Dissertation zur Erlangung des Doktorgrades
der Fakultät für Chemie und Pharmazie
der Ludwig-Maximilians-Universität München

Kank family proteins comprise a novel type of talin activator

Zhiqi Sun
aus Anshun, Guizhou, China

2015

Erklärung
Diese Dissertation wurde im Sinne von § 7 der Promotionsordnung vom 28. November 2011 von Herrn Prof. Dr. Reinhard Fässler betreut.

Eidesstattliche Versicherung

Diese Dissertation wurde selbstständig, ohne unerlaubte Hilfe erarbeitet.

München, ……..

_____
(Zhiqi Sun)

Dissertation eingereicht am 03.07.2015

1. Gutachterin / 1. Gutachter: Prof. Dr. Reinhard Fässler

2. Gutachterin / 2. Gutachter: Prof. Dr.med. Markus Sperandio

Mündliche Prüfung am 6.11.2015

Table of contents

Abbreviations

ADMIDAS	metal ion-dependent adhesion site
APC	adenomatous polyposis coli
ARP2/3	actin-related protein 2/3
ATAT1	α-tubulin N-acetyltransferase 1
CDK5	cyclin-dependent kinase 5
CFEOM1	congenital fibrosis of the extraocular muscles type 1
CLASP	cytoplasmic linker associated protein
CRAPome	contaminant repository for affinity purification
Dab2	disabled homolog 2
DD	dimerization domain
DLC1	deleted in liver cancer 1
DOK1	docking protein 1
ECM	extracellular matrix
EGF	epidermal growth factor
EM	electron microscopy
Eps8	epidermal growth factor receptor pathway substrate 8
EZH2	enhancer of zeste homolog 2
FA	focal adhesion
FAEI	focal adhesion enrichment index
FAK	focal adhesion kinase
FB	fibrillar adhesion
FCHO2	FCH domain only 2
FERM	4.1/ezrin/radixin/moesin
FN	fibronectin
FRAP	fluorescence recovery after photobleaching
GEF	guanine nucleotide exchange factor
HDAC6	histone deacetylase 6
hMSC	human mesenchymal stem cell
IBS	integrin binding site
ICAP1	integrin cytoplasmic domain-associated protein 1
ILK	integrin-linked kinase
IMC	inner membrane clasp
IRSp53	insulin receptor substrate p53
Kank	KN motif and ankyrin repeat domains
LADIII	leukocyte adhesion deficiency type III
LATS	large tumor suppressor
LIMBS	or ligand-induced metal ion binding site
MDGI	mammary-derived growth inhibitor
METTL8	methyltransferase-like protein 8
MIDAS	metal ion-dependent adhesion site
MRL	Mig-10/RIAM/Lamellipodin
MST	STE20-like protein kinase
MT1-MMP	membrane type 1 matrix metalloprotease
MYPT1	myosin phosphatase-targeting subunit 1
NA	nascent adhesion
NMR	nuclear magnetic resonance
OMC	outer membrane clasp

PH	pleckstrin homology
PIPKIγ90	phosphatidylinositol 4-phosphate 5-kinase Type Iγ 90
PP2A	protein phosphatase 2A
PSI	plexin-semaphorin-integrin
PTB	phospho-tyrosine binding
RA	Ras-association
RIAM	Rap1–GTP-interacting adapter molecule
ROCK	Rho-associated coiled-Coil containing protein kinase
SAXS	small angle X‑ray scattering
SHARPIN	SHANK-associated RH domain-interacting protein
Smurf1	SMAD ubiquitination regulatory factor 1
SNX	sorting nexin
SRC	steroid receptor coactivator
SRF	serum-responsive factor
SyMBS	synergistic metal ion binding site
TAZ	transcriptional co-activator with PDZ-binding motif
TEAD	TEA domain
THATCH	talin/HIP1R/Sla2p actin tethering C-terminal homology
TMD	transmembrane domain
VASP	vasodilator-stimulated phosphoprotein
VASP	vasodilator-stimulated phosphoprotein
VBS	vinculin-binding site
WAVE2	WASP-family verprolin-homologous protein-2
YAP	Yes-associated protein

1. Summary

Cell adhesion to the extracellular matrix (ECM) is mainly mediated by integrins, which are heterodimeric transmembrane receptors composed of α and β subunits. 18 different α subunits and 8 different β subunits assemble into 24 different integrin heterodimers recognizing specific ECM ligands.

Prior to the assembly of an adhesion site, integrins have to be activated. Integrin activation is characterized by switching the unbound integrin from a low affinity (inactive) to a high affinity (active) state, which is followed by binding ECM substrates. Upon activation and ligand binding, integrins recruit adaptor and signaling proteins and cluster into nascent adhesions (NAs). NAs are small (with a diameter less than 1 μm) and short-lived adhesions that emerge at the leading edge of cell protrusions. While most NAs are rapidly dissolved, a small population of them are coupled to F-actin and undergo maturation into large focal adhesions in an actomyosin-dependent manner. During this process, mechanical force generated by non-muscle myosin-II acts on mechano-sensitive proteins in the adhesion leading to conformational changes and further recruitment of adaptor and signaling proteins. At a later step and only of cells that adhere to fibronectin (FN), fibrillar adhesions are formed during fibrillogenesis through the centripetal translocation of a5β1 integrins.

The recruitments of the two adaptor proteins, talin and kindlin to two NPxY/NxxY motifs present in β integrin cytoplasmic domains are crucial for integrin activation. Talin is highly conserved ~270kD big protein and composed of an N‑terminal FERM domain (talin head) and a long C-terminal rod domain. The binding of talin FERM domain to the membrane-proximal NPxY motif and juxtamembrane region in β-integrin tails alters β-integrin transmembrane domain topology and promotes the high affinity state in the integrin ectodomain. Moreover, talin plays essential roles in mechano-transduction through its C-terminal rod domain. Besides direct F-actin binding, talin rod domain expose cryptic vinculin binding sites under mechanical force. Vinculin recruitment further strengthens the F-actin linkage with talin. The dynamic connection between talin and the actomyosin system creates a molecular clutch that drives cell migration. Given its important function in integrin activation, talin activity is tightly controlled by an autoinhibitory intramolecular head-rod interaction. RIAM (Rap1–GTP-interacting adapter molecule) and a splice isoform of phosphatidylinositol 4-phosphate 5-kinase

type Iγ (PIPKIγ90) have been shown to activate talin. However, genetic ablations of either gene in mice did not lead to overt phenotypes related to talin dysfunction, indicating the existence of redundant talin activation mechanisms.

Specialized adhesion structures recruit large ensembles of proteins, which are collectively termed adhesome. Literature survey and high resolution quantitative mass spectrometry identified more than one thousand candidate adhesome proteins with versatile functions. However, most of these proteins' localization and enrichment in adhesion sites still lack biochemical validation. In my study, I developed an unbiased focal adhesion enrichment index (FAEI) to quantitatively describe protein enrichment in adhesome. By combining results obtained from FAEI with integrin tail peptide interactome, I identified Kank2 as a novel abundant adhesome protein. Kank2 is a member of evolutionarily conserved Kank family proteins. Cell biology analysis identified Kank2 as marker for a novel focal adhesion subcompartment, the FA belt, which marks the outer border of focal adhesion. Remarkably, Kank2 activates talin through a direct interaction between the KN motif present in the Kank2 N-terminus and the central region of the talin rod. Moreover, Kank2 appears to destabilize talin-actin connection and mobilize talin in adhesion sites. As a consequence, Kank2 suppresses cell migration through talin regulation. Altogether, my study establishes Kank family proteins as novel FA proteins residing in a novel FA compartment where they bind and induce/maintain talin activation and disengage the molecular clutch on talin.

2. Introduction

2.1. Integrin receptors

Multicellular organisms are organized through highly coordinated cell-cell and cell-substratum interactions. Cells constantly sense the biophysical and biochemical properties of their extracellular environment, and translate this information into a wide spectrum of biological outputs including cell migration, cell proliferation, differentiation, etc. While cell-cell adhesion is mediated by cadherin receptors, integrins are the major transmembrane receptors that mediate the interactions between cells and the extracellular matrix (ECM).

Integrins are large family of hetero-dimeric type I transmembrane receptors consisting of one α and one β subunit. The existence of integrin receptor was theorized in 1970s and identified in 1980s (Hynes, 2004). They were termed as 'integrin' due to their ability to 'integrate' the extracellular matrix and the cytoskeleton across the plasma membrane (Hynes, 1987; Tamkun et al., 1986). Integrin receptors are restricted to but universally expressed in metazoan. During evolution, integrin family receptors, together with extracellular matrix proteins, expanded and diversified to accommodate different requirements for organ development, tissue organization as well as tissue homeostasis (Johnson et al., 2009).

2.1.1. Integrin structure

In mammals, the integrin superfamily comprises 18 α- and 8 β-subunits, and together they form 24 different obligate heterodimers, each binding to a specific set of extracellular matrix proteins (Figure 1) (Hynes, 2002). The α-subunits usually contain around 1000 amino acids whereas the β-subunits contain around 750 amino acids. The structure of each subunit could be divided into an ectodomain, a transmembrane domain (TMD) and a short cytoplasmic tail.

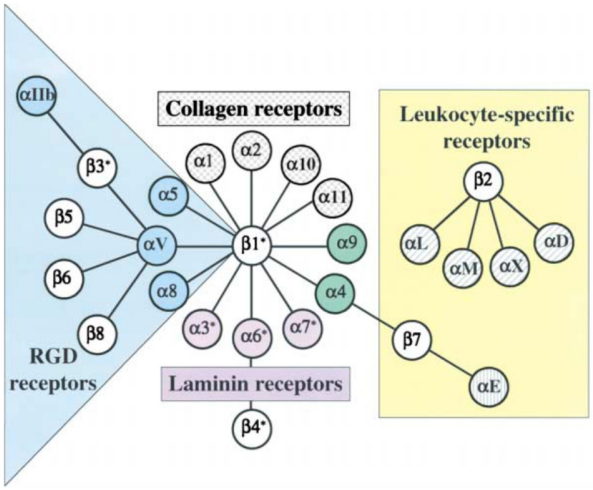

Figure 1. Classification of mammalian integrin family members according to their hetero-dimeric partner and ligand binding specificity. Image is adapted from (Hynes, 2002).

2.1.1.1. Ectodomain

The α-subunit ectodomain consists of 4 or 5 domains dependent on different integrin subtypes (Figure 2). All integrin α-subunits contain an N-terminal β-propeller, followed by a thigh and two calf domains, both of which have similar immunoglobulin-like, β-sandwich folds (Larson et al., 1989; Xiong et al., 2001). The linker between β-propeller domain and the thigh domain and the 'genu' at the junction between the thigh and calf 1 domain confer most of the interdomain flexibility. Nine integrin α-subunits contain an additional α-I domain of around 200 amino acids that is inserted between blade 2 and blade 3 of the β-propeller domain (Larson et al., 1989). The α-I domain is structurally related to von Willebrand factor A domain. In integrins with α-I domain, it is the exclusive ligand binding site. At the N-terminus of the ectodomain of integrin β-subunits, β-I domains are structurally similar with α-I domains and is inserted in a hybrid domain, which is in turn inserted in a plexin-semaphorin-integrin (PSI) domain (Xiong et al., 2004). The PSI domain is followed by four cysteine-rich epidermal growth factor (EGF) domains and a tail domain (Figure 2). The β-tail domain is flexible enough to allow topological rearrangement between ectodomain and TMD. The β-leg exhibits overall more structural flexibility than the α-leg, which undergoes large conformational change during ligand binding, particularly in β-I/hybrid domain (see below). The heterodimerization of integrin ectodomain is mainly mediated by a large interaction interface between the β-I domain in the β-subunit and the β-propeller domain in the α-subunit, which buries ~1700Å2 surface (Figure 2). In integrins that lack α-I domain,

ligand binding occurs at the groove of this interface. Mutations that disrupt this interaction in β2 integrins result in leukocyte adhesion defects (Bunting et al., 2002).

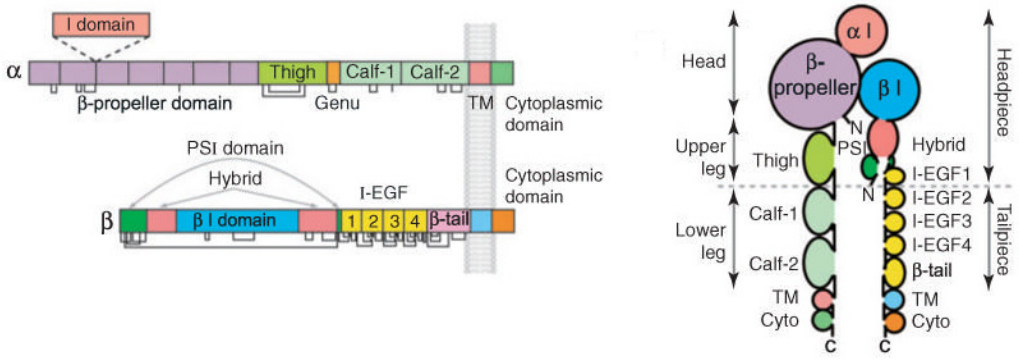

Figure 2. Domain organization in integrin primary structures. Insertion of α-I domain is indicated with dash lines. Disulfide bonds are shown in lines connecting cysteines at corresponding positions. Integrin heterodimerized ectodomain could also be spatially annotated as head, upper leg, lower leg in the α-subunit and headpiece and tailpiece in the β-subunit. Image is adapted from (Luo et al., 2007).

Integrin-ligand interaction could be categorized into four main classes. Two β1 integrins (α5β1 and α8β1), αIIbβ3 integrin and all five αV integrins (αVβ3, αVβ5, αVβ6 and αVβ8) bind RGD tripeptide present in fibronectin (FN), fibrinogen, vitronectin and many other proteins. Four α-I domain-containing β1 integrins (α1β1, α2β1, α10β1 and α11β1) form a laminin/collagen binding integrin subfamily. These integrins recognize the Gly-Phe-Hyp-Gly-Glu-Arg (GFOGER; Hyp or O represent Hydroxyproline) motif in collagen. A third integrin subfamily contains three β1 integrins (α3β1, α6β1 and α7β1) and α6β4 which selectively interact with laminins through unknown motif(s). Another integrin subfamily includes α4β1, α4β7 and α9β1 which interact with the acidic LDV motif in fibronectin and VCAM-1 in a RGD motif-independent manner. Belonging to the same subfamily are leucocyte-specific β2 integrins (αDβ2, αMβ2, αLβ2, αXβ2) and αEβ7 integrin that interact with LDV-related sequences in ICAM, VCAM and E-cadherin through their α-I domains.

Structural studies of both ligand-bound α-I domain and β-I domain conclude that divalent cations are universally required for ligand binding by all integrins (Lee et al.,

1995; Xiao et al., 2004; Zhu et al., 2008a). In order to interact with negatively charged residues in the ligand, the metal ion-dependent adhesion site (MIDAS) binds Mg^{2+} under physiological condition. Two regulatory metal ion binding sites locate adjacently to MIDAS, both of which bind Ca^{2+} under physiological condition. One site positively regulate ligand binding in the presence of Ca^{2+} and thus is termed synergistic metal ion binding site (SyMBS) or ligand-induced metal ion binding site (LIMBS). The other site is called adjacent to metal ion-dependent adhesion site (ADMIDAS) and plays inhibitory role in ligand binding. Thus Ca^{2+} has dual effects on integrin-mediated adhesion that high Ca^{2+} concentration inhibits adhesion whereas low Ca^{2+} concentration promotes adhesion. Replacing Ca^{2+} with Mn^{2+} at ADMIDAS increases ligand binding affinity.

2.1.1.2. Transmembrane domain

The transmembrane domains (TMD) of both α-subunit and β-subunit are highly conserved among different species. Several additional hydrophobic residues locate to the C-terminus of the predicted hydrophobic transmembrane region after a snorkeling lysine residue (Figure 3). It was proposed that these juxtamembrane hydrophobic residues may allow the TMD to be either straight or tilted in the plasma membrane, thus topologically permitting transmembrane signal transduction (Ginsberg et al., 2005). The TMD association is mediated by two types of interaction. Residues with opposing charges (Arg-995 in αIIb integrin and Asp-723 in β3 integrin) at the juxtamembrane region link two TMDs through electrostatic interaction and this site is termed inner membrane clasp (IMC, Figure 3). Inside the membrane, α-TMD contains a conserved GxxxG motif, which is statistically, the most over-represented simple sequence motif among all transmembrane domains (Russ and Engelman, 2000; Senes et al., 2000). Structurally, the two glycines (Gly-972 and Gly-976 in αIIb integrin) form a ‘groove’ that the dimerizing TMD could fit in to closely pack against each other. Any mutation on these glycines will result in a significant disruption of TMD dimerization. This GxxxG motif-mediated integrin TMD association is termed outer membrane clasp (OMC, Figure 3).

Both IMC and OMC are indispensable for the efficient transmembrane association of integrin heterodimer (Kim et al., 2009). Structural analysis of the αIIbβ3 integrin TMD dimer revealed a 25° crossing angle between α-TMD and β-TMD with α-TMD

perpendicular to the membrane and β-TMD tilted in the membrane (Figure 3) (Lau et al., 2009). TMD tilting allows simultaneous formation of both IMC and OMC. Integrin activation is accompanied by topological alteration of the β-TMD that disrupts the transmembrane dimerization (Kim et al., 2012). Both charge reversal of the IMC (R995D or D723R) and bulky mutations in the OMC (G972L or G976L) in αIIbβ3 integrin resulted in constitutive activation of integrin (Hughes et al., 1996; Luo et al., 2005). Thus it is widely accepted that transmembrane dimerization is required to stabilize integrin in its low affinity state for some integrins, although it is debated whether the salt bridge of the IMC is required for all integrins.

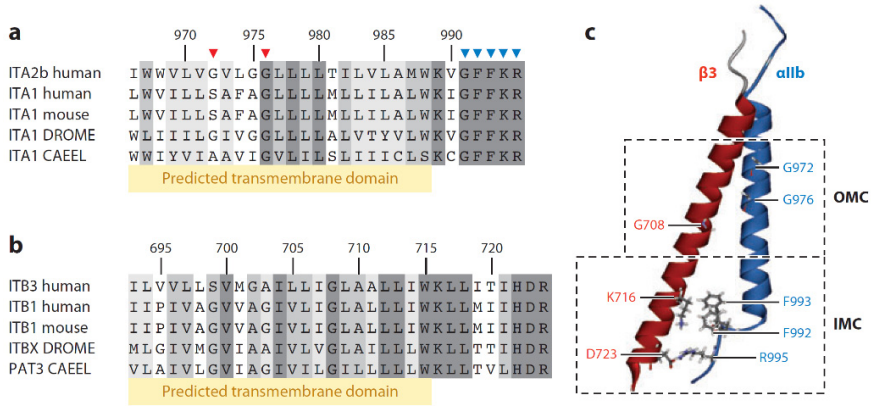

Figure 3. (a) and (b), sequence alignment of α-TMD and β-TMD indicates sequence conservation. Both α-TMD and β-TMD contain additional hydrophobic residues at the C-terminus than predicted transmembrane sequence. Highly conserved GxxxG and GFFKR motifs in α-subunit are indicated by arrows. (c), nuclear magnetic resonance structure of the TMD complex of αIIbβ3 integrin (αIIb TMD in blue and β3 TMD in red). TMD association occurs at two positions termed outer membrane clasp (OMC) and inner membrane clasp (IMC). Residues involved in OMC and IMC are indicated. Picture is adapted from (Kim et al., 2011).

2.1.1.3. Cytoplasmic domain

Unlike receptor tyrosine kinases that transduce growth factor signaling, integrins have short cytoplasmic domain (~20-50 amino acids) with no catalytic activity. One exception is β4 integrin which contains a large cytoplasmic domain of around 1000 amino acids. α6β4 associates with intermediate filaments but not actin in hemidesmosomes. The lack of structural consensus suggests that the short integrin cytoplasmic domains are most likely very flexible by themselves and only adopt certain

secondary structure when complexed with specific adaptor proteins (Campbell and Humphries, 2011).

The cytoplasmic domains of β integrin contains a juxtamembrane HDRR motif, a membrane-proximal NPxY motif and a membrane-distal NxxY motif separated by a serine/threonine-rich linker (TT motif in β1A integrin) (Legate and Fassler, 2009). NPxY and NxxY motifs are commonly recognized by phospho-tyrosine binding (PTB) domains or domains with similar fold (e.g. FERM domain) (Figure 4). Kindlin binding to the TT motif and distal NxxY motif through its FERM domain is crucial for integrin activation. The other integrin activator, talin, uses the FERM domain to interact with the entire sequence from HDRR motif to membrane-proximal NPxY motif. All other integrin tail interactors that compete with kindlin and/or talin are potentially integrin inactivators. Among them, integrin cytoplasmic domain-associated protein 1 (ICAP1) and docking protein 1 (DOK1) interact with the membrane-distal and membrane-proximal NxxY/NPxY motifs, respectively, and thus keep integrin in its inactive state (Bouvard et al., 2013). Recent structural study showed that filamin may inhibit integrin activation by directly competing with kindlin for NxxY motif binding, blocking talin binding via steric hindrance and stabilizing the IMC (Liu et al., 2015). Integrin endocytosis is redundantly mediated by disabled homolog 2 (Dab2) and Numb that interact with NPxY and NxxY motif, although the binding specificity is unclear (Calderwood et al., 2003; Ezratty et al., 2009; Nishimura and Kaibuchi, 2007). Once internalized into endosomes, integrin could be either recycled to the plasma membrane or degraded in lysosome. The FERM-domain containing sorting nexins (SNX17 and SNX31) interact with the membrane-distal NPKY motif in β1 integrin on the endosomes and prevent the lysosomal degradation (Bottcher et al., 2012; Steinberg et al., 2012; Tseng et al., 2014).

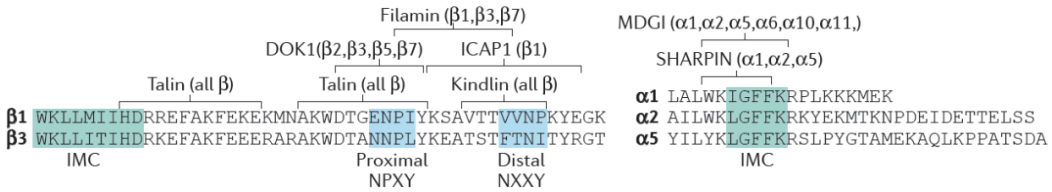

Figure 4. Hot spots of integrin tail binding events are highlighted (blue). The binding regions for several integrin activators and inactivators and their integrin subtype specificity are indicated. Picture is adapted from (Bouvard et al., 2013).

The protein interactions on α integrin cytoplasmic tail are less well studied. Recently it was reported that both SHANK-associated RH domain-interacting protein (SHARPIN) and mammary-derived growth inhibitor (MDGI) interact with the juxtamembrane WKxGFFKR motif in α integrin tail (Figure 4) and inactivate integrin likely through steric hindrance of talin binding as well as IMC stabilization (Nevo et al., 2010; Rantala et al., 2011). It appears that α tail interactions mainly play roles in integrin inactivation. In sum, Integrin tail binding proteins control the entire life cycle of integrin including activation, inactivation, endocytosis, recycling and degradation. How these mutually exclusive binding events are dynamically regulated needs further research.

2.1.2. Allosteric integrin activation

It is well accepted that integrin activation and ligand binding is accompanied by large conformational changes (Figure 5). The X-ray crystal structure of the αVβ3 integrin ectodomain is in a V-shaped bent conformation with the globular N-terminal ligand binding domain juxtaposed to the membrane-proximal region of the leg pieces (Xiong et al., 2001). Bent conformation may restrict the accessibility of the ligand binding site and thus represent physiological low-affinity state. Electron microscopy (EM) study could confirm that αVβ3 integrin ectodomain stays in a bent conformation in its resting state. Ligand or Mn^{2+} can induce a switchblade-like opening to an extended conformation with the head piece facing upwards and two leg pieces separated (Takagi et al., 2002). This concept is further validated for αIIbβ3 integrin reconstituted in phospholipid nanodiscs (Ye et al., 2010). While the majority of αIIbβ3 integrins stay in compact bent conformation with ~11nm in height, integrin activation induced by the talin head domain (see below) or ligand binding promotes the ectodomain extension with ~19nm in height.

The low-affinity bent conformation is stabilized by several weak interactions including the interface between α and β leg pieces, between the head piece and the lower leg piece and the TMD dimerization (Figure 5 (1)). Structural perturbations of the cytoplasmic domain and/or transmembrane domain favor the extended conformation in which the ligand binding site is more accessible (Figure 5 (2)). Extrinsic ligand binding to β-I or α-I domains induces conformational changes in the head piece so that the βI-α7-helix pistons downward and induces a remodeling of the interface between β-I/α-I domain and hybrid domain, leading to a 60˚ degree swing-out of the hybrid

domain, 70 Å away from the α subunit. The hybrid domain swing-out translates the local interface change into a global conformational rearrangement and eventually an overall open conformation of the integrin ectodomain (Figure 5 (3)). For integrins with α-I domain, extrinsic ligand binding on α-I induces intrinsic ligand binding to β-I domain (Luo et al., 2007).

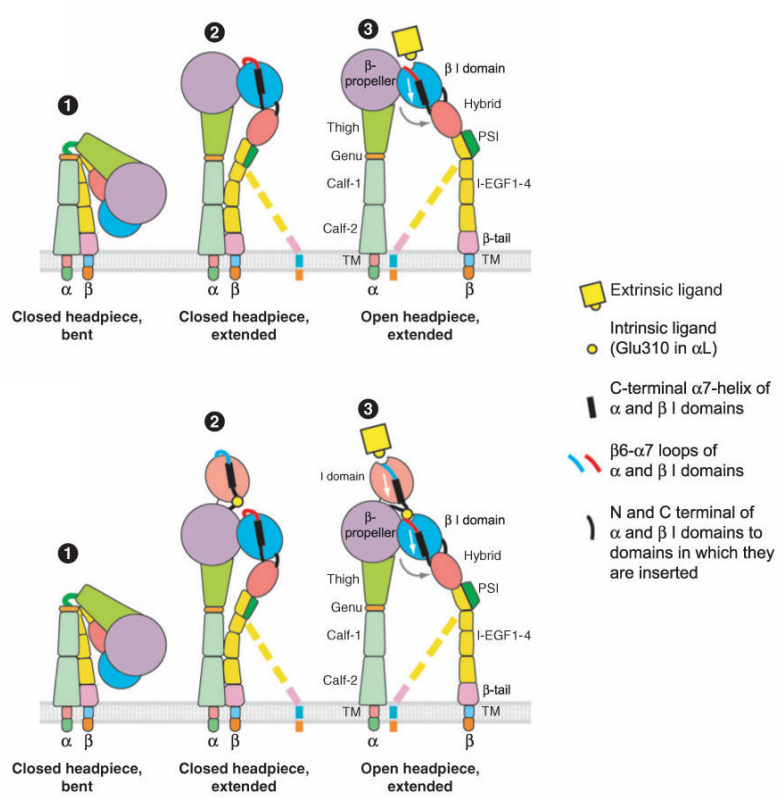

Figure 5. Schematic illustration of the conformation change during integrin activation for integrins that lack (upper panel) or contain (lower panel) α-I domain. Image is adapted from (Luo et al., 2007).

2.2. Talin-dependent integrin activation

Among various integrin tail binding proteins, talin plays a critical role in integrin activation. Like integrins, talin is conserved throughout metazoans. Mammals express two talin paralogue genes, talin-1 and talin-2, with different tissue specificity. While talin-1 is ubiquitously expressed in all tissues as a single isoform, full length talin-2 is

mainly expressed in muscle and neuronal lineages with multiple alternatively spliced isoforms expressed in other tissues. The milestone discovery that overexpression of talin head domain (see below) induced the high affinity conformation of αIIbβ3 integrin and shRNA-mediated knockdown of talin suppressed integrin activation established talin as the first integrin activator (Tadokoro et al., 2003). Genetic analysis of talin genes in *D.melanogaster* (Brown et al., 2002) and *C.elegans* (Cram et al., 2003) as well as in mice (Monkley et al., 2000; Petrich, 2009) have all demonstrated that talin is essential for integrin-mediated functions.

2.2.1. Talin structure and autoinhibition

Talin is a large cytosolic protein with a molecular weight of ~270 kDa. It was initially found to connect integrin cytoplasmic domain with vinculin (Burridge and Mangeat, 1984; Horwitz et al., 1986). Talin comprises a globular N-terminal head domain and a large C-terminal rod domain connected by a flexible linker (Critchley, 2009) (Figure 6). The talin head contains a FERM domain which shares homology with those found in the band 4.1/ezrin/radixin/moesin family cytoskeletal proteins (Fehon et al., 2010). The talin FERM domain can be divided into four subdomains: F0, F1, F2, and F3. While both F0 and F1 subdomains are ubiquitin-like folds, the F3 subdomain has a phosphotyrosinebinding (PTB)-like fold which is responsible for the interaction with integrin (integrin-binding site 1; IBS1), phosphatidylinositol 4-phosphate 5-kinase type Iγ 90 (PIPKIγ90) and the hyaluronan receptor layilin in a structurally similar mode (Anthis et al., 2009; de Pereda et al., 2005; Wegener et al., 2008). Talin head also interacts with focal adhesion kinase (FAK), Tiam, actin-related protein 2/3 (ARP2/3) and actin (Lawson et al., 2012; Lee et al., 2004; Wang et al., 2012). Moreover, the F1-3 domains contain positively charged patches of basic amino acids that interact with negatively charged PtdIns (4,5)P_2 and facilitate talin-integrin binding at plasma membrane (Wang, 2012).

Talin rod domain contains 62 α-helices that are packed into 13 helical bundles (R1-R13) followed by a single helix dimerization domain (DD), which dimerizes in anti-parallel manner (Figure 6). Among them, R1, R5-R7 and R9-R13 are 5-helix bundles and the others are 4-helix bundles. The successive 4-helix bundles between R2 and R4 create a relatively compact cluster since their N-terminal and C-terminal ends are centripetally oriented. R7 and R8 domain adopt unique fold with the 4-helix bundle R8

inserted in the R7 bundles (Gingras et al., 2010). The talin rod domain contains numerous binding sites for actin, vinculin, Rap1–GTP-interacting adapter molecule (RIAM) and a second integrin binding site (IBS2) (Critchley, 2009). R8 domain in the talin rod is able to recruit tumor suppressor Rho GTPase activating protein, deleted in liver cancer 1 (DLC1) and synemin which links actin with intermediate filaments (Li et al., 2011b; Sun et al., 2008).

Although full length talin 1 structure has been modeled based on crystal and nuclear magnetic resonance (NMR) structures of individual domains, the tertiary structure of talin remains elusive. While in low salt condition talin adopts a compact globular structure, in higher salt concentration (above 150mM KCl), talin adopts a U-shaped flexible conformation with about 56nm in length (Winkler et al., 1997). EM reconstruction of full-length talin at low salt condition based on SAXS (small angle X-ray scattering) analysis of individual domain proposed a donut-shaped talin dimeric structure with two rod domains stacking against each other and the talin head domain embedded within the donut (Goult et al., 2013a). Interestingly, R7-R9, R13 and DD domains are adjacent to each other in this model.

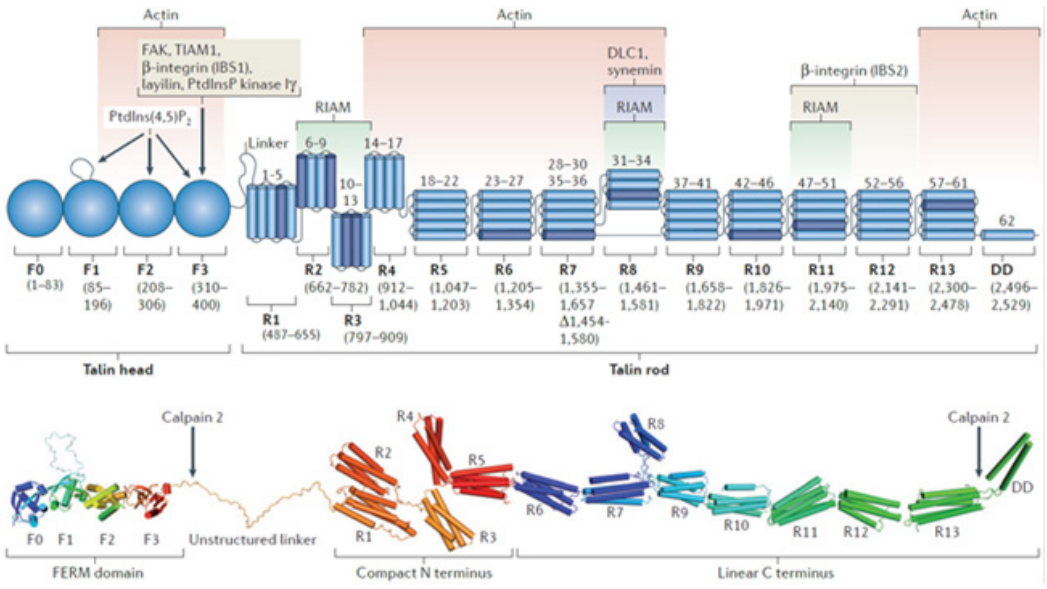

Figure 6. Domain organization and structural model of full-length talin. Talin 1 and talin 2 are predicted to have the same domain structure. Upper panel: Domain boundaries are annotated according to amino acids sequence of human talin-1. Vinculin binding sites (VBSs) are

indicated in dark blue. Lower panel: structural model of talin 1 is assembled from the crystal and nuclear magnetic resonance (NMR) structures of the various domains. Picture is adapted from (Calderwood et al., 2013).

As talin is essential in integrin activation, its activity is tightly controlled. The majority of overexpressed talin stays in the cytosol indicating that most talin molecules stay in an inactive form (Banno et al., 2012). The globular closed conformation of the talin dimer is thought to reflect the autoinhibited conformation of talin in the cytoplasm. Crystal structure analysis revealed an intramolecular interaction between talin F3 subdomain in the head and R9 domain in the rod with sub-micromolar affinity, which masks both the integrin binding site and the PtdIns(4,5)P_2 binding surface in the FERM domain (Goksoy et al., 2008; Song et al., 2012) (Figure 7). Point mutations disrupting the talin autoinhibition enhance talin-mediated integrin αIIbβ3 activation when overexpressed in CHO cells (Song et al., 2012). Other weak intramolecular interactions in talin rod may contribute to the packing of globular dimer structure. Talin autoinhibition is physiologically important as constitutive active talin mutant in flies causes morphogenetic defects such as delayed dorsal closure during development (Ellis et al., 2013).

2.2.2. Talin activation

In order to bind integrin, talin requires an activation step that disrupts the auto-inhibitory head-rod interaction. Several mechanisms promote talin activation and plasma membrane localization to induce integrin activation.

The best characterized talin activator is the Rap1 effector protein Rap1–GTP-interacting adapter molecule (RIAM). RIAM belongs to the MRL (Mig-10/RIAM/Lamellipodin) protein family which contains an N-terminal short talin binding sequence, a Ras-association (RA), pleckstrin homology (PH), and several proline-rich domains (Krause et al., 2004). RIAM has been shown to mediate talin activation downstream of the PKC-Rap1 signaling pathway (Han et al., 2006; Lafuente et al., 2004). The talin rod contains several binding sites for RIAM in the R2R3 domains, R8 domain and R11 domain with the one in R8 showing the highest affinity (Chang et al., 2014). Active Rap1 GTPase-bound RIAM may initially bind the R8 helical bundle and thereby recruits talin to the plasma membrane through the geranylgeranyl group on

the active Rap1 (Lee et al., 2009). After targeting talin to plasma membrane, RIAM is able to bind the F3 subdomain, which leads to the disruption of the autoinhibitory interaction between F3 and R9 domains (Yang et al., 2014a). Since RIAM interacts with the actin elongator, vasodilator-stimulated phosphoprotein (VASP), RIAM may also couple talin activation with actin dynamics to drive membrane protrusion at cell leading edge (Lafuente et al., 2004; Worth et al., 2010).

As the positively charged surface in the F3 domain interacts with both R9 domain and acidic phospholipids, the F3–R9 interaction can be disrupted by PtdIns(4,5)P_2 (Goksoy et al., 2008). PtdIns(4,5)P_2 can also promote MRL protein-mediated talin translocation to the plasma membrane by interacting with the PH domain in RIAM and Lamellipodin (Krause et al., 2004; Wynne et al., 2012). A spliced variant of phosphatidylinositol 4-phosphate 5-kinase Type Iγ, PIPKIγ90, is responsible for localized synthesis of PtdIns(4,5)P_2 in focal adhesions (Legate et al., 2011). Talin recruits and activates PIPK1γ90 by a direct interaction between talin F3 domain and the WVYSPLH sequence in the C-terminus of PIPK1γ90 (Di Paolo et al., 2002; Ling et al., 2002). Cells lacking PIPK1γ90 show delayed cell adhesion and spreading, reduced recruitment of talin to focal adhesions and subsequently impaired force transduction (Legate et al., 2011). However, since integrin tail and PIPKIγ90 have overlapping binding site on the talin head, PIPK1γ90 may only be involved in adhesion reinforcement after the initial talin recruitment to adhesion sites.

Recently it was reported that talin was not detectable in early paxillin-positive nascent adhesions in FAK-null cells (Lawson et al., 2012). Although such an observation does not speak against a role for talin in integrin activation, it is plausible that FAK interacts with talin and promotes its recruitment to early adhesion sites in a positive feedback loop.

In addition, talin contains several actin binding sites, some of which may be initially exposed on the autoinhibitory globular structure. By dynamically interacting with F-actin and the PtdIns(4,5)P_2 on the plasma membrane, the frictional force created by the actin retrograde flow may release the autoinhibited structure, resulting in stochastic talin activation events in cell protrusions. Subsequent engagement with free integrin cytoplasmic domains would lead to a deterministic talin activation event. Although this mechanism is highly speculative, a recent study showed that the actin retrograde flow

has the potential to induce the high affinity state of αLβ2 integrins in the immune synapse mediated by T cells (Comrie et al., 2015).

The lack of overt developmental defects in mice lacking PIPK1γ90 or RIAM suggests that talin activation is either stochastic or entirely mediated by the retrograde actin flow (Legate et al., 2012; Plow and Qin, 2015; Stritt et al., 2015). While RIAM controls talin in cell protrusions, talin in mature focal adhesions still undergoes fast exchange in fluorescence recovery after photobleaching (FRAP) analysis (Goult et al., 2013b). Importantly, talin is directly recruited to mature focal adhesion from cytoplasm without lateral diffusive movement across the plasma membrane (Rossier et al., 2012), suggesting the existence of several, possibly functionally distinct talin activation mechanisms.

2.2.3. Structural basis of Talin-dependent integrin activation

Once activated, talin head domain can interact with the entire N-terminal half of the β integrin cytoplasmic domain from the HDDR motif to the first NPxY motif (Anthis et al., 2009; Wegener et al., 2007) (Figure 7). The F3 subdomain first binds to the NPxY motif, which allows additional interaction between F3 and the juxtamembrane region of the β-integrin tail. At the juxtamembrane region, talin F3 disrupts the salt bridge of IMC by interacting with the conserved Asp residue in β integrin (Asp-723 in β3 integrin) (Figure 7). The loss of IMC destabilizes the integrin TMD dimerization, induces tilting and repositioning of the β-TMD in the membrane and eventually a conformational change of the ectodomain (Kim et al., 2012) (Figure 7).

The interaction between talin head and PtdIns(4,5)P_2 in the plasma membrane plays important role in talin-mediated integrin activation at least partially by strengthening talin-integrin interaction (Moore et al., 2012). Mutations in talin F1 and F2 subdomains that impair talin-membrane interaction result in reduced talin-dependent integrin activation (Anthis et al., 2009; Goult et al., 2010). The simultaneous interactions of talin with both plasma membrane and integrin tail may also coordinate the intramembranous TMD topological change (Figure 7).

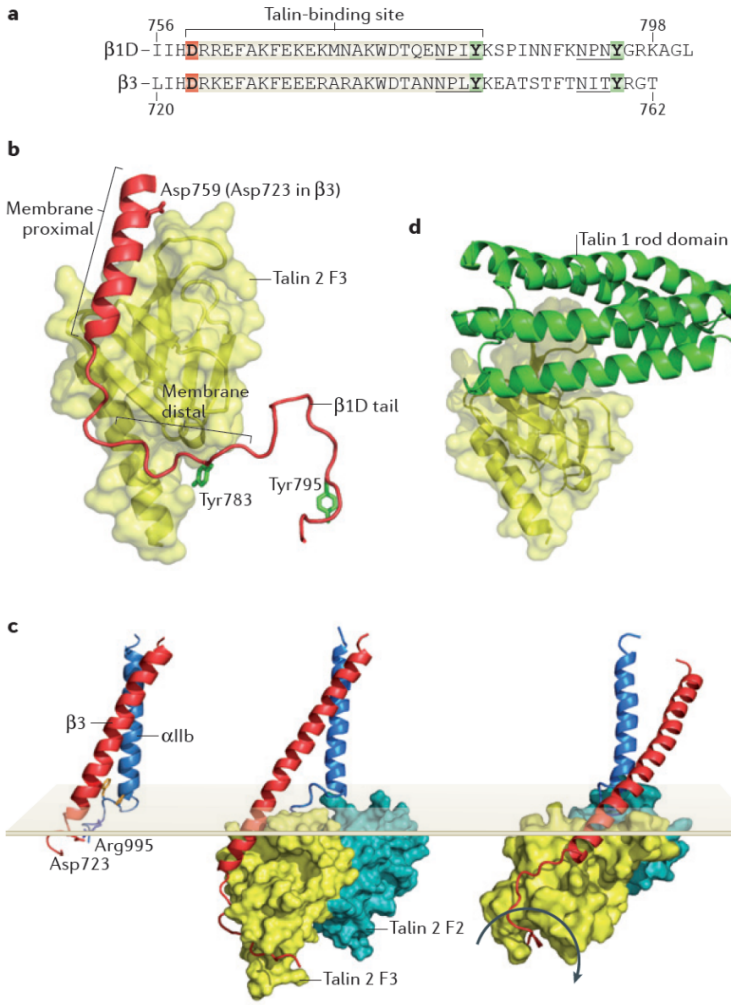

Figure 7. Structural basis of talin-mediated integrin activation. (a) Talin interaction sites are highlighted in β1A and β3 integrin cytoplasmic domain. (b) Crystal structure of talin in complex with the 1D tail. Talin interaction with Asp-759 and Tyr-783 are important for talin-dependent integrin activation and talin-integrin interaction. (c) Talin activates integrin by modulating β integrin TMD topology. TMD dimerization by innermembrane clasp (IMC, Asp-723 and Arg-995) and transmembrane interaction stabilize integrin in inactive state (left); Talin binding to Asp-723 on β3 integrin tail disrupts the IMC (middle); talin binding to plasma membrane tilts β-TMD, induces TMD separation at outer membrane side and promotes conformation change in ectodomain (right). (d) Crystal structure of the autoinhibitory interaction between talin-F3 domain and R9 domain. Picture is adapted from (Calderwood et al., 2013).

2.2.4. Connections between talin and actin

Although talin is clearly required for integrin activation in platelets (Gee et al., 2015; Petrich et al., 2007), the physiological significance of talin-mediated integrin activation in other tissues remains debatable. While talin-2 knockout results in mild muscle dystrophy, talin-1 and talin-2 double knockout (talin-1/2 DKO) in mouse skeletal muscles leads to defects in the myotendinous junction maintenance, myoblast fusion and sarcogenesis (Conti et al., 2009). Strangely, although these phenotypes are similar to muscle-specific ablation of β1 integrin (Schwander et al., 2003), myoblasts from talin-1/2 DKO mice have normal β1 integrin activation and adhesion to various ECM ligands. Furthermore, although talin head domain rescues integrin activation in talin-depleted cells, it fails to rescue cell spreading, focal adhesion kinase activation or traction force generation (Zhang et al., 2008). Genetic studies of different talin truncation mutants in flies also showed that talin-actin connections are essential for tissue-specific talin function (Klapholz et al., 2015; Tanentzapf and Brown, 2006; Tanentzapf et al., 2006). Notably, talin head domain alone failed to rescue any talin-dependent function in flies (Klapholz et al., 2015). Thus at least in some tissues, the major function of talin is to mediate the connection between integrin and actin cytoskeleton.

Talin could interact with actin either directly or indirectly. Early *in vitro* studies found that talin purified from gizzard could interact with both G-actin and F-actin (Goldmann and Isenberg, 1991; Schmidt et al., 1999). However, neither exact locations of actin binding sites, nor the physiological function of these direct actin association are completely understood. At least three F-actin binding sites have been identified (Hemmings et al., 1996). F2 and F3 subdomains in the talin head directly interact with F-actin when pH is below 7.0 and may couple integrin with F-actin (Lee et al., 2004). The R7R8 domains in talin rod also directly interact with F-actin (Gingras et al., 2010). The best characterized actin binding site locates at the C-terminal end of the talin rod which contains the R13 helical bundle and the dimerization domain. This actin binding domain is now referred as THATCH domain (talin/HIP1R/Sla2p actin tethering C-terminal homology) due to its structural similarity with a homologous region in HIP1R. Notably, efficient actin binding only occurs when two THATCH domains dimerize through the dimerization domain (Gingras et al., 2008). In silico modeling suggested

that the flexible linker between R13 and DD could allow different talin dimer geometries depending on the orientation of mechanical force (Golji and Mofrad, 2014).

The indirect linkage between talin and F-actin is mainly mediated by vinculin. Vinculin is a 116 kDa protein containing a talin-binding head domain and an actin-binding tail domain linked by a short proline-rich sequence (Ziegler et al., 2006). Crystal structures of full length vinculin revealed that both talin-binding and actin-binding sites are masked in the resting state through an autoinhibitory interaction between head and tail domains (Borgon et al., 2004; Ziegler et al., 2006). Talin rod domain contains multiple (up to 11) potential vinculin-binding sites (VBSs) with the consensus sequence of LxxAAxxVAxxVxxLIxxA that are distributed in different helical bundles along the talin rod (Gingras et al., 2005). Most of these VBSs are buried in the α-helix bundles and thus cryptic. Tensile force in the pico newton range is sufficient to unfold the talin rod domain to expose the cryptic VBSs. Vinculin binding in turn stabilizes talin in the unfolded state (del Rio et al., 2009; Yao et al., 2014). In sum, talin is a mechanosensitive protein whose linkage to F-actin is sensitive to both geometry and magnitude of mechanical force.

2.2.5. Post-translational regulation of talin function

With the exception of a few examples, little is known about the post-translational regulation of talin. Much of the efforts have been focused on the flexible linker region that contains several phosphorylation sites as well as a calpain-2 cleavage site. Calpain-2 mediated cleavage at Gln-433 separates talin head domain from talin rod domain and thus may liberate talin head from the autoinhibition. Isolated talin head is much more potent in integrin binding than full length talin *in vitro* mainly due to a higher on-rate (Yan et al., 2001). However in living cells, cleaved talin head domain is susceptible to Smurf1 (SMAD ubiquitination regulatory factor 1)-mediated ubiquitination and degradation (Huang et al., 2009). A point mutation (L432G) in the linker region renders talin insensitive to calpain-2 and leads to reduced adhesion disassembly rate (Franco et al., 2004). A mutation that disrupt a C-terminal calpain cleavage site (Glu-2492 in talin-1) also inhibits adhesion disassembly (Bate et al., 2012). Thus the major function of calpain-mediated talin cleavage is to disconnect integrins from the actin cytoskeleton and destabilize focal adhesion. Interestingly, CDK5 (cyclin-dependent kinase 5)-mediated phosphorylation at Ser-425 residue

prevents talin head ubiquitination and counteracts calpain-induced adhesion destabilization (Huang et al., 2009). Although in SH-SY5Y cells, both S425A and S425D mutants inhibit cells migration in a wound healing assay, CDK5-dependent talin phosphorylation at Ser-425 promotes β1 integrin activation and bone metastasis in metastatic prostate cancer (PCa) cells, suggesting that the *in vivo* function of talin phosphorylation is context-dependent (Jin et al., 2015). CDK5 may also orchestrate the activation of RhoGAP DLC1 and talin function (Tripathi et al., 2014).

Other types of post-translational regulation are recently emerging. It was shown that arginylation of a C-terminal calpain-released talin fragment regulates cell-cell contact (Zhang et al., 2012). Moreover, methylation of the talin C-terminal THATCH domain by histone methyltransferase enhancer of zeste homolog 2 (Ezh2) partially liberates talin from F-actin. Loss of Ezh2 leads to larger focal adhesion, aberrant stress fiber, reduced adhesion dynamics and reduced transendothelial migration of innate leukocytes and dendritic cells (Gunawan et al., 2015). In sum, post-translational modifications play important roles in regulating the talin connection to actin and adhesion dynamics.

2.3. Kindlin-dependent integrin activation

Recently, kindlins are identified as a new family of integrin activators. The kindlin family in mammals comprises three members (kindlin1-3) that have different tissue expression patterns. While kindlin-1 is preferentially expressed in epithelial cells, kindlin-3 expression is restricted in hematopoietic cells; and kindlin-2 is widely expressed in non-hematopoietic cells (Ussar et al., 2006).

Mutations in kindlin genes are linked to human genetic diseases with pathological manifestations traced to integrin defects. Mutations in kindlin-1 cause Kindler syndrome which is characterized by skin blisters, photosensitivity, mucosal errosion, etc. (Jobard et al., 2003; Siegel et al., 2003). Genetic studies in kindlin-1 knockout mice have attributed at least some of these phenotypes to defects in integrin-mediated adhesion (Meves et al., 2013; Rognoni et al., 2014; Ussar et al., 2008). Mutations in human kindlin-3 cause leukocyte adhesion deficiency type III (LADIII) characterized by severe bacterial infections and bleedings (Karakose et al., 2010). Using kindlin-3 knockout mice, it was shown kindlin-3 is required for the functions of multiple integrins in hematopoietic lineages (Moser et al., 2009; Moser et al., 2008; Schmidt et al., 2011).

Constitutive kindlin-2 knockout in mice results in peri-implantation lethality due to the defective integrin-mediated adhesion of the primitive endoderm and the epiblast to the basement membrane (Montanez et al., 2008). The conserved function of kindlins could be validated in other model organisms. *C.elegans* expresses one kindlin homologue gene called unc-112. UNC-112 colocalizes with PAT-3/β-integrin at muscle-epidermal attachment sites. Homozygous mutants of unc-112 genes exhibit defective assembly of dense bodies and M-lines, loss of integrin at the muscle attachment sites and a severe Pat (paralyzed, arrested elongation at twofold) phenotype similar to integrin mutants (Rogalski et al., 2000). *D.melanogaster* expresses two kindlin homologues (Fit-1 and Fit-2). Simultaneous knockdown of both Fit-1 and Fit-2 results in muscle rounding up, similar to the phenotype of integrin knockdown (Bai et al., 2008).

Like the talin head domain, kindlins consist of a FERM domain with an insertion of a pleckstrin homology (PH) domain into the F2-subdomain (Karakose et al., 2010). The PH domain interacts with plasma membrane and facilitates kindlin-mediated integrin activation (Yates et al., 2012). The F3 subdomain of Kindlin FERM interacts with the membrane distal NPxY motif. A serine/threonine-rich motif before the NPxY as well as the carboxyl terminus of β1 integrin tails also significantly contribute to Kindlin binding affinity and specificity (Fitzpatrick et al., 2014; Harburger et al., 2009).

It is clear that integrin activation requires a cooperation between talin and kindlin as genetic disruption of either binding on β1 integrin tail phenocopies β1 knockout defects (Meves et al., 2013). Eventhough kindlin-2 is not expressed in platelets, in an artificial system, kindlin-2 overexpression can enhance the activation of αIIbβ3 but not α5β1 only in the presence of overexpressed talin head (Ma et al., 2008). One possible explanation is that different integrin subtypes have different sensitivities in activation assays due to their different affinities for kindlin. How kindlin contributes to integrin activation is mechanistically unclear. In contrast to talin, kindlin binding to β integrin tails is not sufficient to disrupt the inner membrane clasp (Bledzka et al., 2012). Recent studies on αIIbβ3 integrin suggest that while talin allosterically activates integrin, kindlin may promote integrin clustering and thus avidity for multivalent ligands (Ye et al., 2013). Notably, the talin head domain has aslo been shown to induce active integrin clustering both *in vitro* and *in vivo* (Ellis et al., 2014; Saltel et al., 2009). Whether talin and kindlin cooperate in integrin clustering remains to be investigated.

2.4. A molecular clutch between integrins and actomyosin required for migration

Various migratory strategies are exploited *in vivo* in a cell type and tissue context-dependent manner. For instance, cancer cells can rapidly disseminate in 3 dimensional matrix with membrane bleb protrusions, which are formed by a polarized rupture of the actin cortex and inflation of cytosolic content (Paluch and Raz, 2013). Interestingly, interstitial leukocyte migration shows a typical amoeboid migration mode with actin-rich lobopodia protrusions (Lammermann and Sixt, 2009). Notably, in physically confined three dimensional space, both bleb and lobopodia protrutions could intercalate with extracellular matrix fibers and thus immobilize the migrating front without necessarily relying on transmembrane receptors (Lammermann et al., 2008; Renkawitz and Sixt, 2010). Mesenchymal migration is another prototype of cell migration widely used by highly spread cells including epithelial cells and fibroblasts. During mesenchymal migration, a mechanical coupling is formed between polymerized actin and integrin-based adhesion (Gardel et al., 2010). Notably, different migratory strategies could be combined *in vivo* by a single cell to achieve maximal migration efficiency in complex tissue environment (Diz-Munoz et al., 2010). Regardless which migratory strategy is exploited, dynamic actin polymerization and actomyosin contraction provide the driving force for cell deformation and ultimate movement (Charras and Paluch, 2008; Parsons et al., 2010; Renkawitz and Sixt, 2010).

2.4.1. Actin structures and dynamics in mesenchymal migration

Cell protrusions in mesenchymal migration are driven by lamellipodia protrusions and/or by filopodia protrusions. Lamellipodia are thin sheet-like protrusions which emerge at the leading edge plasma membrane and extend 2-4 µm towards the cell center (Pollard and Borisy, 2003) (Figure 9). They are formed by the rapid polymerization of dendritic F-actin network mainly through the actin-related protein 2/3 (ARP2/3) complex and actin severing factor, cofilin. ARP2/3 complex is the major actin nucleator in the lamellipodium. When the ARP2/3 complex binds to the side of pre-existing actin filaments, it mimics the barbed end of an actin filament from which a new actin-filament can branch out (Goley and Welch, 2006). Loss of ARP2/3 results in loss of lamellipodia formation, reduced 2-D migration speed and defective haptotaxis

(Suraneni et al., 2012; Wu et al., 2012). The full activity of the ARP2/3 complex requires nucleation-promoting factors (NPF). WASP-family verprolin-homologous protein-2 (WAVE2) complex, as an effector of PtdIns(3,4,5)P_3 and Rac1 GTPase, is responsible for ARP2/3 activation in the leading edge (Oikawa et al., 2004; Yamazaki et al., 2003).

Once the actin branching point is established by the ARP2/3 complex, new actin filaments can elongate spontaneously. However, spontaneous actin assembly is kinetically inefficient and the free barbed ends could be blocked by actin capping proteins (Edwards et al., 2014). Two classes of actin elongators, vasodilator-stimulated phosphoprotein (VASP) and formins, protect the barbed ends from capping proteins and promote elongation of unbranched filaments (Campellone and Welch, 2010). Actin elongators also play roles in linking actin barbed ends with plasma membrane at the leading edge (Block et al., 2012). The balance between ARP2/3-mediated branching and unbranched elongation determines the dynamics of lamellipodia. While high WAVE2 activity results in denser actin network which protrudes slower but more persistently; high actin elongation activity results in unstable protrusions that retract frequently (Bear et al., 2002).

Filopodia are thin spike-like protrusions that usually originate from dendritic actin network of lamellipodia (Mattila and Lappalainen, 2008) (Figure 9). They contain tightly bundled parallel actin filaments with their barbed ends facing the plasma membrane. The formation of filopodia rely on actin elongators including VASP and formins and actin bundling proteins including fascin, insulin receptor substrate p53 (IRSp53) and epidermal growth factor receptor pathway substrate 8 (Eps8) (Mattila and Lappalainen, 2008). Myosin-X is also required for filopodia formation since it transports VASP proteins and integrins into filopodia tips (Tokuo and Ikebe, 2004; Zhang et al., 2004). Point-like integrin-based adhesions are often found at the tips of filopodia (Galbraith et al., 2007). Filopodia thus can sense the extracelullar microenvironment, initiate and orientate the following lamellipodia extensions (Johnson et al., 2015). Depletion of fascin results in the loss of filopodia and haptotaxis but not chemotaxis (Vignjevic et al., 2006). Irrespective of their different structures, lamellipodia and filopodia exhibit actin polymerization at the protruding plasma membrane and

depolymerization at cell-proximal area, which results in the retrograde treadmilling flow of actin filaments.

Behind the dynamic protrusions sites is the contractile lamella consisting of stress fibers and transverse arcs. Transverse arcs are formed by lateral annealing of F-actin meshwork from lamellipodia; in contrast, stress fibers are assembled through formin activity at focal adhesions (Hotulainen and Lappalainen, 2006). Both stress fibers and transverse arcs are composed of periodic α-actinin/myosin-II patches interspersed by short (<5 μm) anti-parallel F-actin filaments. The non-muscle myosin-II activity also drives the retrograde movement of these structure although at much slower speed than that in lamellipodia, forming an integrated treadmilling contractile structure (Burnette et al., 2014; Hotulainen and Lappalainen, 2006).

2.4.2. Molecular clutch between integrin and actomyosin

The retrograde actin movements are mechanical coupled to integrin-based adhesion structures through a 'molecular clutch'. The 'molecular clutch' model predicts bifurcated transmission of retrograde actin flow into membrane protrusion at the leading edge and traction force at adhesion sites which pulls the cell body forward (Figure 8) (Giannone et al., 2009). The clutch engagement results in loss of retrograde flow, traction force generation, and persistent membrane protrusion (Gardel et al., 2010).

Several actin binding proteins, including talin, vinculin, α-actinin, filamin, tensin and integrin-linked kinase (ILK), can directly or indirectly mediate the engagement of the integrin cytoplasmic tail with F-actin (Brakebusch and Fassler, 2003). As direct integrin binding protein with several actin-binding sites, talin mediates the initial clutch between ligand-bound integrin and actin filaments with slip bonds of 2 pN amplitude (Jiang et al., 2003). Individual integrin molecules bear large tension up to 50pN during cell adhesion (Wang and Ha, 2013). Force in this range partially unfolds talin molecules and reveals multiple cryptic sites for vinculin (del Rio et al., 2009). Vinculin recruitments further strengthen the connection between talin and F-actin, hence resulting in a stronger clutch. Vinculin is essential for the molecular clutch since depletion of vinculin results in excessive actin retrograde flow into the lamellum and ambiguous lamellipodium–lamellum border (Thievessen et al., 2013). As talin is required for the recruitment of vinculin to integrin, depletion of talin also leads to

excessive retrograde F-actin flow at the initial cell spreading stage (Johnson et al., 2015; Zhang et al., 2008). α-actinin forms an anti-parallel rod-shaped dimer with actin-binding sites at both end of the rod and bundles actin filaments (Ribeiro Ede et al., 2014; Sjoblom et al., 2008). α-actinin is also able to directly interact with integrin cytoplasmic tails, actin and vinculin head through distinct domains and stabilize the molecular clutch between integrin and actin (Ziegler et al., 2006).

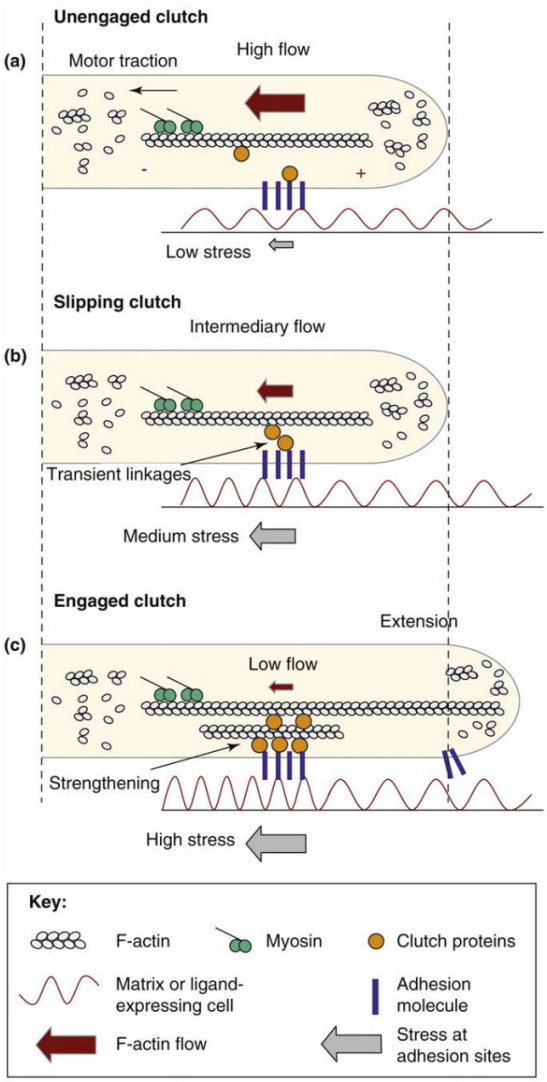

Figure 8. Dynamic engagement of the molecular clutch between adhesion complexes and actomyosin system. (a) Unengaged clutch with no coupling between actomyosin and adhesion complexes results in fast actin retrograde flow, no traction force on ECM and no membrane protrusion.(b) When transient connections are formed between the F-actin flow and adhesion complexes, low traction force is produced at the expense of reduced F-actin flow. (c) With a

strong coupling between F-actin and adhesion complexes, high traction force and persistent membrane protrusion are produced to drive cell migration. Image is adapted from (Giannone et al., 2009).

The molecular clutch engagement at adhesion site is dynamically regulated. With fluorescent speckle microscopy, it was observed that clutch proteins including talin, vinculin and α-actinin, all move retrogradely at intermediary velocities between the fast F-actin retrograde flow rate and the stationary integrins (Hu et al., 2007). Thus, these findings confirm that a slip clutch is formed at the interface between integrin and F-actin through dynamic binary interactions. By regulating a tunable force-transmitting linkage through clutch engagement at different levels, the slip clutch theoretically allows sensitive cellular adaptation to external mechanical cues (Chan and Odde, 2008).

2.4.3. Mechano-sensing and transduction

Mechano-sensing and transduction describe the ability of adherent cells to measure and translate the mechanical stimuli of the biological environment into biochemical signals and adapt their physiological processes accordingly (Jaalouk and Lammerding, 2009). *In vivo*, sensory cells including inner ear hair cells, sensory neurons, etc. acutely respond to mechanical changes in the environment and convert them into electrochemical signals. Also, physical properties of the extracellular environment including rigidity, geometry and nanoscale topology influence cell proliferation, differentiation and death. Consequently, mechano-sensing and transduction are essential for embryonic development and tissue homeostasis and play an important role in pathology.

Force-induced functionality is the central mechanism of mechano-sensing and transduction. Cells probe the rigidity of extracellular environment by pulling on ECM or neighboring cells and thereby detect their effective displacements. Contractile forces produced by the actomyosin apparatus are transduced to the ECM through the 'molecular clutch' mentioned above. Considering that individual force-bearing integrins link to a force-transducing molecular chain, tensile force builds up until the weakest protein-protein interaction interface ruptures, which results in a local failure of the force-transducing chain; or the displacement of the extracellular ligand which results

in force relaxation. Within this time window, intra- and extracellular force-bearing proteins can be increasingly stretched into different functional states. These force-induced functionality could be achieved by exposing cryptic binding sites as is shown for talin and filamin or by altering enzymatic reactivity as is shown for p130Cas and titin kinase (del Rio et al., 2009; Ehrlicher et al., 2011; Puchner et al., 2008; Rognoni et al., 2012; Sawada et al., 2006). Force-induced functionality thus allows protein complex remodeling and biochemical signal transduction.

In addition to the induction of protein interactions and kinase activation, the formation of catch bonds is also an essential type of force-induced functionality. With a constant protein-protein interaction interface, the bond lifetime decreases exponentially with the force applied. These types of interfaces are referred as slip bonds. Interestingly, some bond interfaces can be allosterically activated by mechanical forces, which leads to significantly increased bond lifetimes. These types of interfaces are referred to as catch bonds. The presence of catch bond interfaces in the integrin-based adhesion structures greatly prolongs the time window within which force-bearing proteins can be switched into new functional states.

Robust mechano-transduction also relies on lateral clustering of multiple force-transducing linkages. On one hand, the lateral interactions within an adhesion plaque allow the tensile force to be distributed across multiple mechanical linkages, which reduces the force per molecule and thus the likelihood of local bond rupture (Howard, 2009). Moreover, clustered linkages also allow the broken bond to reform before the collapse of other remaining bonds resulting in the stabilization of the tensile connection. As a result, clustered mechanical linkages forms a bistable system: when the bond numbers stay above a critical threshold, the cluster could survive multiple local single-bond ruptures; when the bond number is below the critical threshold, the system fails completely. Consistent with this model, autonomous force fluctuations were observed within single adhesion site (Plotnikov et al., 2012).

By establishing a tension balance between intracellular and extracellular opposing force elements, cells stiffen the force-bearing cytoskeleton as prestressed tensegrity structure (Ingber, 2003a, b). According to the tensegrity model, mechanical stress propagates along prestressed element in a speed of ~30m/s, much faster than diffusion-mediated and motor mediated signal propagation (usually in speed of a few

micrometers per second) (Wang et al., 2009). Moreover, cellular tensegrity allows the mechanical force to be propagated with little dissipation for long distance (Wang et al., 2009). Consistent with this model, only when cells are prestressed in a more rigid ECM environment, locally applied mechanical force can trigger rapid Src kinase activation at both local force-bearing site and long distance sites in an integrin-dependent manner (Bai et al., 2008). The long range transduction of locally generated biochemical signaling allows rapid delivery of extracellularly stored mechanical information to multiple intracellular organelles including the nucleus.

One of the most impressive example of mechano-sensing and transduction is transcriptional reprograming of stem cell differentiation under different biophysical stimuli. Human mesenchymal stem cells (hMSC) isolated from bone marrow can differentiate into multiple mesenchymal lineages, including adipocytes and osteoblasts, when induced with defined soluble factors (Pittenger et al., 1999). While adipocytes adopt rounded shapes with loose adhesion, osteoblasts usually show large spreading areas. *In vivo*, adipocytes and osteoblasts reside in tissue environments of different rigidities. The seminal work of McBeath et al. demonstrated that single hMSC confined in small adhesive island preferentially undergo adipogenic differentiation, while on large adhesive patch, single hMSCs tend to differentiate into osteoblasts (McBeath et al., 2004). Thus cell shape can instruct stem cell fate determination. The landmark work by Engler et al. unequivocally showed that various substrate elasticities predispose hMSCs to different lineages with corresponding stiffness even in the absence of soluble differentiation inducers (Engler et al., 2006). Moreover, parallel nanogratings induce the expression of neuronal markers in hMSCs (Yim et al., 2007). Remarkably, cell shape and ECM stiffness converge with soluble differentiation cues on RhoA GTPase and its effector Rho-associated coiled-coil containing protein kinase (ROCK) to regulate stem cell fate. Inhibition of cellular tension by the actin depolymerizating agent cytochalasin D, or by ROCK inhibitor Y-27632, promotes adipogenic differentiation of hMSCs. Conversely, overexpression of constitutively active ROCK restores osteogenic fate in hMSCs that are confined on small adhesive island. Moreover, dominant negative RhoA overrides soluble osteogenic cues and induces adipogenesis (Engler et al., 2006; McBeath et al., 2004).

How could mechano-transduction regulate cell fate decision at the transcriptional level? Yes-associated protein (YAP) and transcriptional co-activator with PDZ-binding motif (TAZ) are the major downstream transcriptional factors of RhoA/ROCK pathway in mechano-transduction (Low et al., 2014). Initially, YAP and TAZ are identified as major targets of the Hippo pathway. Hippo pathway comprises a regulatory kinase cascade including mammalian homologues of the Hippo kinase in *D.melanogaster*, STE20-like protein kinase 1 (MST1) and MST2, their downstream kinases large tumor suppressor 1 (LATS1) and LATS2 and the YAP/TAZ transcriptional factors. YAP/TAZ shuttle between cytoplasm and nucleus and function as transcriptional co-activators for TEA domain (TEAD) containing proteins to induce pro-proliferative and anti-apoptotic gene expressions. MST1/2 phosphorylate and activate LATS1/2 which in turn phosphorylate YAP/TAZ. Phosphorylated YAP/TAZ is sequestered in cytoplasm by 14-3-3 and eventually degraded in the proteasome. Interestingly, ECM rigidity, cell geometry and density control cell proliferation and stem cell differentiation by regulating YAP/TAZ activity (Aragona et al., 2013; Dupont et al., 2011). While these regulations depend on the actin cytoskeleton and the RhoA/ROCK pathway, they do not rely on the activation status of LATS1/2, thus should be considered as a non-canonical Hippo signaling pathway. In contrast to the static mechanical state, cyclic stretch regulates YAP/TAZ via canonical Hippo signaling through JNK kinase pathway (Codelia et al., 2014; Mohseni et al., 2014).

Beside YAP/TAZ, mechano-transduction regulates gene expression at different time scale and on multiple levels through different transcriptional factors including serum-responsive factor (SRF), NF- κB, etc. (Olson and Nordheim, 2010; Sero et al., 2015). Mechano-responsive regulation of mRNA splicing has also been reported for the epigenetic regulators such as methyltransferase-like protein 8 (METTL8) (Jakkaraju et al., 2005). Thus, long range mechano-transduction allows the mechanical information of the extracellular environment to affect long term gene expression in the nucleus.

2.5. Molecular organization of integrin-based adhesions

A hallmark of integrin family receptors is their ability to sense the dynamic biochemical and biophysical properties of extracellular matrices with specialized adhesion structures of distinct morphology, subcellular localization, mechanical properties as well as protein composition. To achieve efficient cell migration, different integrin-based

adhesion structures undergo highly dynamic life cycles in which both the actin and microtubule cytoskeletons participate. Accumulating evidences also suggest that specialized endocytosis/exocytosis events occur in close vicinity around adhesion complexes.

2.5.1. Nascent adhesion (NA)

Initial integrin activation and ligand binding trigger the formation of short-lived nascent adhesions (NAs) with a diameter less than 0.5μm at the leading edge of cell protrusions (Gardel et al., 2010) (Figure 9). NAs emerge at the border between lamellipodium and lamellum where the actin retrograde flow switches from fast flow rate to slow flow rate (Hu et al., 2007).

Several principles govern NA formation. First, an integrin-ligand bond must be formed and stabilized for the initial NA nucleation. Lack of the integrin activator, kindlin, led to total failure of NA formation (Theodosiou et al, in preparation). Interestingly however, talin appeared to be dispensable for the formation of NAs during initial cell spreading (Zhang et al., 2008). Second, clustering of active integrin is important for NA formation. Integrin-mediated adhesion requires the presence of nanoscale RGD clusters on which at least three integrins could bind with inter-distances less than ~70nm (Cavalcanti-Adam et al., 2007; Coussen et al., 2002; Maheshwari et al., 2000). EM-tomography analysis of the thin lamellipodium indeed revealed uniform doughnut-shaped particles with diameters of around 25nm, presumably representing integrin nano-clusters (Patla et al., 2010). Moreover, kindlin-3 was shown to promote multivalent ligand binding through integrin clustering (Ye et al., 2013). Third, since NAs are not coupled to thick stress fibers and show high turnover rates, integrins in nascent adhesion must have fast ligand binding kinetics under low mechanical force. Interestingly, in fibroblasts, α5β1 integrin but not αVβ3 integrin participates in the formation of NAs (Schiller et al., 2013). Consistently, β1 integrin is less immobilized on its ligand in comparison to β3 integrin at a single molecular level and such difference requires the extracellular domain (Rossier et al., 2012). Fourth, intracellular adaptor proteins that are recruited to integrin cytoplasmic tails are also important in NA formation either through stabilizing integrin clusters or downstream signaling events. For instance, β3 integrin-enriched NAs could be artificially forged by fusing IPP complex components to β3 integrin cytoplasmic domain (Elad et al., 2013). Finally,

the molecular clutch between integrin and actin is essential for NA formation since either deletion of vinculin or inhibition of the actin retrograde flow by targeting the ARP2/3 complex leads to reduced NA formation (Alexandrova et al., 2008; Thievessen et al., 2013). Consistent with the mechanisms mentioned above, recent microscopic analysis revealed that NAs initiate as a cluster of α5β1 integrins. While Kindlin-2 forms constitutive complex with β1 throughout the NA life time, talin:integrin stoichiometry increases from 1:2 to 1:1 in a myosin-II dependent manner (Bachir et al., 2014).

Dynamic formation of NAs is essential for a productive and processive lamellipodium protrusion during cell migration in a 2 dimensional environment (Gardel et al., 2010). On one hand, coupling between NAs and actin retrograde flow converts actin treadmilling into the force that pushes the leading edge membrane forward (Gardel et al., 2008). On the other hand, NAs could function as a signaling hub to promote actin dynamics in the lamellipodium through β-PIX-Rac1-ARP2/3 axis (Kuo et al., 2011) or kindlin-paxillin-p130Cas-Rac axis (Theodosiou et al., in preparation). Since the molecular clutch is required for NA formation, actin dynamics and NAs form a positive feedback loop to drive cell protrusions. Most NA complexes are rapidly dissolved within minutes and only a small population of them eventually undergoes maturation into focal adhesions (FAs) behind lamellum in an actomyosin-dependent manner (Choi et al., 2008) (Figure 9). It is not clear whether the disassembly of NAs is a default fate or an actively controlled process.

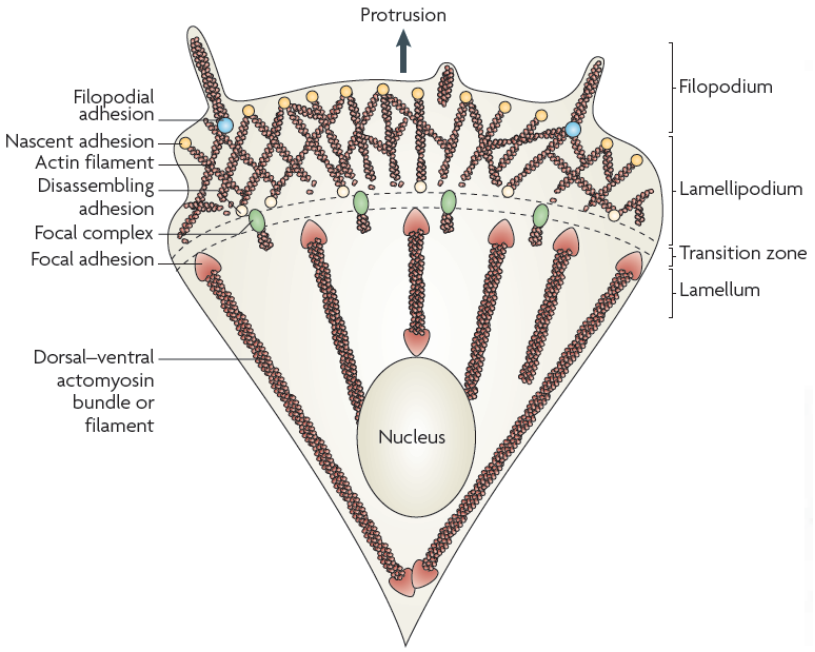

Figure 9. Spatial organization of actin-based structures are linked to dynamic integrin-based adhesive structures in mesenchymal migration. Lamellipodium protrusion in supported by Arp2/3-induced dendritic actin network which links to nascent adhesions. Filopodia originate from lamellipodia through actin elongators including VASP and formins. Nascent adhesions under go either disassembly or force-dependent maturation into focal adhesion in the transition zone between lamellipodia and lamellum. Mature focal adhesions are connected to thick stress fibers. Image is adapted from (Parsons et al., 2010).

2.5.2. Focal adhesion (FA)

FAs have diameters ranging from 1μm to 5μm with a lifetime up to 20 minutes. FA maturation is a coordinated process requiring integrin clustering, actin bundling, and actin-integrin linkage reinforcement (Figure 9).

Although clustering of active integrins already occurs in NAs, the fact that most NAs dissolve without connection to the contractile stress fiber suggests that crosslinked actin bundles could serve as a structural template for FA growth. One candidate that links integrin clustering to the actin template is α-actinin. α-actinin is also able to directly interact with integrin cytoplasmic tails, indicating that it is sufficient to oligomerize integrin receptors in growing FAs along the actin filament (Roca-Cusachs

et al., 2013). Bulky β1 integrin clusters are co-recruited with α-actinin into growing FAs in periodic manner (Bachir et al., 2014). siRNA mediated depletion of the actin crosslinker α-actinin impairs FA maturation without significantly reducing the contractile feature of lamella and traction force generation (Choi et al., 2008; Oakes et al., 2012). Thus, α-actinin is able to promote β1 integrin clustering and set up a connection between the integrin cluster and the actin cytoskeleton. However, overexpression of a motor-dead myosin IIA mutant which retains actin crosslinking activity is sufficient to restore FA maturation in α-actinin knockdown cells, suggesting that the actin bundling is sufficient to guide FA clustering without α-actinin (Choi et al., 2008). In mature FAs, α-actinin regulates mechano-transduction probably by stabilizing the integrin-actin linkage as the chromophore-assisted laser inactivation of actinin-GFP in FAs induced rapid disconnection of stress fibers from FAs (Rajfur et al., 2002; Roca-Cusachs et al., 2013). Given the low affinity between talin head and integrin cytoplasmic domain (Anthis et al., 2010), bundled actin filaments in mature FAs can also stabilize integrin clustering by immobilizing talin through its C-terminal actin binding site and promoting avidity between talin and integrin clusters (Rossier et al., 2012).

The transition from NAs to FAs is stimulated by mechanical force which is generated by non-muscle myosin II activity and transduced via F-actin (Balaban et al., 2001). Inhibiting non-muscle myosin-II activity by blebbistatin blocks FA maturation and induces massive formation of NAs (Straight et al., 2003; Vicente-Manzanares et al., 2008). Several mechanisms could explain the force-dependent FA maturation processes. First, mechanical force exerted on certain FA proteins may induce conformational changes or partial protein unfolding leading to the exposure of cryptic binding sites for downstream adaptor proteins. Since talin could interact with both the integrin cytoplasmic tails and actin filaments at the same time, it transduces the mechanical force to integrins. Stretching force in the pico newton range is sufficient to unfold the talin rod domain and promote the recruitment of vinculin, which in turn stabilize talin in the unfolded state (del Rio et al., 2009; Yao et al., 2014). Thus vinculin is recruited to FAs in a force-dependent manner and further reinforces the connection between integrins and F-actin (Cohen et al., 2006; Humphries et al., 2007). A large group of proteins, particularly LIM domain containing proteins, are recruited to FAs in force-dependent manner to promote FA growth, probably through a similar mechanism

(Schiller et al., 2011). Second, tension-induced conformational changes may alter kinase/phosphatase activity or substrate specificity/accessibility within FA and trigger downstream signal transduction. For instance, p130Cas is more efficiently phosphorylated by Src family kinases when stretched both *in vitro* and *in vivo* (Sawada et al., 2006). It has also been suggested that, PR65, a scaffolding subunit of protein phosphatase PP2A, could change conformation and alter substrate specificity under tension (Grinthal et al., 2010). Finally, the mechanical force induces catch-bonds between α5β1 integrins and fibronectin (Friedland et al., 2009; Kong et al., 2009). Thus mechanical force promotes FA maturation not only by promoting adaptor protein recruitment and enhancing integrin signaling but also by stabilizing integrin-ligand interaction.

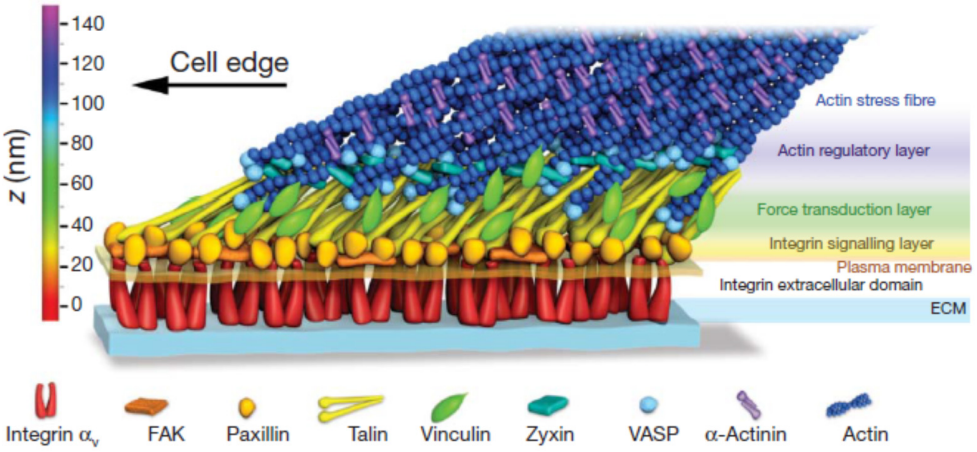

Figure 10. Vertical hierarchy of the molecular organization in mature focal adhesion. Interferometric photoactivated localization microscopy was used to measure the position of different focal adhesion proteins relative to the integrin-ligand interface with a resolution of ~5nm. Several functional layers are designated according to their respective marker proteins. Picture is adapted from (Kanchanawong et al., 2010).

RhoA GTPase activity plays a central role in FA maturation since it can promote actin elongation through the formin pathway and myosin-dependent force generation through the ROCK pathway. Since actin bundling and mechanical force promote FA growth differently, FA size is not always correlated with or predicted by the traction force transmitted to FAs. For instance, depletion of mDia reduces FA size without

impairing the cell traction force (Oakes et al., 2012). Similarly, fibroblasts expressing only αVβ3 and αVβ5 integrins assemble large FA but apply smaller traction force in comparison to fibroblasts expressing only α5β1 integrins, which is likely caused by integrin subtype-specific RhoA activation and its differential coupling to downstream effectors (Schiller et al., 2013).

Hundreds of different proteins are recruited into focal adhesion and form a dynamic interaction network, whose connectivity, complexity and plasticity massively increase during FA maturation (Winograd-Katz et al., 2014). Nevertheless, mature FAs still exhibit a laminated modular molecular organization. Three-dimensional super-resolution fluorescence microscopy of several key FA components revealed that different functional modules in mature FAs are spatially organized into stratified layers of nanometer scale, with integrin-ligand binding module spanning 20nm across the plasma membrane, followed by integrin activator/signaling module containing the talin head, FAK and paxillin 20nm above the plasma membrane, a force transduction module containing the stretched talin rod domain and vinculin, and an actin regulatory module which is connected with actin stress fibers (Kanchanawong et al., 2010) (Figure 10). This organization fits well with the molecular clutch model. While the components in the integrin signaling module stay stationary on the substrate with integrin, the retrograde flow velocities increase from the force transduction module to actin regulatory module (Hu et al., 2007). The lateral organization of focal adhesion structure is less appreciated, probably due to the fact that all current FA markers show a homogeneous staining pattern and the lack of definition of the lateral border of FAs. Mature FAs maintain their equilibrium by symmetrical exchange of pre-assembled protein complex in individual functional modules (Hoffmann et al., 2014). It is possible that the spatiotemporally uniform FA building blocks in the cytosol could maintain the steady state FA but not NAs, which have non-equilibrium protein composition.

2.5.3. Fibrillar adhesion (FB)

Fibrillar adhesions (FBs) are cell-matrix adhesion structures that form in cells cultured on fibronectin. They locate towards the cell center with elongated streak-like morphology or as dotty arrays (Geiger and Yamada, 2011; Zaidel-Bar et al., 2004). Fibrillar adhesions arise from centripetal myosin-II-driven translocation of α5β1-integrins from mature FAs along the underlying fibronectin matrix (Zamir et al., 2000).

This myosin-dependent translocation pre-stresses the fibronectin dimers to expose cryptic binding sites and promote their assembly into fibrils (Singh et al., 2010).

Although the initial phase of FB formation relies upon actin stress fibers (Pankov et al., 2000), once formed, assembled FBs lack the linkage to thick stress fiber and persist even when the force is relaxed (Zamir et al., 2000). Notably, the formation of FBs on a uniformly fibronectin-coated 2-dimensional surface requires translocation of fibronectin molecules as covalently conjugated fibronectin suppresses FB formation (Katz et al., 2000). These observations suggest that unlike FAs, the mechanical coupling between the contractile actomyosin system and integrin-ligand complexes in FBs must be weak. Consistent with this hypothesis, the force-responsive signature of FAs (e.g. phospho-Tyrosine, pTyr397FAK) or force dependent integrin subtypes (e.g. αVβ3 integrin) are not observed in FB (Schiller et al., 2013; Zamir et al., 1999). As a consequence, FBs do not provide pulling force to promote cell migration; instead, they regulate cell migration by increasing adhesiveness or curbing cell orientation along pre-existing matrix fibers. FBs play more important roles during extracellular matrix remodeling in tissue homeostasis (Bonnans et al., 2014).

2.5.4. Adhesion sliding

FA sliding, defined as the translocation of adhesion plaques along the substratum, could be due to a combination of different mechanisms. At both the front and the rear end of migrating fibroblasts, asymmetric force distribution within FAs could lead to focal adhesion growth at the proximal and disassembly at the distal end, resulting in a treadmilling-type movement of adhesion (Ballestrem et al., 2001; Hu et al., 2007; Olberding et al., 2010). Adhesion treadmilling is directed toward the actomyosin contractility along the structural template of the attached stress fiber (Olberding et al., 2010).

Adhesion structure may also slide without turnover when several requirements are fulfilled. First, the integrins in the sliding adhesions must bind their ligands through slip-bonds rather than catch-bonds so the integrins can dissociate and rebind the substratum during sliding; second, integrins must be maintained in their active conformation so that the sliding adhesions do not detach; third, integrin clustering must be stabilized so that the sliding adhesions do not disintegrate. This theory predicts that adhesion sliding uncouples or loosens the mechanical clutch between actomyosin and

integrin. Interestingly, in sharp contrast to motile fibroblasts where FA sliding occur only at the rear end, sliding adhesions are frequently observed in stationary fibroblasts, suggesting that the force coupling and the forward pulling is compromised by adhesion sliding (Smilenov et al., 1999). How to maintain active integrin clustering when the mechanical force is uncoupled? It has been shown that overexpression of vinculin head domain could induce aberrant active integrin clusters that are insensitive to F-actin disruption (Humphries et al., 2007). Since vinculin head is able to stabilize talin in its open conformation, the formation of a the talin-integrin complex at low mechanical force may be the key to this question. However, since full length vinculin only exposes its talin binding site under force, this task is likely accomplished by other, still unknown proteins.

2.5.5. Focal adhesion disassembly

The dynamic adhesion turnover is crucial for cell migration. For NAs, it appears that the disassembly is the default fate if FA maturation does not occur. Spatial and temporal regulation of FA disassembly is required for efficient forward movement of the cell body (Webb et al., 2002). Microscopic studies of FA assembly and disassembly revealed similar kinetics (Stehbens and Wittmann, 2014). However, given the high degree of complexity and plasticity in the protein interaction network in FA, a simple reversion of the molecular events in FA assembly most likely cannot effectively disrupt FAs (Ezratty et al., 2005). A bottom-up strategy, in which FA disassembly mechanism specifically targets the most liable nodes in the integrin adhesome to induce a collapse of the network, is much more likely. Another preferred strategy for FA disassembly is to collectively attack multiple nodes in adhesome network to generally destabilize the FA structure.

FAs are assembled around the short cytoplasmic tails of β integrin subunits. Importantly, unlike the rest of the adhesome network, the linkage between integrin tail and the rest of adhesome mostly relies upon two integrin activators, talin and kindlin. Thus, displacement of talin and/or kindlin from the β integrin cytoplasmic tail is probably the converging point of all FA disassembly pathways. While little is known about how kindlin is regulated during FA disassembly, cells exploit several mechanisms to destabilize the integrin-talin-actin linkage to promote FA disassembly. The calcium-dependent protease calpain cleaves talin and several other FA proteins,

and inhibition of calpain perturbs FA disassembly (Bhatt et al., 2002; Franco et al., 2004). Intriguingly, EZH2, a histone methyl-transferase which was thought to only act in nuclei, can also methylate C-terminal F-actin binding motif of talin and disrupt talin-F-actin interaction (Gunawan et al., 2015). EZH2-mediated talin methylation promotes adhesion turnover and transendothelial migration of neutrophils and dendritic cell (Gunawan et al., 2015). Moesin, a highly abundant cell cortex-enriched FERM domain-containing protein, can be phosphorylated by MAP4K4 kinase and then compete with talin for integrin binding and thereby induce adhesion disassembly (Vitorino et al., 2015). Interestingly, the *D.melanogaster* MAP4K4 homologue, *misshapen*, enriches at the trailing edge of migrating cell and promotes epithelial cell migration by decreasing integrin levels (Lewellyn et al., 2013).

In an extreme scenario, global microtubule disruption by nocodazole leads to aberrant FA growth and nocodazole wash-out triggers microtubule re-growth towards FA and subsequent FA disassembly by integrin endocytosis (Ezratty et al., 2005). Several endocytic adaptor proteins including Dab2, the closely related ARH (autosomal recessive hypercholesterolemia) and Numb concentrate around disassembling FAs, directly compete with talin and kindlin for the NxxY/NPxY motifs in β integrin cytoplasmic tails and promote clathrin-mediated integrin internalization and FA disassembly (Calderwood et al., 2003; Chao and Kunz, 2009; Ezratty et al., 2009; Nishimura and Kaibuchi, 2007). Both Dab2 and Numb are able to bridge the integrins with the AP2 complex and the clathrin coat (McMahon and Boucrot, 2011). Consistently, silencing either AP2 or dynamin results in enlarged FAs (Chao et al., 2010; Chao and Kunz, 2009; Ezratty et al., 2005). Proteins in the integrin signaling module actively regulate clathrin-mediated integrin internalization and FA disassembly. For instance, dynamin is recruited to FAs by FAK and subsequently activated by Src kinase (Ezratty et al., 2005; Wang et al., 2011). Talin may also regulate FA disassembly by regulating the RIAM-MEK-ERK1/2 pathway (Colo et al., 2012).

In contrast to the constitutive integrin endocytosis-recycling cycle in non-adhesive plasma membrane areas, endocytosis-mediated FA disassembly most likely requires internalization of ECM-engaged integrins. Thus, proteolytic release of integrin-bound ECM fragment from the fibrillary matrix at FAs can greatly facilitate FA disassembly.

The membrane type 1 matrix metalloprotease (MT1-MMP) is exocytosed around FAs in Rab6 GTPase dependent manner and mediates focused ECM degradation during FA disassembly (McNiven, 2013; Stehbens et al., 2014; Takino et al., 2007; Wang and McNiven, 2012) (Figure 11). Consequently, MT1-MMP is required for integrin and fibronectin endocytosis as well as normal FA turnover (Shi and Sottile, 2011; Takino et al., 2006). Similar to clathrin-dependent integrin internalization, MT1-MMP is regulated by FAK and Src kinases. FAK recruits MT1-MMP recruitment to FAs and Scr kinase stabilizes the FAK-p130Cas-MT1-MMP complex by phosphorylating Tyr573 at the cytoplasmic tail of MT1-MMP (Wang and McNiven, 2012).

Most FA plaque proteins are not endocytic cargo and are dismissed during FA disassembly by releasing the mechanical force. All FA disassembly mechanisms eventually lead to tension relaxation by disrupting ECM-integrin-actin linkage. FAs rapidly disassemble when actomyosin-dependent force is inhibited by blebbistatin or ROCK inhibitor even in the presence of MT1-MMP inhibitor (Carisey et al., 2013; Stehbens et al., 2014). Although microtubule regrowth-induced FA disassembly is RhoA and Rac1 independent, under physiological condition, integrin internalization in FA must be coordinated with tension release through Rho GTPase signaling (Ezratty et al., 2005).

2.5.6. Microtubules target FAs

Spatial and temporal regulation of FA turnover is mediated by microtubules. Microtubules explore intracellular space by stochastically switching between growing and shortening phases, a behavior called dynamic instability (Mitchison and Kirschner, 1984). Interestingly, microtubules and FAs mutually regulate each other at the cell periphery. Individual microtubules repeatedly target FAs where they switch from a growing phase to a shortening phase in a frequency that is fivefold higher than in cytoplasm (Efimov et al., 2008; Kaverina et al., 1998). The growing microtubules tips bend towards the adhesion sites at the cell periphery where they reach to 50nm near the ECM, as close as the integrin signaling module (Krylyshkina et al., 2003; Stehbens et al., 2014). Frequent microtubule targeting correlates with FA disassembly (Kaverina et al., 1999). It was thus initially proposed that microtubules may deliver certain FA relaxation factors to promote FA disassembly (Kaverina et al., 1999). Microtubule

targeting to FAs participates in all major FA disassembly mechanisms described above.

First of all, microtubules can influence FA dynamics by local modulation of Rho GTPase signaling. Global microtubule depolymerization induces rapid RhoA activation and high cell contractility, which correlates with FA stabilization (Ren et al., 1999). RhoA GTPases are activated by guanine nucleotide exchange factors (GEF). The microtubule depolymerization-induced RhoA activation is almost completely mediated by GEF-H1 (also known as ArhGEF2) as depletion of GEF-H1 abrogates nocodazole-induced RhoA activity and cell contractility (Chang et al., 2008; Krendel et al., 2002). The inactive GEF-H1 is sequestered by dynein light chain Tctex on microtubules and released into the cytosol upon its activation downstream of protein kinase A (PKA) as well as G protein coupled receptor signaling (Krendel et al., 2002; Meiri et al., 2012; Meiri et al., 2014). Although global microtubule depolymerization completely release GEF-H1 into the cytosol, under physiological conditions, GEF-H1 is required for RhoA activation at the cell leading edge (Nalbant et al., 2009), suggesting that the GEF-H1 activity is locally regulated. Therefore, microtubules around FAs may locally regulate RhoA activity by sequestering or releasing active GEF-H1. Microtubule targeting can also suppress RhoA activity by activating Rac1, a functionally antagonizing GTPase of RhoA. Microtubule-associated RacGEF, Tiam 1 and Tiam 2, have been shown to activate Rac1 during microtubule regrowth and are required for FA disassembly (Even-Ram et al., 2007; Rooney et al., 2010).

Microtubules also control FA dynamics by locally regulating endocytosis and exocytosis (Figure 11). Clathrin-mediated endocytosis is initiated by the nucleation of FCH domain only 2 (FCHO2) proteins on PtdIns(4,5)P_2, followed by cargo selection through AP2 and other cargo specific adaptors, subsequently followed by clathrin coat assembly and membrane scission through the dynamin GTPase activity (Ezratty et al., 2009). The observations that AP2, Dab2, Numb, clathrin and dynamin all concentrate around FAs after nocodazole treatment suggest that microtubules are not required for the delivery of endocytic adaptors to FAs but required to enable integrin internalization. This may be due to a microtubule-dependent signaling pathway. For instance, microtubule mediates the targeting of MAP4K4 kinase to FAs, where MAP4K4 not only promotes talin displacement by Moesin but also promotes integrin internalization

through activating Arf6 GTPase (Vitorino et al., 2015; Yue et al., 2014). Besides clathrin-dependent integrin endocytosis, caveolae may also mediate integrin internalization (del Pozo et al., 2005). Importantly, caveolin-containing vesicles are targeted to FAs along microtubules (Wickstrom et al., 2010) (Figure 11). In addition, MT1-MMP-containing exocytic carriers travel along microtubules toward FAs (Figure 11), where the exocyst complex can be recognized and activated by GEF-H1 (Grigoriev et al., 2007; Pathak et al., 2012).

Although microtubules frequently target FAs, the interaction is transient and the switch between growing and shortening phase is stochastic and not synchronized. Thus, the ultimate FA disassembly signal(s) may originate from FAs or actin cytoskeleton and microtubule targeting serves as a spatio-temporal cue. Interestingly, mechanically loaded FAs resist external force by recruiting GEF-H1 and activating RhoA GTPase independent of microtubule stability (Guilluy et al., 2011). Moreover, mechanical force stabilizes FAs and stimulates microtubule growth toward FAs at the same time (Kaverina et al., 2002). Thus the mechanical state of FAs can override the microtubule-induced FA disassembly supporting the notion that microtubules regulate but do not deliver the ultimate trigger for FA disassembly.

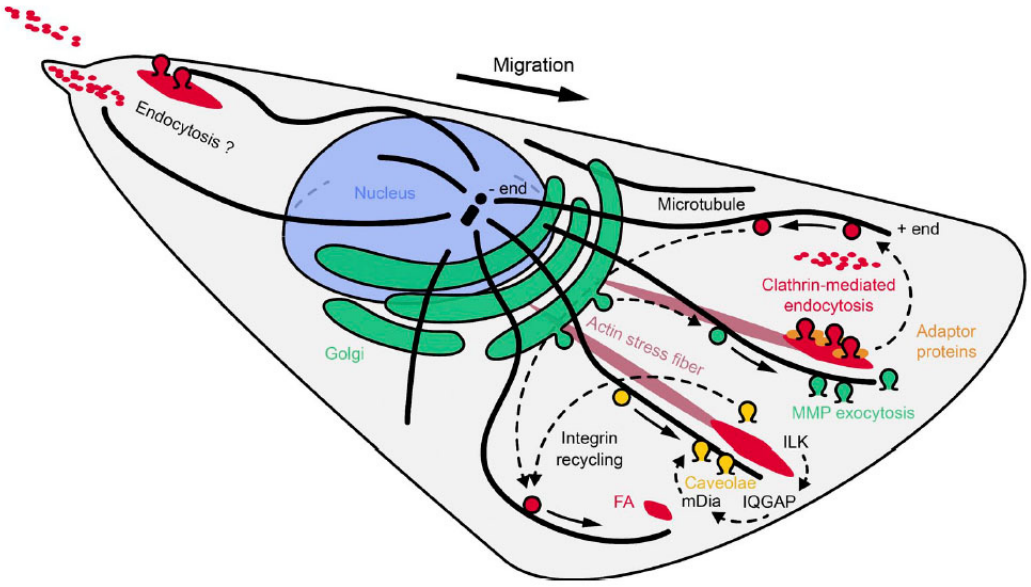

Figure 11. Microtubules target to focal adhesions and influence FA life cycle. The image is adapted from (Stehbens and Wittmann, 2012). Microtubule targeting to FAs promotes FA disassembly by local exocytosis of metalloprotease MT1-MMP and promoting clathrin-

mediated integrin endocytosis. Internalized integrins could be recycled back to cell surface. ILK-IQGAP1-mDia axis stabilize microtubule around FAs and promote stable insertion of caveolin into the plasma membrane.

FAs also reciprocally regulate microtubule dynamics. For instance, ILK, FAK and paxillin were shown to be required for microtubule stabilization at cell periphery. ILK recruits the IQGAP1-mDia1 complex, which promotes microtubule stabilization at the downstream of RhoA signaling likely through the adenomatous polyposis coli (APC) complex (Wen et al., 2004; Wickstrom et al., 2010). Moreover, integrin-dependent FAK activation is required to couple RhoA with the mDia1-dependent microtubule stabilization pathway (Palazzo et al., 2004). Lys-40 acetylation on α tubulin reflects stable microtubules, which is mainly catalyzed *in vivo* by α-tubulin N-acetyltransferase 1 (ATAT1) and removed by histone deacetylase 6 (HDAC6) (Aguilar et al., 2014; Zhang et al., 2003). At the downstream of ILK, myosin phosphatase-targeting subunit 1 (MYPT1, also known as PPP1R12A) could inhibit both non-muscle myosin II and HDAC6 activity, thus coordinating actomyosin with microtubule stability (Joo and Yamada, 2014). Paxillin can also inhibit HDAC6 in cell protrusions and promote polarized microtubule stabilization (Deakin and Turner, 2014). Moreover, ATAT1 partially colocalizes with paxillin in FAs and loss of ATAT1 leads to impaired cell adhesion and spreading (Aguilar et al., 2014; Montagnac et al., 2013). Interestingly, ATAT1 is also recruited to early endocytic sites by AP2 complex (Montagnac et al., 2013), indicating a correlation between microtubules stabilization in cell protrusions and endocytosis-mediated FA disassembly. The mutual regulation between FAs and microtubules thus maintains an intricate balance between cellular contractility and microtubule stability.

2.5.7. Cortical complexes around FAs

Despite the functional links between FAs and the complex for microtubule targeting, the microtubule targeting complex does not penetrate into FAs. Instead, this complex clusters on the plasma membrane around FAs. The cortical microtubule targeting complex is composed of two groups of proteins: a microtubule guidance module containing adenomatous polyposis coli (APC), actin cross-linking family protein 7 (ACF7) and cytoplasmic linker associated proteins (CLASPs) that guides growing

microtubule ends towards the cell periphery and a microtubule anchorage module containing liprin-α, liprin-β, ELKS, LL5 that captures the microtubule ends on the cell cortex. This complex is also the docking sites for exocytic carrier vesicles.

APC, ACF7 and CLASPs are recruited to microtubule plus ends by EB1 (Akhmanova and Steinmetz, 2008). APC is a large multifunctional adaptor protein initially identified as a tumor suppressor frequently mutated in familial and sporadic colon cancer (Aoki and Taketo, 2007). Beside its function in regulating the canonical Wnt signaling pathway, APC clusters at plus ends of a subset of stable microtubules in cell protrusions where it regulates FA assembly and directional cell migration (Matsumoto et al., 2010). ACF7 is a spectraplakin family protein that crosslinks microtubule with F-actin and may guide microtubule growth along F-actin toward FAs (Suozzi et al., 2012). Loss of ACF7 leads to disorganized peripheral microtubule bundles and reduced FA turnover rates, suggesting that ACF7 is required for microtubule-dependent FA disassembly (Wu et al., 2008; Wu et al., 2011). Interestingly, depletion of either CLASPs or LL5β with siRNA results in defects in microtubule targeting and large FAs resembling the ACF7 knockout (Mimori-Kiyosue et al., 2005; Stehbens et al., 2014). GSK3β-mediated phosphorylation of APC, ACF7 and CLASPs negatively control their association with EB1 (Etienne-Manneville and Hall, 2003; Kumar et al., 2009; Wu et al., 2011). β1 integrin activation in the leading edge of migratory cells leads to local activation of Cdc42 GTPase and GSK3β inactivation, which can in turn promote stable microtubule anchorage around FAs (Etienne-Manneville and Hall, 2003).

The microtubule guidance module further links microtubule plus ends with cell cortex through a plasma membrane-associated microtubule anchorage complex consisting of at least liprin-α, liprin-β, ELKS and LL5 (Astro and de Curtis, 2015). Four liprin-α (1-4) and two liprin-β (1-2) belong to the liprin family scaffold proteins that are characterized by an N-terminal coiled-coil domain and C-terminal SAM domain repeats. Liprin-α and liprin-β form heterodimers with each other through the SAM domain repeats (Wei et al., 2011) and homodimers through the coiled-coil domain (Taru and Jin, 2011). Liprin-α recruits multiple signaling and adaptor proteins involved in cytoskeletal regulation and vesicle trafficking, including ELKS (Dai et al., 2006; Ko et al., 2003a; Ko et al., 2003b; Shin et al., 2003). ELKS family proteins consisting of ELKS1 and ELKS2, are coiled-coil proteins with no defined domain structure. ELKS1

interacts with Rab6-GTPase and serves as the major docking site for Rab6-containing exocytic vesicles (Grigoriev et al., 2007; Ohtsuka et al., 2002). LL5 family proteins, LL5α and LL5β, are coiled-coil proteins with a C-terminal PH domain. Importantly, LL5β directly interacts with CLASP proteins on microtubule plus ends (Lansbergen et al., 2006). Moreover, LL5β also interacts with ELKS through the coiled-coil structure and PtdIns(3,4,5)P_3 on the plasma membrane through the PH domain (Lansbergen et al., 2006). The extensive homo- and hetero-dimerization as well as the interaction with phospholipids promote the nucleation of liprin-β-liprin-α-ELKS1-LL5β complex on the cell cortex. Depletion of either component or inhibition of PI3K-dependent PtdIns(3,4,5)P_3 synthesis reduces the clustering of the microtubule anchorage complex on the cell cortex (Lansbergen et al., 2006). Importantly, although the microtubule anchorage complex does not colocalize with FAs, it tends to cluster around mature FAs and integrin-mediated adhesion is required for the complex nucleation on the basal side of epithelial cells (Hotta et al., 2010). Mechanical force has been shown to activate PI3K and promote PtdIns(3,4,5)P_3 synthesis, which may in turn promote liprin-α-liprin-β-ELKS1-LL5β complex clustering (Rubashkin et al., 2014). It is not clear whether there is a physical linkage between the cortical microtubule anchorage complex and integrins in FAs.

The internalization of ligand-bound integrins also occurs around FAs. Although most endocytic adaptors have uniform distribution across the basal cell cortex, the integrin–specific cargo selector Numb shows polarized distribution in cell protrusions in close vicinity to FAs (Nishimura and Kaibuchi, 2007; Taylor et al., 2011). Similar to the microtubule anchorage complex, depletion of Numb interferes with directional persistence of cell migration (Nishimura and Kaibuchi, 2007). However, Numb-positive endocytic sites and liprin-β1-positive microtubule anchorage sites show mutually exclusive localization. Therefore, plasma membrane around FAs seems to be specialized into different functional domains.

2.6. Integrin adhesome analysis

Large ensemble of proteins, collectively termed ‘integrin adhesome’, are assembled into macro-complexes on integrin clusters with defined nano-scale organization and molecular stoichiometry (Schiller and Fassler, 2013; Winograd-Katz et al., 2014). Ever since the identification of vinculin and talin as the first adhesion adaptors in 1980s,

microscopic analysis has been the major driving force for discovery of new adhesome components (Geiger and Zaidel-Bar, 2012). By 2006, through data mining of published microscopic observations as well as biochemical analysis, Zaidel-Bar et al summarized the first adhesome list containing 156 components and 690 interactions (Zaidel-Bar et al., 2007).

With the help of quantitative mass spectrometry and novel adhesion complex isolation methods, several labs extended the integrin adhesome list to more than 1000 proteins (Humphries et al., 2009; Kuo et al., 2011; Schiller et al., 2011; Schiller et al., 2013). Notably however, the degree of overlap between three adhesome analysis are unexpectedly low, with less than 100 proteins in common (Geiger and Zaidel-Bar, 2012). Several reasons could explain the major deviance between these studies. First, they used different adhesion complex isolation methods. While Schiller et al. and Kuo et al. isolated adhesion from adherent cells seeded on fibronectin coated plastic culture dishes with the help of osmotic pressure and hydrodynamic shear force, Humphries et al. isolated adhesion complex from suspended cells by incubating them with ligand-coated latex beads. Moreover, Schiller et al. and Humphries et al. used different chemical crosslinkers to stabilize the integrin adhesion complex. Furthermore, different cell types were used to bind integrin ligand for different times in these studies. Finally, while both Kuo et al. and Humphries et al. used spectral counts for quantification, Schiller et al. used high resolution mass spectrometry combined with a label-free quantification algorithm.

As mentioned before, each adherent cell contains heterogeneous adhesion populations due to different mechanical tensions and integrin conformations. Fibrillary adhesions assembled on the dorsal side of cells may be removed by the hydrodynamic force thus lost in the adhesome analysis. The slip-bond integrin complex may be less crosslinked and thus underrepresented (Friedland et al., 2009). The power of adhesome analysis is more obvious when adhesion states are synchronized with genetic or pharmaceutical manipulations. By inhibiting focal adhesion maturation with blebbistatin, Schiller et al. revealed that LIM domain proteins are recruited during FA maturation in a tension-dependent manner (Schiller et al., 2011). With similar approaches, Kuo et al. discovered that β-PIX protein is enriched in nascent adhesion to promote Rac GTPase activation and membrane protrusion (Kuo et al., 2011).

Adhesome analysis under the condition of global microtubule depolymerization has led to the discovery of MAP4K4 as microtubule-dependent FA relaxation factor (Yue et al., 2014). By synchronizing integrin conformation with conformation-specific antibodies, Byon, A, et al. showed that microtubules are preferentially attracted to active integrins (Byron et al., 2015).

The strikingly high number of integrin adhesome components is largely due to the 'non-canonical adhesome', including ribosomes, translation initiation factors, and heterogeneous nuclear ribonucleoproteins (hnRNPs) (Humphries et al., 2009; Humphries et al., 2015; Kuo et al., 2011; Schiller et al., 2011). These observations are in line with the proposed function of localized protein translation in cell migration and axon guidance. For instance, mRNAs encoding β-actin are transported to cell leading edge by RNA binding protein ZBP1, where Src kinase locally activates β-actin mRNA translation (Huttelmaier et al., 2005). Forced localization of β-actin mRNA at adhesion sites slightly increases adhesion complex stability (Katz et al., 2012). Moreover, paxillin was shown to bind multiple hnRNP proteins including hnRNPK to form the spreading initiation center (de Hoog et al., 2004). However, many of these non-canonical adhesome components are highly abundant in cells and belong to the category of CRAPome (contaminant repository for affinity purification) (Mellacheruvu et al., 2013). Their over-representation may be due to high abundance and unspecific binding or crosslinking. For instance, hnRNPK is among the most frequently detected proteins in all affinity-purified samples, suggesting its high propensity to participate in non-specific interaction in biochemical purification procedures (Mellacheruvu et al., 2013). The apparent adhesion-dependent enrichment of these RNA binding proteins may be due to nuclear export induced by integrin signaling (e.g. ERK kinase) (Habelhah et al., 2001). One possible improvement of adhesome analysis is to quantify relative enrichment of individual proteins in isolated adhesion complex after normalizing their levels in FA fraction against total cell expression levels.

In summary, although recent advances in quantitative mass spectrometry have greatly facilitated the comprehensive profiling of the integrin adhesome, conventional cell biology approaches are still indispensable to validate each candidate. Furthermore, it remains to be a challenging task to understand the self-assembly logic of various adhesion structures and how they interact with other cellular components.

2.7. Kank family proteins

Kank family proteins are evolutionarily conserved from *C.elegans* to humans. KANK stands for 'KN motif and ankyrin repeat domains' due to the presence of a unique and evolutionarily conserved N-terminal KN motif and C-terminal ankyrin repeats or 'kidney ankyrin repeat-containing protein' due to its initial identification in kidney tissue and kidney-derived cell lines.

The founding member of Kank family proteins, Kank1, was initially identified as candidate tumor suppressor in a screening for loss of heterozygosity in renal carcinoma cell lines (Sarkar et al., 2002). Consistently, overexpression of Kank1 is sufficient to induce cell cycle arrest and apoptosis in glioma cell lines *in vitro* (Guo et al., 2014). Homology searching in human genome revealed the presence of three more family members termed Kank2, Kank3 and Kank4 (Kakinuma et al., 2009). As indicated above, the hall mark of this Kank family is the presence of a unique KN motif at the N-terminus and five ankyrin repeats at the C-terminus (Figure 12). Another well conserved structural element is the coiled-coil domain in the central region of the protein (Figure 12). However, this coiled-coil domain is lost in Kank4 (Kakinuma et al., 2009). Due to their high structural similarity, Kank family proteins most likely have overlapping and redundant functions.

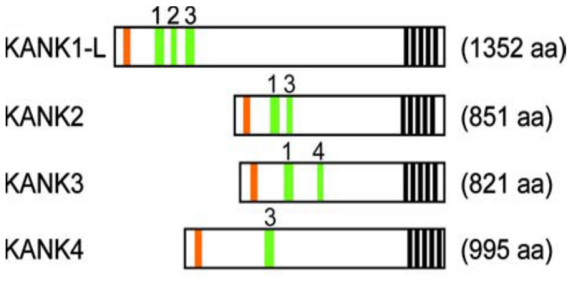

Figure 12. Domain organization of mammalian Kank family proteins. Evolutionarily conserved domains are indicated. KN motif locates at the N-terminus of the protein (Red). Several coiled-coil domains (green) locate in the central part of the proteins with the first coiled-coil domain to be the most conserved during evolution. All Kank family proteins contain five ankyrin repeats (black) at the C-terminus. Picture is adapted from (Kakinuma et al., 2009)

Several rare human genetic diseases have been linked to mutations and deletions in Kank family gene locus. The genomic deletion of Kank1 gene locus has been associated with a neurodegenerative disease similar to cerebral palsy (type 2 spastic quadriplegic cerebral palsy) (Lerer et al., 2005). Moreover, p.Ala670Val mutation in Kank2 has been linked to Naxos and Carvajal syndrome characterized by keratoderma and woolly hair phenotypes (Ramot et al., 2014). Recently, several mutations in Kank1 (p.E454K), Kank2 (p.S181G and p.S684F) and Kank4 (p.Y801H) are linked with nephrotic syndromes including minimal change kidney disease and focal segmental glomerulosclerosis (Gee et al., 2015). p.Y801H mutation in Kank4 may also result in facial dysmorphism, intellectual disability, dilated cardiomyopathy, atrial septal defect and leukocytosis (Gee et al., 2015). Interestingly, Kank2 knockdown in zebrafish also results nephrotic syndrome-like phenotypes characterized by proteinuria and podocyte foot process effacement. Interestingly, it is known that both dysregulated RhoA GTPase and defects in integrin-mediated podocytes adhesion also lead to nephrotic syndromes (Gee et al., 2013; Tian et al., 2014). Kank2 forms a complex with RhoGDIα and siRNA knockdown of Kank1 or Kank2 upregulate active RhoA GTPase activity in podocytes.

Although identified as disease-related proteins in humans, much of our knowledge of Kank family genes' *in vivo* function is based on the studies in *C.elegans*. Unlike high vertebrates, *C.elegans* has only one Kank homologue, called VAB-19. VAB-19 was found to localize at muscle-epidermal attachment sites in a myotactin-dependent manner. Both the KN motif and the conserved coiled-coil domain are required for this localization. The epidermal elongation during *C.elegans* embryo development requires coordinated actomyosin-mediated lateral epidermal cell shape change as well as a stable muscle-epidermal linkage. VAB-19 mutants are defective in epidermal elongation and muscle attachment to the epidermis, which leads to developmental arrest and subsequent embryonic lethality (Ding et al., 2003). Notably, aberrant actin cytoskeleton organization was also observed in VAB-19 mutants (Ding et al., 2003). VAB-19 may regulate the actin cytoskeleton organization in the epidermis through binding to Eps8, an actin bundling and capping protein whose mutation also leads to epidermal elongation defects in *C.elegans* (Ding et al., 2008). Interestingly, the embryonic lethal phenotype could be largely rescued with an α-spectrin null mutant, suggesting that VAB-19 may regulate cell cortex organization.

Other genetic studies in *C.elegans* suggested that VAB-19 may be a general stabilizer of the muscle-epidermal attachment due to the synthetic lethality between conditional VAB-19 mutant allele with other mutants that affect basement membrane components or ECM receptor (Zahreddine et al., 2010). Moreover, like UNC-97 (PINCH homologue) and UNC-112 (Kindlin homologue), VAB-19 also regulates directional HSN (hermaphrodite specific motor neurons) axon outgrowth towards netrin (Yang et al., 2014b).

Definitive evidence for an involvement of VAB-19 in integrin-mediated cell adhesion came from the study of basement membrane remodeling during uterine-vulval attachment. During the mid-L3 larval stage in *C.elegans*, the ventral uterine and vulval-precursor cells are separated by basement membranes. A specialized gonadal cell called anchor cell initially breaches the basement membranes by locally degrading the basement membrane through metalloproteinase. Later, to complete the attachment between neighboring uterine and vulval tissue, the initial basement membrane gap is widened due to basement membrane sliding. It was noticed that VAB-19 and the C.*elegans* integrin homologue INA/PAT-3 cooperate to stabilize the basement membrane gap (Ihara et al., 2011). Furthermore, cell cycle arrest, laminin deposition, and increased integrin levels in non-dividing vulval cells are also essential to stabilize the basement membrane gap (Matus et al., 2014).

Using zebrafish as model organism, it was demonstrated that Kank3 localizes to cell-cell and cell basement membrane adhesions where it controls cell adhesion and convergence and extension movements during gastrulation and neural tube closure. Knockdown of Kank3 in zebrafish resulted in embryonic epidermal detachment with various penetrance, further supporting a functional link between Kank and integrin (Boggetti et al., 2012). Interestingly, zebrafish Kank3 uses a conserved NGGY motif to interact with the PTB domain of Numb. Double knockdown of both Kank3 and Numb leads to more severe phenotypes than single gene knockdown (Boggetti et al., 2012). Thus, Kank3 may coordinate integrin adhesion with endocytic trafficking.

The *D.melanogaster* contains only one Kank homolog (dKank) which is encoded by the gene CG10249. dKank has been shown to localize to mature muscle-tendon attachment sites and to bind the microtubule plus end protein EB1 (Clohisey et al., 2014). However, this EB1 binding site is not evolutionarily conserved and is not

present in other Kank family members. Although complete deletion of dKank does not lead to severe developmental defects, knockdown of dKank leads to defects in pericardial nephrocyte function (Gee et al., 2015; Zhang et al., 2013) and altered neuron morphology (Sepp et al., 2008).

At the cellular level, Kank family proteins regulate both actin and microtubule cytoskeleton architecture. Kank1 has been shown to inhibit cell spreading on fibronectin through binding to IRSp53. IRSp53 is a downstream effector protein of both Rac1 and Cdc42 during lamellipodia and filopodia formation respectively (Scita et al., 2008). Kank1 inhibits the association between IRSp53 and Rac1 but not with Cdc42. Consequently, Kank1 could suppress Rac1-dependent lamellipodia formation and thereby promote Cdc42-induced filopodia formation (Roy et al., 2009). Notably, IRSp53 forms a functional complex with Eps8 to promote F-actin bundling (Kast et al., 2014), suggesting that IRSp53, Eps8 and Kank1 may form a tertiary complex to regulate filopodia formation. Moreover, Kank1 in mammalian cells also blocks RhoA activation induced by insulin signaling. Although the exact molecular mechanism remains elusive, Akt-dependent phosphorylation of the flexible loop before the central coiled-coil domain and subsequent recruitment of 14-3-3 seem to be involved (Kakinuma et al., 2008). Moreover, it was suggested that Kank1 regulates RhoA activity by interacting with deleted in liver cancer 1 (DLC1), a talin-binding RhoGAP (Kakinuma et al., 2008). Accordingly, all Kank family members in mammalian cells could antagonize stress fiber formation likely through attenuating RhoA activity (Zhu et al., 2008b).

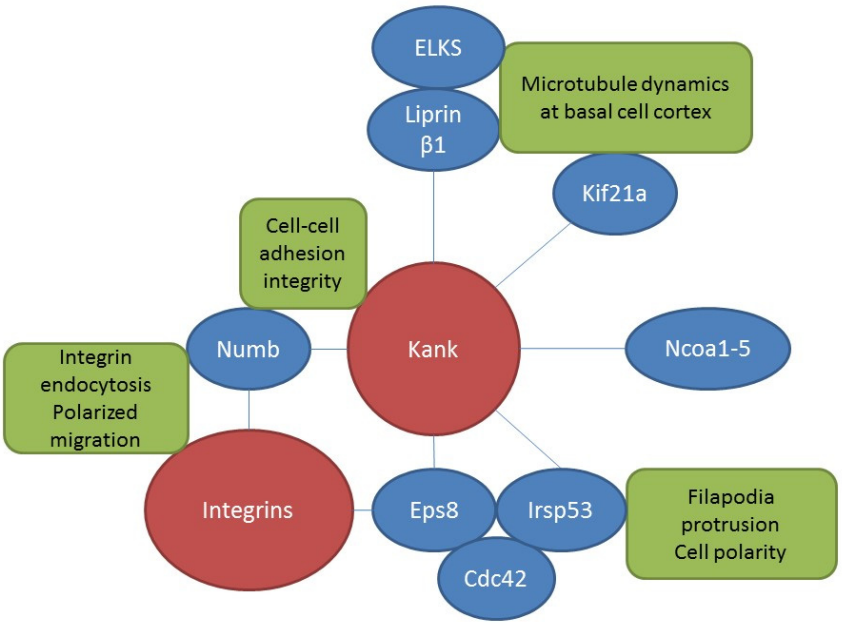

Figure 13. Summary of known Kank (red) interacting protein complexes (blue) and their association with integrins (red). Cellular processes controlled by individual complex proposed in literatures are highlighted in green boxes.

A recent paper reported that Kank1 can form a complex with liprin-β1 via its conserved coiled-coil region and kinesin 21a (KIF21a) via its ankyrin repeats (van der Vaart et al., 2013). These interactions are conserved during evolution as they are also detected in flies (Guruharsha et al., 2011). Interestingly, this tertiary complex could inhibit microtubule plus end outgrowth at the periphery of cell cortex (van der Vaart et al., 2013). Consistently, depletion of Kank1 through siRNA resulted in aberrant microtubule bundles at cell periphery in Hela cells resembling the ACF7 knockout and leading to abnormal axon morphology in neurons (Li et al., 2011a; van der Vaart et al., 2013). Interestingly, a KIF21a mutation causing congenital fibrosis of the extraocular muscles type 1 (CFEOM1) disease characterized by abnormal oculomotor nerve migration was shown to result in a constitutive active KIF21a that concomitantly enhanced Kank1 recruitment to the plasma membrane, suggesting that Kank1 may be involved in the disease development (Cheng et al., 2014; Kakinuma and Kiyama, 2009). A role of Kank1 in neuronal migration may also be the underlying mechanism

of type 2 spastic quadriplegic cerebral palsy. Notably, mRNP particles containing Kank2 mRNA were shown to be transported to the filopodia tips where they associate with APC on stabilized microtubules (Mili et al., 2008). Thus, microtubules may control localized translation of Kank2 proteins in cell protrusions.

Besides cytoskeletal functions, Kank family proteins also participate in the transcriptional regulation. For instance, Kank2 sequesters steroid receptor coactivators (SRC1-5) in the cytoplasm to dampen the transcriptional response of estrogen and vitamin D receptors (Ramot et al., 2014; Zhang et al., 2007). Moreover, Kank1 may regulate β-catenin signaling by escorting it into nuclei (Wang et al., 2006). In summary, despite accumulating evidences suggesting that Kank family proteins may coordinate the actin and microtubule cytoskeleton architecture, how these processes are linked to integrin based-adhesion by Kank proteins needs further investigations.

3. Aim of the thesis

As introduced above, quantitative mass spectrometry analysis have greatly expanded the inventory of integrin-based adhesomes and linked FAs to some non-canonical adhesion functions (e.g. protein translation, RNA splicing, etc.). However, since the previous approaches are potentially biased by the total protein abundance, the specificity of the adhesome analysis remains questionable.

Thus, the **1st aim** of my PhD study was to develop an integrative, quantitative and abundance-independent description of protein enrichment in FAs and recruitment to integrin tail complexes. Based upon this analysis, we have identified many novel adhesion proteins, one of which is Kank2.

Numerous reports in the literature indicated that Kank proteins play important role in integrin-mediated adhesion and migration. As **2nd aim** of my PhD study, I combined cell biology and biochemistry to gain mechanistic insights into the functions of Kank proteins during integrin-mediated processes. Our data establish Kank family proteins as a novel type of talin activator.

Kank family genes have been implicated in rare congenital human diseases including cerebral palsy, nephrotic syndrome, keratoderma and renal tumors. The **3rd aim** of my PhD study is to generate Kank1 and Kank2 conditional knockout mice in order to study their *in vivo* functions. The phenotype analysis is ongoing and thus not included in the manuscripts that are summarized below.

4. Short summary of manuscripts

4.1. Kank family proteins comprise a novel type of talin activator

Zhiqi Sun, Hui-Yuan Tseng, Sally J. Deeb, Dirk Dedden, Maik Veelders, Naoko Mizuno, Matthias Mann, Reinhard Fässler (Manuscript in preparation)

In this manuscript, we developed an integrative adhesome analysis by combining a focal adhesion enrichment index with integrin tail interactome to identify novel FA proteins. Using this approach we identified the evolutionarily conserved Kank protein family as novel FA proteins. Interestingly, Kank2 concentrates at the lateral border of FAs (which we term the FA belt), a previously unrecognized FA sub-compartment. Mechanistically, Kank directly binds the talin R7 domain through its evolutionarily conserved KN motif and promotes talin activation in a force- and F-actin-independent manner. Consequently, Kank2 induces and/or maintains the formation of active integrins at sites deprived of actomyosin coupling. Our data identify Kank family proteins as novel type of talin activator, which specifically stabilize integrin-talin complexes that are uncoupled from the actomyosin system.

4.2. β1- and αv-class integrins cooperate to regulate myosin II during rigidity sensing of fibronectin-based microenvironments

Schiller HB, Hermann MR, Polleux J, Vignaud T, Zanivan S, Friedel CC, Sun Z, Raducanu A, Gottschalk KE, Théry M, Mann M, Fässler R. **Nat Cell Biol 2013, 15, 625.**

At the beginning of my PhD study, I supported Dr. Herbert Schiller in his analysis of integrin subtype specific signaling. In this study, β1- and αV-class integrins were expressed in integrin-null fibroblasts. Notably, while α5β1-class integrins promote NA formation and cell protrusions, αV-class integrins induce the formation of large FAs Combining functional assays with adhesome and phosphoproteome analyses, we found that β1- and αV-class integrins differentially activate and couple RhoA to downstream effectors. While α5β1 integrins induce a RhoA-Rock-myosin II pathway, αv-class integrins couple RhoA to the formin mDia1 but not myosin II. Moreover, αv-class integrins recuit GEF-H1 to activate RhoA in FAs. Optimal mechano-sensing is achieved by the synergistic effects of both integrin classes in fibroblasts. This study assigns specific functions to distinct fibronectin-binding integrins. My major

contribution to this project is to analyze the RhoA and Rac1 activities and perform GEF-H1 knockdown experiments.

4.3. A firm grip does not always pay off: a new Phact(r) 4 integrin signaling

Sun Z, Fässler R. **Gene Dev 2012, 26, 1-5.**

Hirschsprung disease is a congenital disorder of the distal colon due to the absence of the enteric nervous system. The lack of enteric neurons can be caused by impaired proliferation, differentiation, or migration of enteric neural crest cells into the distal colon and rectum. β1 integrin plays a critical role in enteric neural crest cell migration. Too much or too low β1 integrin signaling can lead to enteric neural crest cell migration defects and hence Hirschsprung disease-like phenotypes. During my PhD study, I wrote a perspective for Genes & Development with my PhD supervisor summarizing the current understanding of β1 integrin signaling during enteric neural crest cell migration.

4.4. Nascent Adhesions: From Fluctuations to a Hierarchical Organization

Sun Z, Lambacher A, Fässler R. **Curr Biol 2014, 24, R801-R803.**

Integrins assemble a complex network of proteins termed adhesome at cell–matrix adhesion sites. The large inventory of proteins makes it an intimidating task to comprehend the underlying logic of their assembly. In this short dispatch, we commented on a recent attempt by Bachir et al. In their paper, Bachir et al. used fluorescence correlation microscopy to measure the spatial and temporal regulation of complex stoichiometry during assembly and stabilization of NAs. This work suggested a new model of NA assembly: kindlin-2 binds to β1 integrin and induces the high-affinity state of α5β1; α-actinin promotes β1 integrin clustering and sets up a transient connection between the integrin cluster and the actin cytoskeleton; talin subsequently replaces α-actinin and establishes a more stable integrin–actin linkage with the help of vinculin.

5. References

Aguilar, A., Becker, L., Tedeschi, T., Heller, S., Iomini, C., and Nachury, M.V. (2014). Alpha-tubulin K40 acetylation is required for contact inhibition of proliferation and cell-substrate adhesion. Molecular biology of the cell *25*, 1854-1866.
Akhmanova, A., and Steinmetz, M.O. (2008). Tracking the ends: a dynamic protein network controls the fate of microtubule tips. Nature reviews Molecular cell biology *9*, 309-322.
Alexandrova, A.Y., Arnold, K., Schaub, S., Vasiliev, J.M., Meister, J.J., Bershadsky, A.D., and Verkhovsky, A.B. (2008). Comparative dynamics of retrograde actin flow and focal adhesions: formation of nascent adhesions triggers transition from fast to slow flow. PloS one *3*, e3234.
Anthis, N.J., Wegener, K.L., Critchley, D.R., and Campbell, I.D. (2010). Structural diversity in integrin/talin interactions. Structure *18*, 1654-1666.
Anthis, N.J., Wegener, K.L., Ye, F., Kim, C., Goult, B.T., Lowe, E.D., Vakonakis, I., Bate, N., Critchley, D.R., Ginsberg, M.H.*, et al.* (2009). The structure of an integrin/talin complex reveals the basis of inside-out signal transduction. The EMBO journal *28*, 3623-3632.
Aoki, K., and Taketo, M.M. (2007). Adenomatous polyposis coli (APC): a multi-functional tumor suppressor gene. Journal of cell science *120*, 3327-3335.
Aragona, M., Panciera, T., Manfrin, A., Giulitti, S., Michielin, F., Elvassore, N., Dupont, S., and Piccolo, S. (2013). A mechanical checkpoint controls multicellular growth through YAP/TAZ regulation by actin-processing factors. Cell *154*, 1047-1059.
Astro, V., and de Curtis, I. (2015). Plasma membrane-associated platforms: Dynamic scaffolds that organize membrane-associated events. Science signaling *8*, re1.
Bachir, A.I., Zareno, J., Moissoglu, K., Plow, E.F., Gratton, E., and Horwitz, A.R. (2014). Integrin-associated complexes form hierarchically with variable stoichiometry in nascent adhesions. Current biology : CB *24*, 1845-1853.
Bai, J., Binari, R., Ni, J.Q., Vijayakanthan, M., Li, H.S., and Perrimon, N. (2008). RNA interference screening in Drosophila primary cells for genes involved in muscle assembly and maintenance. Development *135*, 1439-1449.
Balaban, N.Q., Schwarz, U.S., Riveline, D., Goichberg, P., Tzur, G., Sabanay, I., Mahalu, D., Safran, S., Bershadsky, A., Addadi, L.*, et al.* (2001). Force and focal adhesion assembly: a close relationship studied using elastic micropatterned substrates. Nature cell biology *3*, 466-472.
Ballestrem, C., Hinz, B., Imhof, B.A., and Wehrle-Haller, B. (2001). Marching at the front and dragging behind: differential alphaVbeta3-integrin turnover regulates focal adhesion behavior. The Journal of cell biology *155*, 1319-1332.
Banno, A., Goult, B.T., Lee, H., Bate, N., Critchley, D.R., and Ginsberg, M.H. (2012). Subcellular localization of talin is regulated by inter-domain interactions. The Journal of biological chemistry *287*, 13799-13812.
Bate, N., Gingras, A.R., Bachir, A., Horwitz, R., Ye, F., Patel, B., Goult, B.T., and Critchley, D.R. (2012). Talin contains a C-terminal calpain2 cleavage site important in focal adhesion dynamics. PloS one *7*, e34461.
Bear, J.E., Svitkina, T.M., Krause, M., Schafer, D.A., Loureiro, J.J., Strasser, G.A., Maly, I.V., Chaga, O.Y., Cooper, J.A., Borisy, G.G.*, et al.* (2002). Antagonism between Ena/VASP proteins and actin filament capping regulates fibroblast motility. Cell *109*, 509-521.
Bhatt, A., Kaverina, I., Otey, C., and Huttenlocher, A. (2002). Regulation of focal complex composition and disassembly by the calcium-dependent protease calpain. Journal of cell science *115*, 3415-3425.

Bledzka, K., Liu, J., Xu, Z., Perera, H.D., Yadav, S.P., Bialkowska, K., Qin, J., Ma, Y.Q., and Plow, E.F. (2012). Spatial coordination of kindlin-2 with talin head domain in interaction with integrin beta cytoplasmic tails. The Journal of biological chemistry *287*, 24585-24594.
Block, J., Breitsprecher, D., Kuhn, S., Winterhoff, M., Kage, F., Geffers, R., Duwe, P., Rohn, J.L., Baum, B., Brakebusch, C*., et al.* (2012). FMNL2 drives actin-based protrusion and migration downstream of Cdc42. Current biology : CB *22*, 1005-1012.
Boggetti, B., Jasik, J., Takamiya, M., Strahle, U., Reugels, A.M., and Campos-Ortega, J.A. (2012). NBP, a zebrafish homolog of human Kank3, is a novel Numb interactor essential for epidermal integrity and neurulation. Developmental biology *365*, 164-174.
Bonnans, C., Chou, J., and Werb, Z. (2014). Remodelling the extracellular matrix in development and disease. Nature reviews Molecular cell biology *15*, 786-801.
Borgon, R.A., Vonrhein, C., Bricogne, G., Bois, P.R., and Izard, T. (2004). Crystal structure of human vinculin. Structure *12*, 1189-1197.
Bottcher, R.T., Stremmel, C., Meves, A., Meyer, H., Widmaier, M., Tseng, H.Y., and Fassler, R. (2012). Sorting nexin 17 prevents lysosomal degradation of beta1 integrins by binding to the beta1-integrin tail. Nature cell biology *14*, 584-592.
Bouvard, D., Pouwels, J., De Franceschi, N., and Ivaska, J. (2013). Integrin inactivators: balancing cellular functions in vitro and in vivo. Nature reviews Molecular cell biology *14*, 430-442.
Brakebusch, C., and Fassler, R. (2003). The integrin-actin connection, an eternal love affair. The EMBO journal *22*, 2324-2333.
Brown, N.H., Gregory, S.L., Rickoll, W.L., Fessler, L.I., Prout, M., White, R.A., and Fristrom, J.W. (2002). Talin is essential for integrin function in Drosophila. Developmental cell *3*, 569-579.
Bunting, M., Harris, E.S., McIntyre, T.M., Prescott, S.M., and Zimmerman, G.A. (2002). Leukocyte adhesion deficiency syndromes: adhesion and tethering defects involving beta 2 integrins and selectin ligands. Current opinion in hematology *9*, 30-35.
Burnette, D.T., Shao, L., Ott, C., Pasapera, A.M., Fischer, R.S., Baird, M.A., Der Loughian, C., Delanoe-Ayari, H., Paszek, M.J., Davidson, M.W*., et al.* (2014). A contractile and counterbalancing adhesion system controls the 3D shape of crawling cells. The Journal of cell biology *205*, 83-96.
Burridge, K., and Mangeat, P. (1984). An interaction between vinculin and talin. Nature *308*, 744-746.
Byron, A., Askari, J.A., Humphries, J.D., Jacquemet, G., Koper, E.J., Warwood, S., Choi, C.K., Stroud, M.J., Chen, C.S., Knight, D*., et al.* (2015). A proteomic approach reveals integrin activation state-dependent control of microtubule cortical targeting. Nature communications *6*, 6135.
Calderwood, D.A., Campbell, I.D., and Critchley, D.R. (2013). Talins and kindlins: partners in integrin-mediated adhesion. Nature reviews Molecular cell biology *14*, 503-517.
Calderwood, D.A., Fujioka, Y., de Pereda, J.M., Garcia-Alvarez, B., Nakamoto, T., Margolis, B., McGlade, C.J., Liddington, R.C., and Ginsberg, M.H. (2003). Integrin beta cytoplasmic domain interactions with phosphotyrosine-binding domains: a structural prototype for diversity in integrin signaling. Proceedings of the National Academy of Sciences of the United States of America *100*, 2272-2277.
Campbell, I.D., and Humphries, M.J. (2011). Integrin structure, activation, and interactions. Cold Spring Harb Perspect Biol *3*.
Campellone, K.G., and Welch, M.D. (2010). A nucleator arms race: cellular control of actin assembly. Nature reviews Molecular cell biology *11*, 237-251.
Carisey, A., Tsang, R., Greiner, A.M., Nijenhuis, N., Heath, N., Nazgiewicz, A., Kemkemer, R., Derby, B., Spatz, J., and Ballestrem, C. (2013). Vinculin regulates the recruitment and release of core focal adhesion proteins in a force-dependent manner. Current biology : CB *23*, 271-281.

Cavalcanti-Adam, E.A., Volberg, T., Micoulet, A., Kessler, H., Geiger, B., and Spatz, J.P. (2007). Cell spreading and focal adhesion dynamics are regulated by spacing of integrin ligands. Biophysical journal *92*, 2964-2974.
Chan, C.E., and Odde, D.J. (2008). Traction dynamics of filopodia on compliant substrates. Science *322*, 1687-1691.
Chang, Y.C., Nalbant, P., Birkenfeld, J., Chang, Z.F., and Bokoch, G.M. (2008). GEF-H1 couples nocodazole-induced microtubule disassembly to cell contractility via RhoA. Molecular biology of the cell *19*, 2147-2153.
Chang, Y.C., Zhang, H., Franco-Barraza, J., Brennan, M.L., Patel, T., Cukierman, E., and Wu, J. (2014). Structural and mechanistic insights into the recruitment of talin by RIAM in integrin signaling. Structure *22*, 1810-1820.
Chao, W.T., Ashcroft, F., Daquinag, A.C., Vadakkan, T., Wei, Z., Zhang, P., Dickinson, M.E., and Kunz, J. (2010). Type I phosphatidylinositol phosphate kinase beta regulates focal adhesion disassembly by promoting beta1 integrin endocytosis. Molecular and cellular biology *30*, 4463-4479.
Chao, W.T., and Kunz, J. (2009). Focal adhesion disassembly requires clathrin-dependent endocytosis of integrins. FEBS letters *583*, 1337-1343.
Charras, G., and Paluch, E. (2008). Blebs lead the way: how to migrate without lamellipodia. Nature reviews Molecular cell biology *9*, 730-736.
Cheng, L., Desai, J., Miranda, C.J., Duncan, J.S., Qiu, W., Nugent, A.A., Kolpak, A.L., Wu, C.C., Drokhlyansky, E., Delisle, M.M*., et al.* (2014). Human CFEOM1 mutations attenuate KIF21A autoinhibition and cause oculomotor axon stalling. Neuron *82*, 334-349.
Choi, C.K., Vicente-Manzanares, M., Zareno, J., Whitmore, L.A., Mogilner, A., and Horwitz, A.R. (2008). Actin and alpha-actinin orchestrate the assembly and maturation of nascent adhesions in a myosin II motor-independent manner. Nature cell biology *10*, 1039-1050.
Clohisey, S.M., Dzhindzhev, N.S., and Ohkura, H. (2014). Kank Is an EB1 interacting protein that localises to muscle-tendon attachment sites in Drosophila. PloS one *9*, e106112.
Codelia, V.A., Sun, G., and Irvine, K.D. (2014). Regulation of YAP by mechanical strain through Jnk and Hippo signaling. Current biology : CB *24*, 2012-2017.
Cohen, D.M., Kutscher, B., Chen, H., Murphy, D.B., and Craig, S.W. (2006). A conformational switch in vinculin drives formation and dynamics of a talin-vinculin complex at focal adhesions. The Journal of biological chemistry *281*, 16006-16015.
Colo, G.P., Hernandez-Varas, P., Lock, J., Bartolome, R.A., Arellano-Sanchez, N., Stromblad, S., and Teixido, J. (2012). Focal adhesion disassembly is regulated by a RIAM to MEK-1 pathway. Journal of cell science *125*, 5338-5352.
Comrie, W.A., Babich, A., and Burkhardt, J.K. (2015). F-actin flow drives affinity maturation and spatial organization of LFA-1 at the immunological synapse. The Journal of cell biology *208*, 475-491.
Conti, F.J., Monkley, S.J., Wood, M.R., Critchley, D.R., and Muller, U. (2009). Talin 1 and 2 are required for myoblast fusion, sarcomere assembly and the maintenance of myotendinous junctions. Development *136*, 3597-3606.
Coussen, F., Choquet, D., Sheetz, M.P., and Erickson, H.P. (2002). Trimers of the fibronectin cell adhesion domain localize to actin filament bundles and undergo rearward translocation. Journal of cell science *115*, 2581-2590.
Cram, E.J., Clark, S.G., and Schwarzbauer, J.E. (2003). Talin loss-of-function uncovers roles in cell contractility and migration in C. elegans. Journal of cell science *116*, 3871-3878.
Critchley, D.R. (2009). Biochemical and structural properties of the integrin-associated cytoskeletal protein talin. Annual review of biophysics *38*, 235-254.

Dai, Y., Taru, H., Deken, S.L., Grill, B., Ackley, B., Nonet, M.L., and Jin, Y. (2006). SYD-2 Liprin-alpha organizes presynaptic active zone formation through ELKS. Nature neuroscience *9*, 1479-1487.
de Hoog, C.L., Foster, L.J., and Mann, M. (2004). RNA and RNA binding proteins participate in early stages of cell spreading through spreading initiation centers. Cell *117*, 649-662.
de Pereda, J.M., Wegener, K.L., Santelli, E., Bate, N., Ginsberg, M.H., Critchley, D.R., Campbell, I.D., and Liddington, R.C. (2005). Structural basis for phosphatidylinositol phosphate kinase type Igamma binding to talin at focal adhesions. The Journal of biological chemistry *280*, 8381-8386.
Deakin, N.O., and Turner, C.E. (2014). Paxillin inhibits HDAC6 to regulate microtubule acetylation, Golgi structure, and polarized migration. The Journal of cell biology *206*, 395-413.
del Pozo, M.A., Balasubramanian, N., Alderson, N.B., Kiosses, W.B., Grande-Garcia, A., Anderson, R.G., and Schwartz, M.A. (2005). Phospho-caveolin-1 mediates integrin-regulated membrane domain internalization. Nature cell biology *7*, 901-908.
del Rio, A., Perez-Jimenez, R., Liu, R., Roca-Cusachs, P., Fernandez, J.M., and Sheetz, M.P. (2009). Stretching single talin rod molecules activates vinculin binding. Science *323*, 638-641.
Di Paolo, G., Pellegrini, L., Letinic, K., Cestra, G., Zoncu, R., Voronov, S., Chang, S., Guo, J., Wenk, M.R., and De Camilli, P. (2002). Recruitment and regulation of phosphatidylinositol phosphate kinase type 1 gamma by the FERM domain of talin. Nature *420*, 85-89.
Ding, M., Goncharov, A., Jin, Y., and Chisholm, A.D. (2003). C. elegans ankyrin repeat protein VAB-19 is a component of epidermal attachment structures and is essential for epidermal morphogenesis. Development *130*, 5791-5801.
Ding, M., King, R.S., Berry, E.C., Wang, Y., Hardin, J., and Chisholm, A.D. (2008). The cell signaling adaptor protein EPS-8 is essential for C. elegans epidermal elongation and interacts with the ankyrin repeat protein VAB-19. PloS one *3*, e3346.
Diz-Munoz, A., Krieg, M., Bergert, M., Ibarlucea-Benitez, I., Muller, D.J., Paluch, E., and Heisenberg, C.P. (2010). Control of directed cell migration in vivo by membrane-to-cortex attachment. PLoS biology *8*, e1000544.
Dupont, S., Morsut, L., Aragona, M., Enzo, E., Giulitti, S., Cordenonsi, M., Zanconato, F., Le Digabel, J., Forcato, M., Bicciato, S.*, et al.* (2011). Role of YAP/TAZ in mechanotransduction. Nature *474*, 179-183.
Edwards, M., Zwolak, A., Schafer, D.A., Sept, D., Dominguez, R., and Cooper, J.A. (2014). Capping protein regulators fine-tune actin assembly dynamics. Nature reviews Molecular cell biology *15*, 677-689.
Efimov, A., Schiefermeier, N., Grigoriev, I., Ohi, R., Brown, M.C., Turner, C.E., Small, J.V., and Kaverina, I. (2008). Paxillin-dependent stimulation of microtubule catastrophes at focal adhesion sites. Journal of cell science *121*, 196-204.
Ehrlicher, A.J., Nakamura, F., Hartwig, J.H., Weitz, D.A., and Stossel, T.P. (2011). Mechanical strain in actin networks regulates FilGAP and integrin binding to filamin A. Nature *478*, 260-263.
Elad, N., Volberg, T., Patla, I., Hirschfeld-Warneken, V., Grashoff, C., Spatz, J.P., Fassler, R., Geiger, B., and Medalia, O. (2013). The role of integrin-linked kinase in the molecular architecture of focal adhesions. Journal of cell science *126*, 4099-4107.
Ellis, S.J., Goult, B.T., Fairchild, M.J., Harris, N.J., Long, J., Lobo, P., Czerniecki, S., Van Petegem, F., Schock, F., Peifer, M.*, et al.* (2013). Talin autoinhibition is required for morphogenesis. Current biology : CB *23*, 1825-1833.
Ellis, S.J., Lostchuck, E., Goult, B.T., Bouaouina, M., Fairchild, M.J., Lopez-Ceballos, P., Calderwood, D.A., and Tanentzapf, G. (2014). The talin head domain reinforces integrin-mediated adhesion by promoting adhesion complex stability and clustering. PLoS genetics *10*, e1004756.

Engler, A.J., Sen, S., Sweeney, H.L., and Discher, D.E. (2006). Matrix elasticity directs stem cell lineage specification. Cell *126*, 677-689.
Etienne-Manneville, S., and Hall, A. (2003). Cdc42 regulates GSK-3beta and adenomatous polyposis coli to control cell polarity. Nature *421*, 753-756.
Even-Ram, S., Doyle, A.D., Conti, M.A., Matsumoto, K., Adelstein, R.S., and Yamada, K.M. (2007). Myosin IIA regulates cell motility and actomyosin-microtubule crosstalk. Nature cell biology *9*, 299-309.
Ezratty, E.J., Bertaux, C., Marcantonio, E.E., and Gundersen, G.G. (2009). Clathrin mediates integrin endocytosis for focal adhesion disassembly in migrating cells. The Journal of cell biology *187*, 733-747.
Ezratty, E.J., Partridge, M.A., and Gundersen, G.G. (2005). Microtubule-induced focal adhesion disassembly is mediated by dynamin and focal adhesion kinase. Nature cell biology *7*, 581-590.
Fehon, R.G., McClatchey, A.I., and Bretscher, A. (2010). Organizing the cell cortex: the role of ERM proteins. Nature reviews Molecular cell biology *11*, 276-287.
Fitzpatrick, P., Shattil, S.J., and Ablooglu, A.J. (2014). C-terminal COOH of integrin beta1 is necessary for beta1 association with the kindlin-2 adapter protein. The Journal of biological chemistry *289*, 11183-11193.
Franco, S.J., Rodgers, M.A., Perrin, B.J., Han, J., Bennin, D.A., Critchley, D.R., and Huttenlocher, A. (2004). Calpain-mediated proteolysis of talin regulates adhesion dynamics. Nature cell biology *6*, 977-983.
Friedland, J.C., Lee, M.H., and Boettiger, D. (2009). Mechanically activated integrin switch controls alpha5beta1 function. Science *323*, 642-644.
Galbraith, C.G., Yamada, K.M., and Galbraith, J.A. (2007). Polymerizing actin fibers position integrins primed to probe for adhesion sites. Science *315*, 992-995.
Gardel, M.L., Sabass, B., Ji, L., Danuser, G., Schwarz, U.S., and Waterman, C.M. (2008). Traction stress in focal adhesions correlates biphasically with actin retrograde flow speed. The Journal of cell biology *183*, 999-1005.
Gardel, M.L., Schneider, I.C., Aratyn-Schaus, Y., and Waterman, C.M. (2010). Mechanical integration of actin and adhesion dynamics in cell migration. Annual review of cell and developmental biology *26*, 315-333.
Gee, H.Y., Saisawat, P., Ashraf, S., Hurd, T.W., Vega-Warner, V., Fang, H., Beck, B.B., Gribouval, O., Zhou, W., Diaz, K.A.*, et al.* (2013). ARHGDIA mutations cause nephrotic syndrome via defective RHO GTPase signaling. The Journal of clinical investigation *123*, 3243-3253.
Gee, H.Y., Zhang, F., Ashraf, S., Kohl, S., Sadowski, C.E., Vega-Warner, V., Zhou, W., Lovric, S., Fang, H., Nettleton, M.*, et al.* (2015). KANK deficiency leads to podocyte dysfunction and nephrotic syndrome. The Journal of clinical investigation.
Geiger, B., and Yamada, K.M. (2011). Molecular architecture and function of matrix adhesions. Cold Spring Harbor perspectives in biology *3*.
Geiger, T., and Zaidel-Bar, R. (2012). Opening the floodgates: proteomics and the integrin adhesome. Current opinion in cell biology *24*, 562-568.
Giannone, G., Mege, R.M., and Thoumine, O. (2009). Multi-level molecular clutches in motile cell processes. Trends in cell biology *19*, 475-486.
Gingras, A.R., Bate, N., Goult, B.T., Hazelwood, L., Canestrelli, I., Grossmann, J.G., Liu, H., Putz, N.S., Roberts, G.C., Volkmann, N.*, et al.* (2008). The structure of the C-terminal actin-binding domain of talin. The EMBO journal *27*, 458-469.
Gingras, A.R., Bate, N., Goult, B.T., Patel, B., Kopp, P.M., Emsley, J., Barsukov, I.L., Roberts, G.C., and Critchley, D.R. (2010). Central region of talin has a unique fold that binds vinculin and actin. The Journal of biological chemistry *285*, 29577-29587.

Gingras, A.R., Ziegler, W.H., Frank, R., Barsukov, I.L., Roberts, G.C., Critchley, D.R., and Emsley, J. (2005). Mapping and consensus sequence identification for multiple vinculin binding sites within the talin rod. The Journal of biological chemistry *280*, 37217-37224.
Ginsberg, M.H., Partridge, A., and Shattil, S.J. (2005). Integrin regulation. Curr Opin Cell Biol *17*, 509-516.
Goksoy, E., Ma, Y.Q., Wang, X., Kong, X., Perera, D., Plow, E.F., and Qin, J. (2008). Structural basis for the autoinhibition of talin in regulating integrin activation. Molecular cell *31*, 124-133.
Goldmann, W.H., and Isenberg, G. (1991). Kinetic determination of talin-actin binding. Biochemical and biophysical research communications *178*, 718-723.
Goley, E.D., and Welch, M.D. (2006). The ARP2/3 complex: an actin nucleator comes of age. Nature reviews Molecular cell biology *7*, 713-726.
Golji, J., and Mofrad, M.R. (2014). The talin dimer structure orientation is mechanically regulated. Biophysical journal *107*, 1802-1809.
Goult, B.T., Bouaouina, M., Elliott, P.R., Bate, N., Patel, B., Gingras, A.R., Grossmann, J.G., Roberts, G.C., Calderwood, D.A., Critchley, D.R.*, et al.* (2010). Structure of a double ubiquitin-like domain in the talin head: a role in integrin activation. The EMBO journal *29*, 1069-1080.
Goult, B.T., Xu, X.P., Gingras, A.R., Swift, M., Patel, B., Bate, N., Kopp, P.M., Barsukov, I.L., Critchley, D.R., Volkmann, N.*, et al.* (2013a). Structural studies on full-length talin1 reveal a compact auto-inhibited dimer: implications for talin activation. Journal of structural biology *184*, 21-32.
Goult, B.T., Zacharchenko, T., Bate, N., Tsang, R., Hey, F., Gingras, A.R., Elliott, P.R., Roberts, G.C., Ballestrem, C., Critchley, D.R.*, et al.* (2013b). RIAM and vinculin binding to talin are mutually exclusive and regulate adhesion assembly and turnover. The Journal of biological chemistry *288*, 8238-8249.
Grigoriev, I., Splinter, D., Keijzer, N., Wulf, P.S., Demmers, J., Ohtsuka, T., Modesti, M., Maly, I.V., Grosveld, F., Hoogenraad, C.C.*, et al.* (2007). Rab6 regulates transport and targeting of exocytotic carriers. Developmental cell *13*, 305-314.
Grinthal, A., Adamovic, I., Weiner, B., Karplus, M., and Kleckner, N. (2010). PR65, the HEAT-repeat scaffold of phosphatase PP2A, is an elastic connector that links force and catalysis. Proceedings of the National Academy of Sciences of the United States of America *107*, 2467-2472.
Guilluy, C., Swaminathan, V., Garcia-Mata, R., O'Brien, E.T., Superfine, R., and Burridge, K. (2011). The Rho GEFs LARG and GEF-H1 regulate the mechanical response to force on integrins. Nature cell biology *13*, 722-727.
Gunawan, M., Venkatesan, N., Loh, J.T., Wong, J.F., Berger, H., Neo, W.H., Li, L.Y., Win, M.K., Yau, Y.H., Guo, T.*, et al.* (2015). The methyltransferase Ezh2 controls cell adhesion and migration through direct methylation of the extranuclear regulatory protein talin. Nature immunology.
Guo, X., Fan, W., Bian, X., and Ma, D. (2014). Upregulation of the Kank1 gene-induced brain glioma apoptosis and blockade of the cell cycle in G0/G1 phase. International journal of oncology *44*, 797-804.
Guruharsha, K.G., Rual, J.F., Zhai, B., Mintseris, J., Vaidya, P., Vaidya, N., Beekman, C., Wong, C., Rhee, D.Y., Cenaj, O.*, et al.* (2011). A protein complex network of Drosophila melanogaster. Cell *147*, 690-703.
Habelhah, H., Shah, K., Huang, L., Ostareck-Lederer, A., Burlingame, A.L., Shokat, K.M., Hentze, M.W., and Ronai, Z. (2001). ERK phosphorylation drives cytoplasmic accumulation of hnRNP-K and inhibition of mRNA translation. Nature cell biology *3*, 325-330.
Han, J., Lim, C.J., Watanabe, N., Soriani, A., Ratnikov, B., Calderwood, D.A., Puzon-McLaughlin, W., Lafuente, E.M., Boussiotis, V.A., Shattil, S.J.*, et al.* (2006). Reconstructing and

deconstructing agonist-induced activation of integrin alphaIIbbeta3. Current biology : CB *16*, 1796-1806.
Harburger, D.S., Bouaouina, M., and Calderwood, D.A. (2009). Kindlin-1 and -2 directly bind the C-terminal region of beta integrin cytoplasmic tails and exert integrin-specific activation effects. The Journal of biological chemistry *284*, 11485-11497.
Hemmings, L., Rees, D.J., Ohanian, V., Bolton, S.J., Gilmore, A.P., Patel, B., Priddle, H., Trevithick, J.E., Hynes, R.O., and Critchley, D.R. (1996). Talin contains three actin-binding sites each of which is adjacent to a vinculin-binding site. Journal of cell science *109 (Pt 11)*, 2715-2726.
Hoffmann, J.E., Fermin, Y., Stricker, R.L., Ickstadt, K., and Zamir, E. (2014). Symmetric exchange of multi-protein building blocks between stationary focal adhesions and the cytosol. eLife *3*, e02257.
Horwitz, A., Duggan, K., Buck, C., Beckerle, M.C., and Burridge, K. (1986). Interaction of plasma membrane fibronectin receptor with talin--a transmembrane linkage. Nature *320*, 531-533.
Hotta, A., Kawakatsu, T., Nakatani, T., Sato, T., Matsui, C., Sukezane, T., Akagi, T., Hamaji, T., Grigoriev, I., Akhmanova, A.*, et al.* (2010). Laminin-based cell adhesion anchors microtubule plus ends to the epithelial cell basal cortex through LL5alpha/beta. The Journal of cell biology *189*, 901-917.
Hotulainen, P., and Lappalainen, P. (2006). Stress fibers are generated by two distinct actin assembly mechanisms in motile cells. The Journal of cell biology *173*, 383-394.
Howard, J. (2009). Mechanical signaling in networks of motor and cytoskeletal proteins. Annual review of biophysics *38*, 217-234.
Hu, K., Ji, L., Applegate, K.T., Danuser, G., and Waterman-Storer, C.M. (2007). Differential transmission of actin motion within focal adhesions. Science *315*, 111-115.
Huang, C., Rajfur, Z., Yousefi, N., Chen, Z., Jacobson, K., and Ginsberg, M.H. (2009). Talin phosphorylation by Cdk5 regulates Smurf1-mediated talin head ubiquitylation and cell migration. Nature cell biology *11*, 624-630.
Hughes, P.E., Diaz-Gonzalez, F., Leong, L., Wu, C., McDonald, J.A., Shattil, S.J., and Ginsberg, M.H. (1996). Breaking the integrin hinge. A defined structural constraint regulates integrin signaling. J Biol Chem *271*, 6571-6574.
Humphries, J.D., Byron, A., Bass, M.D., Craig, S.E., Pinney, J.W., Knight, D., and Humphries, M.J. (2009). Proteomic analysis of integrin-associated complexes identifies RCC2 as a dual regulator of Rac1 and Arf6. Science signaling *2*, ra51.
Humphries, J.D., Paul, N.R., Humphries, M.J., and Morgan, M.R. (2015). Emerging properties of adhesion complexes: what are they and what do they do? Trends in cell biology.
Humphries, J.D., Wang, P., Streuli, C., Geiger, B., Humphries, M.J., and Ballestrem, C. (2007). Vinculin controls focal adhesion formation by direct interactions with talin and actin. The Journal of cell biology *179*, 1043-1057.
Huttelmaier, S., Zenklusen, D., Lederer, M., Dictenberg, J., Lorenz, M., Meng, X., Bassell, G.J., Condeelis, J., and Singer, R.H. (2005). Spatial regulation of beta-actin translation by Src-dependent phosphorylation of ZBP1. Nature *438*, 512-515.
Hynes, R.O. (1987). Integrins: a family of cell surface receptors. Cell *48*, 549-554.
Hynes, R.O. (2002). Integrins: bidirectional, allosteric signaling machines. Cell *110*, 673-687.
Hynes, R.O. (2004). The emergence of integrins: a personal and historical perspective. Matrix biology : journal of the International Society for Matrix Biology *23*, 333-340.
Ihara, S., Hagedorn, E.J., Morrissey, M.A., Chi, Q., Motegi, F., Kramer, J.M., and Sherwood, D.R. (2011). Basement membrane sliding and targeted adhesion remodels tissue boundaries during uterine-vulval attachment in Caenorhabditis elegans. Nature cell biology *13*, 641-651.

Ingber, D.E. (2003a). Tensegrity I. Cell structure and hierarchical systems biology. Journal of cell science *116*, 1157-1173.
Ingber, D.E. (2003b). Tensegrity II. How structural networks influence cellular information processing networks. Journal of cell science *116*, 1397-1408.
Jaalouk, D.E., and Lammerding, J. (2009). Mechanotransduction gone awry. Nature reviews Molecular cell biology *10*, 63-73.
Jakkaraju, S., Zhe, X., Pan, D., Choudhury, R., and Schuger, L. (2005). TIPs are tension-responsive proteins involved in myogenic versus adipogenic differentiation. Developmental cell *9*, 39-49.
Jiang, G., Giannone, G., Critchley, D.R., Fukumoto, E., and Sheetz, M.P. (2003). Two-piconewton slip bond between fibronectin and the cytoskeleton depends on talin. Nature *424*, 334-337.
Jin, J.K., Tien, P.C., Cheng, C.J., Song, J.H., Huang, C., Lin, S.H., and Gallick, G.E. (2015). Talin1 phosphorylation activates beta1 integrins: a novel mechanism to promote prostate cancer bone metastasis. Oncogene *34*, 1811-1821.
Jobard, F., Bouadjar, B., Caux, F., Hadj-Rabia, S., Has, C., Matsuda, F., Weissenbach, J., Lathrop, M., Prud'homme, J.F., and Fischer, J. (2003). Identification of mutations in a new gene encoding a FERM family protein with a pleckstrin homology domain in Kindler syndrome. Human molecular genetics *12*, 925-935.
Johnson, H.E., King, S.J., Asokan, S.B., Rotty, J.D., Bear, J.E., and Haugh, J.M. (2015). F-actin bundles direct the initiation and orientation of lamellipodia through adhesion-based signaling. The Journal of cell biology *208*, 443-455.
Johnson, M.S., Lu, N., Denessiouk, K., Heino, J., and Gullberg, D. (2009). Integrins during evolution: evolutionary trees and model organisms. Biochimica et biophysica acta *1788*, 779-789.
Joo, E.E., and Yamada, K.M. (2014). MYPT1 regulates contractility and microtubule acetylation to modulate integrin adhesions and matrix assembly. Nature communications *5*, 3510.
Kakinuma, N., and Kiyama, R. (2009). A major mutation of KIF21A associated with congenital fibrosis of the extraocular muscles type 1 (CFEOM1) enhances translocation of Kank1 to the membrane. Biochemical and biophysical research communications *386*, 639-644.
Kakinuma, N., Roy, B.C., Zhu, Y., Wang, Y., and Kiyama, R. (2008). Kank regulates RhoA-dependent formation of actin stress fibers and cell migration via 14-3-3 in PI3K-Akt signaling. The Journal of cell biology *181*, 537-549.
Kakinuma, N., Zhu, Y., Wang, Y., Roy, B.C., and Kiyama, R. (2009). Kank proteins: structure, functions and diseases. Cellular and molecular life sciences : CMLS *66*, 2651-2659.
Kanchanawong, P., Shtengel, G., Pasapera, A.M., Ramko, E.B., Davidson, M.W., Hess, H.F., and Waterman, C.M. (2010). Nanoscale architecture of integrin-based cell adhesions. Nature *468*, 580-584.
Karakose, E., Schiller, H.B., and Fassler, R. (2010). The kindlins at a glance. Journal of cell science *123*, 2353-2356.
Kast, D.J., Yang, C., Disanza, A., Boczkowska, M., Madasu, Y., Scita, G., Svitkina, T., and Dominguez, R. (2014). Mechanism of IRSp53 inhibition and combinatorial activation by Cdc42 and downstream effectors. Nature structural & molecular biology *21*, 413-422.
Katz, B.Z., Zamir, E., Bershadsky, A., Kam, Z., Yamada, K.M., and Geiger, B. (2000). Physical state of the extracellular matrix regulates the structure and molecular composition of cell-matrix adhesions. Molecular biology of the cell *11*, 1047-1060.
Katz, Z.B., Wells, A.L., Park, H.Y., Wu, B., Shenoy, S.M., and Singer, R.H. (2012). beta-Actin mRNA compartmentalization enhances focal adhesion stability and directs cell migration. Genes & development *26*, 1885-1890.

Kaverina, I., Krylyshkina, O., Beningo, K., Anderson, K., Wang, Y.L., and Small, J.V. (2002). Tensile stress stimulates microtubule outgrowth in living cells. Journal of cell science *115*, 2283-2291.
Kaverina, I., Krylyshkina, O., and Small, J.V. (1999). Microtubule targeting of substrate contacts promotes their relaxation and dissociation. The Journal of cell biology *146*, 1033-1044.
Kaverina, I., Rottner, K., and Small, J.V. (1998). Targeting, capture, and stabilization of microtubules at early focal adhesions. The Journal of cell biology *142*, 181-190.
Kim, C., Lau, T.L., Ulmer, T.S., and Ginsberg, M.H. (2009). Interactions of platelet integrin alphaIIb and beta3 transmembrane domains in mammalian cell membranes and their role in integrin activation. Blood *113*, 4747-4753.
Kim, C., Ye, F., and Ginsberg, M.H. (2011). Regulation of integrin activation. Annu Rev Cell Dev Biol *27*, 321-345.
Kim, C., Ye, F., Hu, X., and Ginsberg, M.H. (2012). Talin activates integrins by altering the topology of the beta transmembrane domain. The Journal of cell biology *197*, 605-611.
Klapholz, B., Herbert, S.L., Wellmann, J., Johnson, R., Parsons, M., and Brown, N.H. (2015). Alternative mechanisms for talin to mediate integrin function. Current biology : CB *25*, 847-857.
Ko, J., Kim, S., Valtschanoff, J.G., Shin, H., Lee, J.R., Sheng, M., Premont, R.T., Weinberg, R.J., and Kim, E. (2003a). Interaction between liprin-alpha and GIT1 is required for AMPA receptor targeting. The Journal of neuroscience : the official journal of the Society for Neuroscience *23*, 1667-1677.
Ko, J., Na, M., Kim, S., Lee, J.R., and Kim, E. (2003b). Interaction of the ERC family of RIM-binding proteins with the liprin-alpha family of multidomain proteins. The Journal of biological chemistry *278*, 42377-42385.
Kong, F., Garcia, A.J., Mould, A.P., Humphries, M.J., and Zhu, C. (2009). Demonstration of catch bonds between an integrin and its ligand. J Cell Biol *185*, 1275-1284.
Krause, M., Leslie, J.D., Stewart, M., Lafuente, E.M., Valderrama, F., Jagannathan, R., Strasser, G.A., Rubinson, D.A., Liu, H., Way, M.*, et al.* (2004). Lamellipodin, an Ena/VASP ligand, is implicated in the regulation of lamellipodial dynamics. Developmental cell *7*, 571-583.
Krendel, M., Zenke, F.T., and Bokoch, G.M. (2002). Nucleotide exchange factor GEF-H1 mediates cross-talk between microtubules and the actin cytoskeleton. Nature cell biology *4*, 294-301.
Krylyshkina, O., Anderson, K.I., Kaverina, I., Upmann, I., Manstein, D.J., Small, J.V., and Toomre, D.K. (2003). Nanometer targeting of microtubules to focal adhesions. The Journal of cell biology *161*, 853-859.
Kumar, P., Lyle, K.S., Gierke, S., Matov, A., Danuser, G., and Wittmann, T. (2009). GSK3beta phosphorylation modulates CLASP-microtubule association and lamella microtubule attachment. The Journal of cell biology *184*, 895-908.
Kuo, J.C., Han, X., Hsiao, C.T., Yates, J.R., 3rd, and Waterman, C.M. (2011). Analysis of the myosin-II-responsive focal adhesion proteome reveals a role for beta-Pix in negative regulation of focal adhesion maturation. Nature cell biology *13*, 383-393.
Lafuente, E.M., van Puijenbroek, A.A., Krause, M., Carman, C.V., Freeman, G.J., Berezovskaya, A., Constantine, E., Springer, T.A., Gertler, F.B., and Boussiotis, V.A. (2004). RIAM, an Ena/VASP and Profilin ligand, interacts with Rap1-GTP and mediates Rap1-induced adhesion. Developmental cell *7*, 585-595.
Lammermann, T., Bader, B.L., Monkley, S.J., Worbs, T., Wedlich-Soldner, R., Hirsch, K., Keller, M., Forster, R., Critchley, D.R., Fassler, R.*, et al.* (2008). Rapid leukocyte migration by integrin-independent flowing and squeezing. Nature *453*, 51-55.
Lammermann, T., and Sixt, M. (2009). Mechanical modes of 'amoeboid' cell migration. Current opinion in cell biology *21*, 636-644.

Lansbergen, G., Grigoriev, I., Mimori-Kiyosue, Y., Ohtsuka, T., Higa, S., Kitajima, I., Demmers, J., Galjart, N., Houtsmuller, A.B., Grosveld, F.*, et al.* (2006). CLASPs attach microtubule plus ends to the cell cortex through a complex with LL5beta. Developmental cell *11*, 21-32.
Larson, R.S., Corbi, A.L., Berman, L., and Springer, T. (1989). Primary structure of the leukocyte function-associated molecule-1 alpha subunit: an integrin with an embedded domain defining a protein superfamily. The Journal of cell biology *108*, 703-712.
Lau, T.L., Kim, C., Ginsberg, M.H., and Ulmer, T.S. (2009). The structure of the integrin alphaIIbbeta3 transmembrane complex explains integrin transmembrane signalling. EMBO J *28*, 1351-1361.
Lawson, C., Lim, S.T., Uryu, S., Chen, X.L., Calderwood, D.A., and Schlaepfer, D.D. (2012). FAK promotes recruitment of talin to nascent adhesions to control cell motility. The Journal of cell biology *196*, 223-232.
Lee, H.S., Bellin, R.M., Walker, D.L., Patel, B., Powers, P., Liu, H., Garcia-Alvarez, B., de Pereda, J.M., Liddington, R.C., Volkmann, N.*, et al.* (2004). Characterization of an actin-binding site within the talin FERM domain. Journal of molecular biology *343*, 771-784.
Lee, H.S., Lim, C.J., Puzon-McLaughlin, W., Shattil, S.J., and Ginsberg, M.H. (2009). RIAM activates integrins by linking talin to ras GTPase membrane-targeting sequences. The Journal of biological chemistry *284*, 5119-5127.
Lee, J.O., Rieu, P., Arnaout, M.A., and Liddington, R. (1995). Crystal structure of the A domain from the alpha subunit of integrin CR3 (CD11b/CD18). Cell *80*, 631-638.
Legate, K.R., and Fassler, R. (2009). Mechanisms that regulate adaptor binding to beta-integrin cytoplasmic tails. Journal of cell science *122*, 187-198.
Legate, K.R., Montag, D., Bottcher, R.T., Takahashi, S., and Fassler, R. (2012). Comparative phenotypic analysis of the two major splice isoforms of phosphatidylinositol phosphate kinase type Igamma in vivo. Journal of cell science *125*, 5636-5646.
Legate, K.R., Takahashi, S., Bonakdar, N., Fabry, B., Boettiger, D., Zent, R., and Fassler, R. (2011). Integrin adhesion and force coupling are independently regulated by localized PtdIns(4,5)2 synthesis. The EMBO journal *30*, 4539-4553.
Lerer, I., Sagi, M., Meiner, V., Cohen, T., Zlotogora, J., and Abeliovich, D. (2005). Deletion of the ANKRD15 gene at 9p24.3 causes parent-of-origin-dependent inheritance of familial cerebral palsy. Human molecular genetics *14*, 3911-3920.
Lewellyn, L., Cetera, M., and Horne-Badovinac, S. (2013). Misshapen decreases integrin levels to promote epithelial motility and planar polarity in Drosophila. The Journal of cell biology *200*, 721-729.
Li, C.C., Kuo, J.C., Waterman, C.M., Kiyama, R., Moss, J., and Vaughan, M. (2011a). Effects of brefeldin A-inhibited guanine nucleotide-exchange (BIG) 1 and KANK1 proteins on cell polarity and directed migration during wound healing. Proceedings of the National Academy of Sciences of the United States of America *108*, 19228-19233.
Li, G., Du, X., Vass, W.C., Papageorge, A.G., Lowy, D.R., and Qian, X. (2011b). Full activity of the deleted in liver cancer 1 (DLC1) tumor suppressor depends on an LD-like motif that binds talin and focal adhesion kinase (FAK). Proceedings of the National Academy of Sciences of the United States of America *108*, 17129-17134.
Ling, K., Doughman, R.L., Firestone, A.J., Bunce, M.W., and Anderson, R.A. (2002). Type I gamma phosphatidylinositol phosphate kinase targets and regulates focal adhesions. Nature *420*, 89-93.
Liu, J., Das, M., Yang, J., Ithychanda, S.S., Yakubenko, V.P., Plow, E.F., and Qin, J. (2015). Structural mechanism of integrin inactivation by filamin. Nature structural & molecular biology *22*, 383-389.

Low, B.C., Pan, C.Q., Shivashankar, G.V., Bershadsky, A., Sudol, M., and Sheetz, M. (2014). YAP/TAZ as mechanosensors and mechanotransducers in regulating organ size and tumor growth. FEBS letters *588*, 2663-2670.
Luo, B.H., Carman, C.V., and Springer, T.A. (2007). Structural basis of integrin regulation and signaling. Annu Rev Immunol *25*, 619-647.
Luo, B.H., Carman, C.V., Takagi, J., and Springer, T.A. (2005). Disrupting integrin transmembrane domain heterodimerization increases ligand binding affinity, not valency or clustering. Proceedings of the National Academy of Sciences of the United States of America *102*, 3679-3684.
Ma, Y.Q., Qin, J., Wu, C., and Plow, E.F. (2008). Kindlin-2 (Mig-2): a co-activator of beta3 integrins. The Journal of cell biology *181*, 439-446.
Maheshwari, G., Brown, G., Lauffenburger, D.A., Wells, A., and Griffith, L.G. (2000). Cell adhesion and motility depend on nanoscale RGD clustering. Journal of cell science *113 (Pt 10)*, 1677-1686.
Matsumoto, S., Fumoto, K., Okamoto, T., Kaibuchi, K., and Kikuchi, A. (2010). Binding of APC and dishevelled mediates Wnt5a-regulated focal adhesion dynamics in migrating cells. The EMBO journal *29*, 1192-1204.
Mattila, P.K., and Lappalainen, P. (2008). Filopodia: molecular architecture and cellular functions. Nature reviews Molecular cell biology *9*, 446-454.
Matus, D.Q., Chang, E., Makohon-Moore, S.C., Hagedorn, M.A., Chi, Q., and Sherwood, D.R. (2014). Cell division and targeted cell cycle arrest opens and stabilizes basement membrane gaps. Nature communications *5*, 4184.
McBeath, R., Pirone, D.M., Nelson, C.M., Bhadriraju, K., and Chen, C.S. (2004). Cell shape, cytoskeletal tension, and RhoA regulate stem cell lineage commitment. Developmental cell *6*, 483-495.
McMahon, H.T., and Boucrot, E. (2011). Molecular mechanism and physiological functions of clathrin-mediated endocytosis. Nature reviews Molecular cell biology *12*, 517-533.
McNiven, M.A. (2013). Breaking away: matrix remodeling from the leading edge. Trends in cell biology *23*, 16-21.
Meiri, D., Marshall, C.B., Greeve, M.A., Kim, B., Balan, M., Suarez, F., Bakal, C., Wu, C., Larose, J., Fine, N.*, et al.* (2012). Mechanistic insight into the microtubule and actin cytoskeleton coupling through dynein-dependent RhoGEF inhibition. Molecular cell *45*, 642-655.
Meiri, D., Marshall, C.B., Mokady, D., LaRose, J., Mullin, M., Gingras, A.C., Ikura, M., and Rottapel, R. (2014). Mechanistic insight into GPCR-mediated activation of the microtubule-associated RhoA exchange factor GEF-H1. Nature communications *5*, 4857.
Mellacheruvu, D., Wright, Z., Couzens, A.L., Lambert, J.P., St-Denis, N.A., Li, T., Miteva, Y.V., Hauri, S., Sardiu, M.E., Low, T.Y.*, et al.* (2013). The CRAPome: a contaminant repository for affinity purification-mass spectrometry data. Nature methods *10*, 730-736.
Meves, A., Stremmel, C., Bottcher, R.T., and Fassler, R. (2013). beta1 integrins with individually disrupted cytoplasmic NPxY motifs are embryonic lethal but partially active in the epidermis. The Journal of investigative dermatology *133*, 2722-2731.
Mili, S., Moissoglu, K., and Macara, I.G. (2008). Genome-wide screen reveals APC-associated RNAs enriched in cell protrusions. Nature *453*, 115-119.
Mimori-Kiyosue, Y., Grigoriev, I., Lansbergen, G., Sasaki, H., Matsui, C., Severin, F., Galjart, N., Grosveld, F., Vorobjev, I., Tsukita, S.*, et al.* (2005). CLASP1 and CLASP2 bind to EB1 and regulate microtubule plus-end dynamics at the cell cortex. The Journal of cell biology *168*, 141-153.
Mitchison, T., and Kirschner, M. (1984). Dynamic instability of microtubule growth. Nature *312*, 237-242.

Mohseni, M., Sun, J., Lau, A., Curtis, S., Goldsmith, J., Fox, V.L., Wei, C., Frazier, M., Samson, O., Wong, K.K., *et al.* (2014). A genetic screen identifies an LKB1-MARK signalling axis controlling the Hippo-YAP pathway. Nature cell biology *16*, 108-117.
Monkley, S.J., Zhou, X.H., Kinston, S.J., Giblett, S.M., Hemmings, L., Priddle, H., Brown, J.E., Pritchard, C.A., Critchley, D.R., and Fassler, R. (2000). Disruption of the talin gene arrests mouse development at the gastrulation stage. Developmental dynamics : an official publication of the American Association of Anatomists *219*, 560-574.
Montagnac, G., Meas-Yedid, V., Irondelle, M., Castro-Castro, A., Franco, M., Shida, T., Nachury, M.V., Benmerah, A., Olivo-Marin, J.C., and Chavrier, P. (2013). alphaTAT1 catalyses microtubule acetylation at clathrin-coated pits. Nature *502*, 567-570.
Montanez, E., Ussar, S., Schifferer, M., Bosl, M., Zent, R., Moser, M., and Fassler, R. (2008). Kindlin-2 controls bidirectional signaling of integrins. Genes & development *22*, 1325-1330.
Moore, D.T., Nygren, P., Jo, H., Boesze-Battaglia, K., Bennett, J.S., and DeGrado, W.F. (2012). Affinity of talin-1 for the beta3-integrin cytosolic domain is modulated by its phospholipid bilayer environment. Proceedings of the National Academy of Sciences of the United States of America *109*, 793-798.
Moser, M., Bauer, M., Schmid, S., Ruppert, R., Schmidt, S., Sixt, M., Wang, H.V., Sperandio, M., and Fassler, R. (2009). Kindlin-3 is required for beta2 integrin-mediated leukocyte adhesion to endothelial cells. Nature medicine *15*, 300-305.
Moser, M., Nieswandt, B., Ussar, S., Pozgajova, M., and Fassler, R. (2008). Kindlin-3 is essential for integrin activation and platelet aggregation. Nature medicine *14*, 325-330.
Nalbant, P., Chang, Y.C., Birkenfeld, J., Chang, Z.F., and Bokoch, G.M. (2009). Guanine nucleotide exchange factor-H1 regulates cell migration via localized activation of RhoA at the leading edge. Molecular biology of the cell *20*, 4070-4082.
Nevo, J., Mai, A., Tuomi, S., Pellinen, T., Pentikainen, O.T., Heikkila, P., Lundin, J., Joensuu, H., Bono, P., and Ivaska, J. (2010). Mammary-derived growth inhibitor (MDGI) interacts with integrin alpha-subunits and suppresses integrin activity and invasion. Oncogene *29*, 6452-6463.
Nishimura, T., and Kaibuchi, K. (2007). Numb controls integrin endocytosis for directional cell migration with aPKC and PAR-3. Developmental cell *13*, 15-28.
Oakes, P.W., Beckham, Y., Stricker, J., and Gardel, M.L. (2012). Tension is required but not sufficient for focal adhesion maturation without a stress fiber template. The Journal of cell biology *196*, 363-374.
Ohtsuka, T., Takao-Rikitsu, E., Inoue, E., Inoue, M., Takeuchi, M., Matsubara, K., Deguchi-Tawarada, M., Satoh, K., Morimoto, K., Nakanishi, H., *et al.* (2002). Cast: a novel protein of the cytomatrix at the active zone of synapses that forms a ternary complex with RIM1 and munc13-1. The Journal of cell biology *158*, 577-590.
Oikawa, T., Yamaguchi, H., Itoh, T., Kato, M., Ijuin, T., Yamazaki, D., Suetsugu, S., and Takenawa, T. (2004). PtdIns(3,4,5)P3 binding is necessary for WAVE2-induced formation of lamellipodia. Nature cell biology *6*, 420-426.
Olberding, J.E., Thouless, M.D., Arruda, E.M., and Garikipati, K. (2010). The non-equilibrium thermodynamics and kinetics of focal adhesion dynamics. PloS one *5*, e12043.
Olson, E.N., and Nordheim, A. (2010). Linking actin dynamics and gene transcription to drive cellular motile functions. Nature reviews Molecular cell biology *11*, 353-365.
Palazzo, A.F., Eng, C.H., Schlaepfer, D.D., Marcantonio, E.E., and Gundersen, G.G. (2004). Localized stabilization of microtubules by integrin- and FAK-facilitated Rho signaling. Science *303*, 836-839.
Paluch, E.K., and Raz, E. (2013). The role and regulation of blebs in cell migration. Current opinion in cell biology *25*, 582-590.
Pankov, R., Cukierman, E., Katz, B.Z., Matsumoto, K., Lin, D.C., Lin, S., Hahn, C., and Yamada, K.M. (2000). Integrin dynamics and matrix assembly: tensin-dependent translocation

of alpha(5)beta(1) integrins promotes early fibronectin fibrillogenesis. The Journal of cell biology *148*, 1075-1090.
Parsons, J.T., Horwitz, A.R., and Schwartz, M.A. (2010). Cell adhesion: integrating cytoskeletal dynamics and cellular tension. Nature reviews Molecular cell biology *11*, 633-643.
Pathak, R., Delorme-Walker, V.D., Howell, M.C., Anselmo, A.N., White, M.A., Bokoch, G.M., and Dermardirossian, C. (2012). The microtubule-associated Rho activating factor GEF-H1 interacts with exocyst complex to regulate vesicle traffic. Developmental cell *23*, 397-411.
Patla, I., Volberg, T., Elad, N., Hirschfeld-Warneken, V., Grashoff, C., Fassler, R., Spatz, J.P., Geiger, B., and Medalia, O. (2010). Dissecting the molecular architecture of integrin adhesion sites by cryo-electron tomography. Nature cell biology *12*, 909-915.
Petrich, B.G. (2009). Talin-dependent integrin signalling in vivo. Thrombosis and haemostasis *101*, 1020-1024.
Petrich, B.G., Marchese, P., Ruggeri, Z.M., Spiess, S., Weichert, R.A., Ye, F., Tiedt, R., Skoda, R.C., Monkley, S.J., Critchley, D.R.*, et al.* (2007). Talin is required for integrin-mediated platelet function in hemostasis and thrombosis. The Journal of experimental medicine *204*, 3103-3111.
Pittenger, M.F., Mackay, A.M., Beck, S.C., Jaiswal, R.K., Douglas, R., Mosca, J.D., Moorman, M.A., Simonetti, D.W., Craig, S., and Marshak, D.R. (1999). Multilineage potential of adult human mesenchymal stem cells. Science *284*, 143-147.
Plotnikov, S.V., Pasapera, A.M., Sabass, B., and Waterman, C.M. (2012). Force fluctuations within focal adhesions mediate ECM-rigidity sensing to guide directed cell migration. Cell *151*, 1513-1527.
Plow, E.F., and Qin, J. (2015). The role of RIAM in platelets put to a test. Blood *125*, 207-208.
Pollard, T.D., and Borisy, G.G. (2003). Cellular motility driven by assembly and disassembly of actin filaments. Cell *112*, 453-465.
Puchner, E.M., Alexandrovich, A., Kho, A.L., Hensen, U., Schafer, L.V., Brandmeier, B., Grater, F., Grubmuller, H., Gaub, H.E., and Gautel, M. (2008). Mechanoenzymatics of titin kinase. Proceedings of the National Academy of Sciences of the United States of America *105*, 13385-13390.
Rajfur, Z., Roy, P., Otey, C., Romer, L., and Jacobson, K. (2002). Dissecting the link between stress fibres and focal adhesions by CALI with EGFP fusion proteins. Nature cell biology *4*, 286-293.
Ramot, Y., Molho-Pessach, V., Meir, T., Alper-Pinus, R., Siam, I., Tams, S., Babay, S., and Zlotogorski, A. (2014). Mutation in KANK2, encoding a sequestering protein for steroid receptor coactivators, causes keratoderma and woolly hair. Journal of medical genetics *51*, 388-394.
Rantala, J.K., Pouwels, J., Pellinen, T., Veltel, S., Laasola, P., Mattila, E., Potter, C.S., Duffy, T., Sundberg, J.P., Kallioniemi, O.*, et al.* (2011). SHARPIN is an endogenous inhibitor of beta1-integrin activation. Nature cell biology *13*, 1315-1324.
Ren, X.D., Kiosses, W.B., and Schwartz, M.A. (1999). Regulation of the small GTP-binding protein Rho by cell adhesion and the cytoskeleton. The EMBO journal *18*, 578-585.
Renkawitz, J., and Sixt, M. (2010). Mechanisms of force generation and force transmission during interstitial leukocyte migration. EMBO reports *11*, 744-750.
Roca-Cusachs, P., del Rio, A., Puklin-Faucher, E., Gauthier, N.C., Biais, N., and Sheetz, M.P. (2013). Integrin-dependent force transmission to the extracellular matrix by alpha-actinin triggers adhesion maturation. Proceedings of the National Academy of Sciences of the United States of America *110*, E1361-1370.
Rogalski, T.M., Mullen, G.P., Gilbert, M.M., Williams, B.D., and Moerman, D.G. (2000). The UNC-112 gene in Caenorhabditis elegans encodes a novel component of cell-matrix adhesion structures required for integrin localization in the muscle cell membrane. The Journal of cell biology *150*, 253-264.

Rognoni, E., Widmaier, M., Jakobson, M., Ruppert, R., Ussar, S., Katsougkri, D., Bottcher, R.T., Lai-Cheong, J.E., Rifkin, D.B., McGrath, J.A.*, et al.* (2014). Kindlin-1 controls Wnt and TGF-beta availability to regulate cutaneous stem cell proliferation. Nature medicine *20*, 350-359.
Rognoni, L., Stigler, J., Pelz, B., Ylanne, J., and Rief, M. (2012). Dynamic force sensing of filamin revealed in single-molecule experiments. Proceedings of the National Academy of Sciences of the United States of America *109*, 19679-19684.
Rooney, C., White, G., Nazgiewicz, A., Woodcock, S.A., Anderson, K.I., Ballestrem, C., and Malliri, A. (2010). The Rac activator STEF (Tiam2) regulates cell migration by microtubule-mediated focal adhesion disassembly. EMBO reports *11*, 292-298.
Rossier, O., Octeau, V., Sibarita, J.B., Leduc, C., Tessier, B., Nair, D., Gatterdam, V., Destaing, O., Albiges-Rizo, C., Tampe, R.*, et al.* (2012). Integrins beta1 and beta3 exhibit distinct dynamic nanoscale organizations inside focal adhesions. Nature cell biology *14*, 1057-1067.
Roy, B.C., Kakinuma, N., and Kiyama, R. (2009). Kank attenuates actin remodeling by preventing interaction between IRSp53 and Rac1. The Journal of cell biology *184*, 253-267.
Rubashkin, M.G., Cassereau, L., Bainer, R., DuFort, C.C., Yui, Y., Ou, G., Paszek, M.J., Davidson, M.W., Chen, Y.Y., and Weaver, V.M. (2014). Force engages vinculin and promotes tumor progression by enhancing PI3K activation of phosphatidylinositol (3,4,5)-triphosphate. Cancer research *74*, 4597-4611.
Russ, W.P., and Engelman, D.M. (2000). The GxxxG motif: a framework for transmembrane helix-helix association. Journal of molecular biology *296*, 911-919.
Saltel, F., Mortier, E., Hytonen, V.P., Jacquier, M.C., Zimmermann, P., Vogel, V., Liu, W., and Wehrle-Haller, B. (2009). New PI(4,5)P2- and membrane proximal integrin-binding motifs in the talin head control beta3-integrin clustering. The Journal of cell biology *187*, 715-731.
Sarkar, S., Roy, B.C., Hatano, N., Aoyagi, T., Gohji, K., and Kiyama, R. (2002). A novel ankyrin repeat-containing gene (Kank) located at 9p24 is a growth suppressor of renal cell carcinoma. The Journal of biological chemistry *277*, 36585-36591.
Sawada, Y., Tamada, M., Dubin-Thaler, B.J., Cherniavskaya, O., Sakai, R., Tanaka, S., and Sheetz, M.P. (2006). Force sensing by mechanical extension of the Src family kinase substrate p130Cas. Cell *127*, 1015-1026.
Schiller, H.B., and Fassler, R. (2013). Mechanosensitivity and compositional dynamics of cell-matrix adhesions. EMBO reports *14*, 509-519.
Schiller, H.B., Friedel, C.C., Boulegue, C., and Fassler, R. (2011). Quantitative proteomics of the integrin adhesome show a myosin II-dependent recruitment of LIM domain proteins. EMBO reports *12*, 259-266.
Schiller, H.B., Hermann, M.R., Polleux, J., Vignaud, T., Zanivan, S., Friedel, C.C., Sun, Z., Raducanu, A., Gottschalk, K.E., Thery, M.*, et al.* (2013). beta1- and alphav-class integrins cooperate to regulate myosin II during rigidity sensing of fibronectin-based microenvironments. Nature cell biology *15*, 625-636.
Schmidt, J.M., Zhang, J., Lee, H.S., Stromer, M.H., and Robson, R.M. (1999). Interaction of talin with actin: sensitive modulation of filament crosslinking activity. Archives of biochemistry and biophysics *366*, 139-150.
Schmidt, S., Nakchbandi, I., Ruppert, R., Kawelke, N., Hess, M.W., Pfaller, K., Jurdic, P., Fassler, R., and Moser, M. (2011). Kindlin-3-mediated signaling from multiple integrin classes is required for osteoclast-mediated bone resorption. The Journal of cell biology *192*, 883-897.
Schwander, M., Leu, M., Stumm, M., Dorchies, O.M., Ruegg, U.T., Schittny, J., and Muller, U. (2003). Beta1 integrins regulate myoblast fusion and sarcomere assembly. Developmental cell *4*, 673-685.
Scita, G., Confalonieri, S., Lappalainen, P., and Suetsugu, S. (2008). IRSp53: crossing the road of membrane and actin dynamics in the formation of membrane protrusions. Trends in cell biology *18*, 52-60.

Senes, A., Gerstein, M., and Engelman, D.M. (2000). Statistical analysis of amino acid patterns in transmembrane helices: the GxxxG motif occurs frequently and in association with beta-branched residues at neighboring positions. Journal of molecular biology *296*, 921-936.
Sepp, K.J., Hong, P., Lizarraga, S.B., Liu, J.S., Mejia, L.A., Walsh, C.A., and Perrimon, N. (2008). Identification of neural outgrowth genes using genome-wide RNAi. PLoS genetics *4*, e1000111.
Sero, J.E., Sailem, H.Z., Ardy, R.C., Almuttaqi, H., Zhang, T., and Bakal, C. (2015). Cell shape and the microenvironment regulate nuclear translocation of NF-kappaB in breast epithelial and tumor cells. Molecular systems biology *11*, 790.
Shi, F., and Sottile, J. (2011). MT1-MMP regulates the turnover and endocytosis of extracellular matrix fibronectin. Journal of cell science *124*, 4039-4050.
Shin, H., Wyszynski, M., Huh, K.H., Valtschanoff, J.G., Lee, J.R., Ko, J., Streuli, M., Weinberg, R.J., Sheng, M., and Kim, E. (2003). Association of the kinesin motor KIF1A with the multimodular protein liprin-alpha. The Journal of biological chemistry *278*, 11393-11401.
Siegel, D.H., Ashton, G.H., Penagos, H.G., Lee, J.V., Feiler, H.S., Wilhelmsen, K.C., South, A.P., Smith, F.J., Prescott, A.R., Wessagowit, V.*, et al.* (2003). Loss of kindlin-1, a human homolog of the Caenorhabditis elegans actin-extracellular-matrix linker protein UNC-112, causes Kindler syndrome. American journal of human genetics *73*, 174-187.
Singh, P., Carraher, C., and Schwarzbauer, J.E. (2010). Assembly of fibronectin extracellular matrix. Annual review of cell and developmental biology *26*, 397-419.
Smilenov, L.B., Mikhailov, A., Pelham, R.J., Marcantonio, E.E., and Gundersen, G.G. (1999). Focal adhesion motility revealed in stationary fibroblasts. Science *286*, 1172-1174.
Song, X., Yang, J., Hirbawi, J., Ye, S., Perera, H.D., Goksoy, E., Dwivedi, P., Plow, E.F., Zhang, R., and Qin, J. (2012). A novel membrane-dependent on/off switch mechanism of talin FERM domain at sites of cell adhesion. Cell research *22*, 1533-1545.
Stehbens, S., and Wittmann, T. (2012). Targeting and transport: how microtubules control focal adhesion dynamics. The Journal of cell biology *198*, 481-489.
Stehbens, S.J., Paszek, M., Pemble, H., Ettinger, A., Gierke, S., and Wittmann, T. (2014). CLASPs link focal-adhesion-associated microtubule capture to localized exocytosis and adhesion site turnover. Nature cell biology *16*, 561-573.
Stehbens, S.J., and Wittmann, T. (2014). Analysis of focal adhesion turnover: a quantitative live-cell imaging example. Methods in cell biology *123*, 335-346.
Steinberg, F., Heesom, K.J., Bass, M.D., and Cullen, P.J. (2012). SNX17 protects integrins from degradation by sorting between lysosomal and recycling pathways. The Journal of cell biology *197*, 219-230.
Straight, A.F., Cheung, A., Limouze, J., Chen, I., Westwood, N.J., Sellers, J.R., and Mitchison, T.J. (2003). Dissecting temporal and spatial control of cytokinesis with a myosin II Inhibitor. Science *299*, 1743-1747.
Stritt, S., Wolf, K., Lorenz, V., Vogtle, T., Gupta, S., Bosl, M.R., and Nieswandt, B. (2015). Rap1-GTP-interacting adaptor molecule (RIAM) is dispensable for platelet integrin activation and function in mice. Blood *125*, 219-222.
Sun, N., Critchley, D.R., Paulin, D., Li, Z., and Robson, R.M. (2008). Identification of a repeated domain within mammalian alpha-synemin that interacts directly with talin. Experimental cell research *314*, 1839-1849.
Suozzi, K.C., Wu, X., and Fuchs, E. (2012). Spectraplakins: master orchestrators of cytoskeletal dynamics. The Journal of cell biology *197*, 465-475.
Suraneni, P., Rubinstein, B., Unruh, J.R., Durnin, M., Hanein, D., and Li, R. (2012). The Arp2/3 complex is required for lamellipodia extension and directional fibroblast cell migration. The Journal of cell biology *197*, 239-251.

Tadokoro, S., Shattil, S.J., Eto, K., Tai, V., Liddington, R.C., de Pereda, J.M., Ginsberg, M.H., and Calderwood, D.A. (2003). Talin binding to integrin beta tails: a final common step in integrin activation. Science *302*, 103-106.
Takagi, J., Petre, B.M., Walz, T., and Springer, T.A. (2002). Global conformational rearrangements in integrin extracellular domains in outside-in and inside-out signaling. Cell *110*, 599-511.
Takino, T., Saeki, H., Miyamori, H., Kudo, T., and Sato, H. (2007). Inhibition of membrane-type 1 matrix metalloproteinase at cell-matrix adhesions. Cancer research *67*, 11621-11629.
Takino, T., Watanabe, Y., Matsui, M., Miyamori, H., Kudo, T., Seiki, M., and Sato, H. (2006). Membrane-type 1 matrix metalloproteinase modulates focal adhesion stability and cell migration. Experimental cell research *312*, 1381-1389.
Tamkun, J.W., DeSimone, D.W., Fonda, D., Patel, R.S., Buck, C., Horwitz, A.F., and Hynes, R.O. (1986). Structure of integrin, a glycoprotein involved in the transmembrane linkage between fibronectin and actin. Cell *46*, 271-282.
Tanentzapf, G., and Brown, N.H. (2006). An interaction between integrin and the talin FERM domain mediates integrin activation but not linkage to the cytoskeleton. Nature cell biology *8*, 601-606.
Tanentzapf, G., Martin-Bermudo, M.D., Hicks, M.S., and Brown, N.H. (2006). Multiple factors contribute to integrin-talin interactions in vivo. Journal of cell science *119*, 1632-1644.
Taru, H., and Jin, Y. (2011). The Liprin homology domain is essential for the homomeric interaction of SYD-2/Liprin-alpha protein in presynaptic assembly. The Journal of neuroscience : the official journal of the Society for Neuroscience *31*, 16261-16268.
Taylor, M.J., Perrais, D., and Merrifield, C.J. (2011). A high precision survey of the molecular dynamics of mammalian clathrin-mediated endocytosis. PLoS biology *9*, e1000604.
Thievessen, I., Thompson, P.M., Berlemont, S., Plevock, K.M., Plotnikov, S.V., Zemljic-Harpf, A., Ross, R.S., Davidson, M.W., Danuser, G., Campbell, S.L.*, et al.* (2013). Vinculin-actin interaction couples actin retrograde flow to focal adhesions, but is dispensable for focal adhesion growth. The Journal of cell biology *202*, 163-177.
Tian, X., Kim, J.J., Monkley, S.M., Gotoh, N., Nandez, R., Soda, K., Inoue, K., Balkin, D.M., Hassan, H., Son, S.H.*, et al.* (2014). Podocyte-associated talin1 is critical for glomerular filtration barrier maintenance. The Journal of clinical investigation *124*, 1098-1113.
Tokuo, H., and Ikebe, M. (2004). Myosin X transports Mena/VASP to the tip of filopodia. Biochemical and biophysical research communications *319*, 214-220.
Tripathi, B.K., Qian, X., Mertins, P., Wang, D., Papageorge, A.G., Carr, S.A., and Lowy, D.R. (2014). CDK5 is a major regulator of the tumor suppressor DLC1. The Journal of cell biology *207*, 627-642.
Tseng, H.Y., Thorausch, N., Ziegler, T., Meves, A., Fassler, R., and Bottcher, R.T. (2014). Sorting nexin 31 binds multiple beta integrin cytoplasmic domains and regulates beta1 integrin surface levels and stability. Journal of molecular biology *426*, 3180-3194.
Ussar, S., Moser, M., Widmaier, M., Rognoni, E., Harrer, C., Genzel-Boroviczeny, O., and Fassler, R. (2008). Loss of Kindlin-1 causes skin atrophy and lethal neonatal intestinal epithelial dysfunction. PLoS genetics *4*, e1000289.
Ussar, S., Wang, H.V., Linder, S., Fassler, R., and Moser, M. (2006). The Kindlins: subcellular localization and expression during murine development. Experimental cell research *312*, 3142-3151.
van der Vaart, B., van Riel, W.E., Doodhi, H., Kevenaar, J.T., Katrukha, E.A., Gumy, L., Bouchet, B.P., Grigoriev, I., Spangler, S.A., Yu, K.L.*, et al.* (2013). CFEOM1-associated kinesin KIF21A is a cortical microtubule growth inhibitor. Developmental cell *27*, 145-160.

Vicente-Manzanares, M., Koach, M.A., Whitmore, L., Lamers, M.L., and Horwitz, A.F. (2008). Segregation and activation of myosin IIB creates a rear in migrating cells. The Journal of cell biology *183*, 543-554.
Vignjevic, D., Kojima, S., Aratyn, Y., Danciu, O., Svitkina, T., and Borisy, G.G. (2006). Role of fascin in filopodial protrusion. The Journal of cell biology *174*, 863-875.
Vitorino, P., Yeung, S., Crow, A., Bakke, J., Smyczek, T., West, K., McNamara, E., Eastham-Anderson, J., Gould, S., Harris, S.F.*, et al.* (2015). MAP4K4 regulates integrin-FERM binding to control endothelial cell motility. Nature *519*, 425-430.
Wang, J.H. (2012). Pull and push: talin activation for integrin signaling. Cell research *22*, 1512-1514.
Wang, N., Tytell, J.D., and Ingber, D.E. (2009). Mechanotransduction at a distance: mechanically coupling the extracellular matrix with the nucleus. Nature reviews Molecular cell biology *10*, 75-82.
Wang, S., Watanabe, T., Matsuzawa, K., Katsumi, A., Kakeno, M., Matsui, T., Ye, F., Sato, K., Murase, K., Sugiyama, I.*, et al.* (2012). Tiam1 interaction with the PAR complex promotes talin-mediated Rac1 activation during polarized cell migration. The Journal of cell biology *199*, 331-345.
Wang, X., and Ha, T. (2013). Defining single molecular forces required to activate integrin and notch signaling. Science *340*, 991-994.
Wang, Y., Cao, H., Chen, J., and McNiven, M.A. (2011). A direct interaction between the large GTPase dynamin-2 and FAK regulates focal adhesion dynamics in response to active Src. Molecular biology of the cell *22*, 1529-1538.
Wang, Y., Kakinuma, N., Zhu, Y., and Kiyama, R. (2006). Nucleo-cytoplasmic shuttling of human Kank protein accompanies intracellular translocation of beta-catenin. Journal of cell science *119*, 4002-4010.
Wang, Y., and McNiven, M.A. (2012). Invasive matrix degradation at focal adhesions occurs via protease recruitment by a FAK-p130Cas complex. The Journal of cell biology *196*, 375-385.
Webb, D.J., Parsons, J.T., and Horwitz, A.F. (2002). Adhesion assembly, disassembly and turnover in migrating cells -- over and over and over again. Nature cell biology *4*, E97-100.
Wegener, K.L., Basran, J., Bagshaw, C.R., Campbell, I.D., Roberts, G.C., Critchley, D.R., and Barsukov, I.L. (2008). Structural basis for the interaction between the cytoplasmic domain of the hyaluronate receptor layilin and the talin F3 subdomain. Journal of molecular biology *382*, 112-126.
Wegener, K.L., Partridge, A.W., Han, J., Pickford, A.R., Liddington, R.C., Ginsberg, M.H., and Campbell, I.D. (2007). Structural basis of integrin activation by talin. Cell *128*, 171-182.
Wei, Z., Zheng, S., Spangler, S.A., Yu, C., Hoogenraad, C.C., and Zhang, M. (2011). Liprin-mediated large signaling complex organization revealed by the liprin-alpha/CASK and liprin-alpha/liprin-beta complex structures. Molecular cell *43*, 586-598.
Wen, Y., Eng, C.H., Schmoranzer, J., Cabrera-Poch, N., Morris, E.J., Chen, M., Wallar, B.J., Alberts, A.S., and Gundersen, G.G. (2004). EB1 and APC bind to mDia to stabilize microtubules downstream of Rho and promote cell migration. Nature cell biology *6*, 820-830.
Wickstrom, S.A., Lange, A., Hess, M.W., Polleux, J., Spatz, J.P., Kruger, M., Pfaller, K., Lambacher, A., Bloch, W., Mann, M.*, et al.* (2010). Integrin-linked kinase controls microtubule dynamics required for plasma membrane targeting of caveolae. Developmental cell *19*, 574-588.
Winkler, J., Lunsdorf, H., and Jockusch, B.M. (1997). Energy-filtered electron microscopy reveals that talin is a highly flexible protein composed of a series of globular domains. European journal of biochemistry / FEBS *243*, 430-436.
Winograd-Katz, S.E., Fassler, R., Geiger, B., and Legate, K.R. (2014). The integrin adhesome: from genes and proteins to human disease. Nature reviews Molecular cell biology *15*, 273-288.

Worth, D.C., Hodivala-Dilke, K., Robinson, S.D., King, S.J., Morton, P.E., Gertler, F.B., Humphries, M.J., and Parsons, M. (2010). Alpha v beta3 integrin spatially regulates VASP and RIAM to control adhesion dynamics and migration. The Journal of cell biology *189*, 369-383.
Wu, C., Asokan, S.B., Berginski, M.E., Haynes, E.M., Sharpless, N.E., Griffith, J.D., Gomez, S.M., and Bear, J.E. (2012). Arp2/3 is critical for lamellipodia and response to extracellular matrix cues but is dispensable for chemotaxis. Cell *148*, 973-987.
Wu, X., Kodama, A., and Fuchs, E. (2008). ACF7 regulates cytoskeletal-focal adhesion dynamics and migration and has ATPase activity. Cell *135*, 137-148.
Wu, X., Shen, Q.T., Oristian, D.S., Lu, C.P., Zheng, Q., Wang, H.W., and Fuchs, E. (2011). Skin stem cells orchestrate directional migration by regulating microtubule-ACF7 connections through GSK3beta. Cell *144*, 341-352.
Wynne, J.P., Wu, J., Su, W., Mor, A., Patsoukis, N., Boussiotis, V.A., Hubbard, S.R., and Philips, M.R. (2012). Rap1-interacting adapter molecule (RIAM) associates with the plasma membrane via a proximity detector. The Journal of cell biology *199*, 317-330.
Xiao, T., Takagi, J., Coller, B.S., Wang, J.H., and Springer, T.A. (2004). Structural basis for allostery in integrins and binding to fibrinogen-mimetic therapeutics. Nature *432*, 59-67.
Xiong, J.P., Stehle, T., Diefenbach, B., Zhang, R., Dunker, R., Scott, D.L., Joachimiak, A., Goodman, S.L., and Arnaout, M.A. (2001). Crystal structure of the extracellular segment of integrin alpha Vbeta3. Science *294*, 339-345.
Xiong, J.P., Stehle, T., Goodman, S.L., and Arnaout, M.A. (2004). A novel adaptation of the integrin PSI domain revealed from its crystal structure. The Journal of biological chemistry *279*, 40252-40254.
Yamazaki, D., Suetsugu, S., Miki, H., Kataoka, Y., Nishikawa, S., Fujiwara, T., Yoshida, N., and Takenawa, T. (2003). WAVE2 is required for directed cell migration and cardiovascular development. Nature *424*, 452-456.
Yan, B., Calderwood, D.A., Yaspan, B., and Ginsberg, M.H. (2001). Calpain cleavage promotes talin binding to the beta 3 integrin cytoplasmic domain. The Journal of biological chemistry *276*, 28164-28170.
Yang, J., Zhu, L., Zhang, H., Hirbawi, J., Fukuda, K., Dwivedi, P., Liu, J., Byzova, T., Plow, E.F., Wu, J*., et al.* (2014a). Conformational activation of talin by RIAM triggers integrin-mediated cell adhesion. Nature communications *5*, 5880.
Yang, Y., Lee, W.S., Tang, X., and Wadsworth, W.G. (2014b). Extracellular matrix regulates UNC-6 (netrin) axon guidance by controlling the direction of intracellular UNC-40 (DCC) outgrowth activity. PloS one *9*, e97258.
Yao, M., Goult, B.T., Chen, H., Cong, P., Sheetz, M.P., and Yan, J. (2014). Mechanical activation of vinculin binding to talin locks talin in an unfolded conformation. Scientific reports *4*, 4610.
Yates, L.A., Lumb, C.N., Brahme, N.N., Zalyte, R., Bird, L.E., De Colibus, L., Owens, R.J., Calderwood, D.A., Sansom, M.S., and Gilbert, R.J. (2012). Structural and functional characterization of the kindlin-1 pleckstrin homology domain. The Journal of biological chemistry *287*, 43246-43261.
Ye, F., Hu, G., Taylor, D., Ratnikov, B., Bobkov, A.A., McLean, M.A., Sligar, S.G., Taylor, K.A., and Ginsberg, M.H. (2010). Recreation of the terminal events in physiological integrin activation. J Cell Biol *188*, 157-173.
Ye, F., Petrich, B.G., Anekal, P., Lefort, C.T., Kasirer-Friede, A., Shattil, S.J., Ruppert, R., Moser, M., Fassler, R., and Ginsberg, M.H. (2013). The mechanism of kindlin-mediated activation of integrin alphaIIbbeta3. Current biology : CB *23*, 2288-2295.
Yim, E.K., Pang, S.W., and Leong, K.W. (2007). Synthetic nanostructures inducing differentiation of human mesenchymal stem cells into neuronal lineage. Experimental cell research *313*, 1820-1829.

Yue, J., Xie, M., Gou, X., Lee, P., Schneider, M.D., and Wu, X. (2014). Microtubules regulate focal adhesion dynamics through MAP4K4. Developmental cell *31*, 572-585.
Zahreddine, H., Zhang, H., Diogon, M., Nagamatsu, Y., and Labouesse, M. (2010). CRT-1/calreticulin and the E3 ligase EEL-1/HUWE1 control hemidesmosome maturation in C. elegans development. Current biology : CB *20*, 322-327.
Zaidel-Bar, R., Cohen, M., Addadi, L., and Geiger, B. (2004). Hierarchical assembly of cell-matrix adhesion complexes. Biochemical Society transactions *32*, 416-420.
Zaidel-Bar, R., Itzkovitz, S., Ma'ayan, A., Iyengar, R., and Geiger, B. (2007). Functional atlas of the integrin adhesome. Nature cell biology *9*, 858-867.
Zamir, E., Katz, B.Z., Aota, S., Yamada, K.M., Geiger, B., and Kam, Z. (1999). Molecular diversity of cell-matrix adhesions. Journal of cell science *112 (Pt 11)*, 1655-1669.
Zamir, E., Katz, M., Posen, Y., Erez, N., Yamada, K.M., Katz, B.Z., Lin, S., Lin, D.C., Bershadsky, A., Kam, Z.*, et al.* (2000). Dynamics and segregation of cell-matrix adhesions in cultured fibroblasts. Nature cell biology *2*, 191-196.
Zhang, F., Saha, S., and Kashina, A. (2012). Arginylation-dependent regulation of a proteolytic product of talin is essential for cell-cell adhesion. The Journal of cell biology *197*, 819-836.
Zhang, F., Zhao, Y., and Han, Z. (2013). An in vivo functional analysis system for renal gene discovery in Drosophila pericardial nephrocytes. Journal of the American Society of Nephrology : JASN *24*, 191-197.
Zhang, H., Berg, J.S., Li, Z., Wang, Y., Lang, P., Sousa, A.D., Bhaskar, A., Cheney, R.E., and Stromblad, S. (2004). Myosin-X provides a motor-based link between integrins and the cytoskeleton. Nature cell biology *6*, 523-531.
Zhang, X., Jiang, G., Cai, Y., Monkley, S.J., Critchley, D.R., and Sheetz, M.P. (2008). Talin depletion reveals independence of initial cell spreading from integrin activation and traction. Nature cell biology *10*, 1062-1068.
Zhang, Y., Li, N., Caron, C., Matthias, G., Hess, D., Khochbin, S., and Matthias, P. (2003). HDAC-6 interacts with and deacetylates tubulin and microtubules in vivo. The EMBO journal *22*, 1168-1179.
Zhang, Y., Zhang, H., Liang, J., Yu, W., and Shang, Y. (2007). SIP, a novel ankyrin repeat containing protein, sequesters steroid receptor coactivators in the cytoplasm. The EMBO journal *26*, 2645-2657.
Zhu, J., Luo, B.H., Xiao, T., Zhang, C., Nishida, N., and Springer, T.A. (2008a). Structure of a complete integrin ectodomain in a physiologic resting state and activation and deactivation by applied forces. Mol Cell *32*, 849-861.
Zhu, Y., Kakinuma, N., Wang, Y., and Kiyama, R. (2008b). Kank proteins: a new family of ankyrin-repeat domain-containing proteins. Biochimica et biophysica acta *1780*, 128-133.
Ziegler, W.H., Liddington, R.C., and Critchley, D.R. (2006). The structure and regulation of vinculin. Trends in cell biology *16*, 453-460.

6. Acknowledgement

First of all, I would like to thank my PhD supervisor, Prof. Reinhard Fässler. Besides the fantastic infrastructure in his department, he generously provides me with finacial and material supports to accomplish my scientific goals. Throughout my PhD study, with his trust and patience, he creates a research environment with maximal freedom, supports my independent thinking and tolerates my stubbornness and stupidities. More importantly, he guides me through difficult periods of my research with open-minded and inspirational discussions. Most importantly, by working with him, I become a more professional and more disciplined scientist.

Second, I greatly appreciate my thesis advisory board members, Dr. Katja Strässer, Dr. Herbert Schiller, Dr. Carsten Grashoff, for their time and helpful discussion. Dr. Herbert Schiller introduced me to the lab and helped me to inititiate my first project. Dr. Carsten Grashoff kindly shared with me the unpublished data and materials from his lab.

Third, I would like to thank all my collaborators and those who provide technical assistance. I worked closed with Hui-Yuang Tseng from Prof. Reinhard Fässler's department and Dr. Sally J. Deeb from Prof. Matthias Mann's department in my project. Dr. Naoko Mizuno, Dirk Dedden and Katharina Austen provided critical material for my research. Dr. Madis Jakobson, Dr. Maik Veelders, Dr. Julien Polleux, Dr. Ralph Böttcher have provided helps with experiments within their expertise. Dr. Nagarjuna Nagaraj and Dr. Sabine Suppmann from the core facility provided excellent technical assistance regarding mass spectrometry and recombinant protein production. Dr. Armin Lambacher provided technical assistance with microscopy, which is critical for my research. I would also like to thank Dr. Olivier Rossier and Dr. Grégory Giannone, with whom I have ongoing collaboration, for cheerful and productive discussion.

Finally, I would like to thank my family, especially my wife for her continuous and selfless supports and my son for demonstrating another perspective of life.

Publications

Reseach articles

- Schiller, H.B., Hermann, M.R., Polleux, J., Vignaud, T., Zanivan, S., Friedel, C.C., Sun, Z.Q., Raducanu, A., Gottschalk, K.E., Thery, M., et al. (2013). beta(1)- and alpha(v)-class integrins cooperate to regulate myosin II during rigidity sensing of fibronectin-based microenvironments. ***Nat Cell Biol 15, 625.***

Highlighted in Faculty 1000 post-publication peer review.

- Sun, Z.Q. *, Gong, J.Y. *, Wu, H., Xu, W.Y., Wu, L.Z., Xu, D.J., Gao, J.L., Wu, J.W., Yang, H.Y., Yang, M.J., et al. (2013). Perilipin1 promotes unilocular lipid droplet formation through the activation of Fsp27 in adipocytes. ***Nat Commun 4.*** (*Equal contribution)

- Gong, J.*, Sun, Z.*, Wu, L., Xu, W., Schieber, N., Xu, D., Shui, G., Yang, H., Parton, R.G., and Li, P. (2011). Fsp27 promotes lipid droplet growth by lipid exchange and transfer at lipid droplet contact sites. ***J Cell Biol 195, 953-963.*** (*Equal contribution)

Cover story.
Highlighted in Faculty 1000 post-publication peer review.

- Nian, Z.*, Sun, Z.*, Yu, L.*, Toh, S.Y., Sang, J., and Li, P. (2010). Fat-specific protein 27 undergoes ubiquitin-dependent degradation regulated by triacylglycerol synthesis and lipid droplet formation. ***The Journal of biological chemistry 285, 9604-9615.*** (*Equal contribution)

Reviews

- Sun, Z.Q., Lambacher, A., and Fassler, R. (2014). Nascent Adhesions: From Fluctuations to a Hierarchical Organization. ***Curr Biol 24, R801-R803.***
- Sun, Z.Q., and Fassler, R. (2012). A firm grip does not always pay off: a new Phact(r) 4 integrin signaling. ***Gene Dev 26, 1-5.***
- Gong, J.Y., Sun, Z.Q., and Li, P. (2009). CIDE proteins and metabolic disorders. ***Curr Opin Lipidol 20, 121-126.***

Book chapters

- Sun, Z.Q., Gong, J.Y., Wu, L.Z., and Li, P. (2013). Imaging Lipid Droplet Fusion and Growth. ***Method Cell Biol 116, 253-268.***

8. Appendix

8.1. Publication 1

Kank family proteins comprise a novel type of talin activator (manuscript in preparation)

8.2. Publication 2

β1- and αv-class integrins cooperate to regulate myosin II during rigidity sensing of fibronectin-based microenvironments

8.3. Publication 3

A firm grip does not always pay off: a new Phact(r) 4 integrin signaling

8.4. Publication 4

Nascent Adhesions: From Fluctuations to a Hierarchical Organization

Kank family proteins comprise a novel type of talin activator

Zhiqi Sun, Hui-Yuan Tseng, Sally J. Deeb, Dirk Dedden, Maik Veelders, Naoko Mizuno, Matthias Mann, Reinhard Fässler

Max Planck Institute of Biochemistry, Martinsried, Germany

Key words: integrin, adhesion, talin, actin

Running title: Kank proteins are talin activators

Abstract

We developed an integrative adhesome analysis by combining a focal adhesion enrichment index with integrin tail interactome to identify novel FA proteins. Using this approach we identified the evolutionarily conserved Kank protein family as novel FA proteins. Interestingly, Kank2 concentrates at the lateral border of FAs (which we term the FA belt), a previously unrecognized FA sub-compartment. Mechanistically, Kank directly binds the talin R7 domain through its evolutionarily conserved KN motif and promotes talin activation in a force- and F-actin-independent manner. Consequently, Kank2 induces and/or maintains the formation of active integrins and destabilizes talin-actin connection. Our data identify Kank family proteins as novel type of talin activator, which specifically stabilize integrin-talin complexes that are uncoupled from the actomyosin system.

Introduction

Mesenchymal migration relies on integrin receptors, a large family of α/β heterodimers that couple the extracellular matrix (ECM) to the actin cytoskeleton [1]. To allow cell adhesion and migration, integrins have to be activated. Integrin activation is characterized by shifting the unbound form of the integrin from a low to a high affinity conformation followed by ligand binding [2]. Ligand bound integrins then cluster and assemble a mechano-sensitive macro-protein complex (called the adhesome) around their cytoplasmic domains [3, 4]. The initial adhesion complex are small, short-lived nascent adhesions (NAs) formed at the periphery of cell protrusions. A limited number of NAs subsequently couple to F-actin and actomyosin-mediated pulling forces reinforce the integrin-ligand interaction and promote the recruitment of more proteins to form large, mature focal adhesions (FAs). The dynamic engagement between integrin and actomyosin serves as a molecular clutch that promotes both forward membrane protrusion and rearward traction force to drive cell migration [5].

Talin and kindlin directly bind to β integrin cytoplasmic tails and play key roles in integrin activation and coupling to actin [6]. Talin is a large, ~270 kD protein composed of an N-terminal FERM (protein 4.1, ezrin, radixin, moesin) domain, also called talin head domain (THD), and a long C-terminal rod domain consisting of 13 helical bundles (R1-R13 domains). The THD is divided into four subdomains (F0, F1, F2, F3). The F3 subdomain of the THD binds β integrin tails and negatively charged lipids on the plasma membrane, and mediates integrin activation. The rod domain contains two F-actin binding sites, several binding sites for RIAM, numerous binding sites for vinculin and a dimerization domain at the extreme C-terminus [7]. The F-actin binding through talin rod couples the integrin/talin complexes to actomyosin, which is required for adhesion re-enforcement and rigidity sensing.

Talin cycles between plasma membrane, where it activates integrins, and cytosol, where it adopts an auto-inhibited form, presumably as a compact globular dimer [8] with an intramolecular interaction between the F3 subdomain and the R9 domain [9, 10]. Since this interaction masks the integrin binding site, talin requires an activation step that disrupts the auto-inhibitory head-rod interaction. A prime candidate for talin activation is the Rap1 effector protein RIAM (Rap1–GTP-interacting adapter molecule), which binds the R8 helical bundle [11], relieves the autoinhibitory interaction and recruits talin to the plasma membrane [12, 13]. A second, potential talin activator is PtdIns(4,5)P_2 [10]. A splice isoform of phosphatidylinositol 4-phosphate 5-kinase type Iγ (PIPKIγ90) locally synthesizes

PtdIns(4,5)P_2 upon recruitment to FAs through direct binding to talin F3 subdomain [14]. Finally, the actin retrograde flow was shown to induce the high affinity state of αLβ2 (LFA-1) on T cells [15], although it is not clear whether talin is the target of the actin flow. However, it is clear from genetic studies that talin activation is a highly redundant process, as neither RIAM- nor PIPKIγ90-deficient mice have apparent phenotypes [16, 17].

In the present paper we developed a FA enrichment index to identify novel FA proteins through high-resolution quantitative mass spectrometry (MS). We identified the evolutionarily conserved Kank protein family as novel FA proteins. Kank family proteins consist of 4 members (Kank1-4) characterized by an N-terminal Kank (KN) motif, several central coil-coil domains and C-terminal ankyrin repeats [18]. Kank1 was shown to restrict microtubule outgrowth at cell cortex by recruiting Kif21a to liprin β1 [19]. Overexpressed Kank proteins inhibit stress fiber formation and migration probably by downregulating RhoA [20]. A single Kank ortholog in *C.elegans*, called VAB19, controls epidermis-muscle attachment [21], neuronal migration [22] and basement membrane sliding during vulval morphogenesis [23]. The Kank3 knockdown in zebrafish leads to epidermal detachment [24]. We found that Kank localizes to the outer border of FAs (which we term the FA belt) and to central fibrillar adhesion, and induces and/or maintains the formation of active integrins at sites lacking actomyosin coupling. Mechanistically, Kank directly binds the talin R7 domain through its evolutionarily conserved KN motif and promotes talin activation in a force- and F-actin-independent manner. Our data identify Kank as novel talin activator, which specifically stabilizes integrin-talin complex that are uncoupled from the actomyosin system.

Results

Kank is a novel FA protein

To identify highly enriched proteins in integrin adhesion sites, we seeded mouse kidney-derived fibroblasts for 3 hours on FN, isolated whole cell lysates and the crosslinked FA fraction and quantified their proteome using high-resolution mass spectrometry combined with the label free protein quantification algorithm (MaxLFQ) (suppl. Fig. 1a). We identified 7954 proteins in the total proteome and 2378 proteins in the corresponding FA-enriched protein fractions. Proteins that were highly abundant in the total proteome were over-represented in the FA-enriched subproteome (suppl. Fig. 1b) pointing to an abundance-dependent unspecific enrichment. We used the false discovery rate (FDR) controlled 2D annotation enrichment algorithm to systematically compare the relative abundance of functional categories between the total proteome and the FA-enriched subproteome and found that proteins involved in cell adhesion including the known adhesome proteins as well as ECM components were strongly enriched in the FA-enriched subproteome, while proteins from intracellular organelles and cytosol such as the endoplasmic reticulum, mitochondria, proteasome were significantly underrepresented in the FA-enriched protein fraction (suppl. Fig. 1c). To identify true FA proteins, we determined the enrichment for each protein of the FA fraction relative to the total proteome abundance (FA enrichment index; FAEI) by calculating ratios of MS-intensity in the FA-enriched subproteome and the total proteome (n=2378; Table S1, suppl. Fig. 1a). The FAEI fits a typical Gaussian distribution (Fig. 1a) with a correlation coefficient of $R2 > 0.98$. Among the proteins in the upper 10% quartile of the FAEI distribution (Table S1), were several novel proteins that have been shown to regulate potentially integrin-regulated processes such as cell adhesion or migration. They include the Kank family member Kank2 (Fig. 1a), three kinases (Csnk1a1, Taok1 and CDK11b) and two phosphatases (Ptp4a2 and Ppp1cc, Table S1).

To identify novel adhesome proteins that associate with β1 integrin tails, we overlaid the FAEI with MS results of β1 integrin tail peptide pulldowns from whole cell lysate. Several known FA proteins enriched with β1 tail peptide pulldown including talin, kindlin and the members of the IPP complex showed high FAEI scores. Proteins such as Dab2 [25], known to bind β1 tails during endocytosis, or SNX17 [26], known to bind β1 tails in the endosomal compartment displayed a low FAEI score. Interestingly, Kank2 was among the proteins that showed a high FAEI score and strong β1 tail binding (Fig. 1a, b). Unlike kindlin2 or c-Src, which preferentially bind β1 and β3 integrin tails respectively, Kank2 bound β1 and

β3 tails with similar efficiencies (Fig. 1c). Immunostaining with polyclonal anti-Kank2 antibodies revealed Kank2-positive puncta closely attached to mature FAs (Fig.1d arrow heads). The nuclear signal is likely unspecific, as it remained in Kank2-depleted cells (data not shown). Interestingly, Kank2-specific immunostaining signals were absent from small NAs. The absence of Kank2 from NAs was confirmed by inhibiting myosin-II with blebbistatin. While blebbistatin-treated cells showed no Kank2 co-localisation with paxillin in NAs at protruding cell membranes (Fig. 1d), Kank2 and paxillin overlapped in thin and long trailing tails (Fig. 1d). Using line intensity profile measurements we observed that endogenous Kank2 puncta peaked at the outer border of FAs (termed FA belt) where conventional FA proteins including talin, kindlin-2, ILK, paxillin and vinculin showed ~50% of their plateau intensity (Fig. 1e-g).

To test whether the localisation of Kank2 to the FA belt depends on the presence of a specific FN-binding integrin class, we overexpressed Kank2-GFP in cells expressing α5β1 and/or αvβ3 and αvβ5 integrins [27], seeded them on FN and determined Kank2 localisation. The experiments revealed that overexrpessed Kank2-GFP localized to the FA belt in β1 as well as αv-class integrin expressing fibroblasts (suppl. Fig 1d), indicating that FA belt localization of Kank2 is integrin class-independent.

Kank is targeted to FAs via the KN motif

To determine the protein domain(s) of Kank2 that is(are) responsible for Kank2 recruitment to FA belt, we generated GFP-tagged Kank2 expression constructs lacking evolutionarily conserved domains (Fig. 2a): the Kank2ΔKN-GFP lacked the Kank (KN) motif; the Kank2ΔCoil-GFP lacked the liprin-binding coiled-coil domain; the Kank2(1-670)-GFP lacked the Kif21a-binding C-terminal ankyrin repeats; and the Kank2ΔKNΔCoil-GFP lacked the KN and coil-coil domains. The constructs were stably transduced into FN-cultured, Kank2-depleted cells (Fig. 2b), and immunostained for paxillin and for F-actin with phalloidin. Similar to endogenous Kank2, full length Kank2-GFP localized to the belt of paxillin-positive FAs and to fibrillar adhesions. In sharp contrast, Kank2ΔKN-GFP did not concentrate on FA belts and fibrillar adhesion but accumulated outside FAs (Fig. 2c-e) co-localizing with liprin β1 (suppl. Fig. 2a). Kank2ΔCoil-GFP and Kank2(1-670)-GFP localized to FA belts and to fibrillar adhesions (Fig. 2c-e), indicating that liprin β1 or Kif21a are not required for FA belt localization of Kank2. Interestingly however, Kank2 could recruit liprin-β1 to FA belt through the coiled-coil domain (suppl. Fig.2a). Kank2ΔKNΔCoil-GFP was diffusely distributed throughout the cytosol (Fig. 2c). To test whether the KN

motif alone is sufficient for FA belt localization, we transduced Kank2-depleted cells with a GFP-tagged KN construct and found a complete overlap of GFP with paxillin (Fig. 2c). These findings indicate (i) that the KN motif is essential to localize Kank2 to FA belts and fibrillar adhesions, (ii) that neither the coil-coil nor the ankyrin repeats are required for Kank2 targeting to the FA belt or exclusion from the FA center, and (iii) that the KN motif peptide is not sufficient to restrict Kank2 localisation to the FA belt.

To test whether the Kank2-KN motif associates with β1 integrin cytoplasmic tails, we performed β1 tail pull downs with lysates from Kank2-depleted cells expressing the GFP-tagged Kank2 expression constructs (Fig. 2a,b) and found that Kank2-GFP and KN-GFP but not GFP or Kank2ΔKN-GFP associated with β1 integrin tail peptides (Fig. 2f,g). In line with the high sequence conservation of the KN motifs from Kank1-4, the GFP-tagged KN motifs from Kank1, Kank3 and Kank4 localized to paxillin-positive FAs (suppl. Fig. 2b). Interestingly, when expressed at similar levels as judge by GFP intensity, Kank1-GFP and Kank3-GFP localized to FA belts, while Kank4-GFP did not show a clear FA belt localization, probably due to its additional diffused localization in the cytoplasm (suppl. Fig. 2c).

The talin rod binds the KN motif of Kank2

Pull down experiments of Kank2 with different wild type and mutant integrin tail peptides from wild type fibroblast lysates revealed that β2 integrin tails had the highest affinity for Kank2, β1 tails an intermediate affinity and β5 tails the lowest affinity (Fig. 3a). Interestingly, the binding profile of Kank2 overlapped with that of talin but not kindlin-2 (Fig. 3a), suggesting that talin and Kank2 are co-recruited to integrin tails. In line with this hypothesis, β1 tails, in which the tyrosine-783 was substituted with alanine (β1-Y783A), neither pulled down Kank2 nor talin, but still kindlin-2 (Fig. 3a). To identify novel Kank2 interacting proteins, we expressed GFP alone or GFP-tagged Kank2 in fibroblasts, performed GFP pull-downs and determined their interactors by MS. In line with a previous report, we identified liprin β1 as a binding partner of Kank2 [19]. Furthermore, talin-1 and two dynein light chain isoforms (Dynll1/LC8a and Dynll2/LC8b) were also among Kank2 interacting proteins (Fig. 3b). Strikingly, while β1 integrin tails specifically recruited talin and Kank2 in tyrosine 783-dependent manner, deletion of talin-1 and talin-2 genes in fibroblasts completely abolished Kank2 recruitment to β1 integrin tails (Fig. 3c), indicating that Kank2 recruitment to integrin tails is indeed talin-dependent. To test whether Kank2 forms a complex with talin through the KN motif, we performed GST pull downs with

recombinant GST-KN motif and recombinant talin head domain (THD) or full length talin-1 (suppl. Fig. 3a). These experiments revealed that the GST-KN motif efficiently pulled down full length talin-1 but not the THD (Fig. 3d) indicating that Kank2 is recruited to β integrin tails through a direct interaction between the KN motif and the talin rod. Fluorescence correlation microscopy measurements revealed a binding affinity of 230±70 nM (mean ± error represents 95% confidence interval) between recombinant full length talin and fluorescently labelled KN peptide (suppl. Fig. 3b). To further narrow down the KN-binding site on the talin rod we expressed different GFP-tagged Talin rod domains in fibroblasts, prepared cell lysates, incubated the cell lysates with the recombinant GST-KN motif and immunoprecipitated protein complexes with anti-GFP antibodies. The experiments revealed that the R7R8 domains of the talin rod bind the GST-KN motif (suppl. Fig. 3c). Altogether these findings show that the KN motif of Kank2 can directly bind the R7R8 domains of Talin.

Kank2 induces Talin and β1 integrin activation

The R7R8 domains were shown to bind RIAM, actin and vinculin [28], all of which can induce and/or maintain the active, integrin binding state of talin. Therefore, we tested whether Kank2 binding to the R7R8 domains also controls talin-integrin interactions. First, we incubated normal fibroblast cell lysates with bacterially expressed, recombinant GST-KN polypeptides or chemically synthesized KN peptides and subsequently performed β1 integrin tail pulldowns. The experiments revealed that GST-KN as well as the synthesized KN peptide efficiently displaced endogenous Kank2 from β1 integrin tail peptides and strongly increased talin binding but affected neither kindlin2 nor Dab2 binding (Fig. 4a; suppl. Fig. 4a-d). Second, we depleted Kank2 using specific shRNA and found that Kank2 depletion decreased binding of endogenous talin to β1 integrin tail peptides by ~30% (Fig. 4b), while overexpression of full length Kank2-GFP but not Kank2ΔKN-GFP increased talin binding to β1 integrin tails in a dose-dependent manner (suppl. Fig. 4e, f). Third, we incubated equal molar (10nM) recombinant full length talin protein with either GST-KN or GST and performed integrin tail peptide pulldown assays *in vitro*. We observed that the GST-KN protein but not GST significantly increased talin binding to β1 integrin tails and that GST-KN was co-recruited with talin to β1 integrin tail (Fig. 4c). Finally, co-expression of talin-GFP with Cherry-tagged Kank2, Kank2ΔKN and Kank2-KN in Kank2-depleted fibroblasts revealed that Kank2 as well as Kank2-KN enhanced localization of talin-GFP to kindlin2-positive adhesion sites, while Kank2ΔKN or Cherry left talin-1-GFP to a large

extent in the cytosol (Fig. 4d,e). These findings clearly indicate that Kank2 induces and/or maintains talin binding to integrin β tails through the KN motif.

Since the activation of talin is a pre-requisite for integrin activation we next tested whether Kank2 regulates integrin activation. To this end, we overexpressed Kank2-GFP, Kank2ΔKN-GFP, KN-GFP or GFP in fibroblasts, seeded them on FN and immunostained them with the activation epitope reporting antibody 9EG7. We found that overexpressed Kank2-GFP or KN-GFP co-localized with 9EG7-positive β1 integrins and increased active β1 integrin clusters in the central cell area, while overexpression of Kank2ΔKN-GFP had no influence on the active integrin clusters at the ventral cell cortex compared with GFP alone (Fig.4f,g).

Kank2 regulates Talin turnover, adhesion remodeling and cell migration

It has been shown that overexpression of Kank2 proteins suppressed stress fiber formation [18]. We next co-stained 9EG7 epitope with phalloidin in cell expressing GFP or Kank2-GFP. We noticed that Kank2-GFP strongly co-localized with active integrin clusters that were apparently not linked with thick stress fibers (suppl. Fig.5a). While Kank2-GFP overexpression consistently increased active β1 integrin clusters, the phalloidin-stained F-actin in 9EG7-positive area is significantly reduced (suppl. Fig.5b, c), suggesting that Kank2 may dislodged F-actin from talin. It has been has been shown that talin binding to F-actin plays the dominant role in immobilizing talin within adhesion sites [29, 30]. To test whether Kank2 regulates talin turnover, we performed fluorescence recovery after photobleaching (FRAP) in central adhesion sites of Kank-2-deplted fibroblasts expressing Kank2-mCherry, Kank2ΔKN-mCherry, KN-mCherry or mCherry alone. While neither Kank2ΔKN, nor the KN motif alone affected the mobile fraction of talin in comparison with mCherry control, expression of full length Kank2 increased the mobile fraction of Talin from 63.8±9.0% to 92.4±7.5% (Fig. 5a-c) suggesting that talin is almost completely decoupled from F-actin by full length Kank2. Interestingly, however, when we calculated the recovery rates of talin-GFP by measuring κ ($1/\tau_{1/2}$) we noticed that full length Kank2 but not Kank2ΔKN reduced the recovery rates of Talin by ~50% (Fig.5b,d), which indicates that Talin associated with Kank2 undergoes a more stable association to β integrin tails. While the KN motif alone did not change the mobile fraction of Talin in adhesion sites, it reduced Talin recovery rates in comparison to mCherry, although not to the same extent as full length Kank2 (Fig. 5d).

Next we examined whether Kank2-induced talin turnover changes adhesion dynamics. To this end, we expressed talin-TagRFP in Kank2-depleted cells rescued with either Kank2-GFP or Kank2ΔKN-GFP and imaged individual adhesion sites over a period of 10 min. In Kank2 expressing cells, talin- TagRFP-positive central adhesions underwent rapid lateral sliding movements and shape remodeling (Fig. 5e; suppl. Movie 1). In sharp contrast, in cells expressing Kank2ΔKN, talin-TagRFP-positive central adhesions remained largely immobile before disassembly (Fig. 5e; suppl. Movie 2). As revealed in color-overlaid time lapse images, Kank2-GFP but Kank2ΔKN-GFP induced adhesion sliding throughout the cell (Fig, 5f). Tracking the mass center of the adhesion sites revealed that expression of full length Kank2 induced a significantly higher adhesion sliding velocity in comparison to expression of Kank2ΔKN (Fig, 5g). Moreover, we observed rapid extensional growth of the adhesion structure in cells expressing full length Kank2 (suppl. Fig. 5d; suppl. Movie 3), suggesting that Kank2 is able to promote de novo assembly of adhesion structure. Altogether these findings suggest that Kank2 regulates talin turnover and adhesion remodeling both by stabilizing talin-integrin complexes and by destabilizing talin-actin linkage.

Increased adhesion sliding is correlated with reduced migration [31]. To test whether Kank2 influences integrin-mediated 2D random cell migration, we depleted ~90% of Kank2 using 2 independent shRNA in fibroblasts (Fig. 6a). Kank2 depletion significantly increased cell migration velocity (Fig. 6b), while directional persistence or β1 integrin expression remained unaffected (Fig.6a and data not shown). Conversely, overexpression of Kank2 (Fig. 6c) reduced migration velocity, regardless whether serum was present or absent during the experiment (Fig. 6d). Finally, the accelerated migration speed of Kank2 knockdown cells was normalized by re-expressing full length Kank2-AcGFP but not Kank2ΔKN-AcGFP or Kank2-KN-AcGFP as measured by mean square displacement (Fig. 6.e,f). Together these result indicate that Kank2 suppresses cell migration by stabilizing talin-integrin complex in the absence of stress fiber coupling.

Discussion

Recent advances in focal adhesion isolation and proteomic analysis provided comprehensive profiling of integrin adhesome [4]. However, the protein enrichment analysis based on spectral counting or label free quantification (LFQ) in biochemical fractions are biased by the protein abundance in the raw material [32]. By normalizing the LFQ intensities in purified FA with total expression level, we derived the FA enrichment index (FAEI), which reflects the enrichment of each protein in the FA fraction regardless of its expression level. Combined with β1 integrin tail interactome, we identified Kank2 as a novel component in integrin binding complex. The evolutionarily conserved Kank family proteins have been implicated in cell-ECM adhesion. For instance, Kank homologue, vab19 in *C.elegans* act synergistically with integrin to restrict basement membrane sliding during vulval morphogenesis [23]. Importantly, mutations of Kank1, Kank2 and Kank4 in human lead to nephrotic syndrome [33], which is often caused by defects in integrin-mediated adhesion or hyper-activated Rho GTPase [34, 35]. Kank1 deletion results in cerebral palsy type 2, spastic quadriplegic (CPSQ2) which could be due to neuronal migration defects [36].

Kank2 is connected to integrin through talin as Kank2 recruitment to integrin tail was abolished in talin-1 and talin-2 double knockout cells. We found direct interaction between KN motif in Kank2 and R7 domain in talin rod. Talin is autoinhibited in the cytoplasm by intramolecular interaction between F3 domain in talin head the R9 in talin rod. Its activation is thought to be mediated by Rap1-RIAM complex and $PI(4,5)P_2$ at the plasma membrane. Activated talin couples integrin with actomyosin system through direct and indirect F-actin binding. The affinity between KN motif and full length Talin measured with FCS is 230±70nmol, in the same range of talin auto-inhibitory interaction. R7 and R8 domains have unique folding with R8 domain inserted in R7 domain. Strikingly, Kank2 binding to talin induced talin activation. Notably, Kank-mediated talin activation could be reconstituted in either cell lysate or recombinantly *in vitro* in a force and F-actin-independent manner. Accordingly, Kank2 promotes translocation of overexpressed talin from cytosol to adhesion sites in KN motif-dependent manner. Consistent with the role of talin in integrin activation, overexpression of Kank2 but not KN motif deletion mutant induced more active β1 integrin clusters in adherent cells. Since R7R8 domain also contains high affinity binding sites for RIAM, vinculin and F-actin, all of which are implicated in talin activation, our data indicate that R7R8 fusion domain contains talin activation motifs where protein interactions disturb talin auto-inhibitory conformation.

Whether other proteins (e.g. DLC1 and synemin) [37, 38] that also bind R7R8 domain have similar talin activation activity needs further investigation.

Intriguingly, endogenous and ectopically expressed Kank2 as well as other Kank homologs concentrate at the lateral border of focal adhesions (FA belt) and fibrillar adhesions but not in nascent adhesions. This localization relies on the interaction with talin as KN motif deletion mutant failed to associate with adhesion border but localized to liprin-β1-positive cortical complex ~200nm away from FA border. Thus Kank2 marks the FA belt as a novel FA sub-compartment. The FA belt localization of Kank2 is independent of integrin subtype since Kank2 concentrates at FA belt in cell expressing only α5β1 integrin or αVβ3/β5 integrins. Notably, KN motif alone was not restricted to FA border but also penetrated into the center of FA, indicating that an unknown structural or functional feature in full length Kank2 excludes it from FA center. It has been shown that RIAM and vinculin compete for talin binding and localize to nascent adhesion and focal adhesion respectively in mutually exclusive manner [39, 40]. Similarly, Kank2 may be excluded from FA center by steric hindrance with other talin interacting molecules.

FA center is linked to thick stress fibers and exerts mechanical tension. Overexpression of Kank proteins has been shown to attenuate stress fiber formation at least partially through down-regulating RhoA activity probably by recruiting RhoGDI [33]. We hypothesize that Kank proteins may locally dislodge F-actin from talin-integrin complex. In comparison with the dynamic interaction between talin head domain and integrin, the F-actin binding through talin rod plays a dominant role in talin immobilization within FA. Our FRAP analysis of talin dynamics revealed that Kank2 but not KN motif deletion mutant increased the talin mobile fraction from ~65% to ~94%. Thus Kank2 almost induced complete mobilization of talin within adhesion, indicating that it destabilized talin's linkage to F-actin. On the other hand, Kank2 but not KN motif deletion mutant slowed the talin recovery rate in the mobile fraction, indicating a reduced off-rate due to stabilized talin-integrin complex. Consistent with its FA center localization, KN motif reduced talin recovery rate but failed to mobilize talin. These data suggests that Kank2 uncoupled talin-mediated integrin activation from actomyosin linkage. Consistent with this hypothesis, Kank2 co-localized with active β1 integrin clusters that appeared not linked to stress fibers. Mechanistically it is difficult to envision how Kank2 controls talin coupling to F-actin. Since Kank2 interacts with central region in Talin rod, calpain-dependent cleavage between talin head and rod is unlikely to be the cause. Kank2 binding may directly pose steric hindrance for F-actin binding on talin.

Post-translational modification may also be involved since methylation of Talin C-terminal F-actin binding site by methyltransferase Ezh2 partially liberates Talin from F-actin [41]. Kank2 may also locally inhibit RhoA activity through RhoGDI and thus suppress F-actin filament assembly.

Integrin-mediated cell migration is driven by the molecular clutch between integrins and actomyosin system [5]. The migration velocity is determined by the balance between clutch engagement and adhesiveness [42, 43]. Stationary fibroblasts exhibit more sliding adhesions, reflecting uncoupled actomyosin connection to ECM and reduced catch-bond interaction [31]. DNA hairpin-based digital force sensor revealed that certain adhesion plaques in the cell do not apply force to their ECM ligands [44]. Consistent with our FRAP analysis, Kank2-GFP and talin-1-TagRFP positive adhesion structures underwent rapid sliding movement and shape deformation, suggesting a slip-bond behavior. In sharp contrast, in cells expressing mutant Kank2 lacking KN motif, talin-1-TagRFP-labeled adhesions remained static and underwent only slight uniaxial movement likely along stress fiber. Our observations suggest that Kank2 could maintain adhesive structure with a slip-bond interface and prevented its conversion to a catch-bond interface. While the catch-bond interface applies pulling force to drive cell migration, slip-bond interface provides frictional adhesiveness that inhibits cell migration. In this sense, the excessive basement membrane sliding in vab-19 mutant in *C.elegans* may be caused by reduced cell adhesiveness and increase cell traction force on the ECM. Indeed, Kank2 overexpression strongly suppressed random cell migration velocity. Conversely, Kank2 knockdown led to increase cell migration speed. Although KN motif alone is able to activate talin, it is required in the full length Kank2 but not sufficient by itself to reduce cell migration velocity in Kank2-depleted cells.

Besides regulating talin activation and talin-actin linkage, Kank proteins may control cell migration by regulating local ECM degradation. We have identified liprin-β1 and two dynein light chain subunits dynll1 and dynll2 as Kank2 binding partners. Kank1 has been shown to interact with liprin-β1 and restrict cortical microtubule (MT) growth by recruiting Kif21a [19]. Although we did not find Kif21a in Kank2 interactome probably due to its low expression in fibroblasts, dynein motors are also involved in MT capture on cell cortex [45]. Liprin-β1 forms large protein complex containing at least liprin-α, ELKS and LL5, which captures MT plus end protein CLASPs and mediates focal exocytosis of MT1-MMP around FAs [19, 46-48]. Local metalloprotease exocytosis then facilitates FA disassembly. Although

liprin interaction is not required for Kank2's FA belt localization, Kank2 could recruit liprin-β1 to FA belt. Moreover, in the absence of talin binding, Kank2ΔKN mutant fully colocalized with liprin-β1. Thus, Kank2 is not only able to participate into both integrin-talin and liprin complex but also further bridge these two complexes. Whether Kank proteins coordinate integrin activation with local exocytosis will be investigated in the future.

Despite the importance of talin activation, neither PIPKIγ90 knockout mice nor RIAM knockout mice display obvious developmental defect [16, 17], suggesting that Talin activation mechanisms may be highly redundant in vivo. Moreover, RIAM knockdown decreased melanoma cell migration [49] whereas a Talin mutant with disrupted auto-inhibition led to delayed dorsal epidermal closure in drosophila [50]. Together with these observations, our data support the existence of redundant and more importantly, functionally distinct talin activation mechanisms. Different talin activation modes have different migratory effects according to differential actomyosin or membrane coupling.

References

1. Hynes, R.O. Integrins: bidirectional, allosteric signaling machines. *Cell* **110**, 673-687 (2002).
2. Luo, B.H., Carman, C.V. & Springer, T.A. Structural basis of integrin regulation and signaling. *Annu Rev Immunol* **25**, 619-647 (2007).
3. Schiller, H.B. & Fassler, R. Mechanosensitivity and compositional dynamics of cell-matrix adhesions. *EMBO reports* **14**, 509-519 (2013).
4. Winograd-Katz, S.E., Fassler, R., Geiger, B. & Legate, K.R. The integrin adhesome: from genes and proteins to human disease. *Nature reviews. Molecular cell biology* **15**, 273-288 (2014).
5. Gardel, M.L., Schneider, I.C., Aratyn-Schaus, Y. & Waterman, C.M. Mechanical integration of actin and adhesion dynamics in cell migration. *Annual review of cell and developmental biology* **26**, 315-333 (2010).
6. Calderwood, D.A., Campbell, I.D. & Critchley, D.R. Talins and kindlins: partners in integrin-mediated adhesion. *Nature reviews. Molecular cell biology* **14**, 503-517 (2013).
7. Critchley, D.R. Biochemical and structural properties of the integrin-associated cytoskeletal protein talin. *Annual review of biophysics* **38**, 235-254 (2009).
8. Goult, B.T. *et al.* Structural studies on full-length talin1 reveal a compact auto-inhibited dimer: implications for talin activation. *Journal of structural biology* **184**, 21-32 (2013).
9. Song, X. *et al.* A novel membrane-dependent on/off switch mechanism of talin FERM domain at sites of cell adhesion. *Cell research* **22**, 1533-1545 (2012).
10. Goksoy, E. *et al.* Structural basis for the autoinhibition of talin in regulating integrin activation. *Molecular cell* **31**, 124-133 (2008).
11. Chang, Y.C. *et al.* Structural and mechanistic insights into the recruitment of talin by RIAM in integrin signaling. *Structure* **22**, 1810-1820 (2014).
12. Han, J. *et al.* Reconstructing and deconstructing agonist-induced activation of integrin alphaIIbbeta3. *Current biology : CB* **16**, 1796-1806 (2006).
13. Lafuente, E.M. *et al.* RIAM, an Ena/VASP and Profilin ligand, interacts with Rap1-GTP and mediates Rap1-induced adhesion. *Developmental cell* **7**, 585-595 (2004).
14. Legate, K.R. *et al.* Integrin adhesion and force coupling are independently regulated by localized PtdIns(4,5)2 synthesis. *The EMBO journal* **30**, 4539-4553 (2011).
15. Comrie, W.A., Babich, A. & Burkhardt, J.K. F-actin flow drives affinity maturation and spatial organization of LFA-1 at the immunological synapse. *The Journal of cell biology* **208**, 475-491 (2015).
16. Legate, K.R., Montag, D., Bottcher, R.T., Takahashi, S. & Fassler, R. Comparative phenotypic analysis of the two major splice isoforms of phosphatidylinositol phosphate kinase type Igamma in vivo. *Journal of cell science* **125**, 5636-5646 (2012).
17. Stritt, S. *et al.* Rap1-GTP-interacting adaptor molecule (RIAM) is dispensable for platelet integrin activation and function in mice. *Blood* **125**, 219-222 (2015).
18. Kakinuma, N., Zhu, Y., Wang, Y., Roy, B.C. & Kiyama, R. Kank proteins: structure, functions and diseases. *Cellular and molecular life sciences : CMLS* **66**, 2651-2659 (2009).
19. van der Vaart, B. *et al.* CFEOM1-associated kinesin KIF21A is a cortical microtubule growth inhibitor. *Developmental cell* **27**, 145-160 (2013).
20. Kakinuma, N., Roy, B.C., Zhu, Y., Wang, Y. & Kiyama, R. Kank regulates RhoA-dependent formation of actin stress fibers and cell migration via 14-3-3 in PI3K-Akt signaling. *The Journal of cell biology* **181**, 537-549 (2008).

21. Ding, M., Goncharov, A., Jin, Y. & Chisholm, A.D. C. elegans ankyrin repeat protein VAB-19 is a component of epidermal attachment structures and is essential for epidermal morphogenesis. *Development* **130**, 5791-5801 (2003).
22. Yang, Y., Lee, W.S., Tang, X. & Wadsworth, W.G. Extracellular matrix regulates UNC-6 (netrin) axon guidance by controlling the direction of intracellular UNC-40 (DCC) outgrowth activity. *PloS one* **9**, e97258 (2014).
23. Ihara, S. *et al.* Basement membrane sliding and targeted adhesion remodels tissue boundaries during uterine-vulval attachment in Caenorhabditis elegans. *Nature cell biology* **13**, 641-651 (2011).
24. Boggetti, B. *et al.* NBP, a zebrafish homolog of human Kank3, is a novel Numb interactor essential for epidermal integrity and neurulation. *Developmental biology* **365**, 164-174 (2012).
25. Ezratty, E.J., Bertaux, C., Marcantonio, E.E. & Gundersen, G.G. Clathrin mediates integrin endocytosis for focal adhesion disassembly in migrating cells. *The Journal of cell biology* **187**, 733-747 (2009).
26. Bottcher, R.T. *et al.* Sorting nexin 17 prevents lysosomal degradation of beta1 integrins by binding to the beta1-integrin tail. *Nature cell biology* **14**, 584-592 (2012).
27. Schiller, H.B. *et al.* beta1- and alphav-class integrins cooperate to regulate myosin II during rigidity sensing of fibronectin-based microenvironments. *Nature cell biology* **15**, 625-636 (2013).
28. Gingras, A.R. *et al.* Central region of talin has a unique fold that binds vinculin and actin. *The Journal of biological chemistry* **285**, 29577-29587 (2010).
29. Himmel, M. *et al.* Control of high affinity interactions in the talin C terminus: how talin domains coordinate protein dynamics in cell adhesions. *The Journal of biological chemistry* **284**, 13832-13842 (2009).
30. Rossier, O. *et al.* Integrins beta1 and beta3 exhibit distinct dynamic nanoscale organizations inside focal adhesions. *Nature cell biology* **14**, 1057-1067 (2012).
31. Smilenov, L.B., Mikhailov, A., Pelham, R.J., Marcantonio, E.E. & Gundersen, G.G. Focal adhesion motility revealed in stationary fibroblasts. *Science* **286**, 1172-1174 (1999).
32. Mellacheruvu, D. *et al.* The CRAPome: a contaminant repository for affinity purification-mass spectrometry data. *Nature methods* **10**, 730-736 (2013).
33. Gee, H.Y. *et al.* KANK deficiency leads to podocyte dysfunction and nephrotic syndrome. *The Journal of clinical investigation* (2015).
34. Gee, H.Y. *et al.* ARHGDIA mutations cause nephrotic syndrome via defective RHO GTPase signaling. *The Journal of clinical investigation* **123**, 3243-3253 (2013).
35. Tian, X. *et al.* Podocyte-associated talin1 is critical for glomerular filtration barrier maintenance. *The Journal of clinical investigation* **124**, 1098-1113 (2014).
36. Lerer, I. *et al.* Deletion of the ANKRD15 gene at 9p24.3 causes parent-of-origin-dependent inheritance of familial cerebral palsy. *Human molecular genetics* **14**, 3911-3920 (2005).
37. Li, G. *et al.* Full activity of the deleted in liver cancer 1 (DLC1) tumor suppressor depends on an LD-like motif that binds talin and focal adhesion kinase (FAK). *Proceedings of the National Academy of Sciences of the United States of America* **108**, 17129-17134 (2011).
38. Sun, N., Critchley, D.R., Paulin, D., Li, Z. & Robson, R.M. Identification of a repeated domain within mammalian alpha-synemin that interacts directly with talin. *Experimental cell research* **314**, 1839-1849 (2008).
39. Goult, B.T. *et al.* RIAM and vinculin binding to talin are mutually exclusive and regulate adhesion assembly and turnover. *The Journal of biological chemistry* **288**, 8238-8249 (2013).

40. Lee, H.S., Anekal, P., Lim, C.J., Liu, C.C. & Ginsberg, M.H. Two modes of integrin activation form a binary molecular switch in adhesion maturation. *Molecular biology of the cell* **24**, 1354-1362 (2013).
41. Gunawan, M. *et al.* The methyltransferase Ezh2 controls cell adhesion and migration through direct methylation of the extranuclear regulatory protein talin. *Nature immunology* (2015).
42. Palecek, S.P., Loftus, J.C., Ginsberg, M.H., Lauffenburger, D.A. & Horwitz, A.F. Integrin-ligand binding properties govern cell migration speed through cell-substratum adhesiveness. *Nature* **385**, 537-540 (1997).
43. Gupton, S.L. & Waterman-Storer, C.M. Spatiotemporal feedback between actomyosin and focal-adhesion systems optimizes rapid cell migration. *Cell* **125**, 1361-1374 (2006).
44. Blakely, B.L. *et al.* A DNA-based molecular probe for optically reporting cellular traction forces. *Nat Methods* **11**, 1229-1232 (2014).
45. Hendricks, A.G. *et al.* Dynein tethers and stabilizes dynamic microtubule plus ends. *Current biology : CB* **22**, 632-637 (2012).
46. Stehbens, S.J. *et al.* CLASPs link focal-adhesion-associated microtubule capture to localized exocytosis and adhesion site turnover. *Nature cell biology* **16**, 561-573 (2014).
47. Grigoriev, I. *et al.* Rab6 regulates transport and targeting of exocytotic carriers. *Developmental cell* **13**, 305-314 (2007).
48. Lansbergen, G. *et al.* CLASPs attach microtubule plus ends to the cell cortex through a complex with LL5beta. *Developmental cell* **11**, 21-32 (2006).
49. Colo, G.P. *et al.* Focal adhesion disassembly is regulated by a RIAM to MEK-1 pathway. *Journal of cell science* **125**, 5338-5352 (2012).
50. Ellis, S.J. *et al.* Talin autoinhibition is required for morphogenesis. *Current biology : CB* **23**, 1825-1833 (2013).

Figure legends

Figure 1. Identification of Kank2 as a novel component in integrin complex.

(a) Histogram of focal adhesion enrichment index (FAEI). (b) Scatter plot of β1 integrin tail peptide binding proteins overlay with coloration according to FAEI. The $\log_2$ SILAC ratio of proteins are plotted as the forward pulldown (x axis) against the reverse labelling pulldown (y axis). (c) Westernblot analysis of proteins complex assembled around β1 and β3 integrin tail peptides. (d) Mouse kidney fibroblasts are plated on fibronectin for 3hours, then treated with or without blebbistatin for 1hour, fixed and immunostained for endogenous Kank2, paxillin (Pxn, red), F-actin with phalloidin (blue) and DAPI (grey). Scale bar, 10μm. (e) Line profile analysis of focal adhesion stained with anti-Talin and anti-vinculin antibody together with Kank2. (f) Theoretical definition of the lateral border of focal adhesion and distance to FA border in line profile analysis. (g) Measurement of the distance between Kank2-postive puncta and FA border using different conventional FA protein markers including ILK, kindlin, vinculin, talin and paxillin. The Kank2-positive puncta structures locates at the lateral border of focal adhesion in line profile analysis.

Figure 2. KN motif is essential for Kank2 localization at FA border and recruitment to integrin tail complex.

(a) Domain organization of Kank2 protein and illustration of truncation/deletion mutant design. (b) Westernblot analysis of the expression level of endogenous Kank2 and reconstituted GFP-tagged Kank2 constructs using anti-Kank2 antibody and ant-GFP antibody in cell with stable Kank2 knockdown and reconstitutions with GFP-tagged Kank2 truncation/deletion mutants. Vinculin is used as loading control. (c) Immunofluorescence of GFP-tagged Kank2 constructs (green) co-stained with anti-Paxillin antibody (Pxn, red), phalloidin (blue) and DAPI (grey). Scale bar, 10μm. (d) Line profile analysis for localization of full length Kank2 and Kank2ΔKN mutant. (e) Quantification of the distance between indicated Kank2 wild type and mutants' localization to FA border indicates KN motif is required for FA association. Student t-test ***P<0.0001. (f)&(g) Integrin tail peptide pulldown and westernblot analysis showed that GFP-tagged full length Kank2 and KN motif along but not Kank2ΔKN mutant or GFP control could be recruited to integrin tail complex. Kank2 constructs were detected with anti-GFP antibody. Kindlin2 was used as positive control.

Figure 3. Kank2 is recruited to integrin tail complex through direct interaction with Talin.

(a) Westernblot (upper panel) and densitometry analysis (lower panel) of the recruitments of endogenous Kank2, kindlin2 and talin to wildtype β1, β2, β5 integrin tail and β1 integrin tail with tyrosine to alanine mutation at the position of tyrosine 783 in full length β1 integrin (β1 Y783A). β1 scrambled peptide (β1 scr) was used as universal control. Note that the binding profiles of Kank2 and talin completely overlapped with each other. (b) Scatter plot of LFQ-intensity ratio between Kank2-GFP pulldown and GFP control pulldown identified Ppfibp1, Dynll1, Dynll2 and talin-1 as strongest Kank2 binding partners. (c) Westernblot (upper panel) and densitometry analysis (lower panel) of the recruitments of endogenous Kank2, kindlin2 and talin to wildtype β1 tail and β1 Y783A mutant tail peptides from wildtype cells (Talin-1/2 flox/flox) or talin knockout cells (Talin-1/2 DKO). Kank2 recruitment to integrin tail strictly depends on the presence of talin. Student t-test ***P<0.0001. (d) GST pulldown of GST-KN fusion protein or GST control with full length recombinant talin-1 or talin-head domain (THD).

Figure 4. Kank2 activates talin and promote integrin activation

(a) Westernblot (left panel) and densitometry analysis (right panel) of the recruitments of endogenous Kank2, talin, kindlin-2 and Dab2 to β1 integrin tail peptide in the presence of exogenous KN-GST or GST recombinant protein. GST-KN recombinant protein replaced endogenous Kank2 but promoted Talin recruitment without affecting kindlin-2 or Dab2 binding. (b) Westernblot (left panel) and densitometry analysis (right panel) of the recruitments of endogenous Kank2, talin and kindling-2 to β1 integrin tail in control cells or Kank2-knockdown cells. (c) Westernblot (left panel) and densitometry analysis (right panel) show that purified GST-KN promotes recombinant talin-1 binding to β1 integrin tail in vitro. (d) Talin-AcGFP (shown in rainbow LUT) was co-transfected with Cherry-tagged full length Kank2, Kank2ΔKN mutant, KN motif along or cherry control into Kank2 knockdown cells. Cells are fixed and stained for kindling-2 (blue). Scale bar, 10μm. (e) Quantification of talin-AcGFP intensity ratio between kindling-2-positive adhesion area and kindling-2-negative cytosolic region in (d) revealed that Kank2 promoted talin localization to adhesion sites through KN motif. (f) Kank2 knockdown cells were transfected with GFP-tagged full length Kank2, Kank2ΔKN mutant, KN motif along or GFP control (green), plated on fibronectin and stained for active integrin with 9EG7 antibody (shown in rainbow LUT). Scale bar, 10μm. (g) Kank2 promote active integrin cluster

formation through KN motif. 9EG7 staining intensity per cell area is quantified from (f). Student t-test *P<0.05, **P<0.01, ***P<0.0001.

Figure 5. Kank2 regulate Talin turnover and adhesion dynamics.

(a) Representative timelapse images of Talin-1-AcGFP (shown in rainbow LUT) in FRAP experiments. Talin-1-AcGFP was co-transfected with Cherry-tagged full length Kank2 or Kank2ΔKN mutant into Kank2 knockdown cells. AcGFP signal is bleached in region of interest (ROI, red circle). (b) Fluorescence recovery curves corresponding to FRAP experiments in (a). Mean fluorescence intensity in ROI is plotted as the percentage of the initial intensity after normalization to cytosolic background. Fluorescent recovery curves from 6 FRAP experiments are fitted with one-phase association model (mean±s.d.). (c) Full length Kank2 but not Kank2ΔKN mutant or KN motif along increased talin-1 mobile fraction in adhesion sites. Mobile fraction is quantified from 10 independent FRAP experiment (mean ± sd. one-way ANOVA Tukey test, ***P<0.001). (d) Full length Kank2 and KN motif along but not Kank2ΔKN mutant reduced talin-1-AcGFP recovery rate. Recovery rate is quantified from 10 independent FRAP experiment (mean ± sd. one-way ANOVA Tukey test, *P<0.05, **P<0.01, ***P<0.0001). (e) Timelapse images of talin-1-TagRFP (rainbow LUT) and Kank2-GFP or Kank2ΔKN-GFP. Talin-1-Tag-RFP was co-transfected with Cherry-tagged full length Kank2 or Kank2ΔKN mutant into Kank2 knockdown cells. Scale bar, 5μm. (f) Color overlay of talin timelapse images from 0min (red), 5min (green) and 10min (blue). (g) Sliding velocities of talin-positive adhesion sites were plotted as box and whisker (min to max). Student t-test ***P<0.001.

Figure 6. Kank2 regulates cell migration through talin.

(a) Westernblot analysis of Kank2 and β1 integrin (Itgb1) expression in cells expressing scrambled shRNA control or two different Kank2 shRNA. B-actin is used as loading control. (b) Kank2 knockdown increased velocity of 2-D random migration on fibronectin. Data is illustrated as box and whisker (minimal to maximal value). Student t-test ***P<0.0001. (c) Westernblot analysis of Kank2 and β1 integrin (Itgb1) expression in cells expressing GFP control or Kank-GFP fusion protein. B-actin is used as loading control. (d) Kank2 overexpression decreased velocity of 2-D random migration on fibronectin with or without serum stimulation. Data is illustrated as box and whisker (minimal to maximal value). Student t-test ***P<0.0001. (e) Single cell tracking is plotted for Kank2 knockdown cells rescued with wild type Kank2, Kank2 lacking KN motif, KN motif alone or GFP control. (f)

Mean square displacement analysis showed that only full length Kank2 restored normal cell migration speeds in Kank2 knockdown cells.

Supplementary figure legends

Suppl. Figure 1

(a) Experiment work flow for mass spectrometry analysis and focal adhesion enrichment index (FAEI) calculation. (b) Histogram of LFQ intensity distribution of total proteome for all quantified proteins in whole cell lysates and those identified in isolated adhesion revealed that adhesion isolation method tends to enrich high abundance proteins. (c) False discovery rate (FDR) controlled 2D annotation enrichment analysis of the relative abundance of functional categories between the total proteome and the FA-enriched subproteome. (d) Kank2-EGFP was overexpressed in cells expressing only α5β1 or αvβ3/β5 integrins and stained for paxillin (Pxn, red), F-actin with phalloidin (blue) and DAPI (grey). Scale bar, 10μm.

Suppl. Figure 2

(a) Immunofluorescence of GFP-tagged Kank2 constructs (green) co-stained with anti-paxillin antibody (Pxn, blue), anti-liprin β1 antibody (red) and DAPI (grey). Scale bar, 10μm. (b) GFP-tagged KN motifs from Kank1, Kank3 and Kank4 are transfected into Kank2 knockdown cells and co-stained with anti-Paxillin antibody (Pxn, red), F-actin with phalloidin (blue) and DAPI (grey). Scale bar, 10μm. (c) GFP-tagged Kank1, Kank3 and Kank4 are transfected into normal fibroblasts and co-stained with anti-paxillin antibody (Pxn, red), F-actin with phalloidin (blue) and DAPI (grey). Scale bar, 10μm.

Suppl. Figure 3

(a) SDS-PAGE analysis of purified full length talin-1, talin head domain, GST-KN fusion protein and GST. (b) Fluorescence correlation spectroscopy measurement of complex formation between atto488-leabeled KN peptide and full length talin-1. (c) Different GFP-tagged talin rod truncations were overexpressed. Cell lysates were mixed with GST-KN motif and immunoprecipitated with anti-GFP antibody and analyzed with westerblot.

Suppl. Figure 4

(a-d) Westernblot (a, c) and densitometry analysis (b, d) of the recruitments of endogenous Kank2, talin, kindlin-2 to β1 integrin tail peptide in the presence of recombinant KN-GST (a, b) or chemically synthesized KN peptide (c, d). GST-KN recombinant protein and KN peptide replaced endogenous Kank2 but promoted talin recruitment without affecting kindlin-2 binding in a dose-dependent manner. (e, f) Westernblot and densitometry analysis of the recruitments of talin to β1 integrin tail in the

presence of different doses of overexpressed full length Kank2 or Kank2ΔKN mutant. Student t-test ***P<0.0001.

Suppl. Figure 5

(a) Kank2 knockdown cells reconstituted with GFP control or Kank2-GFP were stained for active integrin with 9EG7 antibody (red) and F-actin with phalloidin (grey). Lower enlarged boxed region shows that Kank2 strongly colocalized with 9EG7 but not phalloidin (see arrow heads). (b) Kank2 promote active integrin cluster formation. 9EG7 staining intensity per cell area is quantified from (a). Student t-test ***P<0.0001. (c) Quantification of F-actin linked to active β1 integrin. Phalloidin intensity in 9EG7-positive area is quantified from (a) and plotted as box and whisker (min to max). Student t-test ***P<0.001. (d) Timelapse images of Talin-1-TagRFP (rainbow LUT) and Kank2-GFP. Scale bar, 5μm.

Supplementary material and methods

Focal adhesion isolation

Focal adhesion isolation with chemical crosslinking was performed as previously described with minor modification. Serum-starved cells were plated on plastic dishes coated with10 µg ml−1 fibronectin at density of 1.5X106 cells per 10cm dish for 3hours. Cells were washed with PBS and crosslinked with 0.5mM DSP and 0.05mM DPDPB at r.t. for 5min and the crosslinker was quenched and washed with buffer containing 134mM NaCl, 50mM TrisHCl. Crosslinked cells were lysed with RIPA buffer (50mM Tris-Hcl pH7.5, 150mM NaCl, 1% Triton-X100, 0.2% SDS, 0.5% sodium deoxycholic acid, and EDTA-free protease inhibitor cocktail) for 30min at 4˚C. Plates were sprayed with high pressure water for 60 second to remove cellular material that was not covalently bound. Crosslinked materials were released in 3ml of lysis buffer (150mM NaCl, 50mMTrisHCl 7.5, 0.1%SDS) at 60°C for 60 minutes and precipitated with cold acetone. Protein pellets were re-dissolved in lysis buffer. Whole cell lysates were collected immediately after crosslinking and quenching in 100mM TrisHCl pH7.5, 4%SDS, 100mM DTT. Samples were snap-freezed in liquid nitrogen for further mass spectrometry sample processing. Experiments were performed in triplicate.

Mass spectrometry analysis

For focal adhesion enrichment index analysis, isolated focal adhesion fractions and total cell lysates were collected in parallel and samples were processed in FASP method. To calculate the FA enrichment index (FAEI), proteins with at least one valid LFQ intensity value in three replicates were filtered and matched according to uniprot ID. After imputation of missing values from normal distribution, ratios between average LFQ intensity in FA and average LFQ intensity in total proteome were calculated and fitted with a Gaussian distribution. FAEI is derived by normalizing mean value of Gaussian distribution to 0.

For in gel digestion and mass spectrometry analysis of EGFP pulldown samples, the samples were loaded on a gel and run for approximately 1 cm length and stopped mainly to incorporate all the proteins onto the gel rather than separating the proteins. Then the whole lane up to where the gel was run was then cut into 1mmX1mm pieces and subjected to a standard in-gel digestion protocol. Briefly the gel pieces were destained in ethanol followed by sequential reduction and alkylation with 10 mM dithiothreitol (DTT) and 40 mM

chloroacetamide (CAA). The gel pieces were then dried and incubated with digestion buffer containing 12.5 ng/µl of trypsin in 25mM Tris pH 8.5. Following overnight digestion the peptides were extracted and purified in StageTips and analyzed in LTQ-Orbitrap XL mass spectrometer. The raw data were processed using MaxQuant computational platform version 1.5.0.26.

Antibodies.

The following antibodies were used for western blotting (WB) and immunofluorescence (IF): GFP (A11122, Life Technologies, 1:1,1000 for WB), Kank2 (HPA015643, Sigma; 1:2,000 for WB and 1:800 for IF), Dab2 (610464, BD Transduction Laboratories, 1:1,000 for WB), actin (A-2066, Sigma; 1:3,000 for WB), β1 integrin (MAB1997, MB1.2, Chemicon; 1:800 for IF), GAPDH (CB1001, 6C5, Calbiochem; 1:5,000 for WB), Kindlin-2 (MAB2617, EMD Millipore 1:1,000 for WB and 1:800 for IF), paxillin (610051, 349, BD Transduction Laboratories, 1:800 for IF), talin-1 (T3287, 8d4, Sigma; 1:1,000 for WB, 1:200 for IF), talin-head specific antibody (sc-15336, Santa Cruz Biotechnology; 1:1000 for WB). A home-made β1-integrin antibodies was used for western blotting (1:10,000 for WB), Phalloidin (Alexa Fluor 546 and Alexa Fluor 647 conjugated, Molecular Probes; 1:50 for IF) was used to stain F-actin. DAPI (Sigma) was used to stain nuclei.

Plasmids and constructs.

cDNA encoding mouse Kank1 and Kank2 were cloned into pEGFP-N1 vector (Clontech) between XhoI and EcoRI sites. Mouse Kank3 was cloned into pEGFP-N1 vector between BglII and EcoRI sites. Mouse Kank4 was cloned into pEGFP-N1 vector between XhoI and AgeI sites. For retrovirus mediated overexpression, DNA fragment encoding Kank2 full length, Kank2ΔKN (a.a.31-56 deleted), Kank2ΔLID (a.a.181-240 deleted), Kank2ΔKNΔLID (a.a.31-56 and a.a.181-240 deleted), Kank2-1-670 (a.a 1-670) and KN motif (a.a. 29-72) were amplified via PCR and inserted between XhoI and EcoRI sites in pRetroQ-AcGFP-N1 vector. To generate NIH3T3 cells stably expressing Kank2-EGFP, AcGFP fragment was replaced with Kank2-EGFP or EGFP fragments from pEGFP-N1-Kank2 with XhoI and NotI cutting sites.

Plasmids for Talin-AcGFP and Talin-TagRFP expression in mammalian cells were generated from pLPCXmod-Talin-1-Ypet (gift from Dr. Carsten Grashoff). Ypet was replaced with either AcGFP sequence or TagRFP-T sequence. Various Talin rod

truncations were amplified with PCR and inserted between XhoI and EcoRI sites in pEGFP-N1 vector.

For retrovirus mediated stable knockdown of mouse Kank2, two shRNA targeting ATACTGTATTCTTGAGTCA (shKank2#1) and AGCCAGAAAGCCAAGCTAC (shKank2#2) in mouse Kank2 3'UTR region were cloned into pSuper.Retro.puro vector (OligoEngine) according to the manufacturer's instruction.

For recombinant protein production, cDNA encoding Kank2 KN motif (a.a 29-72) was inserted into pGEX-6P1 (GE Healthcare) between EcoRI and BamHI sites. Plasmid for recombinant Talin-1 head domain (a.a 405) was cloned in pCoofy vector. Plasmid for full length Talin-1 recombinant protein production (pET101-Talin-FL) was described before [citation].

Cell lines.

Mouse kidney fibroblasts carrying floxed αv and β1 alleles were cultured as previously described and used for focal adhesome analysis. Mouse kidney fibroblasts containing floxed β1-integrin allele were cultured as previously described. NIH3T3 mouse fibroblasts and hTert-RPE1 cells were cultured according to the recommendation of ATCC.

Transient and stable transfection/transduction.

Cells were transiently transfected with Lipofectamine 2000 (Invitrogen) according to the manufacturer's protocol. To generate stable cell lines, VSV-G pseudotyped retroviral vectors were produced by transient transfection of HEK293T (human embryonic kidney) cells. Viral particles were concentrated from cell culture supernatant as described previously and used for infection.

Expression and purification of recombinant proteins.

For GST fusion protein of KN motif, plasmids encoding GST–KN or GST alone were transformed into BL21 (DE3) and protein expression was autoinduced over night at 37˚C. 5g biomass was lysed with high pressure homogenizer in GST binding buffer (TrisHCl 50mM, NaCl 150mM, EDTA 1mM, DTT 1mM, pH 7.5). Protease inhibitor (AEBSF-HCl 1mM, Aprotinin 2µg/ml, Leupeptin 1µg/ml, Pepstatin 1µg/ml) and nuclease (Benzonase) were added during the cell lysis. After clarification, supernatant were incubated with Glutathione Sepharose 4 Fast Flow (GE Healthcare) for 3.5hour at 4˚C followed by 3 times

washing with GST binding buffer and elution with 50 mM Glutathione in the binding buffer. Elute fractions containing were pooled and desalted (Sephadex G-25 in Hi Prep 26/10) in buffer (TrisHCl 50mM, NaCl 150mM, 0.1mM DTT) and further purified with size-exclusion chromatography (Superdex 75 PC 3.2/30) in desalting buffer.

Full length talin recombinant protein production was optimized based on previously published protocol. Briefly, pET101-Talin-FL was transformed into BL21 (DE3) Gold and induced 1 mM IPTG at 18˚C overnight. After lysis with high pressure homogenizer in lysis buffer (50mM TrisHCl pH7.8, 500mM NaCl, 30mM imidazole, 1mM DTT) and clarification of the supernatant, full length Talin was purified by Ni-NTA affinity chromatography (Ni SepharoseHigh Performance, GE Healthcare). Elute fractions with 500mM imidazole in lysis buffer were pooled and loaded on anion exchange (HiTrap Q HP, 6% highly cross linked agarose; strong anion -N+(CH3)3, GE Healthcare) in MES buffer (20mM MES pH6.3, 1mM DTT, gradient from 100mM KCl to 100mM KCl). Elute fractions were pooled and concentrated (Amicon Ultra 15, MWCO 100kD) and further purified by size-exclusion chromatography (Superdex 200 10/300 GL, GE Healthcare) in 50mM TrisHCl pH7.8, 150mM KCl, 1mM DTT. Purified fractions were stored in presence of 50% glycerol in -80˚C.

Talin-1-head (a.a. 1-405) was cloned into pCoofy vector. The recombinant production of talin-1-head (a.a. 1-405) in E. coli Rosetta cells (Merck Millipore) was autoinduced at 24 °C for 22 h. After cell lysis and clarification of the supernatant, talin-1-head was purified by Ni-NTA affinity chromatography (Qiagen). Elute fractions containing talin-1-head were pooled, cleaved with SenP2 protease and purified by size-exclusion chromatography (Superdex 200 26/600, GE Healthcare) yielding unmodified murine talin dead domain.

Immunoprecipitation and GST pulldown

For immunoprecipitation of EGFP tagged proteins, cells were lysed in M-PER buffer and 1mg cells lysates in were immunoprecipitated with µMACS GFP Isolation Kit (Miltenyi Biotec) according to the manufacturer's protocol. Elutes were separated in SDS-PAGE for westernbloting or in-gel digestion and mass spectrometry analysis.

For GST pulldown experiments, full length Talin and Talin-head recombinant protein were re-buffered in the GST binding buffer (137mM NaCl, 13mM KCl, 0.05% Tween-20, 50mM TrisHCl pH7.5) with Zebra Desalt Spin Columns (Thermo Scientific). 200nM GST or GST-

KN fusion proteins were incubated with 100nM full length Talin or 300nM Talin head for 30min at 4˚C and then incubated with Glutathione Sepharose (GE Healthcare) for another 1.5hour at 4˚C. Resin was washed three times with the GST binding buffer and eluted in 2X laemmli buffer at 95˚C for 2min. Samples were analyzed in westernblot using antibody against Talin head and GST.

Fluorescence correlation spectroscopy (FCS)

The diffusion time as a function of talin protein concentration was measured by fluorescence correlation spectroscopy (FCS). FCS experiments were performed on a custom-build confocal microscopy. Prior to the experiment, the known diffusion coefficient of AlexaFluor 488 in water was used to calibrate the confocal volume (D = 400 $\mu m^2/s$). To analyze the interactions between the atto488 fluorescently-labeled KN peptide and talin, the peptide was diluted to a final concentration of ~1 nM in buffer (20 mM HEPES, 150 mM KCl, 0.5 mM EDTA, 1 mM DTT, pH 7.5) and 32 μM of talin was added. The reaction was incubated at room temperature for 3 minutes before subject to the FCS measurement. Lower concentrations in solution of talin were made by subsequent dilution in buffer containing 1nM of atto488-labeled KN peptide. The full dilution series was repeated three times. The fluctuation of fluorescence arising from the fluorescent KN-talin complexes was monitored and auto-correlated using all three measurements and diffusion time was estimated by fitting with a single diffusing species.

Integrin peptide pulldowns.

Peptide pulldowns were performed as described previously with minor modifications with β1 wt cytoplasmic tail peptides (HDRREFAKFEKEKMNAKWDTGENPIYKSAVTTVVNPKYEGK-OH), β1 Y795A tail peptide (HDRREFAKFEKEKMNAKWDTGENPIYKSAVTTVVNPKAEGK-OH), β3 tail peptide (HDRKEFAKFEEERARAKWDTANNPLYKEATSTFTNITYRGT-OH), β5 tail peptide (HDRREFAKFQSERSRARYEMASNPLYRKPISTHTVDFAFNKFNKSYNGSVD-OH), β2 tail peptide (TDLREYRRFEKEKLKSQWNN-DNPLFKSATTTVMNPKFAES-OH), a scrambled peptide (EYEFEPDKVDTGAKGTKMAKNEKKFRNYTVHNIWESRKVAP-OH). All peptides were desthiobiotinylated. Before use, peptides were immobilized on 20 μl Dynabeads MyOne Streptavidine C1 (10 mg ml−1, Invitrogen) in washing buffer containing 137mM NaCl, 13mM KCl, 50mM TrisHCl at pH 7.4, 0.05% Tween-20 for 2hours at 4˚C. Beads were washed twice with washing buffer and once with M-PER buffer. 0.5mg

cell lysate at 1mg/ml collected in M-PER buffer was incubated with the beads for 5hours at 4˚C. After incubation with tail peptides, proteins were eluted with 2X laemmli buffer at 95˚C for 5min. For in vitro Talin activation assay, 10nM recombinant talin diluted in the peptide pulldown washing buffer for 15min and then incubated with 10nM GST or GST-KN motif for 1hour together with the Dynabeads at 4˚C. Beads were washed three times with the washing buffer and eluted with 2X laemmli buffer at 95˚C for 5min.

Immunofluorescence microscopy.

For immunostaining, cells were cultured on glass coated with 10 μg ml−1 fibronectin (Calbiochem) for 5hours in complete culture medium before fixed with cold methanol:acetone (1:1) for 5min at -20˚C (for endogenous Talin staining) followed by 15min rehydration in PBS at r.t. or with 2% PFA/PBS for 15min at r.t. For PFA fixed samples, fixed cells were permeabilized with 0.1% Triton-X100/PBS for 30min at r.t. Cells were blocked with 5%BSA/PBS for 1 h at r.t. followed by incubation with the primary antibodies in 5%BSA/PBS overnight at 4˚C and secondary antibodies for 1 h at r.t. Images were collected at room temperature on a ZEISS (Jena, Germany) LSM780 confocal laser scanning microscope equipped with a ZEISS Plan-APO 63x/NA1.46 oil immersion objective.

Fluorescence recovery after photobleaching and fluorescence live cell imaging

Fluorescence recovery after photobleaching (FRAP) and fluorescence live cell imaging were performed on a ZEISS (Jena, Germany) LSM780 confocal laser scanning microscope equipped with a ZEISS Plan-APO 63x/NA1.46 oil immersion objective with environmental control (5% CO2 and humidification). Cells were transfected with indicated plasmids and cultured on 10 μg ml−1 fibronectin coated glass-bottom live cell imaging chamber (ibidi) for 24 hours. For FRAP experiments, region of interest was bleached with full laser power at 488nm for 30 iterations and fluorescence recovery was monitored for 5min with 20second interval with 1% laser power. No significant photobleaching was observed during the post-bleaching phase. FRAP data was extracted with build-in package in Carl Zeiss ZEN software and analyzed in GraphPad Prism 6. FRAP curves were fitted in one phase association model: Y=Y0 + (Plateau-Y0)*(1-exp(-K*x)). For fluorescence live cell imaging, cells were imaged for 10min with 20second interval with 1% laser power.

Time-lapse video microscopy of 2D-random cell migration.

Indicated cells were seeded sparsely on 6-well plate coated with 5μg/ml fibronectin in the absence of serum for 2hours, then the cell migrations were recorded at 37 °C and 5% CO2 for 6hours with 5min time interval on a Zeiss Axiovert 200 M (Zeiss, Germany) equipped with ×10/.3, ×20/.4 and ×40/.6 objectives, a motorized stage (Märzhäuser) and an environment chamber (EMBL Precision Engineering) with a cooled CCD (charge-coupled device) camera (Roper Scientific). Image acquisition and microscope control were carried out with MetaMorph software (Molecular Devices). The acquired images were analyzed using the manual tracking plugin of ImageJ and the Chemotaxis and Migration Tool (ibidi).

Statistics.

Statistical analysis was performed in GraphPad Prism software (version 5.00, GraphPad Software). Results are illustrated as the mean±sd. unless otherwise indicated.

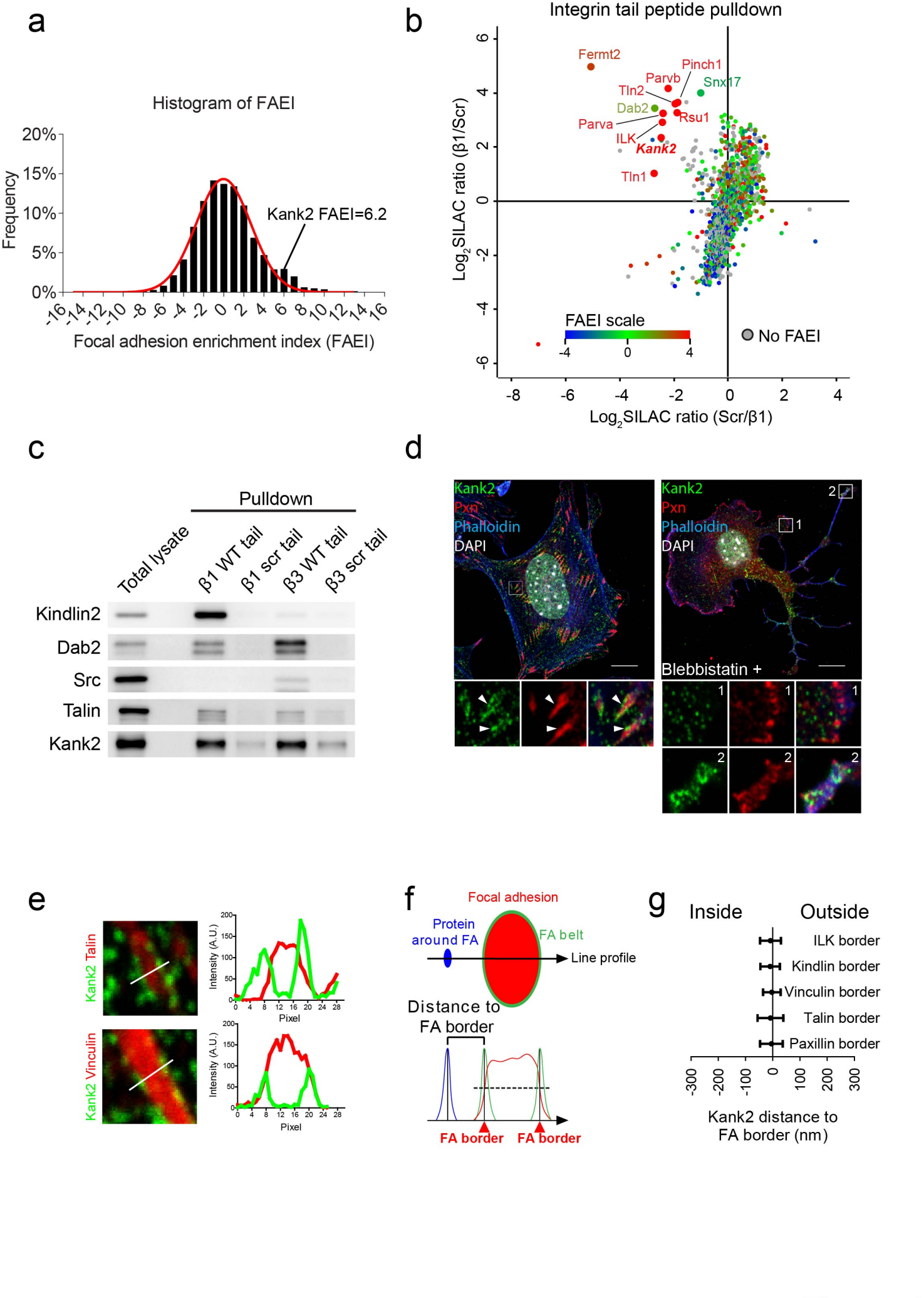
a
Histogram of FAEI
Frequency
20%
15%
10%
5%
0%
Kank2 FAEI=6.2
-16 -14 -12 -10 -8 -6 -4 -2 0 2 4 6 8 10 12 14 16
Focal adhesion enrichment index (FAEI)
b
Integrin tail peptide pulldown
Fermt2
Pinch1
Parvb
Snx17
Tln2
Dab2
Rsu1
Parva
ILK
Kank2
Tln1
FAEI scale
-4 0 4
No FAEI
Log2SILAC ratio (β1/Scr)
Log2SILAC ratio (Scr/β1)
c
Pulldown
Total lysate
β1 WT tail
β1 scr tail
β3 WT tail
β3 scr tail
Kindlin2
Dab2
Src
Talin
Kank2
d
Kank2
Pxn
Phalloidin
DAPI
Blebbistatin +
e
Kank2 Talin
Kank2 Vinculin
Intensity (A.U.)
Pixel
f
Focal adhesion
Protein around FA
FA belt
Line profile
Distance to FA border
FA border
FA border
g
Inside
Outside
ILK border
Kindlin border
Vinculin border
Talin border
Paxillin border
-300 -200 -100 0 100 200 300
Kank2 distance to FA border (nm)

Figure 1

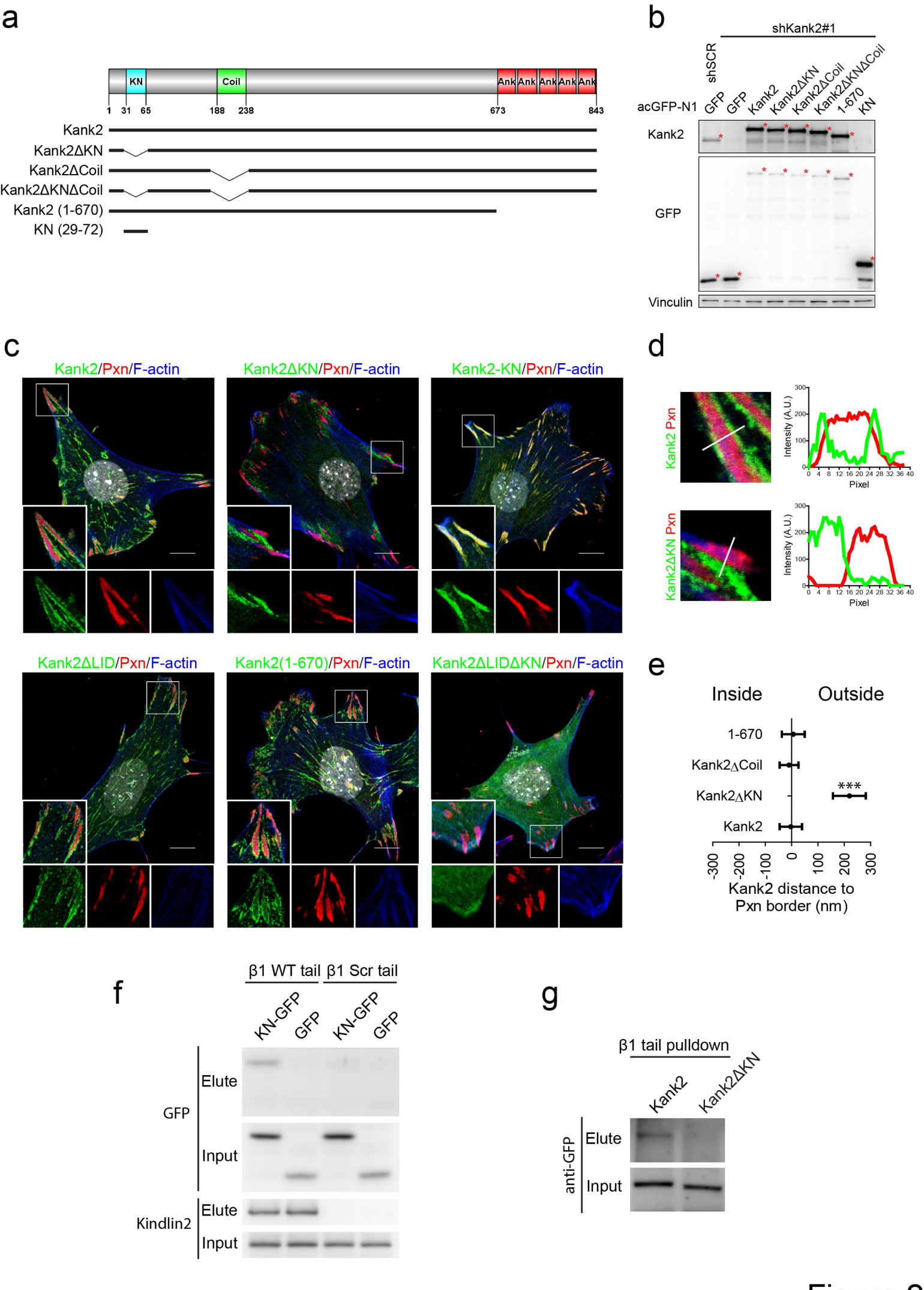
a
KN
Coil
Ank
1
31
65
188
238
673
843
Kank2
Kank2ΔKN
Kank2ΔCoil
Kank2ΔKNΔCoil
Kank2 (1-670)
KN (29-72)
b
shKank2#1
shSCR
acGFP-N1
GFP
GFP
Kank2
Kank2ΔKN
Kank2ΔCoil
Kank2ΔKNΔCoil
1-670
KN
Kank2
GFP
Vinculin
c
Kank2/Pxn/F-actin
Kank2ΔKN/Pxn/F-actin
Kank2-KN/Pxn/F-actin
Kank2ΔLID/Pxn/F-actin
Kank2(1-670)/Pxn/F-actin
Kank2ΔLIDΔKN/Pxn/F-actin
d
Kank2 Pxn
Kank2ΔKN Pxn
Intensity (A.U.)
Pixel
e
Inside
Outside
1-670
Kank2ΔCoil
Kank2ΔKN
Kank2
***
-300
-200
-100
0
100
200
300
Kank2 distance to
Pxn border (nm)
f
β1 WT tail
β1 Scr tail
KN-GFP
GFP
KN-GFP
GFP
GFP
Elute
Input
Kindlin2
Elute
Input
g
β1 tail pulldown
Kank2
Kank2ΔKN
anti-GFP
Elute
Input

Figure 2

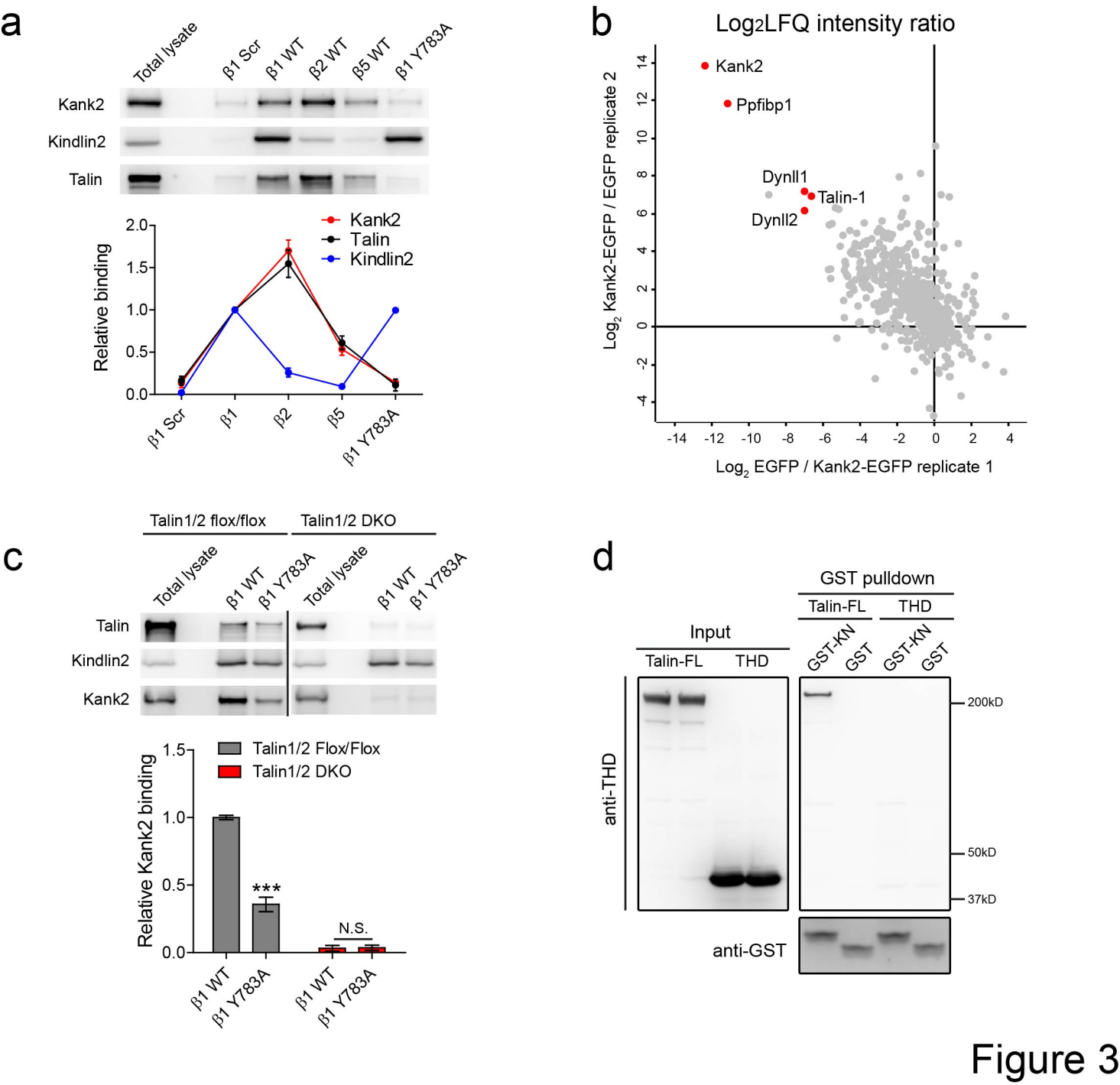
a
Total lysate
β1 Scr
β1 WT
β2 WT
β5 WT
β1 Y783A
Kank2
Kindlin2
Talin
Relative binding
Kank2
Talin
Kindlin2
β1 Scr
β1
β2
β5
β1 Y783A
b
Log2LFQ intensity ratio
Kank2
Ppfibp1
Dynll1
Talin-1
Dynll2
Log2 Kank2-EGFP / EGFP replicate 2
Log2 EGFP / Kank2-EGFP replicate 1
c
Talin1/2 flox/flox
Talin1/2 DKO
Total lysate
β1 WT
β1 Y783A
Talin
Kindlin2
Kank2
Relative Kank2 binding
Talin1/2 Flox/Flox
Talin1/2 DKO
***
N.S.
β1 WT
β1 Y783A
d
GST pulldown
Talin-FL
THD
Input
GST-KN
GST
anti-THD
200kD
50kD
37kD
anti-GST

Figure 3

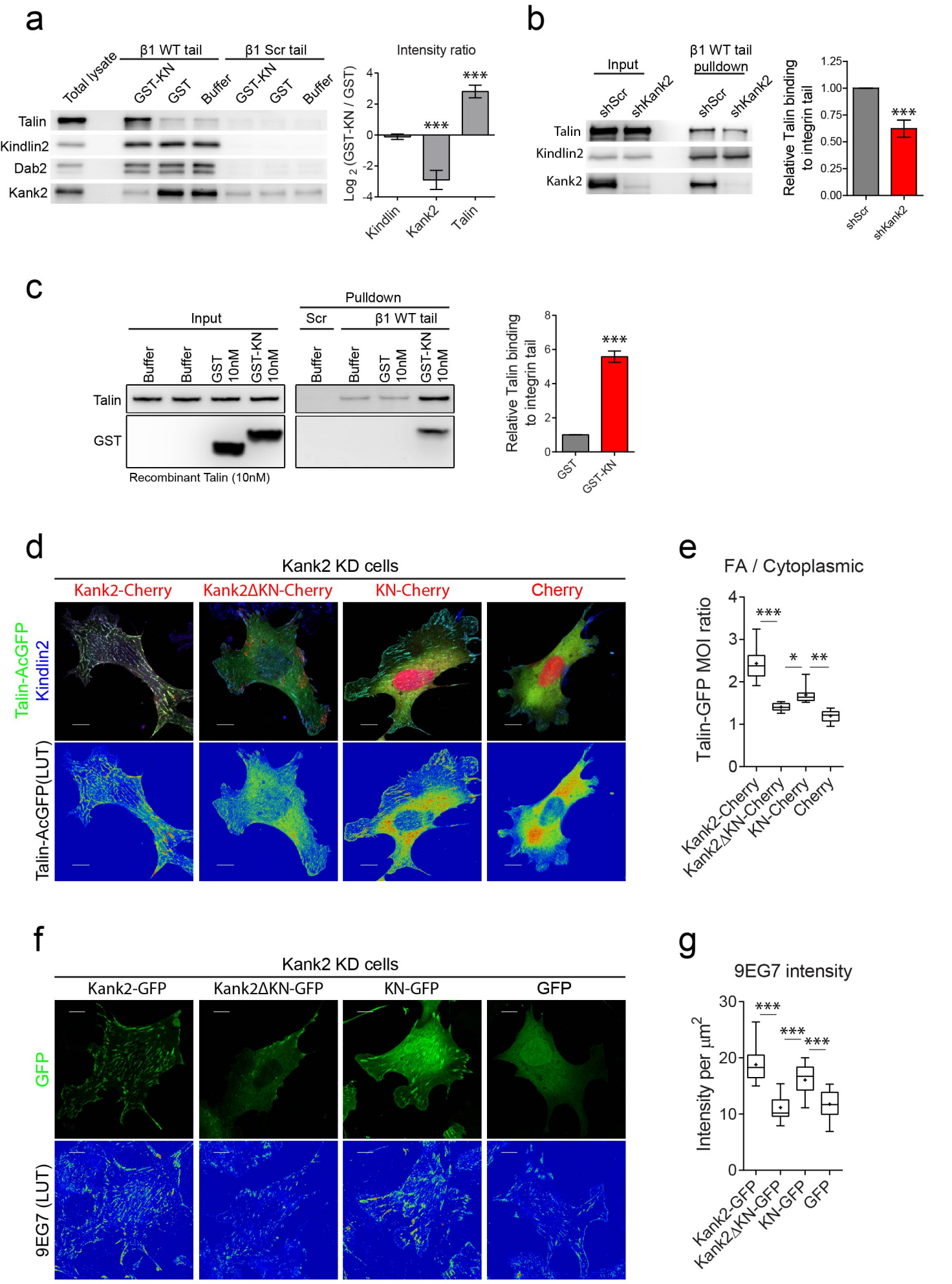
a
Total lysate
β1 WT tail
β1 Scr tail
GST-KN
GST
Buffer
GST-KN
GST
Buffer
Talin
Kindlin2
Dab2
Kank2
Intensity ratio
Log 2 (GST-KN / GST)
***
***
Kindlin
Kank2
Talin
b
Input
β1 WT tail pulldown
shScr
shKank2
shScr
shKank2
Talin
Kindlin2
Kank2
Relative Talin binding to integrin tail
***
shScr
shKank2
c
Pulldown
Input
Scr
β1 WT tail
Buffer
Buffer
GST 10nM
GST-KN 10nM
Buffer
Buffer
GST 10nM
GST-KN 10nM
Talin
GST
Recombinant Talin (10nM)
Relative Talin binding to integrin tail
***
GST
GST-KN
d
Kank2 KD cells
Kank2-Cherry
Kank2ΔKN-Cherry
KN-Cherry
Cherry
Talin-AcGFP
Kindlin2
Talin-AcGFP(LUT)
e
FA / Cytoplasmic
Talin-GFP MOI ratio
***
*
**
Kank2-Cherry
Kank2ΔKN-Cherry
KN-Cherry
Cherry
f
Kank2 KD cells
Kank2-GFP
Kank2ΔKN-GFP
KN-GFP
GFP
GFP
9EG7 (LUT)
g
9EG7 intensity
Intensity per μm2
***
***
***
Kank2-GFP
Kank2ΔKN-GFP
KN-GFP
GFP

Figure 4

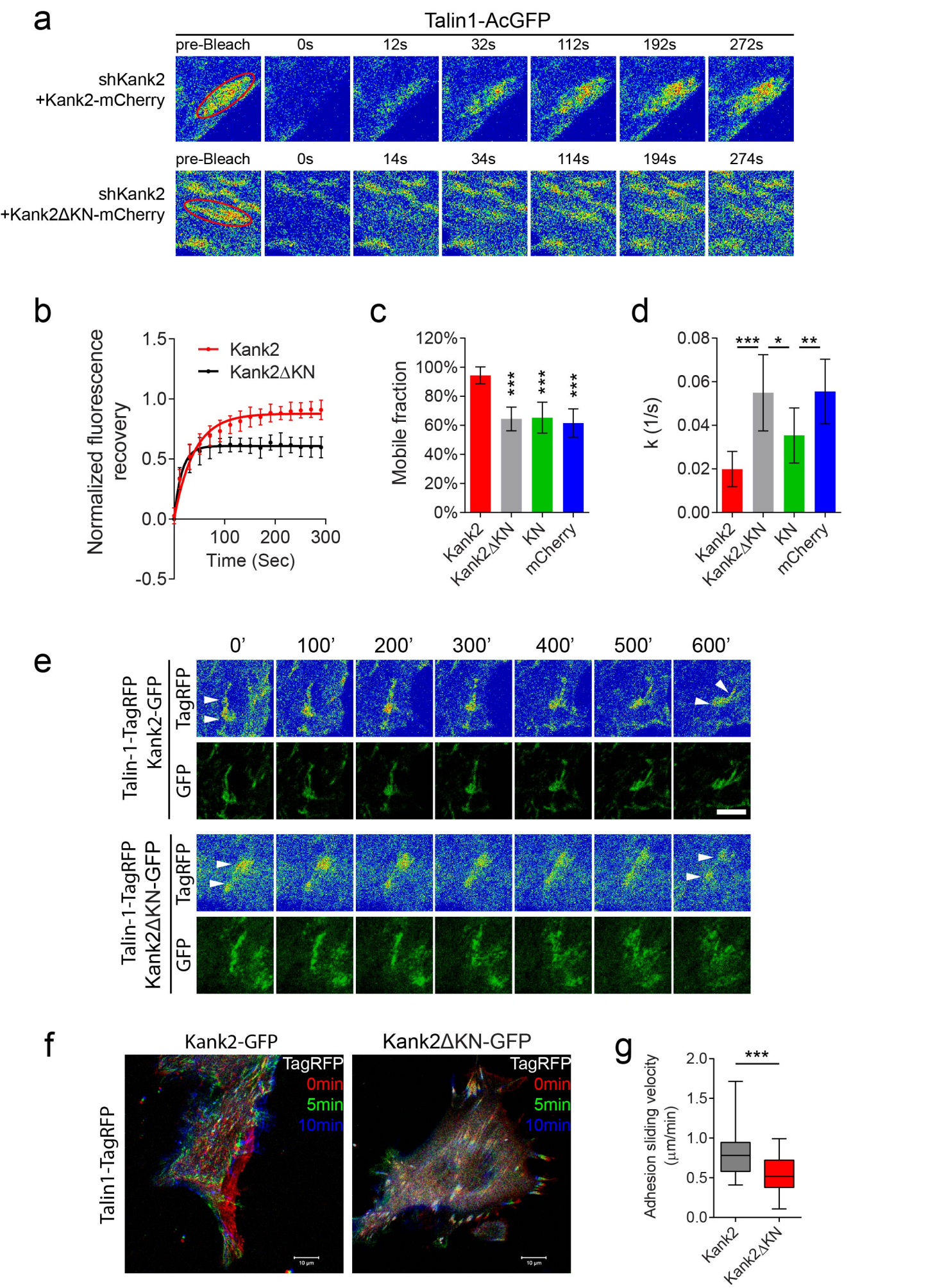
a
Talin1-AcGFP
pre-Bleach
0s
12s
32s
112s
192s
272s
shKank2
+Kank2-mCherry
pre-Bleach
0s
14s
34s
114s
194s
274s
shKank2
+Kank2ΔKN-mCherry
b
Normalized fluorescence recovery
Kank2
Kank2ΔKN
Time (Sec)
c
Mobile fraction
Kank2
Kank2ΔKN
KN
mCherry
d
k (1/s)
Kank2
Kank2ΔKN
KN
mCherry
e
0'
100'
200'
300'
400'
500'
600'
Talin-1-TagRFP
Kank2-GFP
TagRFP
GFP
Talin-1-TagRFP
Kank2ΔKN-GFP
TagRFP
GFP
f
Kank2-GFP
Kank2ΔKN-GFP
Talin1-TagRFP
TagRFP
0min
5min
10min
g
Adhesion sliding velocity (μm/min)
Kank2
Kank2ΔKN

Figure 5

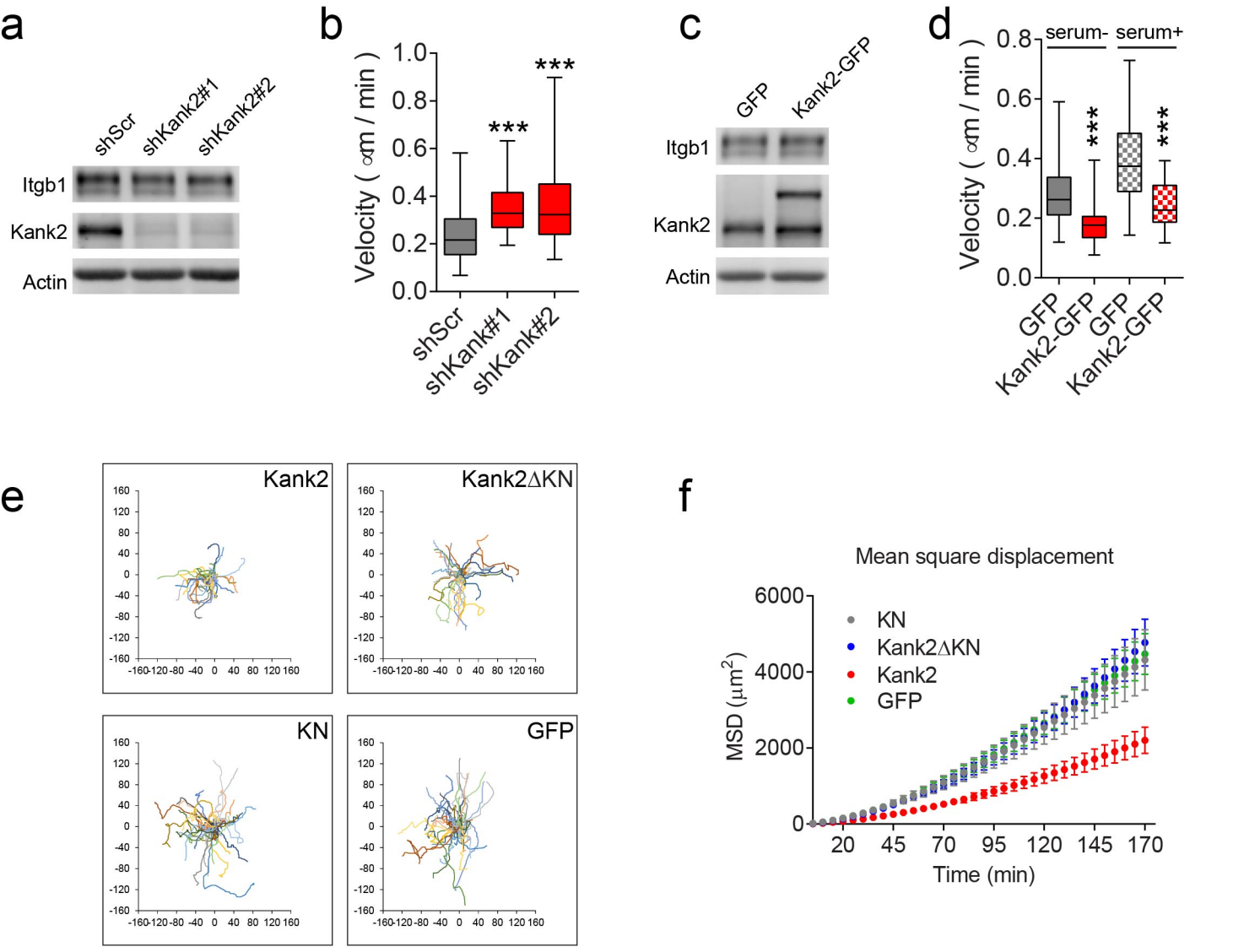
a
shScr
shKank2#1
shKank2#2
Itgb1
Kank2
Actin
b
Velocity (∝m / min)
1.0
0.8
0.6
0.4
0.2
0.0
***
***
shScr
shKank#1
shKank#2
c
GFP
Kank2-GFP
Itgb1
Kank2
Actin
d
serum-
serum+
Velocity (∝m / min)
0.8
0.6
0.4
0.2
0.0
***
***
GFP
Kank2-GFP
GFP
Kank2-GFP
e
Kank2
Kank2ΔKN
KN
GFP
160
120
80
40
0
-40
-80
-120
-160
-160-120-80 -40 0 40 80 120 160
f
Mean square displacement
MSD (μm2)
6000
4000
2000
0
KN
Kank2ΔKN
Kank2
GFP
20
45
70
95
120
145
170
Time (min)

Figure 6

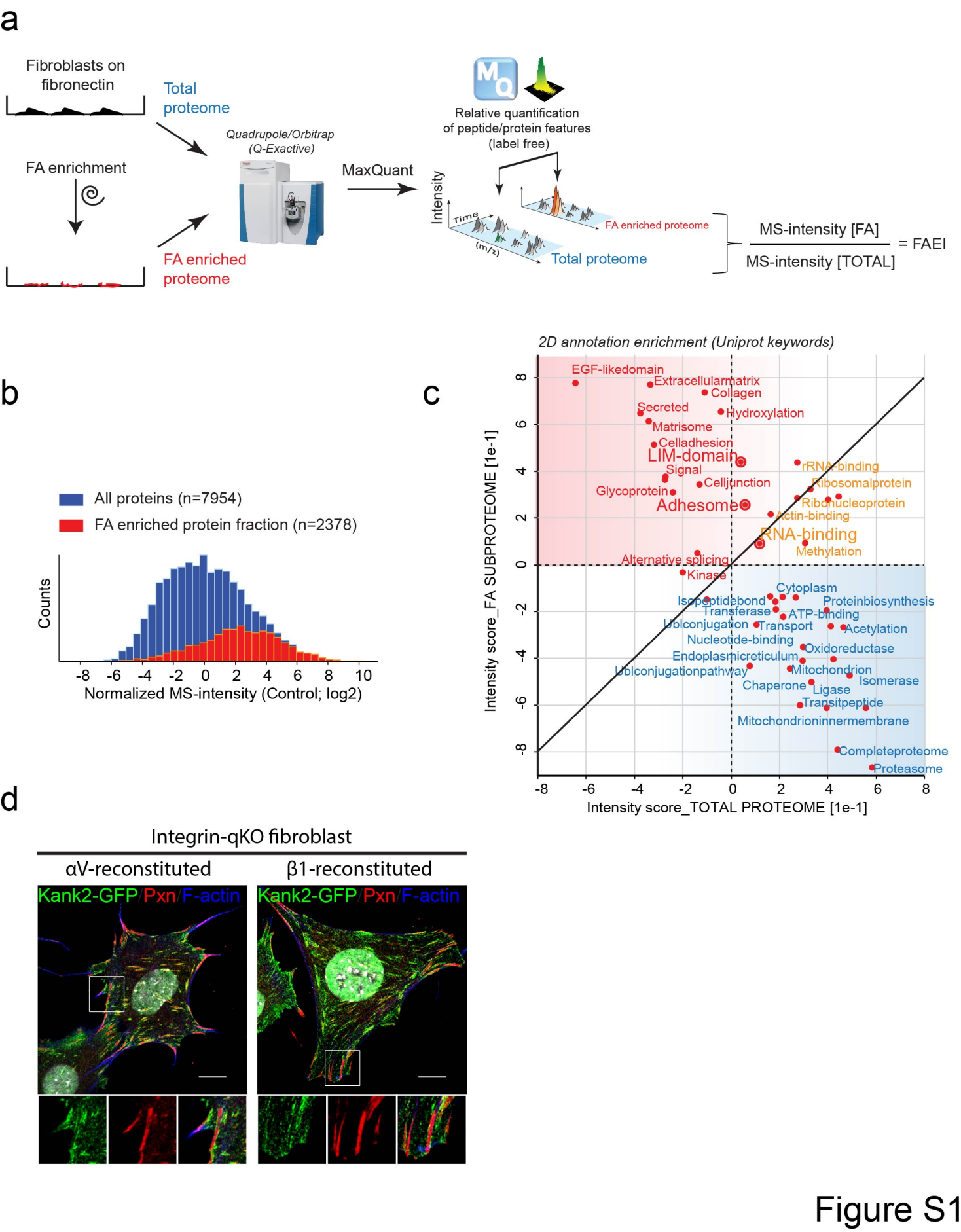
a
Fibroblasts on fibronectin
Total proteome
FA enrichment
Quadrupole/Orbitrap (Q-Exactive)
FA enriched proteome
MaxQuant
Relative quantification of peptide/protein features (label free)
Intensity
Time
(m/z)
FA enriched proteome
Total proteome
MS-intensity [FA] / MS-intensity [TOTAL] = FAEI
b
All proteins (n=7954)
FA enriched protein fraction (n=2378)
Counts
Normalized MS-intensity (Control; log2)
c
2D annotation enrichment (Uniprot keywords)
Intensity score_FA SUBPROTEOME [1e-1]
Intensity score_TOTAL PROTEOME [1e-1]
EGF-likedomain
Extracellularmatrix
Collagen
Secreted
Hydroxylation
Matrisome
Celladhesion
LIM-domain
Signal
Celljunction
Glycoprotein
Adhesome
rRNA-binding
Ribosomalprotein
Ribonucleoprotein
Actin-binding
RNA-binding
Methylation
Alternative splicing
Kinase
Cytoplasm
Isopeptidebond
Proteinbiosynthesis
Transferase
ATP-binding
Ubl conjugation
Transport
Acetylation
Nucleotide-binding
Oxidoreductase
Endoplasmicreticulum
Ubl conjugationpathway
Mitochondrion
Isomerase
Chaperone
Ligase
Transitpeptide
Mitochondrioninnermembrane
Completeproteome
Proteasome
d
Integrin-qKO fibroblast
αV-reconstituted
β1-reconstituted
Kank2-GFP/Pxn/F-actin
Kank2-GFP/Pxn/F-actin

Figure S1

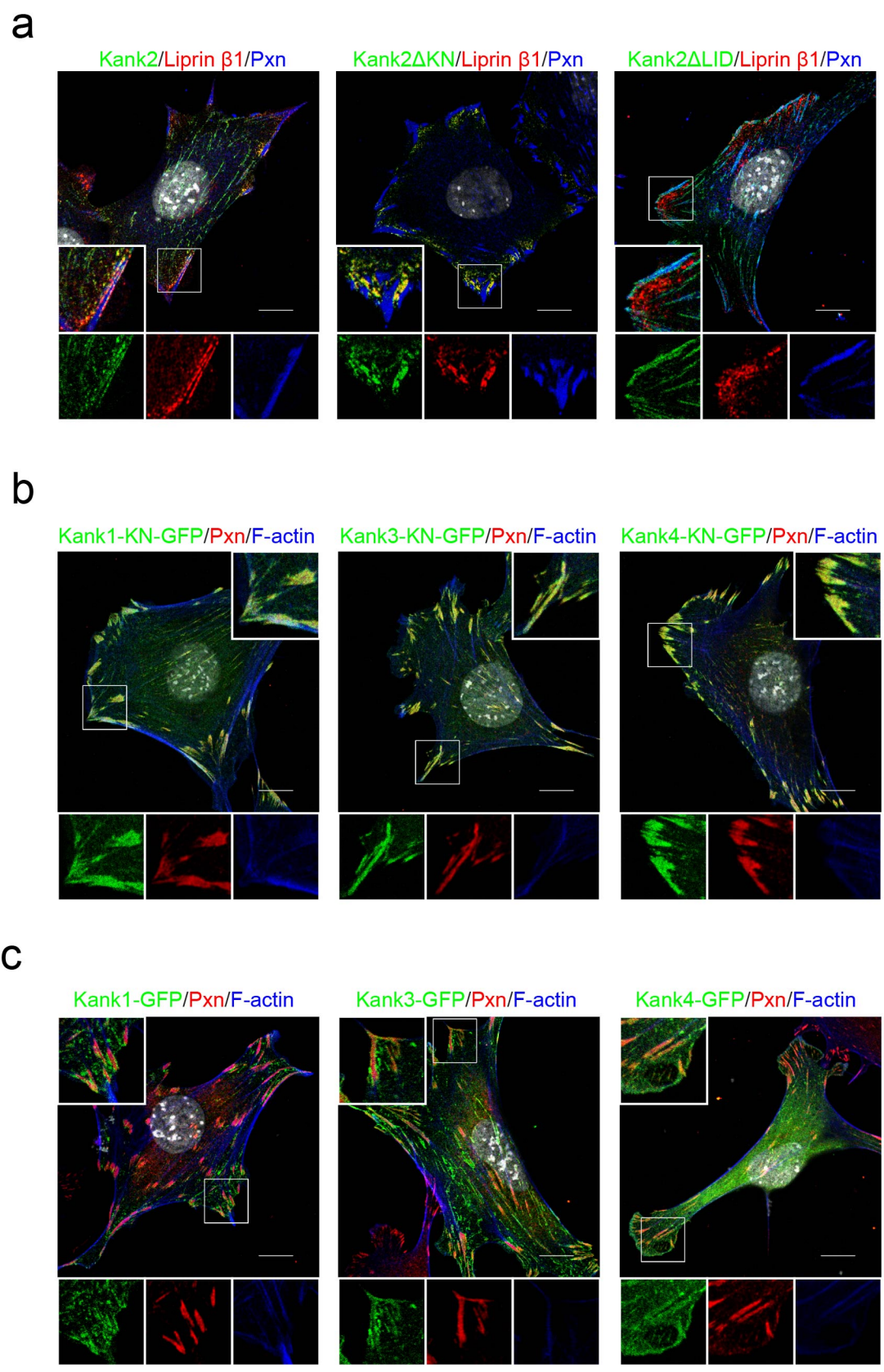
a
Kank2/Liprin β1/Pxn
Kank2ΔKN/Liprin β1/Pxn
Kank2ΔLID/Liprin β1/Pxn
b
Kank1-KN-GFP/Pxn/F-actin
Kank3-KN-GFP/Pxn/F-actin
Kank4-KN-GFP/Pxn/F-actin
c
Kank1-GFP/Pxn/F-actin
Kank3-GFP/Pxn/F-actin
Kank4-GFP/Pxn/F-actin

Figure S2

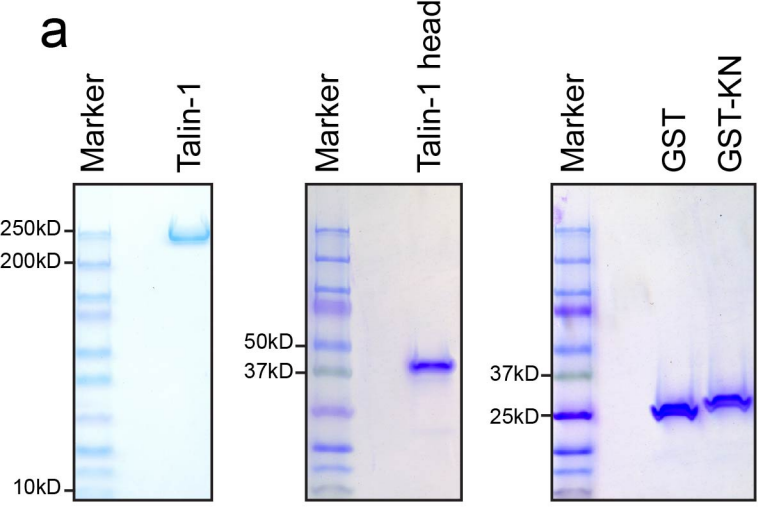
a
Marker
Talin-1
250kD
200kD
10kD
Marker
Talin-1 head
50kD
37kD
Marker
GST
GST-KN
37kD
25kD

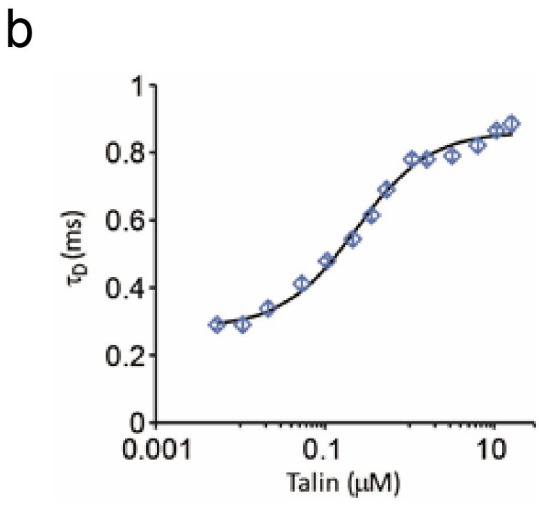
b
1
0.8
0.6
0.4
0.2
0
τD (ms)
0.001
0.1
10
Talin (μM)

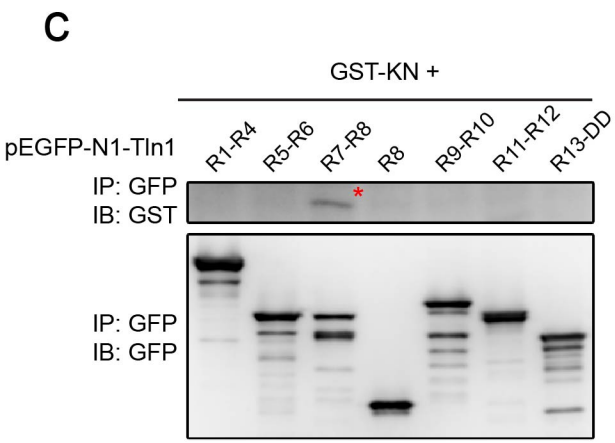
c
GST-KN +
pEGFP-N1-Tln1
R1-R4
R5-R6
R7-R8
R8
R9-R10
R11-R12
R13-DD
IP: GFP
IB: GST
*
IP: GFP
IB: GFP

Figure S3

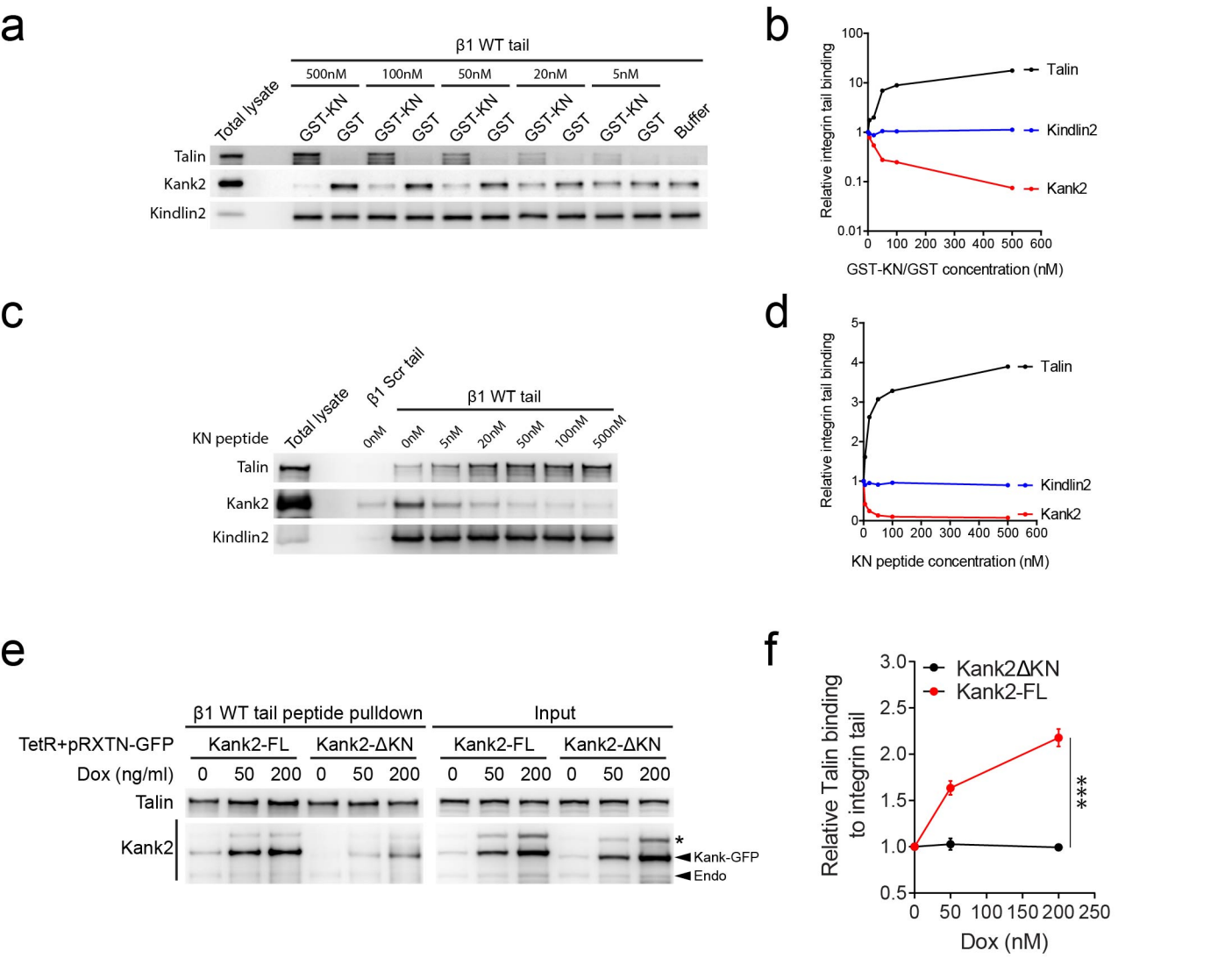
a
β1 WT tail
500nM
100nM
50nM
20nM
5nM
Total lysate
GST-KN
GST
Buffer
Talin
Kank2
Kindlin2
b
Relative integrin tail binding
Talin
Kindlin2
Kank2
GST-KN/GST concentration (nM)
c
β1 Scr tail
β1 WT tail
KN peptide
0nM
5nM
20nM
50nM
100nM
500nM
d
KN peptide concentration (nM)
e
β1 WT tail peptide pulldown
Input
TetR+pRXTN-GFP
Kank2-FL
Kank2-ΔKN
Dox (ng/ml)
0
50
200
Kank-GFP
Endo
f
Kank2ΔKN
Kank2-FL
Relative Talin binding to integrin tail
***
Dox (nM)

Figure S4

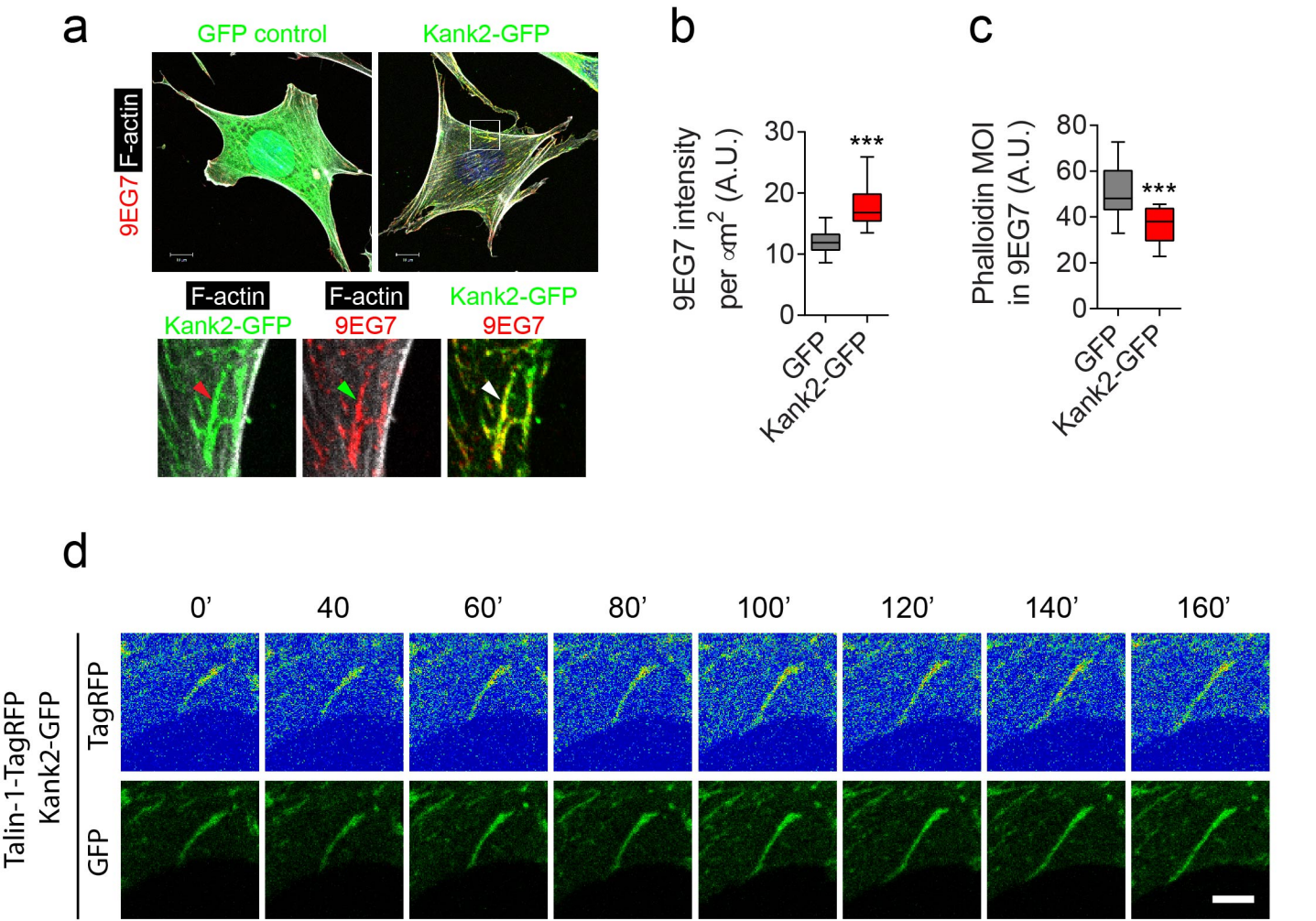
a
GFP control
Kank2-GFP
9EG7 F-actin
F-actin
Kank2-GFP
F-actin
9EG7
Kank2-GFP
9EG7
b
9EG7 intensity per μm² (A.U.)
30
20
10
0
***
GFP
Kank2-GFP
c
Phalloidin MOI in 9EG7 (A.U.)
80
60
40
20
0
***
GFP
Kank2-GFP
d
0'
40
60'
80'
100'
120'
140'
160'
Talin-1-TagRFP
Kank2-GFP
TagRFP
GFP

Figure S5

nature cell biology

β_1- and α_v-class integrins cooperate to regulate myosin II during rigidity sensing of fibronectin-based microenvironments

Herbert B. Schiller[1,6], Michaela-Rosemarie Hermann[1,6], Julien Polleux[1], Timothée Vignaud[2], Sara Zanivan[3], Caroline C. Friedel[4], Zhiqi Sun[1], Aurelia Raducanu[1], Kay-E. Gottschalk[5], Manuel Théry[2], Matthias Mann[3] and Reinhard Fässler[1,7]

How different integrins that bind to the same type of extracellular matrix protein mediate specific functions is unclear. We report the functional analysis of β_1- and α_v-class integrins expressed in pan-integrin-null fibroblasts seeded on fibronectin. Reconstitution with β_1-class integrins promotes myosin-II-independent formation of small peripheral adhesions and cell protrusions, whereas expression of α_v-class integrins induces the formation of large focal adhesions. Co-expression of both integrin classes leads to full myosin activation and traction-force development on stiff fibronectin-coated substrates, with α_v-class integrins accumulating in adhesion areas exposed to high traction forces. Quantitative proteomics linked α_v-class integrins to a GEF-H1–RhoA pathway coupled to the formin mDia1 but not myosin II, and $\alpha_5\beta_1$ integrins to a RhoA–Rock–myosin II pathway. Our study assigns specific functions to distinct fibronectin-binding integrins, demonstrating that $\alpha_5\beta_1$ integrins accomplish force generation, whereas α_v-class integrins mediate the structural adaptations to forces, which cooperatively enable cells to sense the rigidity of fibronectin-based microenvironments.

Integrins are α/β heterodimers that mediate cell adhesion to the extracellular matrix (ECM) and to receptors on other cells[1], thereby regulating numerous biological processes that are essential for development, postnatal homeostasis and pathology[1–4]. The mammalian genome encodes 18 α and 8 β integrin genes, which form 24 heterodimers. Mammalian cells usually co-express several integrins, which recognize ECM components by binding specific amino-acid stretches such as the Arg-Gly-Asp (RGD) motif[1,5]. RGD motifs are found in many matrix proteins including fibronectin, in which RGD mediates binding to $\alpha_5\beta_1$ and all α_v-class integrins[6]. *In vivo* and *in vitro* studies indicated that $\alpha_5\beta_1$ and α_v-class integrins (for example, $\alpha_v\beta_3$) exert both specific and redundant functions[7–15]; however, how these distinct integrins accomplish their individual functions and whether these cooperate remains unclear. The signalling properties and functions of integrins are executed by specialized adhesive structures with distinct morphology, subcellular localization, lifespan and molecular composition. Nascent adhesions are short-lived adhesive structures in membrane protrusions[16] that promote the activity of Rho–GTPases such as Rac1. Some nascent adhesions develop into large focal adhesions that initiate multiple signalling pathways, which activate effectors including myosin II. Myosin II exerts contractile forces resulting in adhesion reinforcement and recruitment of more proteins to focal adhesions, which induces a further increase in myosin II activity[17]. This feedback signalling to myosin II critically depends on biophysical parameters such as ECM stiffness. The identity of mechanosensor(s) in focal adhesions, whether it is an integrin, a focal adhesion protein or a combination of both, is unknown[18]. Quantitative mass spectrometry (MS) was previously used to determine the protein composition of adhesion structures (adhesomes) of cells seeded on fibronectin, and the dynamic changes on myosin-II-induced adhesion maturation[19,20]. As cells recruit different integrin classes to fibronectin-induced adhesions, these studies did not assign specific proteins and signalling outputs to particular integrins.

Here we developed a cell system to investigate the protein composition and signalling properties of adhesion sites anchored selectively through $\alpha_5\beta_1$ and/or α_v-class integrins. We found marked integrin-class-specific differences in the morphology of focal adhesions, in their requirement for mechanical tension, in the protein composition of their adhesomes and their signalling capacity. Furthermore, we

[1]Department of Molecular Medicine, Max Planck Institute of Biochemistry, 82152 Martinsried, Germany. [2]Laboratoire de Physiologie Cellulaire et Végétale, Institut de Recherche en Technologies et Sciences pour le Vivant, CNRS/UJF/INRA/CEA, 17 Rue des Martyrs, 38054 Grenoble, France. [3]Department of Proteomics and Signal Transduction, Max Planck Institute of Biochemistry, 82152 Martinsried, Germany. [4]Institute for Informatics, Ludwig-Maximilians-Universität München, 80333 Munich, Germany. [5]Institute of Experimental Physics, University of Ulm, 89069 Ulm, Germany. [6]These authors contributed equally to this work.
[7]Correspondence should be addressed to R.F. (e-mail: faessler@biochem.mpg.de)

Received 2 November 2012; accepted 4 April 2013; published online 26 May 2013; DOI: 10.1038/ncb2747

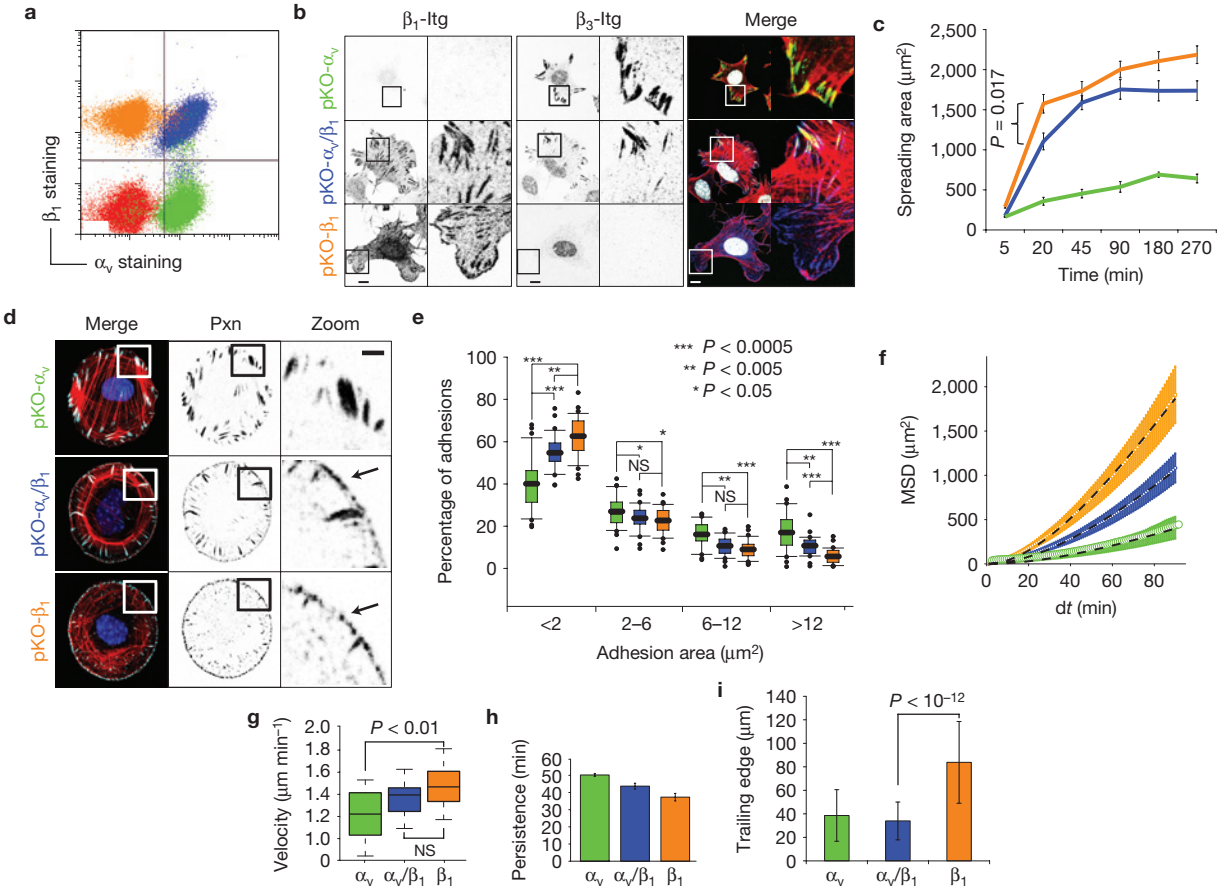

Figure 1 Different morphologies and adhesive functions of pKO-α_v, pKO-β_1 and pKO-α_v/β_1 cells. (**a**) Flow cytometry analysis of β_1 and α_v cell surface levels. (**b**) Immunostaining of indicated cell types plated for 90 min on fibronectin for β_1 and β_3. The merged images show an overlay of integrin (β_1, blue; β_3, green), F-actin (red) and nuclear (DAPI, blue) staining. Scale bars, 10 μm. (**c**) Spreading areas of cells seeded on fibronectin. Error bars represent s.e.m. ($n = 20$ cells per time point; 1 representative of 2 independent experiments is shown). The P value is derived from a t-test. (**d**) Cells were plated on circular fibronectin-coated micropatterns and immunostained for paxillin (Pxn). The merged images show an overlay of paxillin (white), F-actin (red) and nuclear (DAPI, blue) staining. Arrows indicate nascent adhesions (<2 μm²) in the cell periphery. Scale bar, 10 μm. (**e**) Boxplots show the distribution of adhesion size classes. Significance was calculated using a t-test ($n = 30$ cells; 1 representative of 2 independent experiments is shown; boxplot whisker ends are at 1.5 interquartile range and outliers are shown as dots). (**f-h**) Migration velocity (**g**) and mean persistence time (**h**) was determined with the MSD values of cell nuclei (**f**) by filming migrating cells over a period of 90 min with a 1 min time lapse (pKO-α_v $n = 12$, pKO-β_1 $n = 14$, pKO-α_v/β_1 $n = 12$; data aggregated over 5 independent experiments). The P value for velocities (**g**) was calculated using an unpaired Wilcoxon test and the persistence time bar graph (**g**) shows the fit error as implemented in the MatLab software. NS, not significant. (**i**) Trailing edge lengths of migrating cells are shown with mean lengths from the cell rear to the middle of the nucleus. Error bars represent s.d. and the P values were calculated using a t-test (pKO-α_v $n = 51$, pKO-β_1 $n = 66$, pKO-α_v/β_1 $n = 40$; 1 representative of 2 independent experiments is shown). pKO-α_v, green; pKO-α_v/β_1, blue; pKO-β_1, orange.

identified a functional synergy between $\alpha_5\beta_1$ and α_v-class integrin signalling hubs leading to feedback amplification of myosin II activity required for focal-adhesion-mediated rigidity sensing.

RESULTS

Differential functions of $\alpha_5\beta_1$ and α_v-class integrins in adhesion formation and cell migration

To obtain cells expressing β_1- and/or α_v-class integrins we intercrossed mice carrying conditional null mutations for the α_v and β_1 integrin genes and constitutive null mutations for the β_2 and β_7 integrin genes ($\beta_1^{f/f}$, $\alpha_v^{f/f}$, $\beta_2^{-/-}$, $\beta_7^{-/-}$ mice)[21], isolated kidney fibroblasts and immortalized them with the SV40 large T antigen (parental fibroblasts). Deletion of floxed α_v and β_1 integrin genes by adenoviral *Cre* transduction removed all integrins from the parental fibroblast clones (pan-knockouts, pKO; Supplementary Fig. S1a–c). Next we transduced parental fibroblasts with α_v or β_1 or both complementary DNAs and simultaneously transduced *Cre* to delete the floxed integrin alleles. This produced cells expressing α_v (pKO-α_v), β_1 (pKO-β_1) or α_v and β_1 (pKO-α_v/β_1) integrins, respectively (Fig. 1a). The pKO-α_v, pKO-β_1 and pKO-α_v/β_1 cells were sorted for comparable integrin surface levels to the parental cell clones (Supplementary Fig. S1d,e). Using western blotting, flow cytometry and MS we identified the following fibronectin-binding integrins; $\alpha_5\beta_1$ in pKO-β_1 cells, $\alpha_v\beta_3$ and $\alpha_v\beta_5$ in pKO-α_v cells, and $\alpha_5\beta_1$, $\alpha_v\beta_3$ and $\alpha_v\beta_5$ in pKO-α_v/β_1 cells (Supplementary Fig. S1f,g). Calibration of our flow cytometry analysis estimated the presence of 170,000 $\alpha_5\beta_1$ and 300,000 α_v-class integrins on the surface of each cell, resulting in approximately equimolar surface levels for β_1, β_3 and β_5 integrins.

All three cell lines specifically adhered to fibronectin, whereas adhesion on vitronectin was similar for pKO-α_v and pKO-α_v/β_1 cells

and absent for pKO-β_1 cells (Supplementary Fig. S1h). To compare the size distribution of focal adhesions we seeded cells for 90 min on fibronectin and immunostained for paxillin, integrin β_1 and β_3 (Fig. 1b and Supplementary Fig. S2a,b). The percentage of small nascent adhesions ($<2\,\mu m^2$) was significantly elevated in pKO-β_1 and pKO-α_v/β_1 cells, whereas large focal adhesions of 6–12 μm^2 dominated in pKO-α_v cells (Supplementary Fig. S2a,b). The cell spreading area on fibronectin was significantly lower in pKO-α_v relative to pKO-β_1 and pKO-α_v/β_1 cells and reduced in pKO-α_v/β_1 relative to pKO-β_1 (Fig. 1c and Supplementary Fig. S1i). As cell shape and spreading area can affect cell contractility, focal adhesion size and distribution[22], we seeded cells on circular fibronectin-coated micropatterns surrounded by non-adhesive polyethylene glycol (PEG), and confirmed the different adhesion size distribution in the three cell lines (Fig. 1d,e). pKO-α_v/β_1 cells contained both small nascent adhesions and large focal adhesions (Fig. 1d). pKO-β_1 and pKO-α_v/β_1 cells showed increased protrusive activity when compared with pKO-α_v cells (Supplementary Fig. S2a,c), which correlated with increased migration speed. The mean square displacement (MSD) of cells migrating on fibronectin showed that pKO-β_1 cells migrated significantly faster than pKO-α_v cells, and that pKO-α_v/β_1 cells exhibited an intermediate migration speed (Fig. 1f,g). As previously shown[13,23,24], expression of α_v-class integrins increased migration persistence (Fig. 1h). pKO-β_1 cells exhibited a significant defect in trailing edge detachment (Fig. 1i and Supplementary Fig. S2c and Videos S1–S3). These results identify a role for $\alpha_5\beta_1$ in protrusive activities and nascent adhesion formation, whereas co-expression of α_v-class integrins also promotes the production of large, stable focal adhesions and trailing edge detachment in migrating cells.

Differential functions of $\alpha_5\beta_1$ and α_v-class integrins synergize to regulate cell contractility

Adhesion maturation and trailing edge retraction in migrating fibroblasts requires coordinated control of myosin-II-mediated cell contractility[25]. We measured myosin II activity using fibronectin-coated X- or crossbow-shaped micropatterns, which report subtle changes in myosin II activity and traction forces along non-adhesive edges[26–28]. Parental fibroblasts cultured on X-shaped fibronectin-coated micropatterns showed a dose-dependent decrease of phosphoT18/S19-myosin light chain (pMLC), paxillin fluorescence intensities and cell area following treatment with the myosin II inhibitor blebbistatin (Supplementary Fig. S2d–g). Crossbow patterns polarize cells into a low contractile front and a highly contractile rear[28]. Immunofluorescence analysis revealed that pMLC and paxillin intensities were the highest in pKO-α_v/β_1, lower in pKO-β_1 and the lowest in pKO-α_v cells (Fig. 2a). Myosin II activity was low in the cell front (Fig. 2b) and high in the cell rear (Fig. 2c) and the cooperative effect of the two integrin classes on pMLC and paxillin intensities in pKO-α_v/β_1 was most prominent in the cell rear (Fig. 2a–c). Treatment with the α_v-class-specific small-molecule inhibitor cilengitide reduced contractility of pKO-α_v/β_1 cells to intermediate levels (Fig. 2b,c), confirming that the adhesive function of α_v-class integrins is required for the synergy with $\alpha_5\beta_1$. We corroborated these results with fibronectin-coated X-shapes, revealing phenotypes that resembled the rear of crossbow shapes (Supplementary Fig. S2h–j).

The ability to form large focal adhesions and stress fibres indicative of high contractile forces together with low pMLC levels in pKO-α_v cells was surprising. Traction-force microscopy experiments on polyacrylamide gels of 35 kPa stiffness revealed good correlation of traction forces and pMLC levels, confirming that traction forces on fibronectin-coated crossbow micropatterns are the lowest in pKO-α_v, the highest in pKO-α_v/β_1 and intermediate in pKO-β_1 cells (Fig. 2d). Along the cell front, traction forces were significantly higher in pKO-β_1 cells when compared with pKO-α_v cells and the highest in pKO-α_v/β_1 (Fig. 2e). Similar differences were observed by calculating the total contractile energy of individual cells (Fig. 2f).

α_v-class integrins accumulate in areas of high traction force and mediate rigidity sensing

$\alpha_v\beta_3$ integrins are known to become immobilized in large and static focal adhesions, whereas $\alpha_5\beta_1$ integrins are mobile, separate from the $\alpha_v\beta_3$ integrins and translocate rearward to fibrillar adhesions[10,29]. To investigate whether $\alpha_5\beta_1$ and α_v-class integrins segregate owing to differential dependence on myosin-II-mediated tension at focal adhesions we seeded pKO-α_v/β_1 and parental floxed cells on fibronectin-coated crossbow shapes and immunostained β_1 and β_3 integrins. Indeed, β_3 heavily accumulated in areas that were shown to be exposed to the highest traction forces, whereas β_1 levels remained very low at these sites (Fig. 3a,b). The β_3 integrins in contractile focal adhesions at the cell rear were lost following blebbistatin treatment, whereas small β_1-containing focal adhesions in the cell periphery were still forming (Fig. 3a). To confirm these findings we plated pKO-α_v/β_1 cells on 1-μm-thin fibronectin-coated lines separated by 3-μm-wide non-adhesive PEG lines. This set-up allows distinguishing ligand-bound from unbound integrins, which is impossible on uniformly coated fibronectin surfaces. Whereas the β_1 integrin staining co-localized with fibronectin lines almost throughout the entire cell length, small β_3 clusters overlaid with lines in the cell periphery associated with F-actin bundles. Blebbistatin treatment or inhibition of Rock with Y-27632 disassembled the β_3 integrin clusters on fibronectin lines, whereas β_1 remained unchanged (Fig. 3c). The differential dependence of $\alpha_5\beta_1$ and α_v-class integrins on myosin-II-mediated tension at focal adhesions suggested that tension-dependent stabilization of α_v-class integrins contributes to rigidity sensing. In line with this hypothesis, traction-force measurements of pKO-β_1 and pKO-α_v/β_1 cells plated on micropatterned polyacrylamide gels of 3 different rigidities (1.4, 10 and 35 kPa) revealed that only pKO-α_v/β_1, but not pKO-β_1, cells were able to increase contractile energies concomitantly with the substrate rigidity. Most notably, the traction forces and contractile energies generated by pKO-β_1 and pKO-α_v/β_1 cells were similar on soft, 1.4 kPa substrates, whereas they differed significantly on stiffer substrates (Fig. 3d,e). We therefore conclude that stabilization of $\alpha_v\beta_3$–fibronectin bonds through actomyosin-mediated tension is required to adjust cell contractility to defined substrate stiffnesses.

Adhesome composition and stoichiometry is controlled by the integrin class and myosin II activity

Cells sense their environment through integrins and numerous plaque proteins in focal adhesions[17,30]. The composition and stoichiometry of the adhesome in fibronectin-bound fibroblasts is controlled by myosin II (refs 19,20). We therefore reasoned that specific binding activities of the integrin cytoplasmic tails and also the differential myosin II activities in pKO-α_v, pKO-β_1 and pKO-α_v/β_1

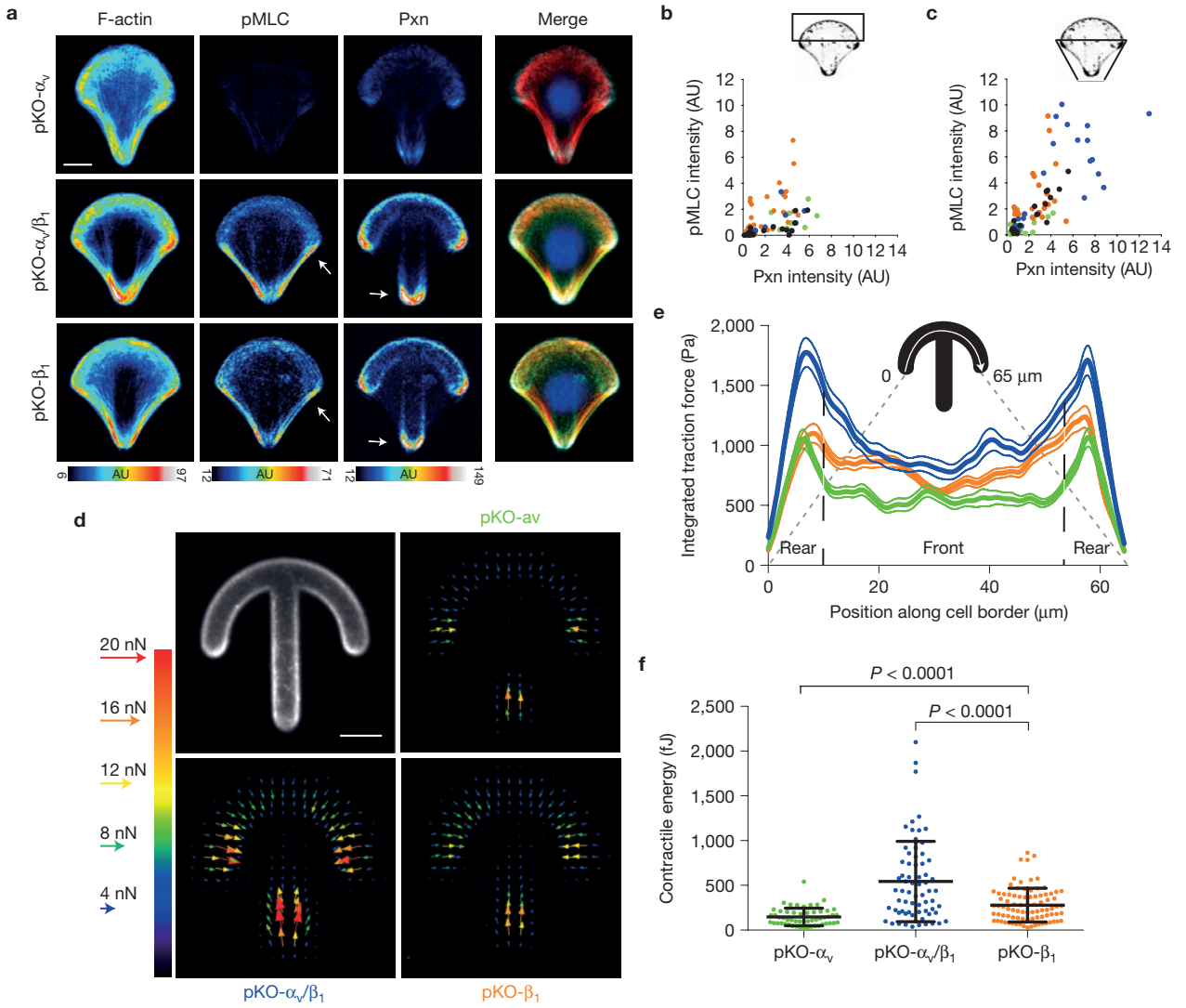

Figure 2 α_v-class integrins cooperate with $\alpha_5\beta_1$ for myosin II reinforcement on stiff fibronectin-coated substrates. (**a**) Averaged confocal images of immunostainings (Merge: F-actin, red; pMLC, green; paxillin, blue; DAPI, blue) of the indicated cell lines plated for 3 h on fibronectin-coated micropatterns (pKO-α_v $n = 55$, pKO-β_1 $n = 36$, pKO-α_v/β_1 $n = 71$; data aggregated over 3 independent experiments). Areas with strong pMLC and paxillin fluorescent signals are marked with arrows. Scale bar, 10 µm. (**b**,**c**) Intensities of pMLC and paxillin (Pxn) fluorescence in the front (**b**) and rear (**c**) regions of individual cells (pKO-α_v $n = 25$, pKO-β_1 $n = 32$, pKO-α_v/β_1 $n = 26$; 1 representative of 3 independent experiments is shown). Optionally, cells were treated with the α_v-class integrin inhibitor cilengitide (1 µM). (**d**) Average traction-force fields of indicated cell types (pKO-α_v $n = 54$, pKO-β_1 $n = 86$, pKO-α_v/β_1 $n = 68$; data aggregated over 3 independent experiments). Arrows indicate force orientation; colour and length represent local force magnitude in nanonewtons. Scale bar, 10 µm. (**e**) Average integrated traction forces along the cell border (pKO-α_v $n = 54$, pKO-β_1 $n = 86$, pKO-α_v/β_1 $n = 58$; data aggregated over 3 independent experiments; thin lines represent s.e.m.). (**f**) Contractile energy of individual cells (pKO-α_v $n = 54$, pKO-β_1 $n = 86$, pKO-α_v/β_1 $n = 68$; data aggregated over 3 independent experiments). Each data point corresponds to the total contractile energy of an individual cell measured by traction-force microscopy. All statistical comparisons were *t*-tests (error bars represent s.e.m.). pKO-α_v (green); pKO-α_v/β_1 (blue); pKO-β_1 (orange); pKOα_v/β_1 + 1 µM cilengitide (black).

cells may contribute to their specific adhesome composition. To test this hypothesis we determined the integrin-class-specific protein composition of focal adhesions. The three cell lines were plated for 45 or 90 min on fibronectin or poly-L-lysine (PLL; permits integrin-independent adhesion) followed by chemical crosslinking and purification of focal adhesions, sample elution and quantitative MS as described previously[19] (Supplementary Fig. S4a and Table S1). Isolated adhesome proteins were quantified using the label-free quantification algorithm of the MaxQuant software[31]. We calculated median MS intensities of 3–4 replicates and performed hierarchical clustering to compare the three cell lines at different time points with and without blebbistatin. This approach allowed identifying protein groups with high correlation of their intensity changes across different substrates, time points and cell lines. We identified a cluster containing 168 proteins significantly enriched for known (previously annotated) focal adhesion proteins. In addition to the 168 proteins, we also considered all previously annotated focal adhesion proteins[32] assigned to other clusters in our analysis. This led to 245 proteins used for further analysis (Supplementary Fig. S4b). Analysis of variance (ANOVA) tests revealed that MS intensities of 62% (152/245) of them were significantly changed

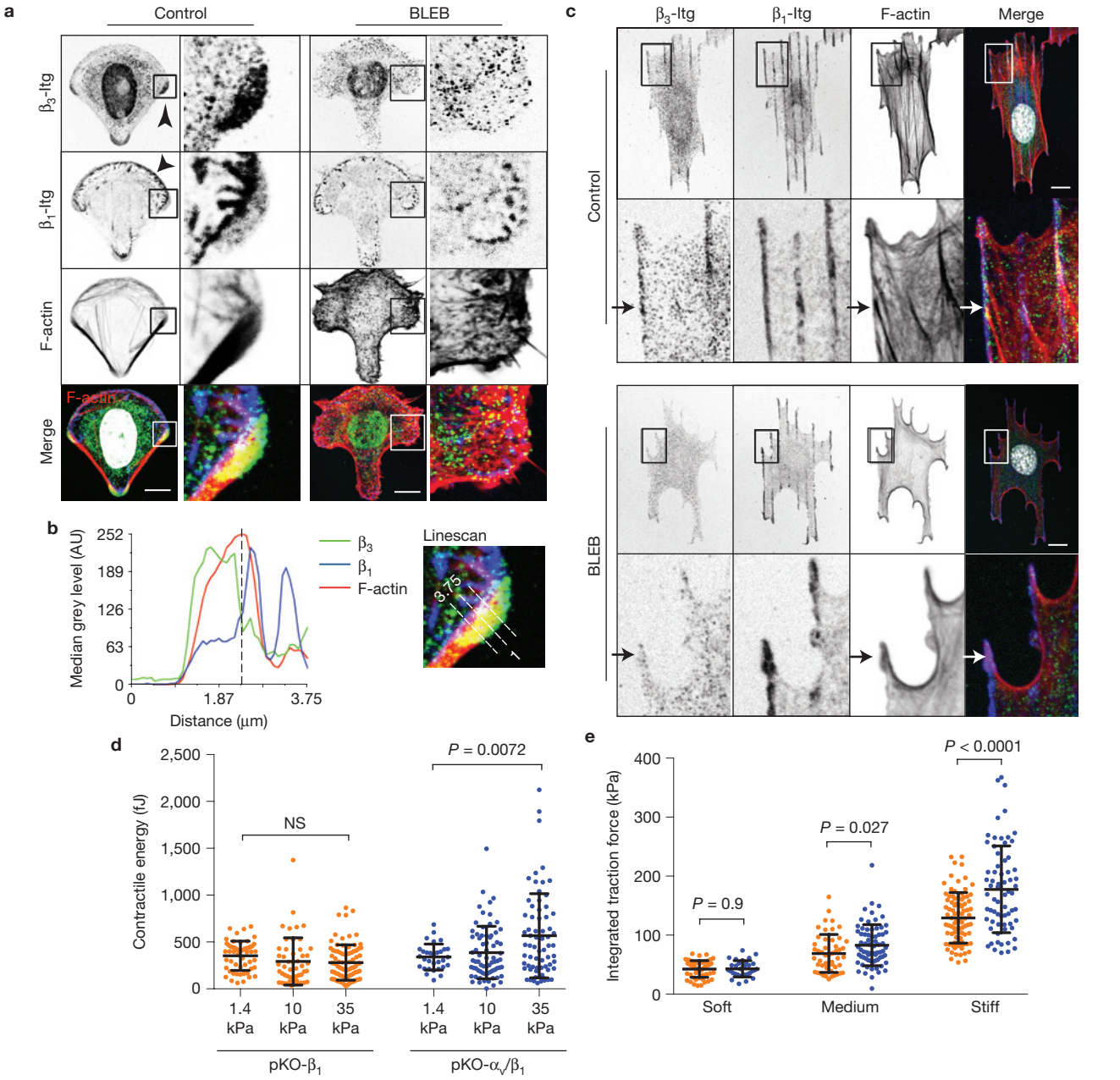

Figure 3 α_v-class integrins accumulate in adhesion areas exposed to high traction force and cooperate with $\alpha_5\beta_1$ for rigidity sensing on fibronectin. (**a**) pKO-α_v/β_1 cells were plated on fibronectin-coated crossbow shapes for 3 h with and without blebbistatin (BLEB) and immunostained for β_1 (blue), β_3 (green) integrins and F-actin (red). Scale bars, 10 μm. DAPI, white (left panel, merge). (**b**) Fluorescence intensity profile of the indicated stainings along the depicted linescan (3.75 μm). (**c**) pKO-α_v/β_1 cells were plated on 1 μm thin fibronectin-coated lines for 90 min with and without blebbistatin and stained for β_1 (blue), β_3 (green) integrin and F-actin (red). Scale bars, 10 μm. DAPI, white (merge). (**d**) Each data point represents the total contractile energy of individual cells measured by traction-force microscopy on gels of indicated rigidities (pKO-β_1: soft $n = 54$, medium $n = 50$, stiff $n = 86$; pKO-α_v/β_1: soft $n = 31$, medium $n = 71$, stiff $n = 68$; data aggregated over 3 independent experiments; all pairwise statistical comparisons from *t*-tests are shown in Supplementary Table S5; NS, not significant). (**e**) Each data point represents the total integrated traction force in kilo Pascal (kPa) of individual cells measured by traction-force microscopy on gels of indicated rigidities (pKO-β_1: soft $n = 54$, medium $n = 50$, stiff $n = 86$; pKO-α_v/β_1: soft $n = 31$, medium $n = 71$, stiff $n = 68$; data aggregated over 3 independent experiments; *P* values of pairwise comparisons were calculated with a *t*-test). pKO-α_v/β_1 (blue); pKO-β_1 (orange).

in at least one of the three cell lines or one of the two time points (Supplementary Table S1).

In line with our previous report[19], blebbistatin induced different intensity reductions in floxed fibroblasts for different classes of adhesome proteins. Following blebbistatin treatment pKO-α_v/β_1 and pKO-β_1 cells were still able to recruit integrin-proximal proteins such as Talin-1, Kindlin-2 and ILK, whereas LIM-domain-containing proteins were reduced to background levels defined by MS intensities from cells seeded on PLL (Fig. 4a). Strikingly, blebbistatin reduced almost all focal adhesion proteins to background levels in pKO-α_v cells, indicating that

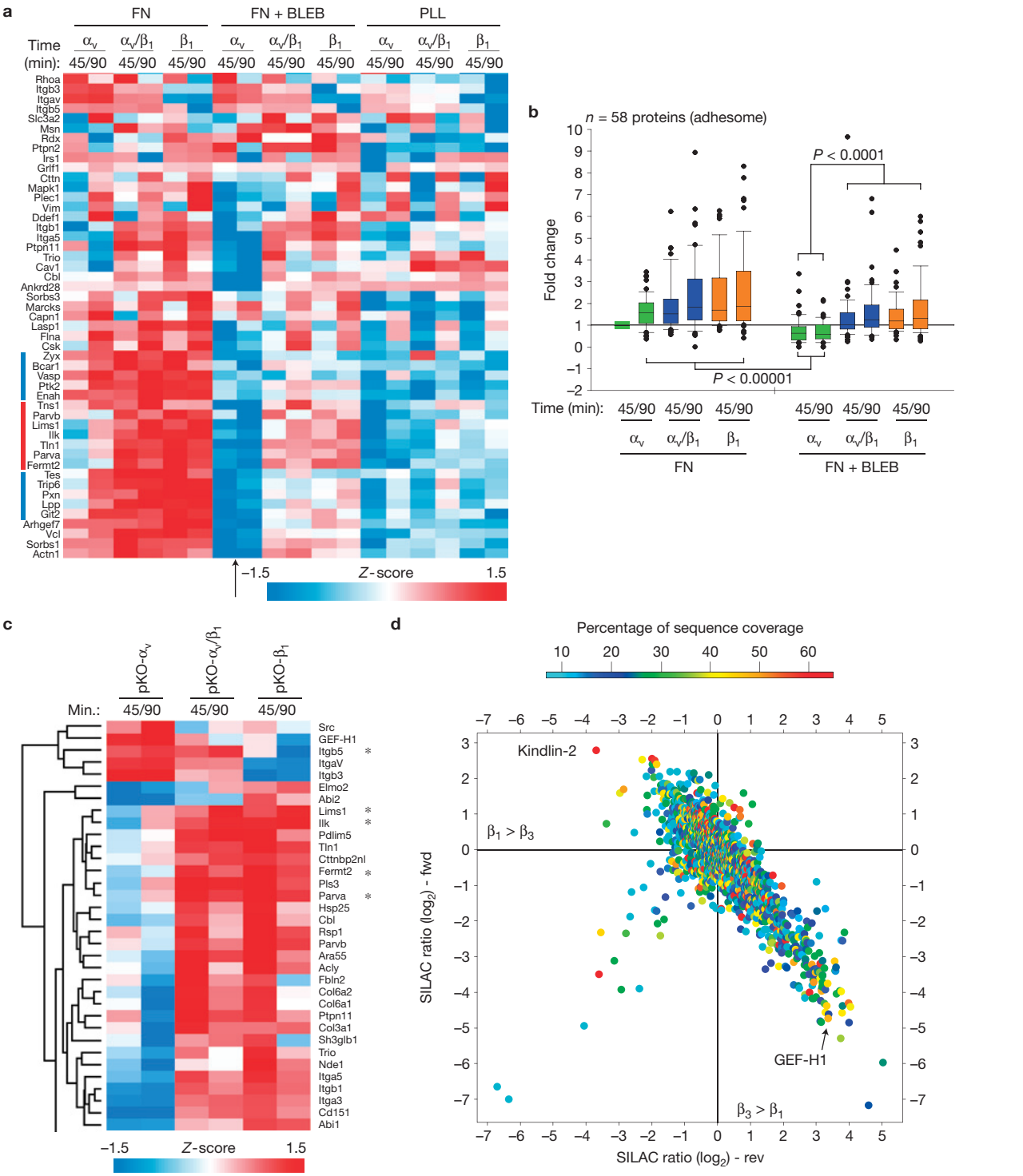

Figure 4 Composition and stoichiometry of the adhesome is determined by the individual integrin and myosin II activity. (**a**) Focal-adhesion-enriched fractions analysed by MS before and after blebbistatin (BLEB) treatment. The *Z*-scores of median MS intensities ($n = 3$–4) are colour coded to show relative protein abundance. A blebbistatin-insensitive cluster is marked with a red bar and blebbistatin-sensitive clusters are marked with blue bars. The arrow highlights the pronounced effect of blebbistatin on pKO-α_v cells. FN, fibronectin. (**b**) Boxplots showing MS intensity differences of 58 known focal adhesion proteins of the indicated cells relative to pKO-α_v cells cultured for 45 min without blebbistatin. A *t*-test revealed significant MS intensity changes after blebbistatin treatment. Boxplot whisker ends are at 1.5 interquartile range and outliers are shown as dots. (**c**) Focal adhesion proteins with similar *Z*-score profiles (colour coded) as $\alpha_5\beta_1$ or α_v-class integrins (selection based on Supplementary Fig. S6) were subjected to hierarchical cluster analysis. Focal-adhesion-enriched fractions were collected 45 and 90 min after plating on fibronectin. (**d**) SILAC ratio plot from label-inverted replicates comparing β_1 with β_3 tail pulldowns. Specific interactors have high SILAC ratios in the forward experiment (fwd) and low SILAC ratios in the label swapped reverse experiment (rev). The colour code shows the percentage of sequence coverage of the proteins identified by MS analysis ($n = 4$; 2 independent experiments). pKO-α_v (green); pKO-α_v/β_1 (blue); pKO-β_1 (orange).

the protein recruitment to focal adhesions in blebbistatin-treated pKO-α_v/β_1 cells was mediated by $\alpha_5\beta_1$ (Fig. 4a). A paired Student's *t*-test for 58 known focal adhesion proteins confirmed a significant reduction of crosslinked focal adhesion proteins in pKO-α_v cells by blebbistatin (Fig. 4b). Furthermore, comparing the 45 and 90 min time points revealed that protein recruitment to focal adhesions was delayed in pKO-α_v cells (Fig. 4a,b). Importantly, blebbistatin did not change the MS intensities of α_v-class integrins, excluding inefficient integrin crosslinking as the cause for the diminished recruitment of focal adhesion proteins, and indicating that short-lived/weak α_v-class integrin–fibronectin interactions occur in the absence of cell contractility and can be crosslinked. These findings together with those depicted in Fig. 3 indicate that $\alpha_5\beta_1$ can cluster and induce adhesome assemblies in the absence of myosin-II-mediated tension, whereas the ability of α_v-class integrins to cluster and recruit adhesome proteins depends on myosin II activation and/or the stress fibre architecture at focal adhesions.

ILK and GEF-H1 are required for myosin II reinforcement on stiff substrates

Consulting published protein–protein interactions within the adhesome[30], we established a putative core interactome of fibronectin-bound $\alpha_5\beta_1$ or α_v-class integrins (Supplementary Fig. S5). Hierarchical cluster analysis of MS intensities of the 125 core proteins of the integrin interactome from all conditions tested (Supplementary Fig. S6) revealed 29 proteins correlating with MS intensities of $\alpha_5\beta_1$ at both time points and 2 proteins correlating with MS intensities of α_v-class integrins (Fig. 4c). In addition to this integrin interactome, we analysed the MS intensities of all actin-binding proteins in the focal-adhesion-enriched fraction and found that WAVE and Arp2/3 complexes, which drive lamellipodia formation, correlated with $\alpha_5\beta_1$, whereas the RhoA effector mDia1 (Diap1), which drives stress-fibre formation, correlated with α_v-class integrins (Supplementary Fig. S7). We performed stable isotope labelling with amino acids in cell culture (SILAC)-based peptide pulldown assays with β_1 and β_3 integrin tail peptides and scrambled control peptides followed by MS (ref. 33) to identify which of the 29 $\alpha_5\beta_1$-enriched and 2 αv-class integrin-enriched adhesome proteins were enriched through differential associations with integrin cytoplasmic tails. Comparison of integrin-tail interactors with scrambled peptide interactors identified common and specific β_1 tail- and β_3 tail-binding proteins (Supplementary Fig. S8). Talin-1 showed equal binding to β_1 and β_3 tails and was therefore used to control the experiments. In line with the adhesome analysis (Fig. 4c) we observed very high β_1-tail-specific enrichment for Kindlin-2 and a lower enrichment for the ILK/PINCH/Parvin (IPP) complex, and a high β_3-tail-specific enrichment of the RhoA guanine nucleotide exchange factor GEF-H1 (Fig. 4d). Thus, the recruitment of Kindlin-2, the IPP complex and GEF-H1 to focal adhesions is controlled by the integrin tail sequence rather than the different focal adhesion architecture in pKO-β_1 and pKO-α_v cells. Ratiometric analysis of fluorescence intensities in focal adhesions confirmed higher Kindlin-2 and ILK levels in pKO-β_1 cells and pKO-α_v/β_1 cells (Fig. 5a–d). To analyse GEF-H1 levels in focal adhesions we first chemically crosslinked and unroofed the cells to remove the large cytoplasmic and microtubule-associated GEF-H1 pool, and then performed immunostainings, which revealed that crosslinked GEF-H1 levels were significantly higher in pKO-α_v and pKO-α_v/β_1 cells than in pKO-β_1 cells (Fig. 5e–g).

To investigate whether the IPP complex and GEF-H1 contribute to myosin II regulation by $\alpha_5\beta_1$ and α_v-class integrins we seeded $ILK^{fl/fl}$ (control) and $ILK^{-/-}$ fibroblasts[34] on fibronectin-coated X-shapes and stained for pMLC. $ILK^{-/-}$ fibroblasts had similarly low pMLC signals as pKO-α_v cells (Fig. 5h,i). Furthermore, inhibition of $\alpha_5\beta_1$ with blocking antibodies or α_v-class integrins with cilengitide in $ILK^{fl/fl}$ cells significantly reduced pMLC levels (Fig. 5h,i), confirming that both fibronectin-binding integrin classes are required to activate myosin II. To examine whether GEF-H1 regulates integrin-mediated activation of myosin II on fibronectin-coated X-shapes we depleted GEF-H1 messenger RNA using short interfering RNA (siRNA; Fig. 5j) and found significantly reduced pMLC levels in GEF-H1-silenced pKO-α_v/β_1 cells, slightly reduced levels in pKO-β_1 cells and unaffected levels in pKO-α_v cells (Fig. 5k,l) indicating that GEF-H1 reinforces myosin II activity in a $\alpha_5\beta_1$-dependent manner.

The IPP complex and GEF-H1 have been implicated in cell contractility regulation by tuning RhoA GTPases[35–37]. Therefore, we investigated whether the activity of RhoA and Rac1 are affected in our cell lines. Seeding the three cell lines for 45 min on fibronectin induced a significantly higher RhoA activity in pKO-α_v cells when compared with pKO-β_1 and pKO-α_v/β_1 cells (Fig. 5m). Rac1 activity was the lowest in pKO-α_v cells, higher in pKO-β_1 and the highest in pKO-α_v/β_1 cells (Fig. 5n). As the high GEF-H1 and RhoA levels in focal adhesions of pKO-α_v cells are not able to promote high pMLC, we conclude that only $\alpha_5\beta_1$ can elicit signals for mediating RhoA-driven myosin II activation.

Integrin-specific signalling pathways cooperate for feedback regulation of myosin II

The coupling of active RhoA to its effector Rock requires unknown signalling events that depend on cell adhesion, cell shape and cytoskeletal tension[22]. To uncover integrin-specific regulators of myosin II upstream and downstream of active RhoA we performed SILAC-based quantitative phosphoproteomics of adhesion signalling on fibronectin. We quantified a total of 3,180 proteins (Supplementary Table S2) and 7,529 phosphorylation sites (Supplementary Table S3) in the three cell lines seeded for 45 min on fibronectin. ANOVA tests of triplicate experiments identified 150 proteins and 1,010 phosphorylation events as significantly regulated in at least one of the three cell lines (Fig. 6a and Supplementary Fig. S9, Tables S2 and S3). Hierarchical cluster analysis of the SILAC ratios of the 1,010 phosphorylation events revealed clusters dominated by $\alpha_5\beta_1$ and clusters dominated by α_v-class integrins. We also observed clusters regulated oppositely by $\alpha_5\beta_1$ and α_v-class integrins, indicating antagonistic regulation, and clusters regulated by both integrin classes, indicating synergistic regulation. Using ratio thresholds for the different pairwise comparisons allowed assignment of 646 of the 1,010 determined phospho-sites into either the antagonistic, dominant or synergistic category (Fig. 6b and Supplementary Table S4).

We searched for phospho-sites that influence myosin II activity in an integrin-dependent manner and found that pKO-β_1 and pKO-$\alpha_v\beta_1$ cells showed increased phosphorylation of the RhoA/Rock targets S693-myosin phosphatase-1 (Mypt1; Fig. 6c–e) and S3-cofilin (Fig. 6c–e). MLC phosphorylation can also be induced by Mlck, whose activity is controlled by Ca^{2+} or Erk2 in focal adhesions[38,39]. We observed synergistic downregulation of S364-Mlck and synergistic

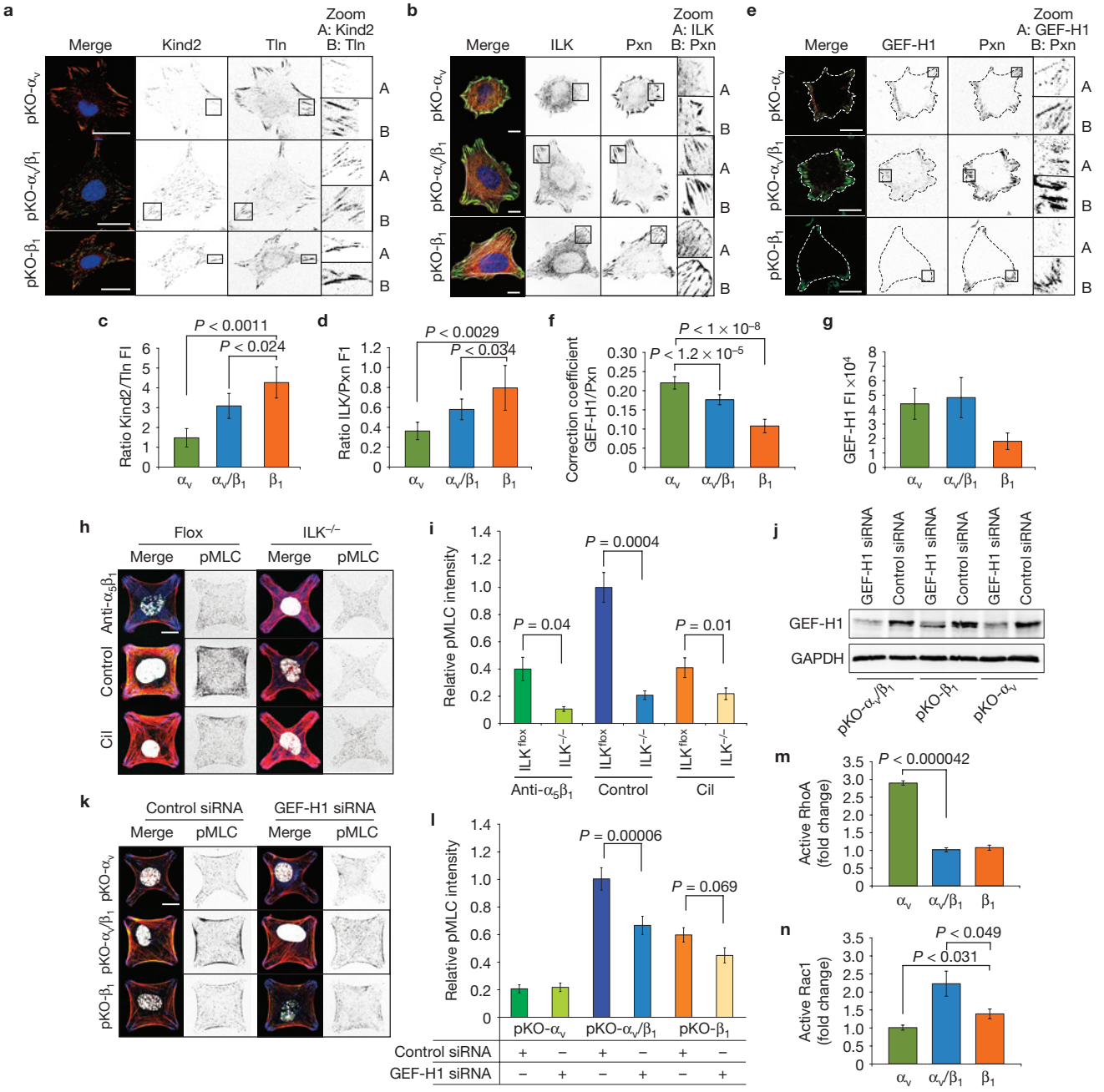

Figure 5 α_v- and β_1-mediated activation of myosin II requires ILK and GEF-H1. (**a**–**f**) Cells were plated on fibronectin-coated glass coverslips for 90 min and immunostained for: Talin-1 (Tln; red) and Kindlin-2 (Kind2; green) (**a**); ILK (red), paxillin (Pxn; green) and F-actin (white) (**b**); or GEF-H1 (red) and paxillin (green) (**e**); scale bars, 10 μm. DAPI, blue (**a**,**b**). Ratios of thresholded fluorescence intensities (FI) were calculated for Kindlin-2 and Talin-1 (pKO-α_v $n = 12$, pKO-β_1 $n = 22$, pKO-α_v/β_1 $n = 22$; results are aggregated over 3 independent experiments) (**c**), and ILK and paxillin (pKO-α_v $n = 33$, pKO-β_1 $n = 40$, pKO-α_v/β_1 $n = 40$; aggregated over 3 independent experiments) (**d**). The correlation coefficient for GEF-H1 and paxillin staining (pKO-α_v $n = 11$, pKO-β_1 $n = 10$, pKO-α_v/β_1 $n = 15$; aggregated over 3 independent experiments) was determined (**f**). (**g**) Total fluorescence intensity of focal-adhesion-retained GEF-H1 after crosslinking and unroofing of cells (pKO-α_v $n = 11$, pKO-β_1 $n = 10$, pKO-α_v/β_1 $n = 15$; aggregated over 3 independent experiments). (**h**) *ILK*$^{-/-}$ and ILK-floxed fibroblasts plated for 3 h on fibronectin-coated X-shapes stained for pMLC, F-actin and paxillin were treated with cilengitide (Cil) to block α_v-class integrins and with monoclonal antibody 2575 to block $\alpha_5\beta_1$. Scale bar, 10 μm. (**i**) Quantification of the relative fluorescence intensities for pMLC to untreated ILK-floxed cells (ILK-flox $n = 26$; ILK-null $n = 17$; ILK-flox +Cil $n = 24$; ILK-null +Cil $n = 12$; ILK-flox +anti-$\alpha_5\beta_1$ $n = 16$, ILK-null anti-$\alpha_5\beta_1$ $n = 10$; data aggregated over 2 independent experiments). (**j**) siRNA-mediated depletion of GEF-H1 confirmed by western blotting. (**k**) Cells were plated on fibronectin-coated X-shapes and stained for pMLC, F-actin and paxillin. Scale bar, 10 μm. (**l**) Quantification of the relative fluorescence intensities for pMLC in siRNA-treated cells (pKO-α_v +control siRNA $n = 24$, pKO-β_1 +control siRNA $n = 48$, pKO-α_v/β_1 +control siRNA $n = 56$, pKO-α_v + GefH1 siRNA $n = 22$, pKO-β_1 + GefH1 siRNA $n = 34$, pKO-α_v/β_1 + GefH1 siRNA $n = 59$; data aggregated over 2 independent experiments). (**m**) Relative RhoA–GTP loading in cells plated for 45 min on fibronectin ($n = 9$; 1 representative of 3 independent experiments is shown). (**n**) Relative Rac1–GTP loading in cells plated for 45 min on fibronectin ($n = 9$; 1 representative out of 3 independent experiments is shown). Error bars represent s.e.m. and *P* values were calculated using a *t*-test. pKO-α_v (green); pKO-α_v/β_1 (blue); pKO-β_1 (orange).

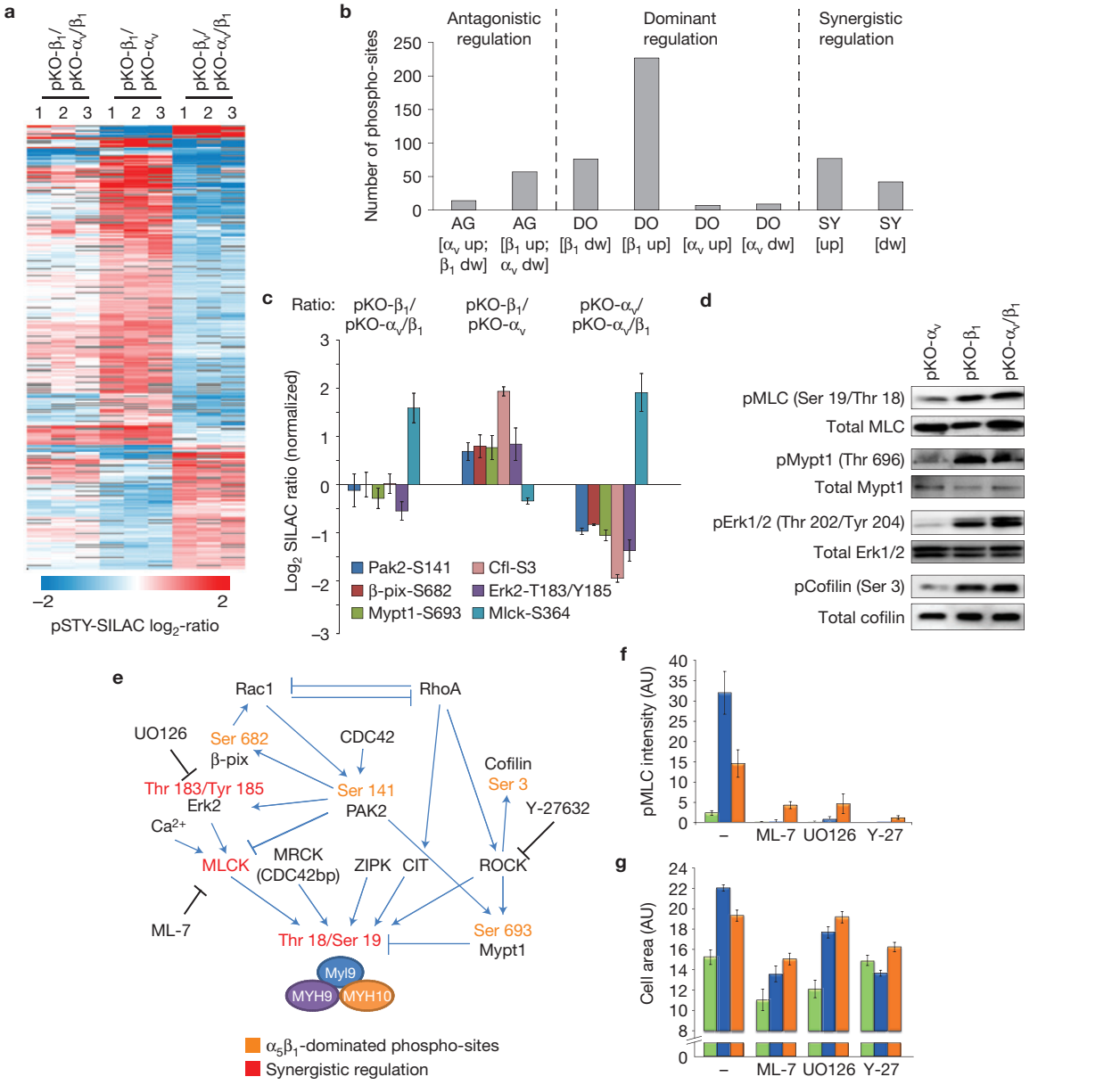

Figure 6 Integrin-specific phosphorylation landscapes on adhesion to fibronectin. (**a**) Hierarchical cluster analysis of SILAC ratios of 1,010 significantly regulated (ANOVA test and Benjamini/Hochberg false discovery rate) phosphorylation events in the indicated cells plated for 45 min on fibronectin from 3 independent replicates. The colour code depicts the normalized $\log_2$ SILAC ratio between cell lines. (**b**) The bar graph shows the number of phosphorylation events grouped into different modes of regulation based on the indicated SILAC ratio threshold criteria. AG, antagonistic; DO, dominant; SY, synergistic. (**c**) SILAC ratios for selected phosphorylation events. The bar graph depicts the median of 3 independent experiments with error bars showing the s.d. (**d**) A selection of differentially regulated phosphorylation events confirmed by western blotting using phospho-site-specific antibodies. (**e**) Signalling network with differentially regulated phosphorylation events shown to be functionally relevant in cell protrusion or contraction. Sites dominated by $\alpha_5\beta_1$ or synergistically upregulated in pKO-α_v/β_1 cells are shown. (**f**,**g**) Mean pMLC fluorescence intensity (**f**) and mean cell area (**g**) on fibronectin-coated X-shapes before and after treatment with ML-7 (25 μM) to inhibit Mlck, UO126 (50 μM) to inhibit ERK and Y-27632 (10 μM) to inhibit Rock. (pKO-α_v: untreated $n = 12$, +ML-7 $n = 10$, +U0126 $n = 15$, +Y-27 $n = 16$; pKO-β_1: untreated $n = 16$, +ML-7 $n = 17$, +U0126 $n = 19$, +Y-27 $n = 21$; pKO-α_v/β_1: untreated $n = 11$, +ML-7 $n = 18$, +U0126 $n = 19$, +Y-27 $n = 30$; 1 representative of 3 independent experiments is shown; all pairwise statistical comparisons using *t*-tests are shown in Supplementary Table S5; error bars represent s.e.m.). pKO-α_v, green; pKO-α_v/β_1, blue; pKO-β_1, orange.

upregulation of pT183/pY185-Erk2 activities in pKO-α_v/β_1 cells (Fig. 6c–e). Western blotting using phospho-site-specific antibodies corroborated these results (Fig. 6d). We uncovered three pathways (Erk2, Rock, Mlck) that were differentially regulated by the two integrin classes following adhesion to fibronectin, and reasoned that inhibition of either one or any combination of these pathways would abrogate synergistic myosin II reinforcement. Indeed, the cooperative activation of myosin II in pKO-α_v/β_1 cells was blocked by inhibiting Erk (UO126), Rock (Y-27632) or Mlck (ML-7; Fig. 6f,g). To confirm the relevance of this finding, we overexpressed constitutively active (ca-) kinase

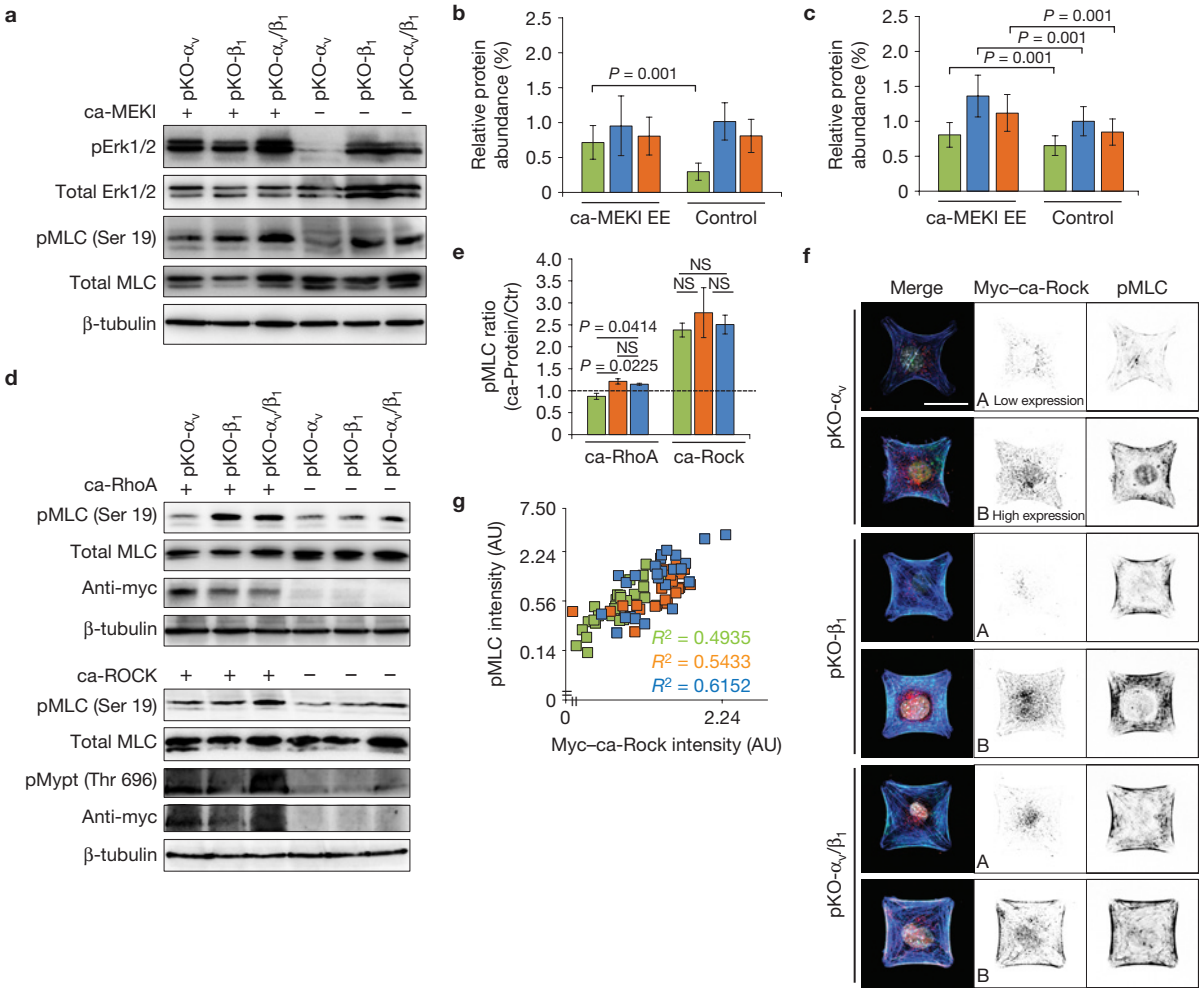

Figure 7 Activation of Rock is $\alpha_5\beta_1$-dependent. (**a**–**c**) Total cell lysates of cells plated for 90 min on fibronectin in the indicated conditions and analysed by western blotting with phospho-specific antibodies. The levels of pErk2 (**b**) and pMLC (**c**) were quantified using densitometry ($n = 3$). (**d**) A representative western blot analysis of cells transfected with myc-tagged ca-RhoA or myc-tagged ca-ROCK constructs and probed with the indicated antibodies. (**e**) Densitometric quantification of western blots ($n = 3$). The bar graphs show ratios of pMLC signals from cells expressing ca-RhoA or ca-Rock over the empty vector control. NS, not significant. (**f**) Confocal image of indicated cells transfected with a myc-tagged ca-ROCK construct, seeded on fibronectin-coated crossbow shapes and immunostained with Myc (red), pMLC (green), F-actin (blue) and DAPI (white). Scale bar, 25 μm. (**g**) Pearson correlation coefficient of fluorescence intensities of pMLC and Myc staining for the three cell lines (pKO-α_v $n = 30$; pKO-β_1 $n = 25$; pKO-α_v/β_1 $n = 25$; 1 representative of 3 independent experiments is shown). All error bars represent s.d. and P values were calculated using a t-test. pKO-α_v (green); pKO-α_v/β_1 (blue); pKO-β_1 (orange). Uncropped images of blots are shown in Supplementary Fig. S10.

constructs and measured their effects on pMLC. Overexpression of ca-MEK1 rescued the low pErk2 levels and significantly increased pMLC in pKO-α_v cells (Fig. 7a–c). The high RhoA and low Rock and pMLC activities in pKO-α_v cells (Figs 5 and 6) suggest that α_v-class integrins are unable to couple active RhoA to Rock, which was tested by overexpressing ca-RhoA or ca-Rock in the three cell lines. Whereas ca-RhoA significantly increased pMLC in pKO-β_1 and pKO-α_v/β_1, pMLC levels remained unchanged in pKO-α_v cells. In sharp contrast, ca-Rock increased pMLC twofold in all three cell lines (Fig. 7d,e), indicating that endogenous Rock in pKO-α_v cells remained inactive even in the presence of high RhoA–GTP. This finding was further confirmed with pMLC staining of cells seeded on fibronectin-coated X shapes (Fig. 7f,g). In conclusion, the Mek1/Erk2 and the RhoA/Rock/pMLC pathways are preferentially induced by $\alpha_5\beta_1$, whereas the high RhoA activity induced in pKO-α_v cells is not coupled to Rock/pMLC.

DISCUSSION

We reconstituted pan-integrin-deficient fibroblasts with β_1- and/or α_v-class integrins and correlated integrin-class-specific cellular phenotypes with integrin-class-specific adhesome composition and signalling events. Fibroblasts exploring fibronectin-based microenvironments engage $\alpha_5\beta_1$ and α_v-class integrins to orchestrate membrane protrusions, cell contractility and cell migration. Our cell line analyses revealed a series of signalling events accomplished by $\alpha_5\beta_1$ integrins, which activate Rac1, induce membrane protrusions, assemble nascent adhesions and generate RhoA/Rock-mediated myosin II activity. In conjunction with these events, mechanosensitive α_v-class integrins accumulate in areas subjected to high tension and reinforce adhesive sites to induce further activation of myosin II and development of large focal adhesions and actomyosin bundles (Fig. 8). Our study uncovers a sequence of tightly integrated biophysical and biochemical events induced by $\alpha_5\beta_1$ and

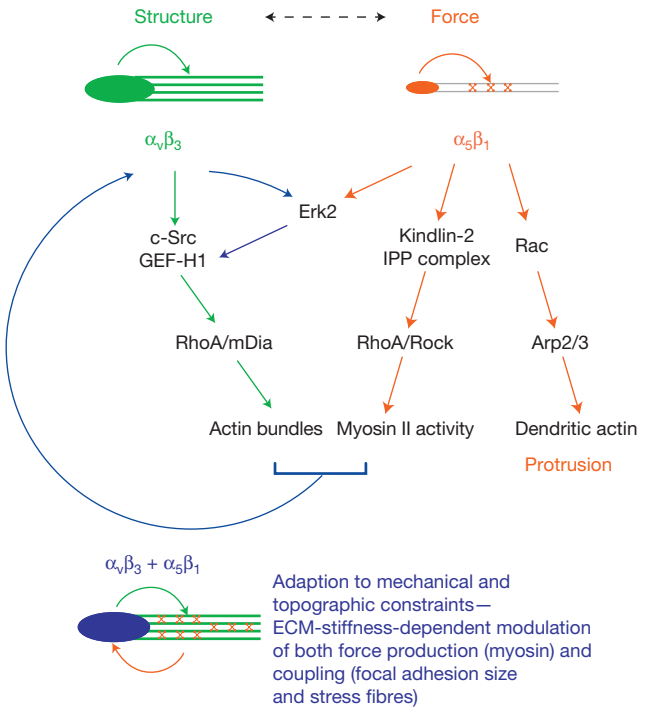

Figure 8 Model of $\alpha_5\beta_1$ and α_v-class integrin cooperation during rigidity sensing. $\alpha_5\beta_1$ integrins adhere to fibronectin, and assemble Kindlin-2- and ILK-rich small peripheral adhesions in a myosin-II-independent manner. The protein assembly in $\alpha_5\beta_1$-containing adhesions activates Rac1, Wave and Arp2/3-driven actin polymerization to induce membrane protrusions, and RhoA/Rock-mediated myosin II activation to induce tension. This tension increases the adhesion lifetime of α_v-class integrins bound to ligand on stiff substrates, which reinforces and stabilizes focal adhesions. α_v-class integrins recruit GEF-H1 to focal adhesions, which reinforces RhoA/myosin II in a $\alpha_5\beta_1$-dependent manner, and increases RhoA activity to promote mDia-mediated stress fibre formation. The combination of α_v-class integrin-mediated structure (focal-adhesion anchoring and stress-fibre formation) with the $\alpha_5\beta_1$-mediated force generation (myosin II activity) constitutes a synergistic system, which is important for adapting cellular contractility and architecture to the rigidity of fibronectin-based microenvironments.

α_v-class integrins that adjust fibroblast contractility to the rigidity of fibronectin-coated substrates. The cooperation of $\alpha_5\beta_1$ and α_v-class integrins to sense the rigidity of fibronectin-based microenvironments predicts that cell migration towards a rigidity gradient, called durotaxis, may also depend on the cooperation of both integrins. These findings have potential ramifications for certain pathologies, such as fibrosis and tumour metastasis where rigidity sensing of fibronectin matrices is crucial in disease progression[40].

To better understand how distinct integrin classes individually and cooperatively probe the biophysical properties of a fibronectin-based microenvironment, we established a cell model system and used proteomics methods to characterize their focal adhesion composition, phospho-signalling and proteome changes. Our comprehensive proteomic data set of adhesion signalling revealed that integrin-class-specific adhesomes and phospho-proteomes are enriched with integrin-specific adapter proteins and signalling intermediates. Several well-known integrin outside-in signalling pathways, including the Rac1/Wave/Arp2,3 and RhoA/Rock pathways, were dominated by $\alpha_5\beta_1$ integrins. Interestingly, the pKO-β_1 cells developed very few stress fibres, indicating that $\alpha_5\beta_1$-induced RhoA activity was preferably used for production of myosin-II-mediated force but not formin-mediated stress-fibre formation. In contrast, the pKO-α_v cells exhibited high RhoA activity, which in turn induced the formation of thick stress fibres, most likely through the activation of mDia, but did not activate Rock/pMLC/myosin II. The coupling of active RhoA to different downstream effectors by distinct integrin classes was unanticipated. The underlying mechanism(s) are unclear, but probably involve specific mark(s) either attached to active RhoA or to the effectors enabling differential interactions with GTP-bound RhoA.

Although forces play an important role in the assembly of focal adhesions, pKO-α_v cells induced the largest focal adhesions among the three cell lines and also exhibited the lowest myosin II activities and traction forces. Focal adhesion size is not the sole predictor of traction forces and the final focal adhesion size can also be determined by an mDia-dependent mechanism[41,42]. Therefore, we propose that the large size of focal adhesions in pKO-α_v cells depends on RhoA/mDia-induced stress fibres rather than on myosin II. However, although the final focal adhesion size in pKO-α_v cells was myosin-II-independent, their formation and/or stability were strictly myosin-II-dependent, evidenced by the pronounced destabilization of α_v-class integrin adhesions with blebbistatin. A role for α_v-class integrins for focal adhesion stabilization has also been obtained from single-protein tracking experiments of β_1 and β_3 integrins, which showed that β_3 integrins are immobilized in large focal adhesions, whereas β_1 integrins are more mobile[29]. The necessity of $\alpha_v\beta_3$ for cell stiffening following force application has also been postulated[43]. Similarly, the recruitment of GEF-H1 to focal adhesions and Erk2 activity was reported as necessary for cell stiffening following force application[35]. Our results link these observations and suggest that force-mediated stabilization of α_v–fibronectin bonds will reinforce focal adhesions, increase local concentrations of GEF-H1 and activate RhoA following $\alpha_5\beta_1$-induced Erk2 activation. Therefore, α_v-class integrins could be capable of forming stronger extracellular catch bonds with fibronectin than $\alpha_5\beta_1$ integrins do[44], resulting in longer bond lifetimes of α_v-class integrins with fibronectin when force is applied. However, as the influence of force on the on and off rates of $\alpha_5\beta_1$ and α_v-class integrins with fibronectin have not been systematically studied, this hypothesis awaits future testing. □

METHODS

Methods and any associated references are available in the online version of the paper.

Note: Supplementary Information is available in the online version of the paper

ACKNOWLEDGEMENTS

We thank J. Cox for software tool development, U. Kuhn and C. Boulegue (MPIB) and A. F. Christ (CNRS/UJF/INRA/CEA) for excellent technical support, and A. Meves, T. Geiger and D. Boettiger for discussions. H.B.S. was a fellow of the European Molecular Biology Organisation (EMBO) and M-R.H. a fellow of the Boehringer Ingelheim fonds. The work was financially supported by the ERC, DFG and the Max Planck Society.

AUTHOR CONTRIBUTIONS

R.F. initiated the project; R.F. and H.B.S. designed the experiments and wrote the paper; H.B.S., M-R.H., T.V., S.Z., J.P., Z.S. and A.R. performed experiments; H.B.S., M-R.H., T.V., S.Z., K-E.G., C.C.F. and R.F. analysed data; J.P., M.T., K-E.G. and M.M. provided important reagents and/or analytical tools; all authors read and approved the manuscript.

COMPETING FINANCIAL INTERESTS
The authors declare no competing financial interests.

Published online at www.nature.com/doifinder/10.1038/ncb2747
Reprints and permissions information is available online at www.nature.com/reprints

1. Hynes, R. O. Integrins: bidirectional, allosteric signaling machines. *Cell* **110,** 673–687 (2002).
2. Desgrosellier, J. S. & Cheresh, D. A. Integrins in cancer: biological implications and therapeutic opportunities. *Nat. Rev. Cancer* **10,** 9–22 (2010).
3. Avraamides, C. J., Garmy-Susini, B. & Varner, J. A. Integrins in angiogenesis and lymphangiogenesis. *Nat. Rev. Cancer* **8,** 604–617 (2008).
4. Liu, H. *et al.* MYC suppresses cancer metastasis by direct transcriptional silencing of α(v) and β(3) integrin subunits. *Nat. Cell Biol.* **14,** 567–574 (2012).
5. Humphries, J. D., Byron, A. & Humphries, M. J. Integrin ligands at a glance. *J. Cell Sci.* **119,** 3901–3903 (2006).
6. Leiss, M., Beckmann, K., Giros, A., Costell, M. & Fassler, R. The role of integrin binding sites in fibronectin matrix assembly *in vivo*. *Curr. Opin. Cell Biol.* **20,** 502–507 (2008).
7. Yang, J. T., Rayburn, H. & Hynes, R. O. Embryonic mesodermal defects in α_5 integrin-deficient mice. *Development* **119,** 1093–1105 (1993).
8. Bader, B. L., Rayburn, H., Crowley, D. & Hynes, R. O. Extensive vasculogenesis, angiogenesis, and organogenesis precede lethality in mice lacking all α_v integrins. *Cell* **95,** 507–519 (1998).
9. Yang, J. T. *et al.* Overlapping and independent functions of fibronectin receptor integrins in early mesodermal development. *Dev. Biol.* **215,** 264–277 (1999).
10. Zamir, E. *et al.* Dynamics and segregation of cell–matrix adhesions in cultured fibroblasts. *Nat. Cell Biol.* **2,** 191–196 (2000).
11. Ballestrem, C., Hinz, B., Imhof, B. A. & Wehrle-Haller, B. Marching at the front and dragging behind: differential $\alpha_v\beta_3$-integrin turnover regulates focal adhesion behavior. *J. Cell Biol.* **155,** 1319–1332 (2001).
12. Danen, E. H., Sonneveld, P., Brakebusch, C., Fassler, R. & Sonnenberg, A. The fibronectin-binding integrins $\alpha_5\beta_1$ and $\alpha_v\beta_3$ differentially modulate RhoA–GTP loading, organization of cell matrix adhesions, and fibronectin fibrillogenesis. *J. Cell Biol.* **159,** 1071–1086 (2002).
13. White, D. P., Caswell, P. T. & Norman, J. C. $\alpha_v\beta_3$ and $\alpha_5\beta_1$ integrin recycling pathways dictate downstream Rho kinase signaling to regulate persistent cell migration. *J. Cell Biol.* **177,** 515–525 (2007).
14. Morgan, M. R., Byron, A., Humphries, M. J. & Bass, M. D. Giving off mixed signals-distinct functions of α(5)β(1) and α(v)β(3) integrins in regulating cell behaviour. *IUBMB Life* **61,** 731–738 (2009).
15. Van der Flier, A. *et al.* Endothelial α_5 and α_v integrins cooperate in remodeling of the vasculature during development. *Development* **137,** 2439–2449 (2010).
16. Choi, C. K. *et al.* Actin and α-actinin orchestrate the assembly and maturation of nascent adhesions in a myosin II motor-independent manner. *Nat. Cell Biol.* **10,** 1039–1050 (2008).
17. Geiger, B., Spatz, J. P. & Bershadsky, A. D. Environmental sensing through focal adhesions. *Nat. Rev. Mol. Cell Biol.* **10,** 21–33 (2009).
18. Bershadsky, A., Kozlov, M. & Geiger, B. Adhesion-mediated mechanosensitivity: a time to experiment, and a time to theorize. *Curr. Opin. Cell Biol.* **18,** 472–481 (2006).
19. Schiller, H. B., Friedel, C. C., Boulegue, C. & Fassler, R. Quantitative proteomics of the integrin adhesome show a myosin II-dependent recruitment of LIM domain proteins. *EMBO Rep.* **12,** 259–266 (2011).
20. Kuo, J. C., Han, X., Hsiao, C. T., Yates Iii, J. R. & Waterman, C. M. Analysis of the myosin II-responsive focal adhesion proteome reveals a role for β-Pix in negative regulation of focal adhesion maturation. *Nat. Cell Biol.* **13,** 383–393 (2011).
21. Lammermann, T. *et al.* Rapid leukocyte migration by integrin-independent flowing and squeezing. *Nature* **453,** 51–55 (2008).
22. Bhadriraju, K. *et al.* Activation of ROCK by RhoA is regulated by cell adhesion, shape, and cytoskeletal tension. *Exp. Cell Res.* **313,** 3616–3623 (2007).
23. Danen, E. H. *et al.* Integrins control motile strategy through a Rho-cofilin pathway. *J. Cell Biol.* **169,** 515–526 (2005).
24. Worth, D. C. *et al.* $\alpha_v\beta_3$ integrin spatially regulates VASP and RIAM to control adhesion dynamics and migration. *J. Cell Biol.* **189,** 369–383 (2010).
25. Huttenlocher, A. & Horwitz, A. R. Integrins in cell migration. *Cold Spr. Harbor Perspec. Biol.* **3,** a005074 (2011).
26. Thery, M. *et al.* Anisotropy of cell adhesive microenvironment governs cell internal organization and orientation of polarity. *Proc. Natl Acad. Sci. USA* **103,** 19771–19776 (2006).
27. Thery, M. Micropatterning as a tool to decipher cell morphogenesis and functions. *J. Cell Sci.* **123,** 4201–4213 (2010).
28. Tseng, Q. *et al.* A new micropatterning method of soft substrates reveals that different tumorigenic signals can promote or reduce cell contraction levels. *Lab on a Chip* **11,** 2231–2240 (2011).
29. Rossier, O. *et al.* Integrins β_1 and β_3 exhibit distinct dynamic nanoscale organizations inside focal adhesions. *Nat. Cell Biol.* **14,** 1057–1067 (2012).
30. Zaidel-Bar, R., Itzkovitz, S., Ma'ayan, A., Iyengar, R. & Geiger, B. Functional atlas of the integrin adhesome. *Nat. Cell Biol.* **9,** 858–867 (2007).
31. Cox, J. & Mann, M. MaxQuant enables high peptide identification rates, individualized p.p.b.-range mass accuracies and proteome-wide protein quantification. *Nat. Biotech.* **26,** 1367–1372 (2008).
32. Zaidel-Bar, R. & Geiger, B. The switchable integrin adhesome. *J. Cell Sci.* **123,** 1385–1388 (2010).
33. Meves, A. *et al.* {β}1 integrin cytoplasmic tyrosines promote skin tumorigenesis independent of their phosphorylation. *Proc. Natl Acad. Sci. USA* **108,** 15213–15218 (2011).
34. Sakai, T. *et al.* Integrin-linked kinase (ILK) is required for polarizing the epiblast, cell adhesion, and controlling actin accumulation. *Genes Dev.* **17,** 926–940 (2003).
35. Guilluy, C. *et al.* The Rho GEFs LARG and GEF-H1 regulate the mechanical response to force on integrins. *Nat. Cell Biol.* **13,** 722–727 (2011).
36. Montanez, E., Wickstrom, S. A., Altstatter, J., Chu, H. & Fassler, R. α-parvin controls vascular mural cell recruitment to vessel wall by regulating RhoA/ROCK signalling. *EMBO J.* **28,** 3132–3144 (2009).
37. Montanez, E. *et al.* Kindlin-2 controls bidirectional signaling of integrins. *Genes Dev.* **22,** 1325–1330 (2008).
38. Holzapfel, G., Wehland, J. & Weber, K. Calcium control of actin-myosin based contraction in triton models of mouse 3T3 fibroblasts is mediated by the myosin light chain kinase (MLCK)-calmodulin complex. *Exp. Cell Res.* **148,** 117–126 (1983).
39. Fincham, V. J., James, M., Frame, M. C. & Winder, S. J. Active ERK/MAP kinase is targeted to newly forming cell–matrix adhesions by integrin engagement and v-Src. *EMBO J.* **19,** 2911–2923 (2000).
40. Butcher, D. T., Alliston, T. & Weaver, V. M. A tense situation: forcing tumour progression. *Nat. Rev. Cancer* **9,** 108–122 (2009).
41. Oakes, P. W., Beckham, Y., Stricker, J. & Gardel, M. L. Tension is required but not sufficient for focal adhesion maturation without a stress fibre template. *J. Cell Biol.* **196,** 363–374 (2012).
42. Stricker, J., Aratyn-Schaus, Y., Oakes, P. W. & Gardel, M. L. Spatiotemporal constraints on the force-dependent growth of focal adhesions. *Biophys. J.* **100,** 2883–2893 (2011).
43. Roca-Cusachs, P., Gauthier, N. C., Del Rio, A. & Sheetz, M. P. Clustering of α(5)β(1) integrins determines adhesion strength whereas α(*v*)β(3) and talin enable mechanotransduction. *Proc. Natl Acad. Sci. USA* **106,** 16245–16250 (2009).
44. Kong, F., Garcia, A. J., Mould, A. P., Humphries, M. J. & Zhu, C. Demonstration of catch bonds between an integrin and its ligand. *J. Cell Biol.* **185,** 1275–1284 (2009).

METHODS

Antibodies. Information about antibodies is provided in Supplementary Table S6.

Isolation, immortalization, viral reconstitution and transfection of cell lines. Mouse pKO fibroblasts and reconstituted pKO-α_v, pKO-β_1 and pKOα_v/β_1 cell lines were generated from fibroblasts (floxed parental) derived from the kidney of 21-day-old male mice carrying floxed α_v and β_1 alleles ($\alpha_v^{flox/flox}$, $\beta_1^{flox/flox}$), and constitutive β_2 and β_7 null alleles ($\beta_2^{-/-}$, $\beta_7^{-/-}$; ref. 21). Individual kidney fibroblast clones were immortalized by retroviral delivery of the SV40 large T. The immortalized floxed fibroblast clones were then retrovirally transduced with mouse α_v and/or β_1 integrin cDNAs and the endogenous floxed β_1 and α_v integrin loci were simultaneously deleted by adenoviral transduction of the *Cre* recombinase. Reconstituted cell lines were FACS sorted to obtain cell populations with comparable integrin surface levels to the parental cell clones. Transduction of ca-RhoA (myc–RhoA pcDNA3.1) and ca-ROCK (myc–ROCKD4 pcDNA3.1) was carried out with Lipofectamine 2000 (Invitrogen through Life Technologies) according to the manufacturer's instructions. The transfection control was an empty pcDNA3.1 vector.

Adhesion and cell migration analysis. Adhesion assays were carried out as previously described[45]. Briefly, cells were plated for 20 min in 96-well plates coated with varying concentrations of ECM ligands. After washing the plates the number of adhered cells that remained on the plate was quantified using attenuance at 595 nm.

To analyse random migration, cell culture dishes were coated with fibronectin (5 μg ml^{-1} in PBS; 2 h at room temperature) and blocked with 1% BSA in PBS. After seeding, video time-lapse microscopy was performed using phase contrast at ×20 magnification. A total of 12 migrating pKO-α_v, 12 migrating pKO-α_v/β_1 and 14 migrating pKO-β_1 cells from 5 independent movies were analysed. One pixel in each cell nucleus was marked manually and served as the cell's coordinate. Each tracked cell j with a track length N_j was recorded by its $x_{j,i}$ and yj,i position for every frame i. A tracking point was made every $D_t = 1$ min. The time difference between the tracking coordinates $x_{j,i}$ and $x_{j,i+n}$ is $t = nD_t$, where n is the frame number. The mean squared displacement (msd) of the cell j at time $t = nD_t$ was calculated by

$$msd_j(t) = \frac{1}{N_j - n}\sum_{i=1}^{N_j-n}\left[\left(x_{j,i+n} - x_{j,i}\right)^2 + \left(y_{j,i+n} - y_{j,i}\right)^2\right]$$

All msd values were calculated for all cells and averaged. The used propagated uncertainty for the $msd(t)$ is the standard deviation of the mean. For an increasing n the number of given tracks contributes to $msd(t)$ decreases as well as the propagated uncertainty caused by the tracking uncertainty increases. Therefore, the $msd(t)$ has been cut at $n = 90$. To determine the persistence time P and the diffusion constant D, Fürths formula

$$msd(t) = 4D\left(t - P\left(1 - \exp\left(-\frac{t}{P}\right)\right)\right)$$

has been fitted through the data. The mean velocity of a cell j has been computed as the average of the distance travelled each time step divided by the time step.

Micropatterning and immunostainings. Micropatterns were generated on PEG-coated glass coverslips with deep-ultraviolet lithography[46]. Glass coverslips were incubated in a 1 mM solution of a linear PEG, CH_3–$(O$–CH_2–$CH_2)_{43}$–NH–CO–NH–CH_2–CH_2–CH_2–$Si(OEt)_3$ in dry toluene for 20 h at 80 °C under a nitrogen atmosphere. The substrates were removed, rinsed intensively with ethyl acetate, methanol and water, and dried with nitrogen. A pegylated glass coverslip and a chromium-coated quartz photomask (ML&C, Jena) were immobilized with vacuum onto a mask holder, which was immediately exposed to deep ultraviolet light using a low-pressure mercury lamp (NIQ 60/35 XL longlife lamp, quartz tube, 60 W from Heraeus Noblelight) at 5 cm distance for 7 min. The patterned substrates were subsequently incubated overnight with 100 μl of fibronectin (20 μg ml^{-1} in PBS) at 4 °C and washed once with PBS.

For immunofluorescence microscopy, cells were seeded on micropatterns in DMEM (GIBCO by Life Technologies) containing 0.5 % FBS at 37 °C, 5% CO_2. After 90 or 180 min the medium was soaked off, and cells were fixed with 3% PFA in PBS for 5 min at room temperature, washed with PBS, blocked with 1% BSA in PBS for 1 h at room temperature and then incubated with antibodies. The fluorescent images were collected with a laser scanning confocal microscope (Leica SP5).

Acrylamide micropatterning. Micropatterns were first produced on glass coverslips as previously described[46]. Briefly, 20 mm square glass coverslips were oxidized through oxygen plasma (FEMTO, Diener Electronics) for 10 s at 30 W before incubating with 0.1 mg ml^{-1} poly-L-lysine (PLL)–PEG (PLL20K-G35-PEG2K, JenKem) in 10 mM HEPES, pH 7.4, for 30 min. After drying, coverslips were exposed to 165 nm ultraviolet (UVO cleaner, Jelight) through a photomask (Toppan) for 5 min. Then, coverslips were incubated with 20 mg ml^{-1} of fibronectin (Sigma) and 2 mg ml^{-1} of rhodamine-labelled fibronectin (Cytoskeleton) in 100 mM sodium bicarbonate solution for 30 min. Acrylamide solution containing acrylamide and bisacrylamide (Sigma) was degassed for 20 min under house vacuum and mixed with passivated fluorescent beads (Invitrogen) by sonication before addition of APS and TEMED. A 25 μl drop of this solution was put directly on the micropatterned glass coverslip. A silanized coverslip was placed over the drop and left polymerizing for 30 min (fluorescent beads passivation and glass silanization were performed as previously described[4]). The sandwich was then put in 100 mM sodium bicarbonate solution and the gel was gently removed from the patterned glass coverslip while staying attached to the other coverslip owing to the silanization treatment. This process transferred the protein micropatterns onto the gel as previously described[47]. Three different solutions of 3%/0.225%, 5%/0.225%, 8%/0.264% acrylamide/bisacrylamide were used. The corresponding Young's modulus of the gels was 1.4, 9.6 and 34.8 kPa respectively as measured using AFM. Coverslips were mounted in magnetic chambers (Cytoo) and washed with sterile PBS before plating cells.

AFM measurements of the Young's modulus of acrylamide gels. We measured gel stiffness through nanoindentation using an atomic force microscope (Bruker Nanoscope) mounted with silica-bead-tipped cantilevers (r(bead) = 2.5 μm, nominal spring constant 0.06 N m^{-1}, Novascan Technologies). Initially, we determined the sensitivity of the photodiode to cantilever deflection by measuring the slope of a force distance curve when pressing the cantilever onto a glass coverslip, and the force constant of the cantilever using the thermal noise method included in the Bruker Nanoscope software. For each acrylamide/bisacrylamide ratio used in the traction-force microscopy measurements we acquired 27 force curves in 3 by 3 grids (2 μm spacing between points) at three different locations on the gels. Before and during indentation experiments gels were kept in PBS. To obtain stiffness values from force curves we used the NanoScope Analysis software. Specifically, we corrected for baseline tilt, and used the linear fitting option for the Hertz model with a Poisson ration of 0.48 on the indentation curve.

Traction-force microscopy and image analysis. Confocal acquisition was performed on an Eclipse TI-E Nikon inverted microscope equipped with a CSUX1-A1 Yokogawa confocal head and an Evolve EMCCD camera (Ropert Scientific, Princeton Instrument). A CFI Plan APO VC oil ×60/1.4 objective (Nikon) was used. The system was driven by the Metamorph software (Universal Imaging).

Traction-force microscopy was performed as previously described[28]. Displacement fields describing the deformation of the polyacrylamide substrate are determined from the analysis of fluorescent bead images before and after removal of the adhering cell with trypsin treatment. Images of fluorescent beads were first aligned to correct experimental drift using the Align slices in stack ImageJ plugin. The displacement field was subsequently calculated by a custom-written particle image velocimetry (PIV) program implemented as an ImageJ (http://rsb.info.nih.gov/ij) plugin. The PIV was performed through an iterative scheme. In all iterations the displacement was calculated by the normalized correlation coefficient algorithm, so that an individual interrogation window was compared with a larger searching window. The next iteration takes into account the displacement field measured previously, so that a false correlation peak due to insufficient image features is avoided. The normalized cross-correlation also allowed us to define an arbitrary threshold to filter out low correlation values due to insufficient beads present in the window. The resulting final grid size for the displacement field was 2.67 × 2.67 μm. The erroneous displacement vectors due to insufficient beads present in the window were filtered out by their low correlation value and replaced by the median value from the neighbouring vectors. With the displacement field obtained from the PIV analysis, the traction-force field was reconstructed by the Fourier transform traction cytometry (FTTC) method with regularized scheme on the same grid (2.67 × 2.67 μm) without further interpolation or remapping. The regularization parameter was set at 1 × 10–11 for all traction-force reconstructions. The Fourier transform traction cytometry code was also written in Java as an ImageJ plugin, so that the whole traction-force microscopy procedure from PIV to force calculation could be performed with ImageJ. The entire package of traction-force microscopy software is available at https://sites.google.com/site/qingzongtseng/tfm. Contractile

DOI: 10.1038/ncb2747

energy was then computed as the integral under the cell of the scalar product of force and displacement vectors using a custom-written code in MatLab. Force profiles along the cell front were generated by integration of the traction maps over the width of the circular part of the pattern. Average pictures were generated after alignment using the Align slices in stack ImageJ plugin. Focal adhesion intensity profiles were generated by integration of the paxillin intensity along the border of the circular part of the micropattern.

Rho–GTPase assays. Cells were serum-starved overnight, detached with trypsin–EDTA and kept in suspension in serum-free medium for 1 h. Cells were then plated on fibronectin-coated dishes (blocked with 1% BSA) in serum-free medium for 45 min. Cell lysis and active Rho–GTPase pulldown was performed using the active Rac1 Pull-Down and Detection Kit or the active Rho Pull-Down and Detection Kit (Cat#16118, 16116, Pierce) according to the manufacturer's instruction. The active GTPase signal was normalized to total protein level of the GTPase. Western blots were quantified with Totallab.

RNA interference. Cells were transiently transfected with a final concentration of 300 nM siRNA (stealth RNAi; Invitrogen) using Lipofectamine 2000 (Invitrogen) according to the manufacturer's protocol, using the targeting sequence sense-5′-CCCGGAACUUUGUCAUCCAUCGUUU-3′ for GEF-H1. As a control we used the scrambled sequence sense-5′-CCCUCAAUGUUCUACCUACGGGUUU-3′.

MS. For proteome and phosphoproteome analysis fibroblasts were cultured in lysine/arginine-free DMEM with 10% FBS (10 KDa dialysed, PAA) and SILAC labelled with light (L-arginine (R0) and L-lysine (K0))], medium (L-arginine-U-$^{13}C_6$ (R6) and L-lysine-$^{2}H_4$(K4)) or heavy (L-arginine-U-$^{13}C_6$ $-^{15}N_4$ (R10) and L-lysine-U-$^{13}C_6$ $-^{15}N_2$ (K8)) amino acids (Cambridge Isotope Laboratories). For phosphoproteome analysis, cells were serum-starved for 6 h and then plated in serum-free medium on fibronectin-coated and BSA-blocked culture dishes for 45 min. Cells were lysed in lysis buffer (100 mM Tris–HCl, at pH 7.5, containing 4% SDS and 100 mM dithiothreitol), boiled 5 min at 95 °C, and sonicated. Lysate was clarified by a 10 min centrifugation at 16,000*g*. Cleared light/medium/heavy proteins were mixed at a 1:1:1 ratio and digested with trypsin using the FASP protocol[48]. For proteome analysis, 40 µg of peptides was separated with strong anion exchange chromatography[49]. For phosphoproteome analysis, 3 mg of peptides was fractionated with strong cation exchange chromatography and enriched for phosphorylated peptides with titanium dioxide (TiO_2) as described previously[50]. Peptides were then analysed on a LTQ-Orbitrap Velos equipped with a nanoelectrospray source (Thermo Fisher Scientific). The full-scan MS spectra were acquired in the Orbitrap with a resolution of 30,000 at m/z 400. The ten most intense ions were fragmented by higher-energy collisional dissociation and the spectra of the fragmented ions were acquired in the Orbitrap analyser with a resolution of 7,500. Peptides were identified and quantified using the MaxQuant software[31] and searched with the Andromeda search engine against the mouse IPI database 3.68 (ref. 51). Phosphorylations were assigned as previously described[50].

The adhesome analysis was performed as previously described[19]. In brief, cells were serum-starved for 4 h and plated for either 45 or 90 min in serum-free medium on fibronectin-coated, BSA-blocked, culture dishes. Optionally, cells were treated with 50 µM blebbistatin for 30 or 75 min. Enrichment for focal-adhesion-associated proteins was achieved by shortly fixing the ventral cell cortex using chemical crosslinkers, followed by removal of non-crosslinked proteins and big organelles by stringent cell lysis and hydrodynamic sheer flow washing. Quantitative mass spectrometric analysis was performed on an LTQ Orbitrap mass spectrometer (Thermo Electron) and analysed using the label-free quantification algorithm[52], which is embedded in the MaxQuant software[31], as previously described[19].

For in-gel digestion, gel bands were cut into 1 mm^3 cubes and washed two times with 50 mM ammonium bicarbonate in 50% ethanol. For protein reduction, gel pieces were incubated with 10 mM dithiothreitol in 50 mM ammonium bicarbonate for 1 h at 56 °C. Alkylation of cysteines was performed with 10 mM iodoacetamide in 50 mM ammonium bicarbonate for 45 min at 25 °C in the dark. Gel pieces were washed two times with 50 mM ammonium bicarbonate in 50% ethanol, dehydrated with 100% ethanol, and dried in a vacuum concentrator. The gel pieces were rehydrated with 12.5 ng µl^{-1} trypsin (sequencing grade, Promega) in 50 mM ammonium bicarbonate and digested overnight at 37 °C. Supernatants were transferred to fresh tubes, and the remaining peptides were extracted by incubating gel pieces two times with 30% acetonitrile in 3% TFA followed by dehydration with 100% acetonitrile. The extracts were combined and desalted using RP-C18 StageTip columns, and the eluted peptides used for mass spectrometric analysis.

For nanoLC–MS/MS, peptide mixtures were separated by on-line nanoLC and analysed by electrospray tandem MS. The experiments were performed on an Agilent 1200 nanoflow system connected to an LTQ Orbitrap mass spectrometer (Thermo Electron) equipped with a nanoelectrospray ion source (Proxeon Biosystems). Binding and chromatographic separation of the peptides took place in a 15-cm fused-silica emitter (75-µm inner diameter from Proxeon Biosystems) in-house packed with reversed-phase ReproSil-Pur C18-AQ 3 µm resin (Dr. Maisch). Peptide mixtures were injected onto the column with a flow of 500 nl min^{-1} and subsequently eluted with a flow of 2500 nl min^{-1} from 2% to 40% acetonitrile in 0.5% acetic acid, in a 100 min gradient. The precursor ion spectra were acquired in the Orbitrap analyser (m/z 300–1,800, $R = 60{,}000$, and ion accumulation to a target value of 1,000,000), and the ten most intense ions were fragmented and recorded in the ion trap. The lock mass option enabled accurate mass measurement in both MS and Orbitrap MS/MS mode as described previously[53]. Target ions already selected for MS/MS were dynamically excluded for 60 s.

For peptide identification and peptide quantification, the data analysis was performed with the MaxQuant software as described previously[31,54], supported by Andromeda as the database search engine for peptide identifications. Peaks in MS scans were determined as three-dimensional hills in the mass-retention time plane. MS/MS peak lists were filtered to contain at most six peaks per 100 Da interval and searched by Andromeda (in-house-developed software) against the Mouse International Protein Index database. The initial mass tolerance in MS mode was set to 7 ppm and MS/MS mass tolerance was 0.5 Da. Cysteine carbamidomethylation was searched as a fixed modification, whereas N-acetyl protein, oxidized methionine, *N*-carbamidomethylated DSP protein and carbamidomethylated DSP lysine were searched as variable modifications. Finally, the label-free quantification algorithm implemented in the MaxQuant software was used as described earlier[52].

SILAC-based peptide pulldowns were carried out with the cytoplasmic tails of β_1 integrin (5′-HDRREFAKFEKEKMNAKWDTGENPIYKSAVTTVVNPKYEGK-3′) and the tails of β_3 integrin (5′-HDRKEFAKFEEERARAKWDTANNPLYKEATS-TFTNITYRGT-3′). The tail peptides were *de novo* synthesized with a desthiobiotin on the amino terminus, coupled to magnetic streptavidin beads (MyOne Streptavidin C1—Invitrogen) and pulldowns from SILAC-labelled cell lysates were performed as described previously[33]. After a mild wash the bound proteins were eluted from the magnet using 16 mM biotin (Sigma-Aldrich). After protein precipitation and in-solution digestion, LC-MS/MS and data analysis was performed as described above. The peptide pulldown experiments were done as reverse SILAC labelling experiments in duplicate (4 biological replicates). We generally considered outliers with high SILAC ratios and high sequence coverage/intensity as more significant than proteins that had only a high SILAC ratio.

Bioinformatics and statistics. ANOVA analysis of the cellular proteome and phosphoproteome was performed using the Perseus bioinformatics toolbox of MaxQuant (J. Cox *et al.*; manuscript in preparation). Multiple testing corrections were performed using the inbuilt permutation method and significant hits were identified at a significance level of 0.01 and 0.05, respectively. ANOVA analysis of the 245 core adhesome proteins was performed using the statistical programming language R (http://www.R-project.org) with the adaptive Benjamini and Hochberg step-up false discovery rate-controlling procedure for multiple testing and a significance level of 0.05. Hierarchical clustering was performed using an average linkage approach and Euclidean distances. Enrichment analysis of clusters for Gene Ontology (GO) terms, KEGG pathways and PFAM and INTERPRO protein domains was performed with the DAVID webserver[55] using the multiple testing correction method by Benjamini and Hochberg and a significance level of 0.05. Protein–protein interactions (PPIs) were compiled from different sources including: PPI databases (DIP (ref. 56; version of December 2009), IntAct (ref. 57) and MINT (ref. 58) (both downloaded on 19 May 2010), BIOGRID (ref. 59; version 3.0.64) and HPRD (ref. 60; Release 9)); the adhesome network database[32]; and the KEGG pathway database[61]. For the adhesome network database, we distinguished between undirected PPIs and directed activating and inhibiting interactions as annotated in the adhesome database and in KEGG. Human and mouse interactions were combined using the orthologue tables of the Mouse Genome Database (MGI) to increase coverage. The high-confidence network of PPIs from public databases contained only interactions reported in at least two separate publications. Networks were visualized using the Cytoscape software. Bar graphs throughout the study were generated in Microsoft Office and depict, unless otherwise indicated, the means and standard errors of the means. Box plots and dot plots were generated using the SigmaPlot software or the MatLab software.

Data deposition. Raw data for the phosphoproteome and proteome analyses of the three cell lines are deposited in the Tranche database (https://proteomecommons.org/tranche/) with the following accession numbers: Schiller_Integrins_Phosphoproteome, on33gw4tEXu5YErn5zrp; Schiller_Integrins_Proteome, EvAbqut9c7fC9OQTyawI.

45. Schiller, H. B., Szekeres, A., Binder, B. R., Stockinger, H. & Leksa, V. Mannose 6-phosphate/insulin-like growth factor 2 receptor limits cell invasion by controlling $\alpha_v\beta_3$ integrin expression and proteolytic processing of urokinase-type plasminogen activator receptor. *Mol. Biol. Cell* **20,** 745–756 (2009).
46. Azioune, A., Carpi, N., Tseng, Q., Thery, M. & Piel, M. Protein micropatterns: a direct printing protocol using deep UVs. *Meth. Cell Biol.* **97,** 133–146 (2010).
47. Rape, A. D., Guo, W. H. & Wang, Y. L. The regulation of traction force in relation to cell shape and focal adhesions. *Biomaterials* **32,** 2043–2051 (2011).
48. Wisniewski, J. R., Zougman, A., Nagaraj, N. & Mann, M. Universal sample preparation method for proteome analysis. *Nat. Methods* **6,** 359–362 (2009).
49. Wisniewski, J. R., Zougman, A. & Mann, M. Combination of FASP and StageTip-based fractionation allows in-depth analysis of the hippocampal membrane proteome. *J. Proteome Res.* **8,** 5674–5678 (2009).
50. Olsen, J. V. *et al*. Global, *in vivo*, and site-specific phosphorylation dynamics in signaling networks. *Cell* **127,** 635–648 (2006).
51. Cox, J. *et al*. Andromeda: a peptide search engine integrated into the MaxQuant environment. *J. Proteome Res.* **10,** 1794–1805 (2011).
52. Luber, C. A. *et al*. Quantitative proteomics reveals subset-specific viral recognition in dendritic cells. *Immunity* **32,** 279–289 (2010).
53. Olsen, J. V. *et al*. Parts per million mass accuracy on an Orbitrap mass spectrometer via lock mass injection into a C-trap. *Mol. Cell Proteomics* **4,** 2010–2021 (2005).
54. Cox, J. *et al*. A practical guide to the MaxQuant computational platform for SILAC-based quantitative proteomics. *Nat. Protocols* **4,** 698–705 (2009).
55. Huang da, W., Sherman, B. T. & Lempicki, R. A. Systematic and integrative analysis of large gene lists using DAVID bioinformatics resources. *Nat. Protocols* **4,** 44–57 (2009).
56. Xenarios, I. *et al*. DIP, the database of interacting proteins: a research tool for studying cellular networks of protein interactions. *Nucleic Acids Res.* **30,** 303–305 (2002).
57. Aranda, B. *et al*. The IntAct molecular interaction database in 2010. *Nucleic Acids Res.* **38,** D525–D531 (2010).
58. Ceol, A. *et al*. MINT, the molecular interaction database: 2009 update. *Nucleic Acids Res.* **38,** D532–D539 (2010).
59. Breitkreutz, B. J. *et al*. The BioGRID Interaction Database: 2008 update. *Nucleic Acids Res.* **36,** D637–D640 (2008).
60. Prasad, T. S., Kandasamy, K. & Pandey, A. Human protein reference database and human proteinpedia as discovery tools for systems biology. *Methods Mol. Biol.* **577,** 67–79 (2009).
61. Kanehisa, M., Goto, S., Sato, Y., Furumichi, M. & Tanabe, M. KEGG for integration and interpretation of large-scale molecular data sets. *Nucleic Acids Res.* **40,** D109–D114 (2012).

DOI: 10.1038/ncb2747

nature cell biology

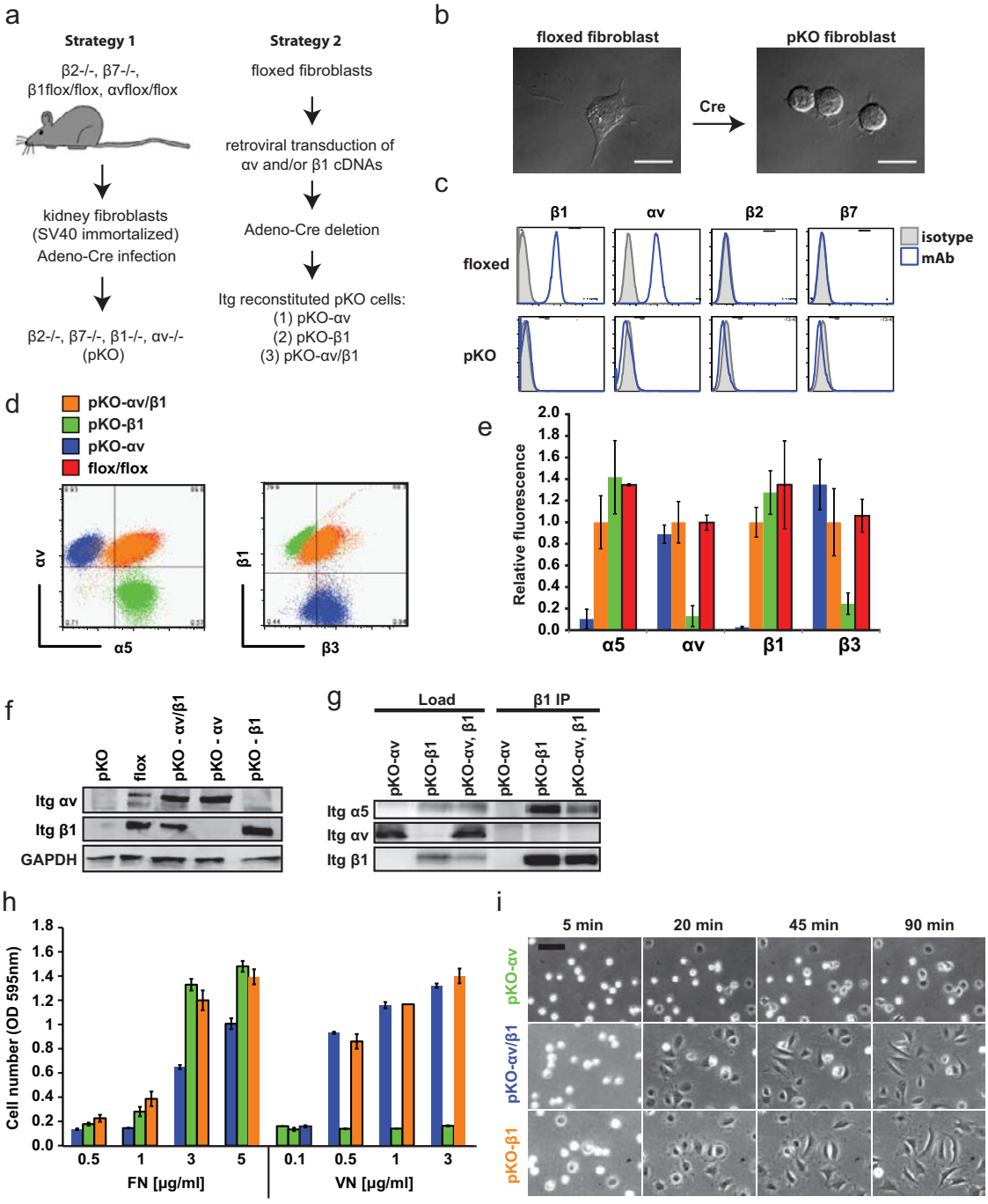

Figure S1 Generation of pKO-αv, pKO-β1 and pKO-αv/β1 cell lines. (**a**) Workflow of the generation of pKO kidney fibroblasts (strategy 1) and integrin reconstituted pKO fibroblasts (strategy 2). (**b**) Phase contrast image of the floxed and pKO cells plated on FN. Scale bar 20 μm. (**c**) Integrin profile of floxed and pKO cells analysed by flow cytometry. (**d**) Cell surface levels of indicated integrins analysed by flow cytometry. (**e**) Relative fluorescence intensities of indicated integrins from three independent stainings analysed by flow cytometry. The means (n=3) and standard deviations are shown. (**f**) Western blots for αv and β1 integrins. GAPDH was used as loading control. (**g**) Cell lysates and immunoprecipitates of β1 integrin were immunoblotted for αv, α5 and β1 integrins. Note that αv does not associate with β1 in pKO-αv/β1 cells. (**h**) Adhesion assay on fibronectin (FN) or vitronectin (VN). Numbers of adherent cells 20 minutes after seeding are shown as relative values of OD=595nm. The bar graph shows the mean and s.e.m. (n=3; one representative out of 2 independent experiments is shown). (i) Cells plated on FN and time-lapse imaged using a phase contrast microscope at 20x magnification. Scale bar 100 μm. pKO-β1 (green); pKO-αv (blue); pKO-αv/β1 (orange); parental β1/αv floxed cell (red).

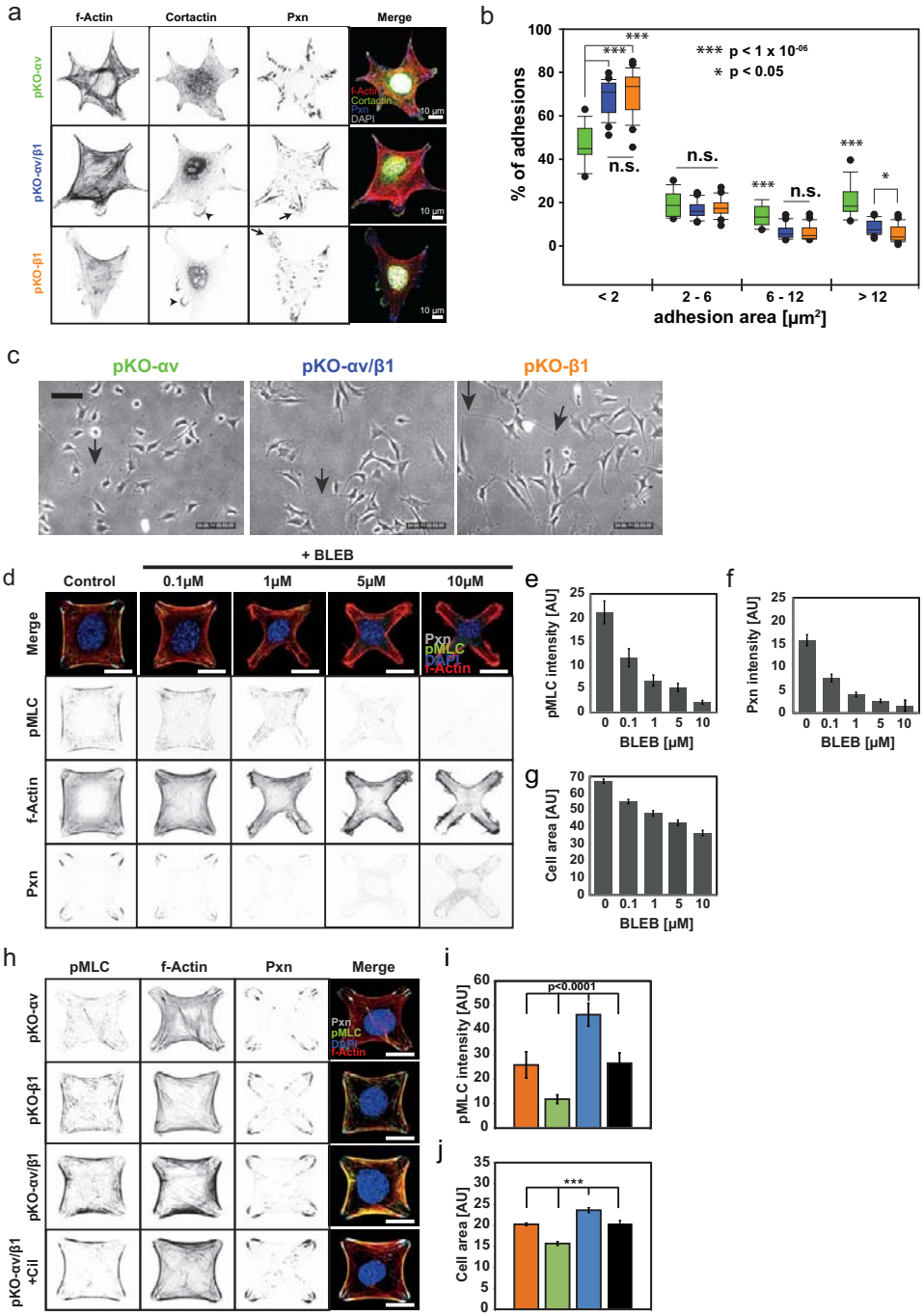

Figure S2 α5β1 and αv-class integrins induce different spreading areas, membrane protrusions and adhesion sites on FN. (**a**) Cells were plated on FN for 90 minutes and immunostained with the indicated antibodies. Arrowheads indicate cortactin-positive lamellipodia and arrows mark the small NAs in lamellipodia. Scale bar 10µm. (**b**) Size distribution of adhesive sites of cells stained with Paxillin calculated with the Metamorph software. Boxplots show the percentage of adhesions in the depicted size classes (pKO-αv n=15; pKO-αv/β1 n= 29; pKO-β1 n=23; one representative out of 2 independent experiments is shown). Boxplot whisker ends are at 1.5 interquartile range and outliers are shown as dots. Significance was calculated using a *t* test (*=p<0.05; ***=p<10 E-06). (**c**) Still pictures taken from supplementary movies S1-S3 showing trailing edge detachment defects indicated by the arrows. Scale bar 100 µm. (**d**) Floxed cells cultured 3 hours on FN-coated X-shapes treated for 1 hour with indicated concentrations of blebbistatin (BLEB), and then stained for Paxillin, pMLC and f-actin. Scale bar 10 µm. (**e**) Fluorescence intensities of pT18/S19-MLC, **(f)** Paxillin (Pxn) and **(g)** cell areas after blebbistatin treatment (n=20 cells; error bars represent s.e.m.). (**h**) Cells plated on FN-coated X-shapes and stained for pMLC, Paxillin and f-actin. Scale bar 10 µm. (**i**) Fluorescence intensities of pS18/T19-MLC and (**j**) cell areas (pKO-αV n=46, pKO-β1 n=46, pKO-αV/β1 n=21, pKO-αV/β1 +Cil n=10; one representative out of 3 independent experiments is shown; error bars represent s.e.m.). Cilengitide (Cil) was used to block αv-class integrins. Significance was calculated using a ttest. pKO-αv (green); pKOαv/β1 (blue); pKO-β1 (orange); pKOαv/β1 + 1 µM cilengitide (black).

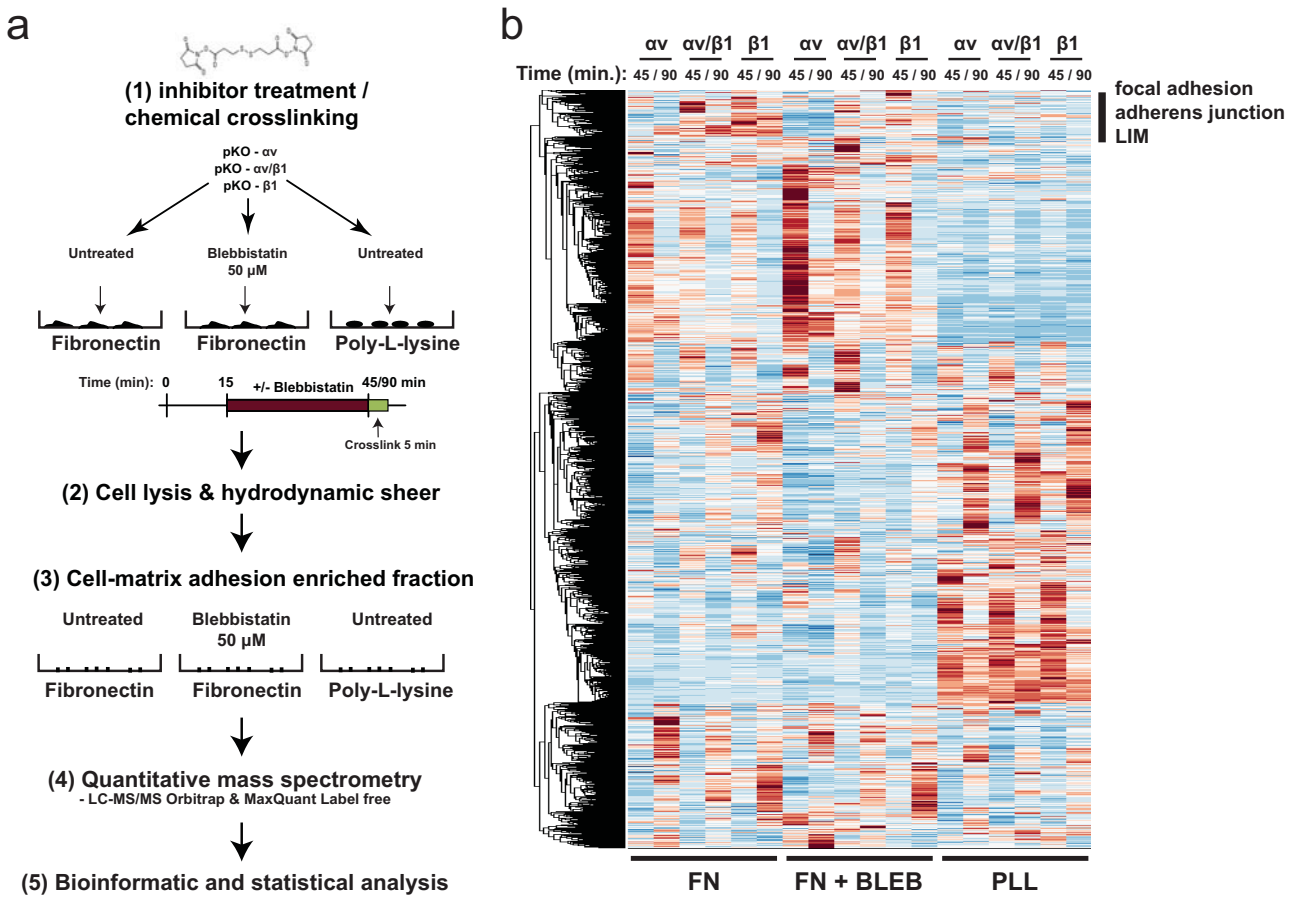

Figure S3 Adhesome analysis of pKO-αv, pKO-β1 and pKOαv/β1 cells. (**a**) Workflow for isolation of FA enriched fractions and analysis of adhesome components. (**b**) Adhesomes derived from cells plated on indicated substrates for 45 or 90 minutes were examined by non-supervised hierarchical cluster analysis of Z-scores of median MS intensities (n=3-4). The labels on the right indicate significantly enriched gene ontology (GO) terms.

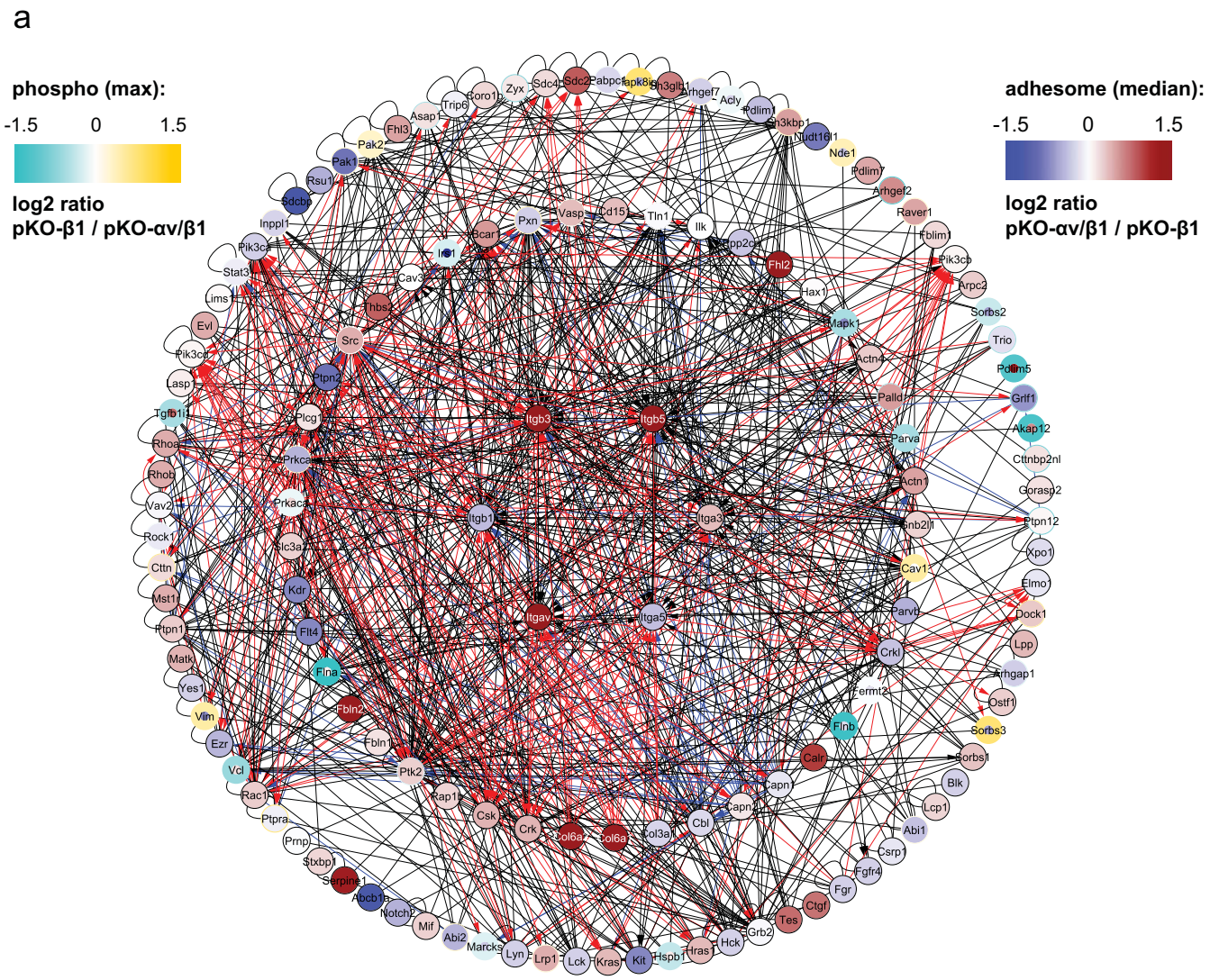

Figure S4 α5β1- and αv-class-specific PPIs and phosphosites. (**a**) The PPI network derived from FA-enriched samples. Integrin subunits are in the centre and their direct and indirect interactors are in the inner and outer circles, respectively. Black lines between nodes indicate high confidence PPI, red arrows indicate activating interactions and blue lines indicate inhibiting interactions. The nodes were labelled with gene symbols and colour-coded according to the MS intensity ratio of pKO-αv/β1 versus pKO-β1. Node edges were colour-coded according to the SILAC ratio of the maximally regulated phosphosite on each significantly regulated protein. (**b**) The PPI-network was derived as in (a). The nodes and node edges were colour-coded according to the MS intensity ratio of pKO-αv versus pKO-αv/β1. (**c**) The PPI-network was derived as described in (a). The nodes and node edges were colour-coded according to the MS intensity ratio of pKO-αv versus pKO-β1.

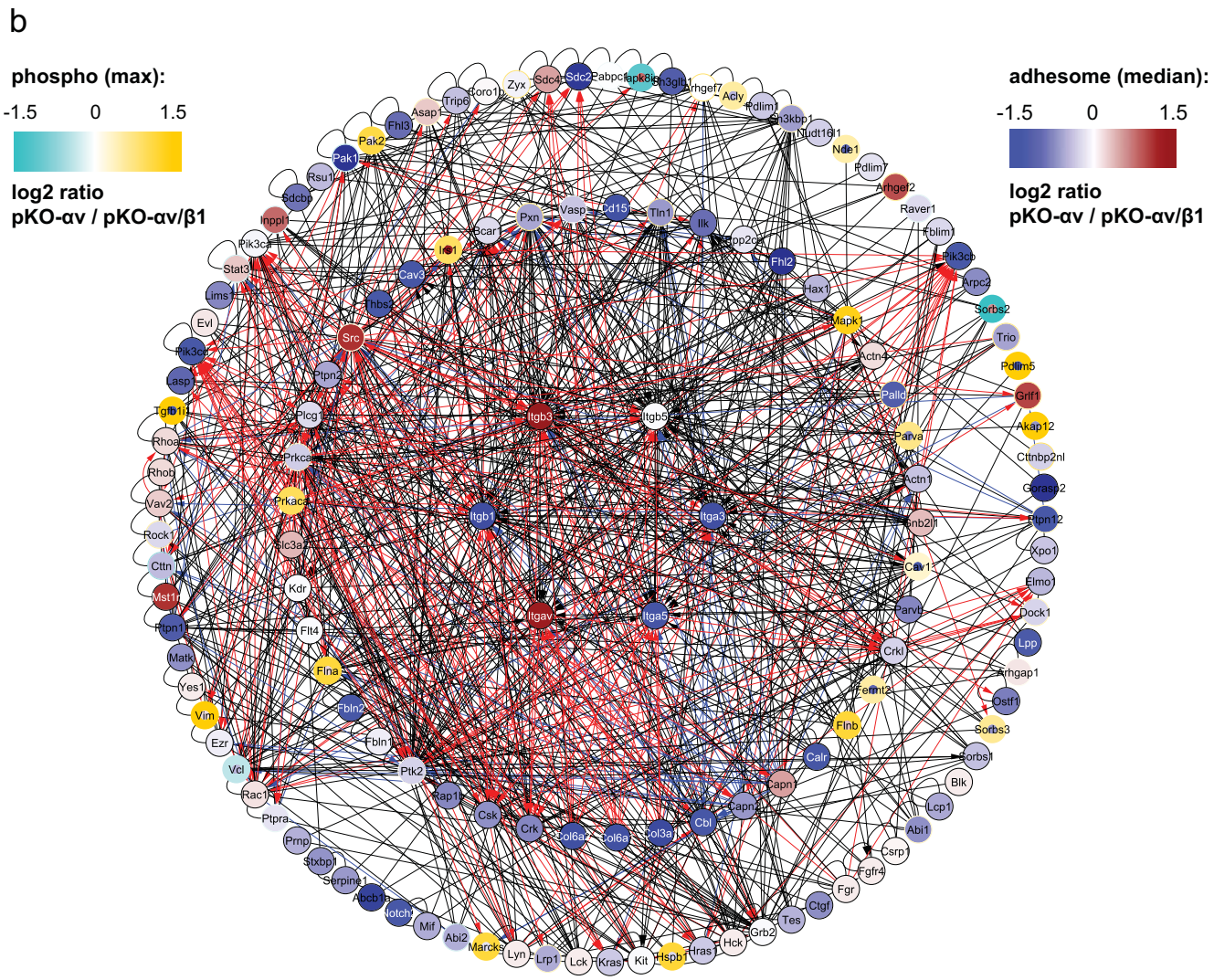

Figure S4 continued

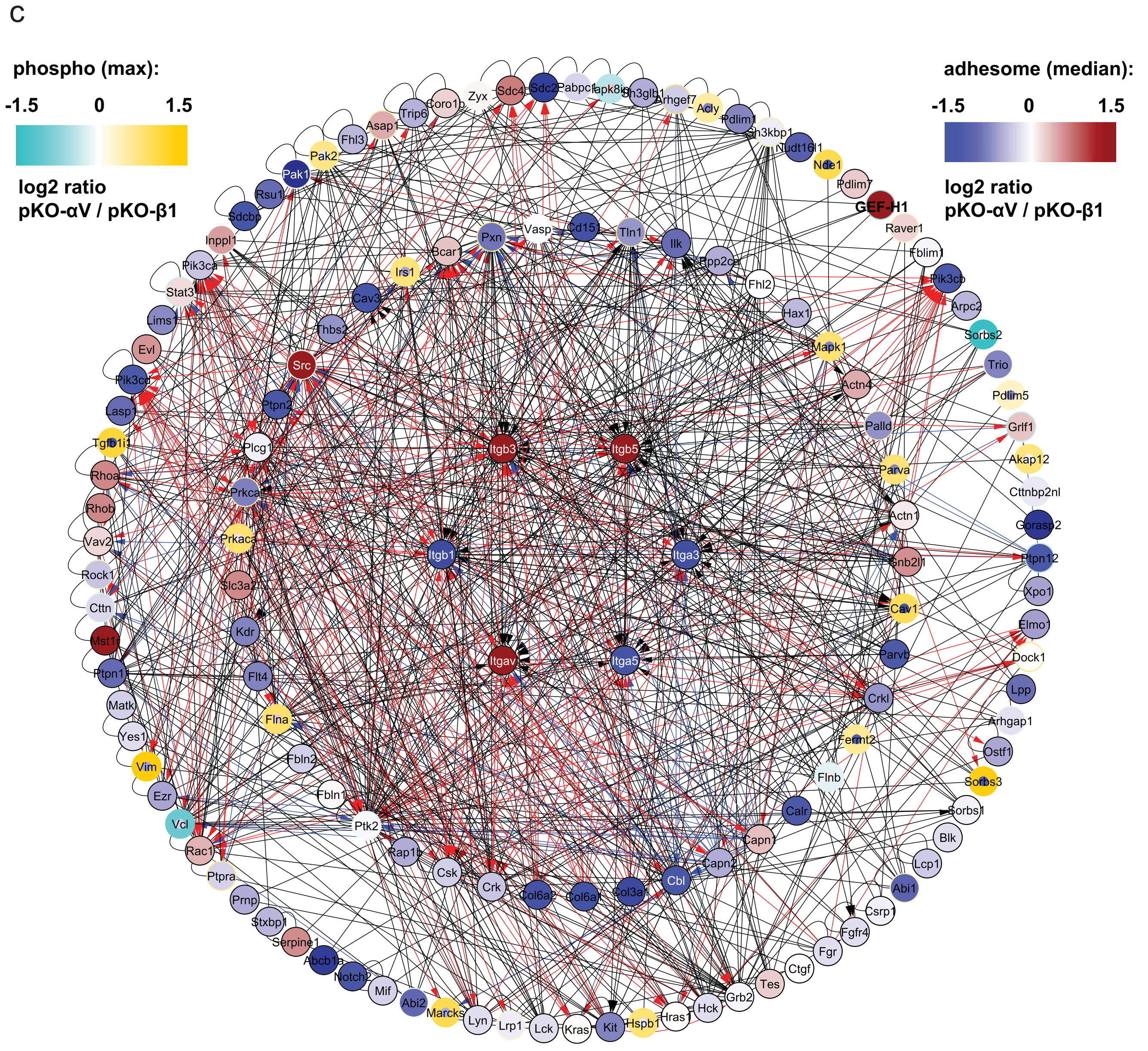

Figure S4 continued

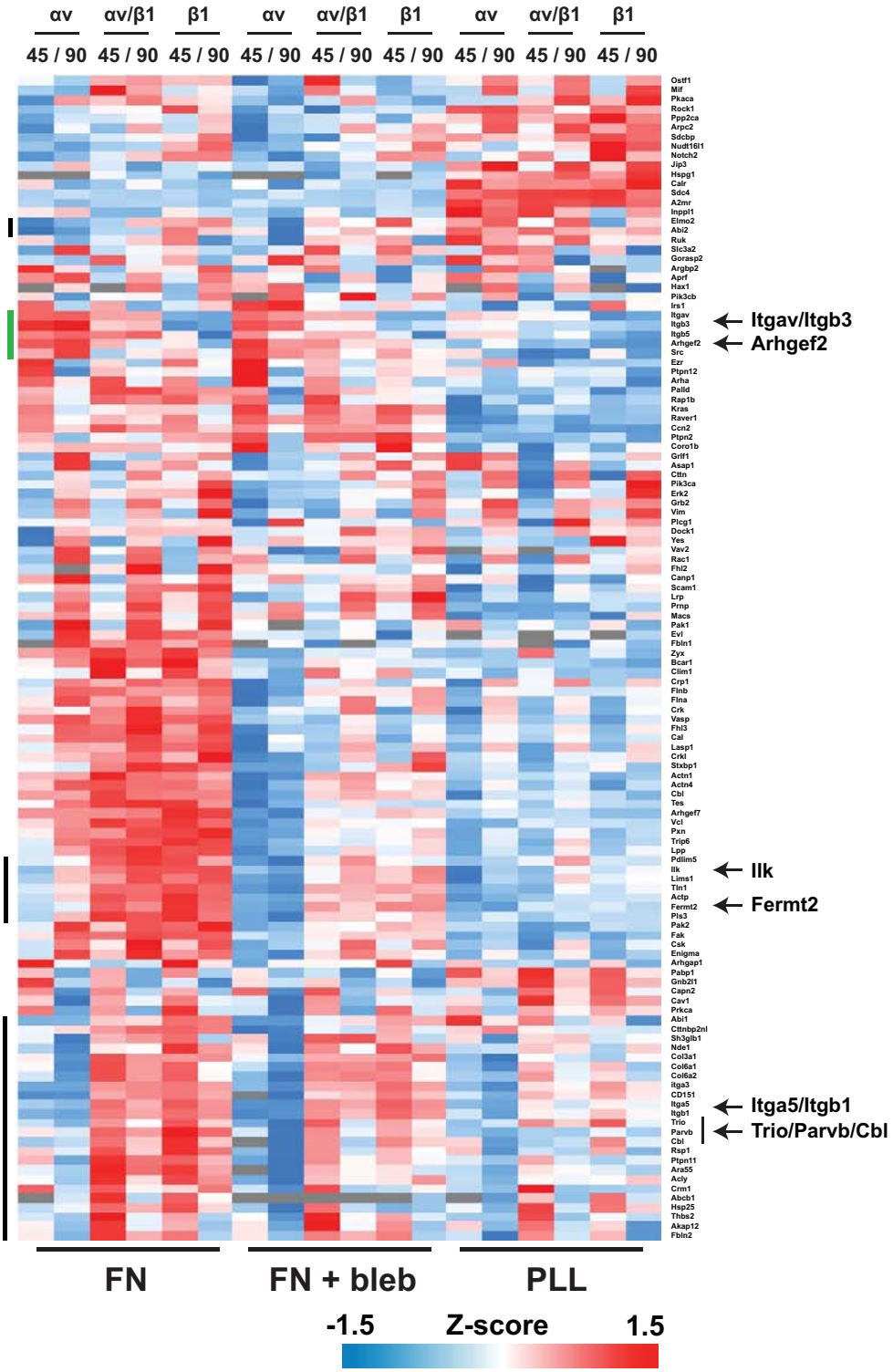

Figure S5 Integrin-specific differences in the "core integrin interactome". The Z-scores of median MS intensities (n=3-4) of the 125 core integrin-interactome proteins (Fig. S4) were subjected to hierarchical clustering. The black bars on the left indicate α5β1-dependent FA proteins, while the green bar indicates the αv-class integrin-dependent FA proteins selected for the clustering in Fig. 4c.

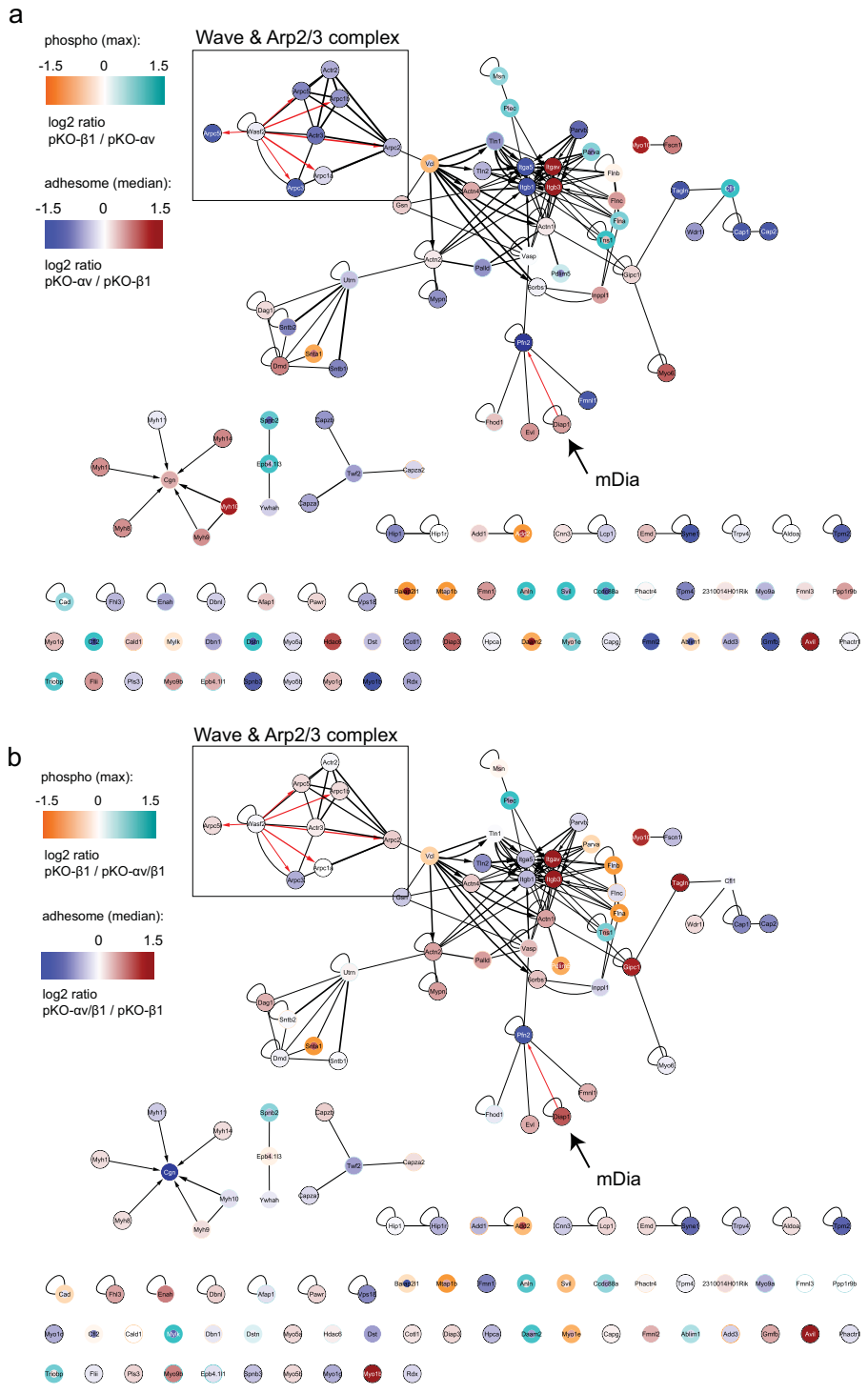

Figure S6 Network analysis of actin binding proteins enriched in the adhesome preparations. (**a**) Actin binding proteins were extracted from the adhesome dataset using gene ontology annotations. Black lines between nodes indicate high confidence PPI, red arrows indicate activating and blue lines indicate inhibiting interactions. The nodes were labelled with gene symbols and colour coded according to the log2 MS intensity ratio of pKO-αv over the pKO-β1 sample. Node edges were colour-coded according to the log2 SILAC ratio of the maximally regulated phosphosite on each significantly regulated protein. The box marks components of the WAVE and Arp2/3 complex, while the arrowhead marks the formin mDia. (**b**) The graph was generated as in (a), except that the nodes were colour-coded according to the log2 MS intensity ratio of pKO-αv/β1 over the pKO-β1 sample.

a

β1-tail:	Desthiobiotin - HDRREFAKFEKEKMNAKWDTGENPIYKSAVTTVVNPKYEGK - OH
β1-tail scr:	Desthiobiotin - ANYETKTNPKFKRAWKDNTKYEVVMSHAGFDIEVPREGKEK - OH
β3-tail:	Desthiobiotin - HDRKEFAKFEEERARAKWDTANNPLYKEATSTFTNITYRGT - OH
β3-tail scr:	Desthiobiotin - AETFLSRHYNKGFDKATKRPAEDRYWNTARENETAKTTIFE - OH

b

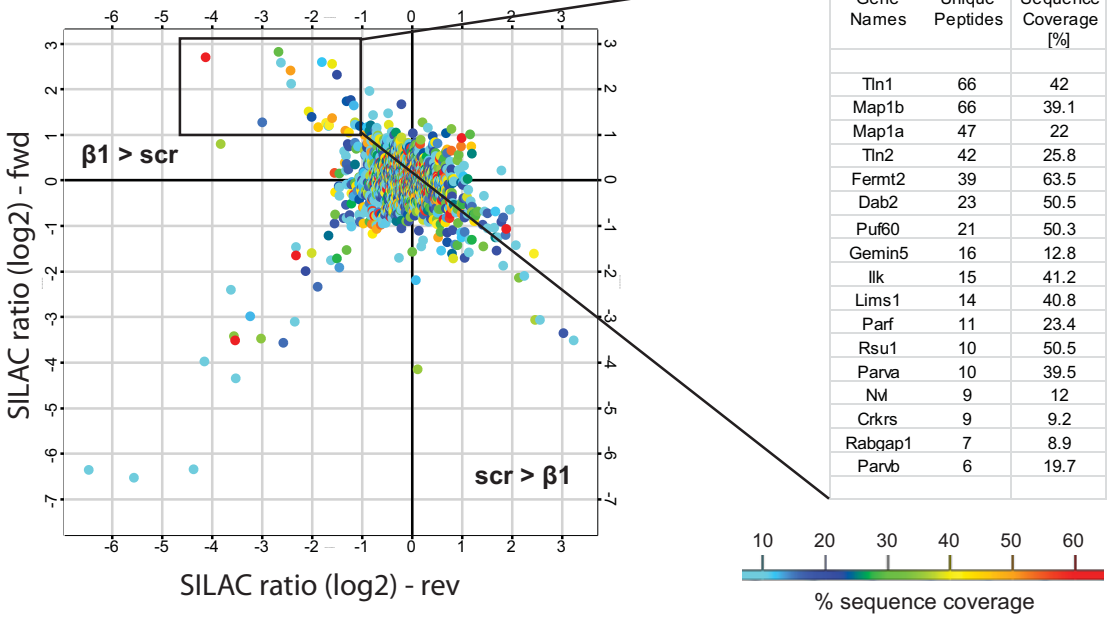

Gene Names	Unique Peptides	Unique Sequence Coverage [%]
Tln1	66	42
Map1b	66	39.1
Map1a	47	22
Tln2	42	25.8
Fermt2	39	63.5
Dab2	23	50.5
Puf60	21	50.3
Gemin5	16	12.8
Ilk	15	41.2
Lims1	14	40.8
Parf	11	23.4
Rsu1	10	50.5
Parva	10	39.5
Nvl	9	12
Crkrs	9	9.2
Rabgap1	7	8.9
Parvb	6	19.7

c

Gene Names	Unique Peptides	Unique Sequence Coverage [%]
Dync1h1	169	43.8
Iqgap1	91	67.2
Tln1	57	35.3
Iqgap2	50	41.1
Vim	49	85.6
Frap1	49	27.5
Usp9x	49	23
Lmo7	48	36.1
Ccdc88a	48	30.3
Fn1	46	29.9
Nes	44	33.4
Arhgef2	38	48.7
Svil	36	20.9
Cep170	35	31.4
Synj1	33	23.6
Hnrnpm	31	48.8
Rictor	31	24.4
Phldb1	31	26.7
KIAA1967	29	44.3

Gene Names	Unique Peptides	Unique Sequence Coverage [%]
Flnc	29	15.9
Irs1	29	34.4
Esf1	28	31.4
Fermt2	28	51
Spata5	27	44.2
Gigyf2	25	25.3
Lmna	25	39.8
Setd2	25	15
Cep55	25	45.2
Dab2	24	53.7
Rgnef	24	19.2
Mcm5	24	43.6
Pik3c2a	23	16
Ctnnd1	23	35.3
Jak1	23	28.6
Hadha	22	37
Dsp	22	9.1
Arhgef17	21	14.4
Rngtt	20	37.2
Dock7	20	11.5

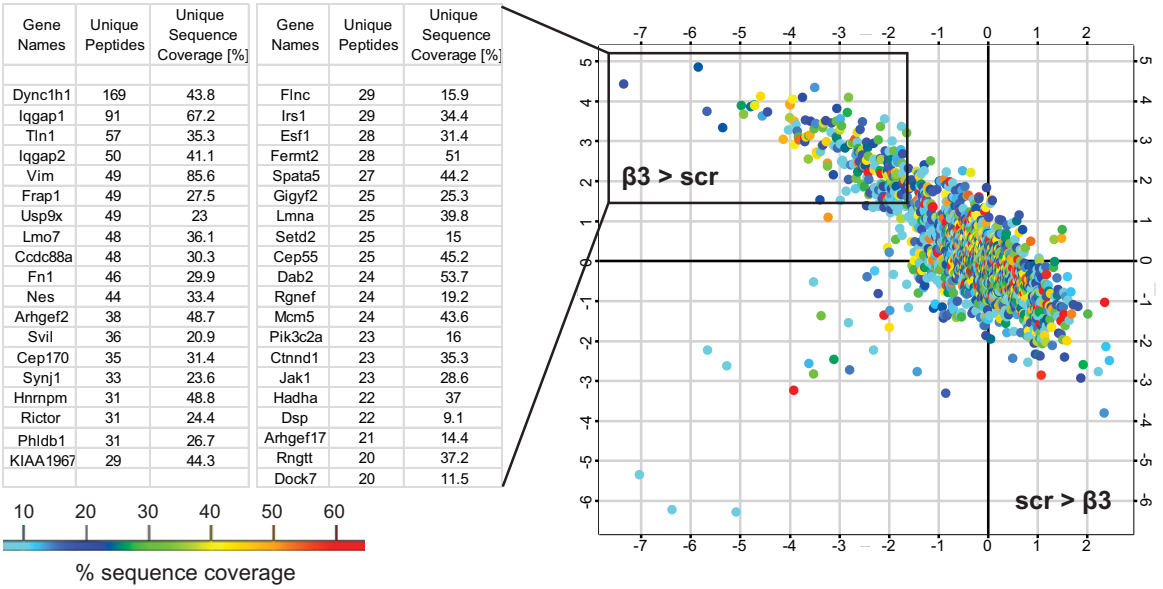

Figure S7 Integrin tail peptide pulldowns. (**a**) Sequence of synthetic desthiobiotinylated peptides used for the pull down experiments. (**b**) SILAC ratio plot from label inverted replicates (specific interactors have high SILAC ratio in the forward experiment and low SILAC ratios in the label swapped reverse experiment) comparing the β1-tail peptide with a scrambled control. The table shows the most intense β1-specific interactors with high sequence coverage that were reproducibly enriched versus the scrambled control peptide (scr) (n=4; 2 independent experiments). (**c**) SILAC ratios of proteins from inverted replicates comparing the β3-tail peptide with a scrambled control. The table shows the most intense β3-specific interactors with high sequence coverage that were reproducibly enriched versus the scrambled control peptide (scr) (n=4; 2 independent experiments).

a

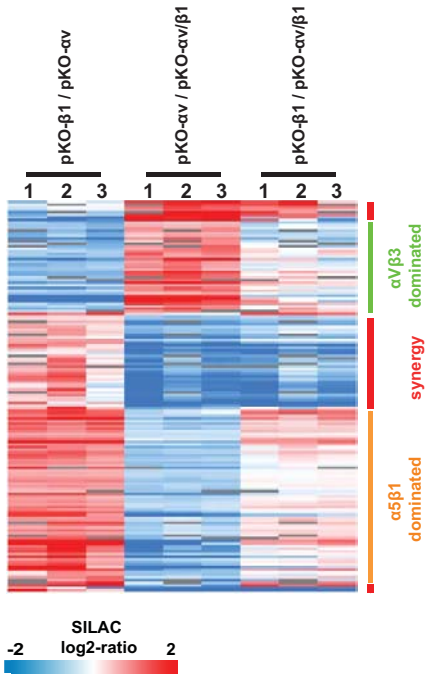

b

Synergy up/down	αvβ3 dominated	α5β1 dominated	α5β1 dominated
Actn1 *	AA881470	Acbd3	Lox
Adir	Abcc4	Acss2	Lxn
Apol9a	Add2	Ahnak2	Man2a1
Ass	Aif1l	Anx1	Mdh2
Bal	Aim1	Anx8	Me2
BC006779	Baiap2l1	Cap	Metap2
Bst2	Bckdha	Capn2	Mme
Clim1	Cadm1	Cav *	Mrc2
Cmpk2	Ctsl	Cdkn2a	Mre11
Ddx58	Daglb	Ckap4	Msra
Dtx3l	Dbt	Clp	Napg
Eif2ak2	Dcoh	Cnn2	Nudt9
G1p2	Dhx33	Col1a1	P4ha1
Galm	Eml2	Col1a2	P4ha2
Garg39	Enpep	Col3a1	Pea15
Garg49	Epb4.1l5	Col6a1	Pk3
Gbp2	Fam129a	Col6a2	Plod2
Gbp3	Fan1	Crabp1	Plod3
Gbp6	Fbxo2	Ctsb	Por
Gstm1	Gsta	D7Ertd671e	Ptmb4
Gstm2	Hist3h2bb	Dpysl3	Rad50
H2-D1	Hk2	Dsn	Rca1
Ifi1	Hmg2a	Ergic53	Rexo2
Ifi205b	Itgav	Fabp5	Rgc32
Ifi35	Jip3	Fam114a1	Sept5
Ifit1	Kiaa0193	Glud	Sparc
Ifitm3	Kiaa1102	H2-K	Svil *
Inf2	Nipsnap1	Igtp	Trp32
Kiaa2005	Polr1d	Ikbip	Tubb6
Mylk *	Ptplad1	Itga3	Ufc1
Nfkb2	Rpl5	Itgb1	Vcl *
Oasl2	Sp2	Kiaa1830	Wdr1
Parp12	Steap	Lamb-1	
Pdlim5	Tjp2	Lbr	
Pml	Wipi2	Lmp7	
Rnf213		Loh11cr2a	
RP23-399J8.4-002			
Sm22			
Stat1			
Tpm1			
Zfp185			

c

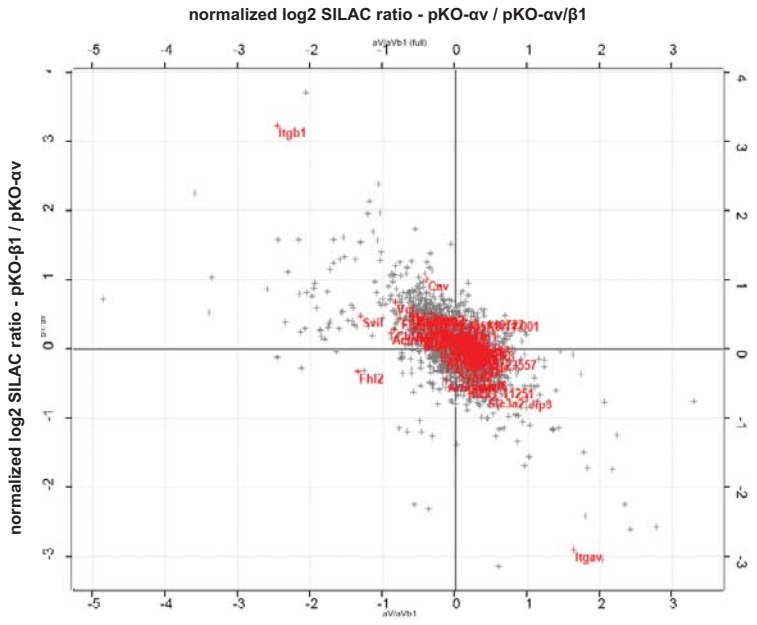

Figure S8 Cellular proteome of pKO-αv, pKO-β1 and pKO-αv/β1 cells. (**a**) SILAC labelled cells cultured on FN for several passages were analysed by MS. SILAC ratios of 150 significantly regulated proteins (ANOVA, Benjamini/Hochberg FDR) were subjected to non-supervised hierarchical cluster analysis and colour coded. The bars depict differentially regulated clusters of proteins. (**b**) Gene names of the 3 differentially regulated groups (a) are shown. Known FA proteins are marked with an asterisk. (**c**) Scatter plot showing SILAC ratios. Previously annotated FA proteins are labelled in red.

Figure 5c

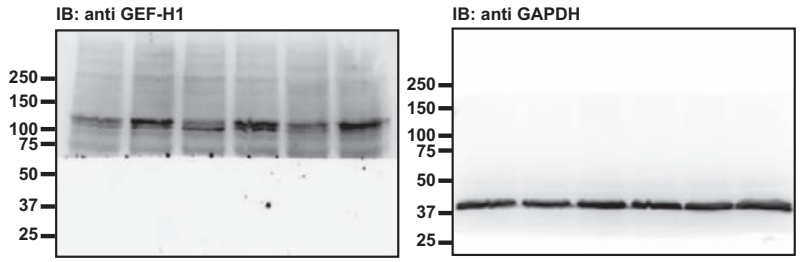

Figure 6d

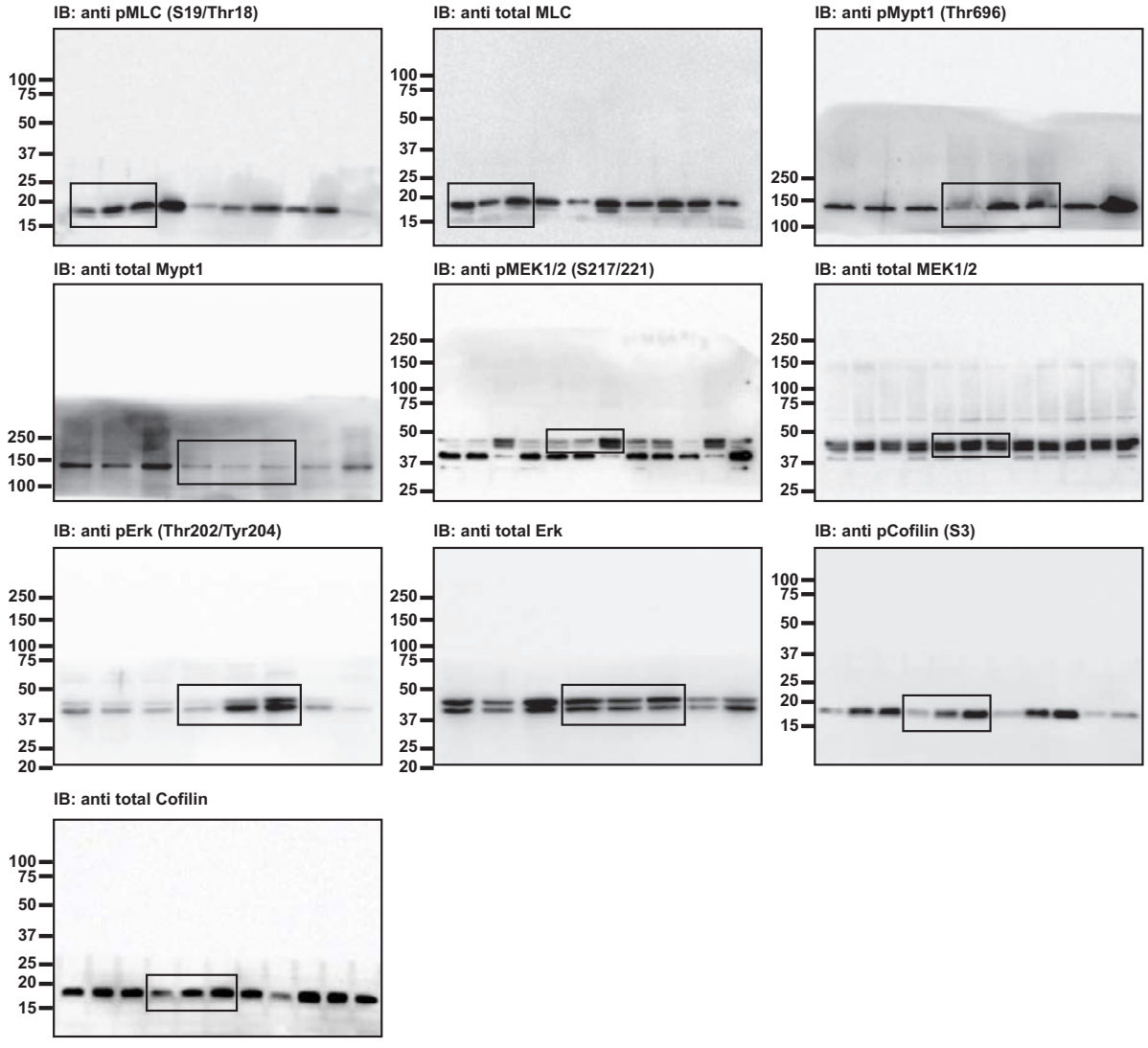

Figure S9 Uncropped western blots.

Figure 7c

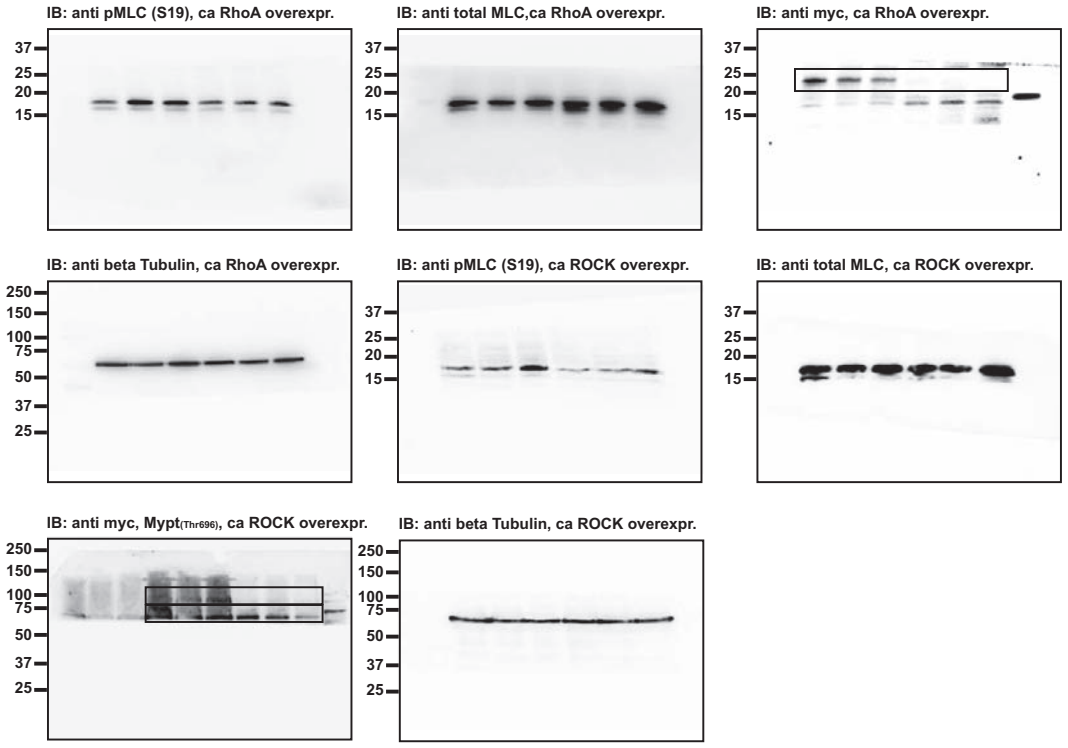

Figure S1f

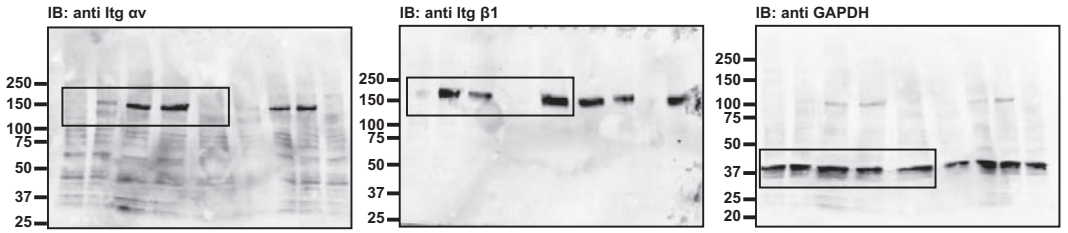

Figure S1g

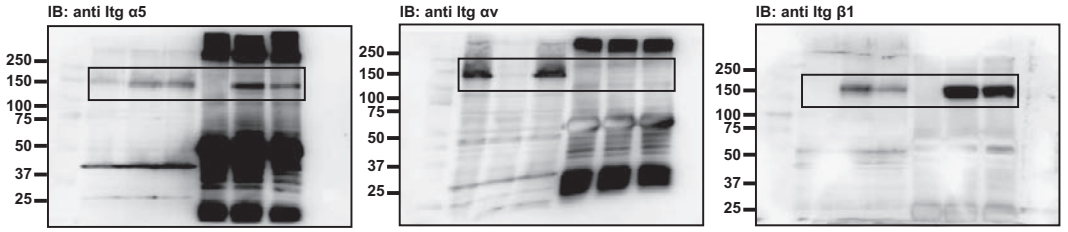

Figure S9 continued

Supplementary video legends

Video S1 Time-lapse movie of pKO-αv cells plated on FN. Cells were plated on FN coated (5 μg/ml; blocked with 1% BSA) tissue culture dishes in presence of 10% serum and video tracked over 20 hours with a frame rate of 1 picture every 4 minutes. Pictures were acquired with a phase contrast microscope at magnification 20x.

Video S2 Time-lapse movie of pKO-αv/β1 cells plated on FN. Cells were plated on FN coated (5 μg/ml; blocked with 1% BSA) tissue culture dishes in presence of 10% serum and video tracked over 20 hours with a frame rate of 1 picture every 4 minutes. Pictures were acquired with a phase contrast microscope at magnification 20x.

Video S3 Time-lapse movie of pKO-β1 cells plated on FN. Cells were plated on FN coated (5 μg/ml; blocked with 1% BSA) tissue culture dishes in presence of 10% serum and video tracked over 20 hours with a frame rate of 1 picture every 4 minutes. Pictures were acquired with a phase contrast microscope at magnification 20x.

PERSPECTIVE

A firm grip does not always pay off: a new Phact(r) 4 integrin signaling

Zhiqi Sun and Reinhard Fässler[1]

Department of Molecular Medicine, Max Planck Institute of Biochemistry, Martinsried 82152, Germany

β1 integrin signaling plays crucial roles in enteric nervous system development. Zhang and colleagues (pp. 69–81) discovered that phosphatase and actin regulator 4 (Phactr4) antagonizes β1 integrin signaling through protein phosphatase 1 (PP1) in focal adhesions of enteric neural crest cells (ENCCs). Loss of Phactr4–PP1 interaction leads to increased β1 integrin signaling, loss of collective and directional migration, and hindgut hypogangaliosis, indicating that the right adjustment of β1 integrin signaling is required for the normal migration and organization of ENCCs.

Hirschsprung disease (HSCR; also called congenital aganglionic megacolon) is a congenital disorder of the distal colon in which the enteric nervous system (ENS) is absent (Brooks et al. 2005). The lack of the enteric neurons leads to a contracted colon, which prevents peristaltic movements of the intestine and obstructs the passage of food residue. The cause for the absent ENS can be due to impaired proliferation, differentiation, or migration of enteric neural crest cells (ENCCs) into the distal colon and rectum (Heanue and Pachnis 2007). ENS development commences at around embryonic days 9–9.5 (E9–E9.5) in mice, when vagal neural crest cells emigrate from the neural tube and invade the foregut (Newgreen and Young 2002). From the foregut, they migrate as ENCCs in a rostrocaudal direction to colonize the developing gastrointestinal tract. When the gastrointestinal tract is colonized, the ENCCs differentiate into different subtypes of neurons and glia, which organize into ganglia and finally interconnect to form the mature ENS (Fig. 1). The differentiation and migration of ENCCs are orchestrated by chemoattractants such as Glial cell line-derived neurotrophic factor (GDNF) and endothelin 3 and their cognate receptors, RET and endothelin-B receptors, respectively (Hearn et al. 1998; Young et al. 2001; Barlow et al. 2003; Burzynski et al. 2009).

The migration of ENCCs has been studied by time-lapse video microscopy in gut explants derived from transgenic mice expressing fluorescent reporter genes in neural crest cells. These studies revealed several intriguing features of their complex migration behavior. ENCCs form long chains in which the cells are tightly connected via cell–cell adhesion (Young et al. 2004). At the migratory wave front of these cell chains are a few solitary cells, also called advanced cells. They detach from the cell chains, explore the environment by continuously protruding their plasma membranes, and aid the forward migration of the following chain of cells (Druckenbrod and Epstein 2005, 2007). ENCCs migrate along most of the gastrointestinal tract with a net migration speed of ~30–40 μm per hour (Young et al. 2004; Druckenbrod and Epstein 2005). When they reach the junction with the caecum, they pause for ~8–12 h. During this period, the migrating chains dissociate into single cells, which move into the caecum, where they show a rapid and nondirectional migration behavior (Druckenbrod and Epstein 2005). Once they have reached the colon, they rejoin into cell chains, form advanced cells at the wave front, and resume the usual migratory mode. The exact reason for the switch of the migratory mode in the caecum is not known. However, it is likely due to the unique signaling and tissue environment of the caecum (Heanue and Pachnis 2007). For instance, the caecum is tremendously rich in extracellular matrix (ECM) proteins such as fibronectin (FN). FN binds to β1 integrins, which were shown to be essential for the migration of ENCCs (Breau et al. 2009).

Integrins are the major cell adhesion molecules for the ECM. They are heterodimeric transmembrane receptors consisting of an α and a β subunit. The human and mouse proteomes contain 18 α and eight β subunits, which can assemble into 24 different integrin heterodimers, each binding to a specific set of ECM proteins (Humphries et al. 2006). A hallmark of integrins is that they must change their conformation before they can bind their ECM ligand (Moser et al. 2009). Following ligand binding, integrins cluster and recruit signaling, adaptor, and actin-binding molecules to their cytoplasmic domains, which results in the coupling of the ECM to the actin cytoskeleton and the formation of a large signaling hub known as focal adhesion (FA) (Geiger et al. 2009). Integrin signaling is finely tuned to control a large number of biological processes, including directional and persistent cell migration. To achieve this, integrins regulate the subcellular activity of small RhoGTPases, which are essential for the dynamic

[*Keywords*: directional cell migration; enteric neural crest cell; Hirschsprung disease; Phactr4; PP1; β1 integrin; cofilin]
[1]Corresponding author.
E-mail: faessler@biochem.mpg.de.
Article is online at http://www.genesdev.org/cgi/doi/10.1101/gad.184192.111.

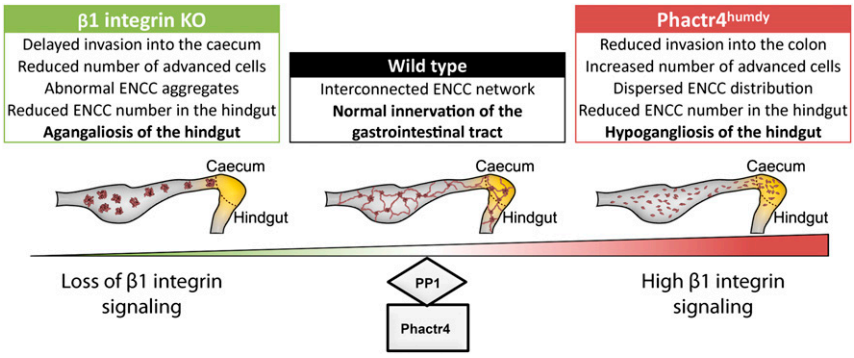

Figure 1. Physiologic β1 integrin signaling is required for the normal migration and organization of ENCCs. The collective migration ENCCs in cell chains establishes an interconnected network, which resembles the organization of the ganglia and the interconnecting neurites of the mature ENS. While the β1 integrin gene ablation leads to abnormal ENCC aggregates and delayed invasion of the caecum, the Phactr4^{humdy} mutation leads to increased β1 integrin signaling, dissociation of ENCCs, loss of collective migration, and hindgut hypogangaliosis.

formation of a stable and persistent lamellipodium at the leading edge of a migrating cell, and adjust the activity of actin-modulating proteins, including actin nucleators such as formins or the Arp2/3 complex, filamentous actin (F-actin)-severing proteins such as cofilin, and others (Petrie et al. 2009). It is important to note that diminished as well as elevated signaling by integrins can lead to pathology. This is nicely demonstrated in mice with decreased and increased β1 integrin function (Bouvard et al. 2007; Legate et al. 2009; Rantala et al. 2011).

The β1 integrin subunit can associate with 12 α subunits and thus forms the largest integrin subfamily. Constitutive deletion of the β1 integrin gene leads to peri-implantation lethality in mice (Fassler and Meyer 1995). Deletion of the β1 integrin gene in neural crest cells affects the formation of multiple neural crest-dependent structures, including the ENS, leading to a HSCR-like phenotype with agangaliosis of the distal part of the colon (Fig. 1; Breau et al. 2006). The ENS defects are due to impaired migration and the formation of abnormal aggregates of ENCCs in the distal midgut, caecum, and hindgut. The major requirement for β1 integrin expression for ENCCs becomes apparent when the migration pauses, and they should dissociate and invade the caecum and the adjacent hindgut. The β1-null ENCCs remain abnormally aggregated and show reduced migration speed and persistence, resulting in diminished colonization of the rostral hindgut with ENCCs and a complete absence in the caudal hindgut (Breau et al. 2009). The migration defect of β1-null ENCCs has not been well studied so far, but it is believed that several factors contribute to the defective hindgut colonization. An abnormal activation of small RhoGTPases through reduced adhesion to FN is most likely the major cause for the impaired migration machinery of β1-null ENCCs. Furthermore, due to the delayed invasion of the caecum and the hindgut, the β1-null ENCCs are believed to meet a growing and differentiating environment that is no longer permissive for incoming ENCCs to migrate efficiently and thus may prevent them from reaching the caudal hindgut. Finally, it has been shown that the density of ENCCs correlates with the efficiency of their own migration (Druckenbrod and Epstein 2005). Therefore, the reduced number of β1-null ENCCs and their clustering in aggregates may also contribute to their failure to reach the rectum. These observations demonstrate that the loss of β1 integrin expression severely compromises the migration of ENCCs and the formation of a functional ENS. In this issue of *Genes & Development*, Zhang et al. (2012) report that phosphatase and actin regulator 4 (Phactr4), a novel adaptor protein, is present in FAs of ENCCs, where it antagonizes β1 integrin signaling and diminishes the activity of the actin-severing protein cofilin. Consequently, impairing Phactr4 function in mice leads to increased β1 integrin signaling in their ENCCs, resulting in severe defects in their migration and colonization of the hindgut.

The Phactr family of proteins consists of four members (Phactr1–4). They were initially identified as protein phosphatase 1 (PP1)-binding proteins in a yeast-two-hybrid screen (Allen et al. 2004). In addition to the C-terminal PP1-binding domain, all four proteins contain three RPEL repeats, which are actin-binding motifs (Miralles et al. 2003). Since immunoprecipitation of Phactr1, Phactr3 (also known as Scapinin), and Phactr4 brings down actin from the soluble fraction of a cell lysate (Allen et al. 2004; Kim et al. 2007; Sagara et al. 2009), it is believed that Phactr proteins bind G-actin. All four members are expressed in the mouse brain; however, each isoform has a distinct distribution and is found in different subcellular compartments (Sagara et al. 2003; Allen et al. 2004; Farghaian et al. 2011). Data on the in vivo functions of these proteins are scarce. In a forward genetic screen for neural tube closure defects in mice, Niswander and colleagues (Kim et al. 2007) identified a R650P missense mutation in Phactr4, which they called *humdy* (Phactr4^{humdy}). The R650P mutation disrupts PP1 binding to Phactr4 and leads to an inhibitory phosphorylation of PP1 at Thr 320 (Fig. 2) and loss of PP1 activity toward the retinoblastoma protein (Rb) (Kim et al. 2007). In the current study, Zhang et al. (2012) report that mice with a homozygous Phactr4^{humdy} mutation develop a HSCR-like phenotype (Fig. 1). In the majority of Phactr4^{humdy} mutant mice, the number of enteric neurons was normal, but they were individually distributed in the stomach, foregut, and midgut, instead of clustered in ganglia, and the neurites were disorganized. The hindgut of Phactr4^{humdy} mutant mice contained fewer neurons, which were also abnormally distributed and without interconnected neurites. In rare cases, neural crest cell invasion of the entire bowel was abolished. Using gut explants combined with time-lapse video microscopy, Zhang et al. (2012) showed that the migration behavior of Phactr4^{humdy} ENCCs is

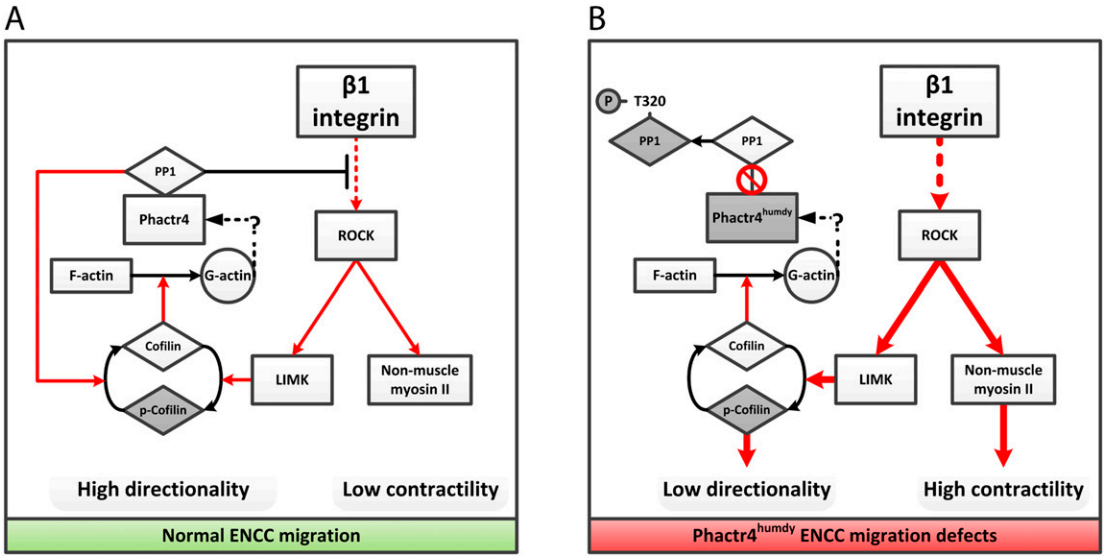

Figure 2. (*A*) Role of the Phactr4–PP1 complex in normal ENCCs. β1 integrin signaling can activate ROCK through multiple, although not completely understood, pathways. ROCK, in turn, activates nonmuscle myosin II (NMII) and LIMK, which promotes the phosphorylation and subsequent inactivation of cofilin. Phactr4 interacts with PP1 and activates its phosphatase activity. The enhanced PP1 activity has two consequences: PP1 directly dephosphorylates and activates cofilin, and PP1 antagonizes β1 integrin signaling (and thus ROCK activation) through unknown mechanisms. The reduced ROCK activity leads to reduced activation of NMII and decreased inactivation of cofilin. The reduced NMII activity dampens the contractility of ENCCs, and the increased cofilin activity enhances directional migration of ENCCs. The increased cofilin activity also liberates G-actin, which can bind Phactr4 and may thereby regulate the functional properties of the Phactr4–PP1 complex in a putative feedback loop. (*B*) Misregulation of PP1 in Phactr4^{humdy} cells. Loss of the interaction between Phactr4 and PP1 in the Phactr4^{humdy} mutant mice leads to decreased and misregulated PP1 activity. Consequently, cofilin is not inactivated and the β1 integrin signaling pathway is not blocked, resulting in the loss of directional migration and increased cell contractility. In both panels, solid red arrows indicate direct activation between proteins; solid black arrows indicate a shift in protein activity (active/inactive cofilin, PP1, and Phactr4) or state (F-actin/G-actin); dotted red arrows indicate an unknown, multistep activation process; dotted black arrows indicate a putative feedback loop; and white protein boxes represent active proteins, while gray boxes represent inactive proteins.

abnormal and is responsible for the aberrant formation of the ENS. The normal number of ENCCs in the foregut and midgut and the reduced number in the hindgut suggests that Phactr4^{humdy} ENCCs may have a defect in exiting the caecum and resuming collective chain migration in the adjacent hindgut. This possibility, however, was not tested, but could be analyzed and confirmed with graft assays.

Zhang et al. (2012) excluded defective proliferation or differentiation of ENCCs as the cause for the HSCR-like phenotype and showed with several imaging experiments that the collective and directional migration of Phactr4^{humdy} ENCCs was abnormal. Imaging ENCC migration in hindgut explants revealed that the Phactr4^{humdy} ENCCs lost their ability to form chains and to migrate in the caudal direction. Instead, they moved as single cells, which showed an erratic and nondirectional migration behavior. When the gut explants were embedded in collagen gels, the invasion of Phactr4^{humdy} ENCCs into the collagen gel could be triggered by exogenous GDNF, albeit with lower efficiency when compared with wild-type cells, suggesting that the Phactr4^{humdy} mutation abrogates the migration machinery of ENCCs rather than the ability to respond to a GDNF gradient. This hypothesis was confirmed with mouse embryonic fibroblasts (MEFs) from Phactr4^{humdy} mutant mice that generate multiple retraction fibers and highly dynamic and unstable lamellipodia when cultured in two dimensions. Clearly, such erratic membrane protrusions and increased cell contractility can account for the loss in directionality.

How could the Phactr4–PP1 complex regulate migration of ENCCs at the molecular level? Experimental results by Zhang et al. (2012) indicate that in Phactr4^{humdy} cells, PP1 activity is diminished and/or misregulated, β1 integrin and Rho kinase (ROCK) activities are high, and cofilin is hyperphosphorylated at Ser 3 (likely through ROCK-mediated LIMK activation), which leads to a diminished severing of F-actin. These findings suggest that PP1 activation through binding to Phactr4 in wild-type cells antagonizes β1 integrin–ROCK–cofilin signaling to enhance cofilin activity and thereby promotes directional migration by maintaining a polarized actin cytoskeleton (Fig. 2). Consistent with a requirement of an active PP1 for persistent directional cell migration, chemical inhibition of PP1 induced a migration defect in wild-type ENCCs of gut tissue explants and in wild-type MEFs that closely resembled the defects observed with Phactr4^{humdy} cells. In both cultured MEF cells and gut tissue explants, functional blockade of β1 integrins using antibodies or RGD peptides or by inhibition of ROCK rescued the migration defect. Strikingly, blocking β1 integrin function in gut tissue explants largely restored the collective migration ENCCs and the net speed of the forward-moving wave front. This

observation strongly suggests that β1 integrin activity needs to be down-regulated, particularly when ENCCs invade the hindgut and are exposed to a change in FN concentration to resume chain migration. One crucial question is at which point Phactr4–PP1 intersects with β1 integrin–ROCK–cofilin signaling. Another unanswered question is how Phactr4–PP1 controls cell contractility. It has been shown that overexpression of constitutively active LIMK (which can phosphorylate cofilin) or phospho-mimicking mutants of cofilin disrupts cell polarity by inducing the formation of multiple lamellipodia (Dawe et al. 2003). However, cofilin does not directly interfere with cell contractility. Contraction along F-actin filaments is mainly mediated by nonmuscle myosin II (NMII) in nonmuscle cells (Vicente-Manzanares et al. 2009). PP1 is the major phosphatase that dephosphorylates myosin regulatory light chain (MRLC) (Matsumura and Hartshorne 2008). On the other hand, it is well known that ROCK activates NMII by phosphorylating the MRLC. ROCK also reduces the activity of PP1 toward MRLC by phosphorylating myosin phosphatase-targeting subunit 1 (Totsukawa et al. 2000). Since chemical inhibition of ROCK restored lamellipodia formation in Phactr4^{humdy} cells, it is conceivable that Phactr4–PP1 regulates integrin signaling upstream of cofilin. However, since ROCK inhibition only partially rescued the collective migration of Phactr4^{humdy} mutant ENCCs, it is likely that Phactr4 also regulates other signaling events downstream from β1 integrin through either controlling PP1 activity or other unknown mechanisms (Fig. 2).

PP1 is a ubiquitously expressed serine/threonine phosphatase that regulates many biological processes, including cell survival, cell division, metabolism, and cytoskeletal reorganizations (Cohen 2002). PP1 consists of a catalytic and a regulatory subunit. There are three isoforms of PP1 catalytic subunits: PP1α, PP1β, and PP1γ. The recruitment of the catalytic subunit of PP1 to regulatory subunits determines the subcellular localization and the substrate specificity of PP1 (Shi 2009). For instance, the actin-binding regulatory subunit spinophilin targets PP1 to actin filaments and cell–cell junctions (Satoh et al. 1998), where it also blocks potential substrate-binding sites on the catalytic subunit and thereby increases substrate specificity (Ragusa et al. 2010). Notably, Phactr4 can interact with all PP1 family members, making Phactr4 a potent and multifunctional regulator of PP1 signaling (Kim et al. 2007). Actin binding by Phactr proteins could add another level of complexity. Biochemical analysis has shown that Phactr proteins interact with G-actin through RPEL repeats. Consistent with this finding, the localization of overexpressed Phactr4 is largely reciprocal with actin stress fibers. The interaction between Phactr and G-actin is likely to reduce actin polymerization in cell protrusions (Sagara et al. 2009). Furthermore, it is currently not known whether G-actin and PP1 binding to Phactr4 are mutually exclusive, synergistic, or independent. Since RPEL repeats abut the PP1 binding domain, it is possible that actin binding to the RPEL repeats might compete with the PP1 recruitment through steric hindrance. Low G-actin concentration might thus lead to the formation of Phactr4–PP1 complexes, which could then activate cofilin to increase the G-actin pool. In such a scenario, Phactr4 could serve as a feedback regulator that senses actin dynamics and modulates PP1 activity accordingly (Fig. 2). To further clarify these issues, structural analysis of the actin–Phactr–PP1 complex will be needed.

The subcellular localization Phactr4 is likely important to locally regulate PP1 activity. Endogenous Phactr4 colocalizes with β1 integrin in mature FAs of MEFs seeded on FN. Whether it also localizes to other subcellular compartments such as cell–cell adhesion sites has not been investigated so far. The immunolocalization of Phactr4 in FAs makes Phactr4 a novel FA protein. Interestingly, Phactr4^{humdy} is also recruited to FAs, indicating that its recruitment does not require the interaction with PP1. FAs have a complex protein composition and an intricate molecular organization and are highly dynamic. As with all classic signaling centers, kinases are abundant in FAs, and many FA proteins become phosphorylated at multiple sites. How PP1 activity is controlled to balance the phosphorylation state of its target proteins and how it achieves substrate specificity in this compartment are not understood. Many potential PP1 regulatory partners have been found. Besides tensin (Eto et al. 2007), PINCH1 has recently been identified as a regulator of PP1α in FAs (Eke et al. 2010). PINCH is a constitutive component of the integrin-linked kinase, PINCH, and parvin (IPP) complex (Legate et al. 2006). PINCH interacts through a consensus PP1 interaction motif in its fifth LIM domain with PP1α, but not with the two other isoforms. This interaction inhibits the activity of PP1α against Akt1 and regulates cell survival (Eke et al. 2010). Since the IPP complex is crucial for β1 integrin-mediated cell motility and adhesion, it is possible that Phactr4 might also regulate β1 integrin signaling by competing with PINCH for PP1α binding. Reciprocally, PINCH binding to PP1α might shift the binding of Phactr4 to other PP1 isoforms and thus modulate the activity and substrate specificity of the Phactr4–PP1 complex.

In conclusion, the work on Phactr4 gives a new flavor to our understanding of how β1 integrin signaling is regulated at different stages of ENCC migration. But, as with all studies describing novel and exciting findings, the study by Zhang et al. (2012) also raises many new questions: How does the Phactr4–PP1 complex intersect with integrin signaling, and is cell–cell adhesion regulated directly by Phactr4–PP1 or indirectly through integrins? Is it possible that Phactr proteins control cell migration not only by regulating PP1 activity, but also by regulating actin dynamics via a feedback regulatory loop involving the binding to PP1 and G-actin? Finally, is the aberrant upregulation of phospho-cofilin the only known substrate of PP1 that disrupts cell polarity, or is the Phactr4^{humdy} phenotype in ENCCs due to a combined dysregulation of many PP1 downstream targets? Time will surely give us the answers!

Acknowledgment

The work in the Fässler laboratory is funded by the Max Planck Society.

References

Allen PB, Greenfield AT, Svenningsson P, Haspeslagh DC, Greengard P. 2004. Phactrs 1–4: A family of protein phosphatase 1 and actin regulatory proteins. *Proc Natl Acad Sci* **101:** 7187–7192.

Barlow A, de Graaff E, Pachnis V. 2003. Enteric nervous system progenitors are coordinately controlled by the G protein-coupled receptor EDNRB and the receptor tyrosine kinase RET. *Neuron* **40:** 905–916.

Bouvard D, Aszodi A, Kostka G, Block MR, Albiges-Rizo C, Fassler R. 2007. Defective osteoblast function in ICAP-1-deficient mice. *Development* **134:** 2615–2625.

Breau MA, Pietri T, Eder O, Blanche M, Brakebusch C, Fassler R, Thiery JP, Dufour S. 2006. Lack of β1 integrins in enteric neural crest cells leads to a Hirschsprung-like phenotype. *Development* **133:** 1725–1734.

Breau MA, Dahmani A, Broders-Bondon F, Thiery JP, Dufour S. 2009. β1 integrins are required for the invasion of the caecum and proximal hindgut by enteric neural crest cells. *Development* **136:** 2791–2801.

Brooks AS, Oostra BA, Hofstra RM. 2005. Studying the genetics of Hirschsprung's disease: Unraveling an oligogenic disorder. *Clin Genet* **67:** 6–14.

Burzynski G, Shepherd IT, Enomoto H. 2009. Genetic model system studies of the development of the enteric nervous system, gut motility and Hirschsprung's disease. *Neurogastroenterol Motil* **21:** 113–127.

Cohen PT. 2002. Protein phosphatase 1—targeted in many directions. *J Cell Sci* **115:** 241–256.

Dawe HR, Minamide LS, Bamburg JR, Cramer LP. 2003. ADF/cofilin controls cell polarity during fibroblast migration. *Curr Biol* **13:** 252–257.

Druckenbrod NR, Epstein ML. 2005. The pattern of neural crest advance in the cecum and colon. *Dev Biol* **287:** 125–133.

Druckenbrod NR, Epstein ML. 2007. Behavior of enteric neural crest-derived cells varies with respect to the migratory wavefront. *Dev Dyn* **236:** 84–92.

Eke I, Koch U, Hehlgans S, Sandfort V, Stanchi F, Zips D, Baumann M, Shevchenko A, Pilarsky C, Haase M, et al. 2010. PINCH1 regulates Akt1 activation and enhances radioresistance by inhibiting PP1α. *J Clin Invest* **120:** 2516–2527.

Eto M, Kirkbride J, Elliott E, Lo SH, Brautigan DL. 2007. Association of the tensin N-terminal protein–tyrosine phosphatase domain with the α isoform of protein phosphatase-1 in focal adhesions. *J Biol Chem* **282:** 17806–17815.

Farghaian H, Chen Y, Fu AW, Fu AK, Ip JP, Ip NY, Turnley AM, Cole AR. 2011. Scapinin-induced inhibition of axon elongation is attenuated by phosphorylation and translocation to the cytoplasm. *J Biol Chem* **286:** 19724–19734.

Fassler R, Meyer M. 1995. Consequences of lack of β1 integrin gene expression in mice. *Genes & Dev* **9:** 1896–1908.

Geiger B, Spatz JP, Bershadsky AD. 2009. Environmental sensing through focal adhesions. *Nat Rev Mol Cell Biol* **10:** 21–33.

Heanue TA, Pachnis V. 2007. Enteric nervous system development and Hirschsprung's disease: Advances in genetic and stem cell studies. *Nat Rev Neurosci* **8:** 466–479.

Hearn CJ, Murphy M, Newgreen D. 1998. GDNF and ET-3 differentially modulate the numbers of avian enteric neural crest cells and enteric neurons in vitro. *Dev Biol* **197:** 93–105.

Humphries JD, Byron A, Humphries MJ. 2006. Integrin ligands at a glance. *J Cell Sci* **119:** 3901–3903.

Kim TH, Goodman J, Anderson KV, Niswander L. 2007. Phactr4 regulates neural tube and optic fissure closure by controlling PP1-, Rb-, and E2F1-regulated cell-cycle progression. *Dev Cell* **13:** 87–102.

Legate KR, Montanez E, Kudlacek O, Fassler R. 2006. ILK, PINCH and parvin: The tIPP of integrin signalling. *Nat Rev Mol Cell Biol* **7:** 20–31.

Legate KR, Wickstrom SA, Fassler R. 2009. Genetic and cell biological analysis of integrin outside-in signaling. *Genes Dev* **23:** 397–418.

Matsumura F, Hartshorne DJ. 2008. Myosin phosphatase target subunit: Many roles in cell function. *Biochem Biophys Res Commun* **369:** 149–156.

Miralles F, Posern G, Zaromytidou AI, Treisman R. 2003. Actin dynamics control SRF activity by regulation of its coactivator MAL. *Cell* **113:** 329–342.

Moser M, Legate KR, Zent R, Fassler R. 2009. The tail of integrins, talin, and kindlins. *Science* **324:** 895–899.

Newgreen D, Young HM. 2002. Enteric nervous system: Development and developmental disturbances—part 2. *Pediatr Dev Pathol* **5:** 329–349.

Petrie RJ, Doyle AD, Yamada KM. 2009. Random versus directionally persistent cell migration. *Nat Rev Mol Cell Biol* **10:** 538–549.

Ragusa MJ, Dancheck B, Critton DA, Nairn AC, Page R, Peti W. 2010. Spinophilin directs protein phosphatase 1 specificity by blocking substrate binding sites. *Nat Struct Mol Biol* **17:** 459–464.

Rantala JK, Pouwels J, Pellinen T, Veltel S, Laasola P, Mattila E, Potter CS, Duffy T, Sundberg JP, Kallioniemi O, et al. 2011. SHARPIN is an endogenous inhibitor of β1-integrin activation. *Nat Cell Biol* **13:** 1315–1324.

Sagara J, Higuchi T, Hattori Y, Moriya M, Sarvotham H, Shima H, Shirato H, Kikuchi K, Taniguchi S. 2003. Scapinin, a putative protein phosphatase-1 regulatory subunit associated with the nuclear nonchromatin structure. *J Biol Chem* **278:** 45611–45619.

Sagara J, Arata T, Taniguchi S. 2009. Scapinin, the protein phosphatase 1 binding protein, enhances cell spreading and motility by interacting with the actin cytoskeleton. *PLoS ONE* **4:** e4247. doi: 10.1371/journal.pone.0004247.

Satoh A, Nakanishi H, Obaishi H, Wada M, Takahashi K, Satoh K, Hirao K, Nishioka H, Hata Y, Mizoguchi A, et al. 1998. Neurabin-II/spinophilin. An actin filament-binding protein with one pdz domain localized at cadherin-based cell–cell adhesion sites. *J Biol Chem* **273:** 3470–3475.

Shi Y. 2009. Serine/threonine phosphatases: Mechanism through structure. *Cell* **139:** 468–484.

Totsukawa G, Yamakita Y, Yamashiro S, Hartshorne DJ, Sasaki Y, Matsumura F. 2000. Distinct roles of ROCK (Rho-kinase) and MLCK in spatial regulation of MLC phosphorylation for assembly of stress fibers and focal adhesions in 3T3 fibroblasts. *J Cell Biol* **150:** 797–806.

Vicente-Manzanares M, Ma X, Adelstein RS, Horwitz AR. 2009. Non-muscle myosin II takes centre stage in cell adhesion and migration. *Nat Rev Mol Cell Biol* **10:** 778–790.

Young HM, Hearn CJ, Farlie PG, Canty AJ, Thomas PQ, Newgreen DF. 2001. GDNF is a chemoattractant for enteric neural cells. *Dev Biol* **229:** 503–516.

Young HM, Bergner AJ, Anderson RB, Enomoto H, Milbrandt J, Newgreen DF, Whitington PM. 2004. Dynamics of neural crest-derived cell migration in the embryonic mouse gut. *Dev Biol* **270:** 455–473.

Zhang Y, Kim T-H, Niswander L. 2012. Phactr4 regulates directional migration of enteric neural crest through PP1, integrin signaling, and cofilin activity. *Genes Dev* (this issue). doi: 10.1101/gad.179283.111.

A firm grip does not always pay off: a new Phact(r) 4 integrin signaling

Zhiqi Sun and Reinhard Fässler

Genes Dev. 2012 26: 1-5
Access the most recent version at doi:10.1101/gad.184192.111

Nascent Adhesions: From Fluctuations to a Hierarchical Organization

Integrins assemble a complex network of molecular interactions at cell–matrix adhesion sites. Fluorescence correlation microscopy has now shed light on the spatial, temporal and numerical distributions of protein complexes during assembly and stabilization of nascent adhesions.

Zhiqi Sun, Armin Lambacher, and Reinhard Fässler*

A hallmark of integrins is their ability to sense the highly dynamic and complex biochemical and mechanical properties of extracellular matrices. To accomplish these tasks, integrins cluster and assemble numerous ancillary proteins in specialized adhesion structures that differ in their morphology, subcellular localization, lifespan and protein composition. Nascent adhesions are the smallest adhesive structures. They emerge at the edge of protruding membranes, are less than 1 μm in diameter and either disassemble after a lifespan of around 1 minute or mature in an actomyosin-dependent manner into large (up to 10 μm^2) and long-lived (several minutes) focal adhesions [1]. The functions that emanate from the various cell–matrix adhesion sites depend on a highly complex network of interacting proteins. Although most adhesion proteins have been identified, little is known about where and when they interact, and to what extent their numbers change during the assembly and stabilization of cell–matrix adhesion sites. In a recent issue of *Current Biology*, Bachir *et al.* [2] used fluorescence correlation microscopy to address such questions during nascent adhesion development [2]. Their results provide a hierarchy of assembly and define the chronology and stoichiometry of protein complexes associated with integrins.

The formation of integrin-containing adhesive sites proceeds in three major steps. It is assumed that all integrins require an activation step that switches the unbound form of integrins from a low-affinity (inactive) state to a high-affinity (active) state [3]. This activation triggers ligand binding and initiates cell adhesion. Integrin activation is induced upon binding of the two adaptor proteins, talin and kindlin, to β integrin cytoplasmic domains. Upon activation, integrins aggregate and recruit integrin-associated proteins into small, signalling-competent clusters that eventually become visible by conventional microscopy as nascent adhesions. Clustering is observed with all integrins and is required to stabilize the integrin–ligand complex, most likely by increasing the probability for dissociated integrin–ligand complexes to rebind before they diffuse away from the adhesion site [4]. Although it is not clear how integrin clustering is achieved at the molecular level, different reports have assigned roles to talin [5], kindlin [6] and the glycocalyx [7]. Finally, a small number of nascent adhesions mature into large and stable focal adhesions, which requires the linkage to the F-actin cytoskeleton and the activation of non-muscle myosin II. Active myosin II generates pulling forces that change the conformation of proteins associated with the integrin tail, such as talin [8] and Cas130 [9], leading to the recruitment of further adhesion-associated proteins. In addition, a force-induced conformational change in the integrin ectodomain leads to increased stability of the integrin–ligand complex, termed adhesion reinforcement [10]. Notably, the newly recruited proteins operate in a positive-feedback manner to further increase F-actin dynamics, myosin II activation and focal adhesion size.

Talin and kindlin are assumed to be the first proteins that bind to integrin cytoplasmic domains [11]. Their recruitment to adhesion sites is thought to be primarily governed by their ability to bind NPxY motifs in β tails — talin to the membrane-proximal motif and kindlin to the membrane-distal motif. It is not clear whether they bind simultaneously or sequentially to integrin tails. Also their function is only partially understood; it is even debated whether both control integrin activation. Similarly, it is also unclear how they regulate integrin clustering and adhesion reinforcement, and whether they share these functions for all integrins and in all cells. For example, although there is ample evidence supporting an essential role for talin in activating integrins in hematopoietic cells, it seems that fibroblasts lacking both talin isoforms (talin-1 and -2) can still adhere to fibronectin and initiate membrane protrusions, although these are short-lived and inappropriate for sustaining cell spreading [12]. Similarly, loss of both talin isoforms in mouse myoblasts leads to severe muscle defects but does not apparently impair activation of β1 integrins and substrate adhesion [13]. Also the function of kindlin is ambiguous. Loss of the hematopoietic isoform (kindlin-3) affects the binding of multiple blood cell types to their substrates and this was thought to be due to an impaired activation of their integrins [14]. A recent study, however, reveals a role for kindlin-3 in integrin clustering rather than activation [6].

Integrin activation and clustering are associated with the recruitment to adhesion sites of a large protein ensemble, which is collectively termed the adhesome [15]. The adhesome was first determined in a meta-survey of the adhesion literature [16] and further refined by systematic studies using high resolution quantitative mass spectrometry [17–20]. The adhesome contains at least 250 proteins, several of which are recruited in a myosin-II-dependent manner. The large inventory of proteins makes it difficult to comprehend the underlying logic of their assembly. Moreover, their recruitment dynamics, stoichiometry, networking, modifications and linkage to the cytoskeleton are poorly understood. In an attempt to address these questions, Bachir *et al.* [2] used fluorescence correlation microscopy to determine the dynamics, stoichiometry and associations of α5β1 integrin, the integrin-binding proteins talin and kindlin-2, and the actin-binding proteins talin, vinculin and α-actinin during the nucleation/assembly and stabilization of nascent adhesions. They fluorescently labelled these proteins, expressed them in CHO cells and analysed their fluorescence

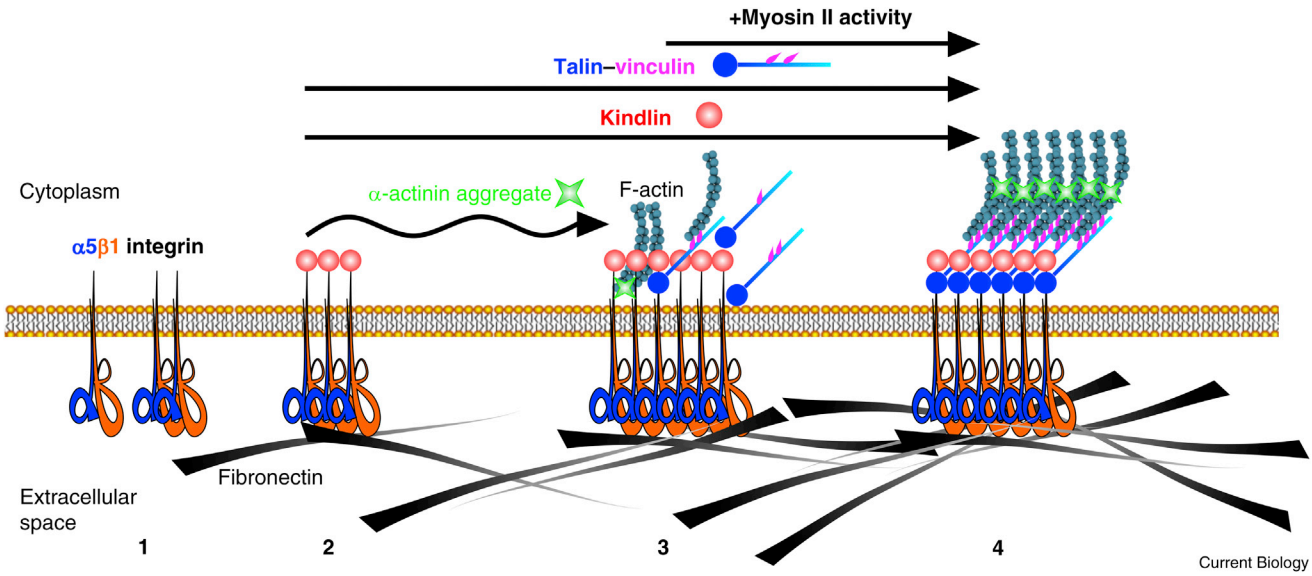

Figure 1. Model of nascent adhesion assembly.

Kindlin-2, talin, vinculin and α-actinin are all recruited to nascent adhesions during their entire lifetime but in different complexes and distinct stoichiometries. Outside of adhesive areas (1), α5β1 integrins remain singly or in clusters of two or three. Kindlin-2 binding to the β1 integrin cytoplasmic domain promotes integrin activation and initiates the nucleation of nascent adhesions (2). Developing nascent adhesions (3) contain talin, which is not associated with α5β1 but forms a complex with vinculin. Aggregates of α-actinin are periodically recruited to nascent adhesions. This is associated with periodic incorporations of further integrins and the initial connection between nascent adhesions and the actin cytoskeleton (3). In stable nascent adhesions (4), integrins reach a 2–3-fold higher degree of aggregation, α-actinin's interaction with integrins is replaced by the talin–vinculin complex, leading to a stable integrin–actin linkage. Myosin II creates pulling forces, resulting in an increased stability of the integrin–ligand interaction, further recruitment of vinculin to the strained talin, and reinforcement of the integrin–actin linkage.

intensity fluctuations in these adhesions using time-lapse total internal reflection fluorescence (TIRF) microscopy. This methodology capitalizes on the movements of the fluorescently labelled proteins, which allows for the determination of their stoichiometry by analyzing the fluctuations of the fluorescence signal with respect to their average intensity, and provides insight into their interactions by simultaneously imaging the fluctuations of two differently labelled proteins and calculating cross-correlations in fluorescence intensities. The results by Bachir *et al.* [2] reveal that the proteins chosen for their study are present throughout the lifetime of nascent adhesions — assembly and stabilization phase — although with different recruitment rates and numbers and in different molecular complexes.

The authors found that neither talin nor kindlin-2 associated with α5β1 integrin in areas adjacent to nascent adhesions, which indicates that α5β1 integrins are not in an activated state outside of adhesion sites. Within nascent adhesions, kindlin-2 and α5β1 co-exist in a 1:1 ratio throughout the lifetime of these adhesions and their positive cross-correlation variance indicates that they are constitutively associated within these adhesions. The association of α5β1 and kindlin-2 is not influenced by the inhibition of myosin II. In contrast, talin, which is also present throughout the lifetime of nascent adhesions, is stably associated with β1 tails only after nascent adhesion assembly is completed, and this interaction is myosin II dependent. Moreover, the stoichiometry of α5β1 and talin is 2:1 in assembling nascent adhesions and 1:1 in mature adhesions.

These findings have significant implications and lead to several important conclusions and hypotheses. The most surprising finding is that kindlin-2 and β1 tails are stably associated in developing nascent adhesions, while talin and β1 tails are not. This suggests that the two integrin activators bind sequentially and that kindlin-2 is probably priming the β1 tails for talin binding. It also suggests that activation of α5β1 is mediated by kindlin-2, while adhesion reinforcement of α5β1 in mature nascent adhesions is mediated by both kindlin-2 and talin, likely by linking the ternary protein complex to actomyosin. The ability of kindlin-2 to activate integrins would be in line with previously published work showing that talin is dispensable for fibroblast adhesion to fibronectin [12] and activation of integrins on mouse myoblasts [13]. However, one should keep in mind that transient interactions of talin with β1 integrin tails that escape detection may very well occur in developing nascent adhesions. Such transient interactions could be sufficient for inducing integrin activation, which is then stabilized by kindlin-2. Nonetheless, the absence of a stable talin–α5β1 integrin complex in developing nascent adhesions excludes a role for talin in integrin clustering during the nucleation of these adhesions. The authors propose that α-actinin may perform this task. Their hypothesis is based on the ability of α-actinin to homodimerize as well as their observation that α-actinin forms aggregates, which are transiently incorporated into developing nascent adhesions. An alternative candidate for integrin clustering and nucleation of nascent adhesions could be kindlin-2, as kindlins were shown to facilitate integrin binding to multivalent ligand [6]. Finally, the lack of association of talin with α5β1 in developing nascent adhesions also indicates that

other adhesome proteins (e.g. RIAM, FAK, vinculin) or lipids (e.g. phosphatidylinositol(4,5)bisphosphate) rather than the integrin tails are responsible for talin recruitment.

In summary, the work of Bachir *et al.* [2] suggests a new model of nascent adhesion assembly and maintenance (Figure 1): kindlin-2 binds to β1 integrin and induces the high-affinity state of α5β1; α-actinin promotes β1 integrin clustering and sets up a transient connection between the integrin cluster and the actin cytoskeleton; and kindlin-2 paves the way for talin recruitment, which replaces α-actinin and establishes a more stable integrin–actin linkage with the help of vinculin, leading to adhesion reinforcement. This sequence of molecular events is both intriguing and provocative, although it may not operate in all cell types and for all integrins, so we look forward to further confirmation in future studies.

References

1. Vicente-Manzanares, M., Ma, X., Adelstein, R.S., and Horwitz, A.R. (2009). Non-muscle myosin II takes centre stage in cell adhesion and migration. Nat. Rev. Mol. Cell Biol. *10*, 778–790.
2. Bachir, A.I., Zareno, J., Moissoglu, K., Plow, E., Gratton, E., and Horwitz, A.R. (2014). Integrin-associated complexes form hierarchically with variable stoichiometry in nascent adhesions. Curr. Biol. *24*, 1845–1853.
3. Shattil, S.J., Kim, C., and Ginsberg, M.H. (2010). The final steps of integrin activation: the end game. Nat. Rev. Mol. Cell Biol. *11*, 288–300.
4. Coussen, F., Choquet, D., Sheetz, M.P., and Erickson, H.P. (2002). Trimers of the fibronectin cell adhesion domain localize to actin filament bundles and undergo rearward translocation. J. Cell Sci. *115*, 2581–2590.
5. Saltel, F., Mortier, E., Hytonen, V.P., Jacquier, M.C., Zimmermann, P., Vogel, V., Liu, W., and Wehrle-Haller, B. (2009). New PI(4,5)P2- and membrane proximal integrin-binding motifs in the talin head control beta3-integrin clustering. J. Cell Biol. *187*, 715–731.
6. Ye, F., Petrich, B.G., Anekal, P., Lefort, C.T., Kasirer-Friede, A., Shattil, S.J., Ruppert, R., Moser, M., Fassler, R., and Ginsberg, M.H. (2013). The mechanism of kindlin-mediated activation of integrin alphaIIbbeta3. Curr. Biol. *23*, 2288–2295.
7. Paszek, M.J., DuFort, C.C., Rossier, O., Bainer, R., Mouw, J.K., Godula, K., Hudak, J.E., Lakins, J.N., Wijekoon, A.C., Cassereau, L., *et al.* (2014). The cancer glycocalyx mechanically primes integrin-mediated growth and survival. Nature *511*, 319–325.
8. del Rio, A., Perez-Jimenez, R., Liu, R., Roca-Cusachs, P., Fernandez, J.M., and Sheetz, M.P. (2009). Stretching single talin rod molecules activates vinculin binding. Science *323*, 638–641.
9. Sawada, Y., Tamada, M., Dubin-Thaler, B.J., Cherniavskaya, O., Sakai, R., Tanaka, S., and Sheetz, M.P. (2006). Force sensing by mechanical extension of the Src family kinase substrate p130Cas. Cell *127*, 1015–1026.
10. Kong, F., Garcia, A.J., Mould, A.P., Humphries, M.J., and Zhu, C. (2009). Demonstration of catch bonds between an integrin and its ligand. J. Cell Biol. *185*, 1275–1284.
11. Calderwood, D.A., Campbell, I.D., and Critchley, D.R. (2013). Talins and kindlins: partners in integrin-mediated adhesion. Nat. Rev. Mol. Cell Biol. *14*, 503–517.
12. Zhang, X., Jiang, G., Cai, Y., Monkley, S.J., Critchley, D.R., and Sheetz, M.P. (2008). Talin depletion reveals independence of initial cell spreading from integrin activation and traction. Nat. Cell Biol. *10*, 1062–1068.
13. Conti, F.J., Monkley, S.J., Wood, M.R., Critchley, D.R., and Muller, U. (2009). Talin 1 and 2 are required for myoblast fusion, sarcomere assembly and the maintenance of myotendinous junctions. Development *136*, 3597–3606.
14. Karakose, E., Schiller, H.B., and Fassler, R. (2010). The kindlins at a glance. J. Cell Sci. *123*, 2353–2356.
15. Winograd-Katz, S.E., Fassler, R., Geiger, B., and Legate, K.R. (2014). The integrin adhesome: from genes and proteins to human disease. Nat. Rev. Mol. Cell Biol. *15*, 273–288.
16. Zaidel-Bar, R., Itzkovitz, S., Ma'ayan, A., Iyengar, R., and Geiger, B. (2007). Functional atlas of the integrin adhesome. Nat. Cell Biol. *9*, 858–867.
17. Schiller, H.B., Friedel, C.C., Boulegue, C., and Fassler, R. (2011). Quantitative proteomics of the integrin adhesome show a myosin II-dependent recruitment of LIM domain proteins. EMBO Rep. *12*, 259–266.
18. Humphries, J.D., Byron, A., Bass, M.D., Craig, S.E., Pinney, J.W., Knight, D., and Humphries, M.J. (2009). Proteomic analysis of integrin-associated complexes identifies RCC2 as a dual regulator of Rac1 and Arf6. Science Sig. *2*, ra51.
19. Schiller, H.B., Hermann, M.R., Polleux, J., Vignaud, T., Zanivan, S., Friedel, C.C., Sun, Z., Raducanu, A., Gottschalk, K.E., Thery, M., *et al.* (2013). beta1- and alphav-class integrins cooperate to regulate myosin II during rigidity sensing of fibronectin-based microenvironments. Nat. Cell Biol. *15*, 625–636.
20. Kuo, J.C., Han, X., Hsiao, C.T., Yates, J.R., 3rd, and Waterman, C.M. (2011). Analysis of the myosin-II-responsive focal adhesion proteome reveals a role for beta-Pix in negative regulation of focal adhesion maturation. Nat. Cell Biol. *13*, 383–393.

Max Planck Institute of Biochemistry, Department of Molecular Medicine, Am Klopferpsitz 18, 82152 Martinsried, Germany.
*E-mail: faessler@biochem.mpg.de

http://dx.doi.org/10.1016/j.cub.2014.07.061

Neuroscience: Waiting for Serotonin

Serotonin dysfunction is implicated in many neuropsychiatric disorders yet the precise behavioral functions of this neuromodulator are not well understood. A new study employs optogenetic methods to activate serotonin neurons during an effort-demanding waiting behavior and demonstrates that serotonin release increases patience, the capacity for self-control.

Sachin Ranade, Hyun-Jae Pi, and Adam Kepecs*

It is downtown Manhattan on a Saturday evening. You decide to go to Ippudu Ramen for dinner. There are no reservations, so the person at the door takes down your name and says, "45 minutes". You are not in a rush but as time passes you get hungrier by the minute and less and less patient. At some point, you give up the wait and decide to look for a slice of pizza instead. We all have been in these situations when we lose the ability for self-control and make impulsive decisions. In a new study in the current issue Miyazaki *et al.* [1] shed light (literally and figuratively) on the neural mechanisms underlying patience. The authors show that patient waiting is enhanced by serotonin, an important neurochemical long hypothesized to be involved in inhibition of impulsive actions.

Serotonin is a major neuromodulator implicated in a broad assortment of behavioral and physiological functions, including aggression, appetite, aversion, behavioral inhibition and impulsivity. Serotonergic neurons are located deep in the midbrain and from there they send extensive, highly divergent projections to virtually all areas of the brain (Figure 1A). The serotonin system is one of the most important targets for the treatment of depression, anxiety, panic and mood disorders and other psychiatric conditions. It has been difficult, however, to explain the diverse effects of serotonin on adaptive behavior within a unified framework.

One of the main theories about serotonin proposes that it is important for behavioral inhibition and self-control. Indeed, a prominent behavioral effect of serotonin manipulation is observed in studies of impulsive choice, in which subjects choose between a small immediate